

REPORT DOCUMENTATION PAGE

Form Approved
OMB No. 0704-0188

Public reporting burden for this collection of information is estimated to average 1 hour per response, including the time for reviewing instructions, searching existing data sources, gathering and maintaining the data needed, and completing and reviewing the collection of information. Send comments regarding this burden estimate or any other aspect of this collection of information, including suggestions for reducing this burden, to Washington Headquarters Services, Directorate for Information Operations and Reports, 1215 Jefferson Davis Highway, Suite 1204, Arlington, VA 22202-4302, and to the Office of Management and Budget, Paperwork Reduction Project (0704-0188), Washington, DC 20503.

| | | | | | | |
|--|--|--|---|---|--|--|
| 1. AGENCY USE ONLY (Leave blank) | | | 2. REPORT DATE Mar 95 | | 3. REPORT TYPE AND DATES COVERED Final Oct 91 - Mar 95 | |
| 4. TITLE AND SUBTITLE CONVENTIONAL WEAPONS EFFECTS ON REINFORCED SOIL WALLS | | | 5. FUNDING NUMBERS PE - 61102F Project - 2302CW Task - 93WL004 | | | |
| 6. AUTHOR(S) Richard A. Reid | | | 7. PERFORMING ORGANIZATION NAME(S) AND ADDRESS(ES) WL/FIVCS 139 BARNES DRIVE, SUITE 2 TYNDALL AFB FL 32403 | | | |
| 8. PERFORMING ORGANIZATION REPORT NUMBER AFOSR-R-95-0314 | | | 9. SPONSORING/MONITORING AGENCY NAME(S) AND ADDRESS(ES) AFOSR/NA 110 DUNCAN AVE, SUITE B115 BOLLING AFB WASHINGTON DC 20332-0001 | | | |
| 10. SPONSORING/MONITORING AGENCY REPORT NUMBER | | | 11. SUPPLEMENTARY NOTES | | | |
| DISTRIBUTION STATEMENT | | | | Approved for public release Distribution Unlimited | | |
| 12a. DISTRIBUTION/AVAILABILITY STATEMENT This report has been reviewed by the Public Affairs Office and is releasable to the National Technical Information Service (NTIS). At NTIS, it will be available to the general public, including foreign nations. | | | 12b. DISTRIBUTION CODE | | | |
| 13. ABSTRACT (Maximum 200 words) A more quantitative understanding of the response of reinforced soil walls to explosions in the retained fill was developed via a single degree of freedom model developed by Drake, et al (1987). A series of full-scale tests were conducted to investigate the response of the walls to free-field blast pressures, and detailed analysis of the test data suggested inertial stresses generated during the crater formation process, not blast pressures, were the governing loading condition. Using full and small-scale test data, the validity of the model is demonstrated through a consistent relationship between system stiffness and displacement. The consistency of the stiffness/displacement relationship for full and scaled tests suggest the centrifuge provides reasonable models of full-scale reinforced soil walls. Application of the test data to the model yields order of magnitude results in prediction of ultimate wall panel displacements. The approach and results of this study provides a significant departure from previous research by identifying the loading mechanisms that govern response, the influence of the engineering properties of the materials, and validation of a model that provides a quantitative description of the physical response of the reinforced soil wall. | | | | | | |
| 14. SUBJECT TERMS Reinforced soil, conventional weapons, protective structures, geosynthetics, geogrid, centrifuge, soil dynamics, inertial stress, plastic stress. | | | | | 15. NUMBER OF PAGES 388 | |
| 16. PRICE CODE | | | | | 17. SECURITY CLASSIFICATION OF REPORT Unclassified | |
| 18. SECURITY CLASSIFICATION OF THIS PAGE Unclassified | | | | | 19. SECURITY CLASSIFICATION OF ABSTRACT Unclassified | |
| 20. LIMITATION OF ABSTRACT UL | | | | | DTIC QUALITY INSPECTED 5 | |

GENERAL INSTRUCTIONS FOR COMPLETING SF 298

The Report Documentation Page (RDP) is used in announcing and cataloging reports. It is important that this information be consistent with the rest of the report, particularly the cover and title page. Instructions for filling in each block of the form follow. It is important to stay *within the lines* to meet *optical scanning requirements*.

Block 1. Agency Use Only (Leave blank).

Block 2. Report Date. Full publication date including day, month, and year, if available (e.g. 1 Jan 88). Must cite at least the year.

Block 3. Type of Report and Dates Covered.

State whether report is interim, final, etc. If applicable, enter inclusive report dates (e.g. 10 Jun 87 - 30 Jun 88).

Block 4. Title and Subtitle. A title is taken from the part of the report that provides the most meaningful and complete information. When a report is prepared in more than one volume, repeat the primary title, add volume number, and include subtitle for the specific volume. On classified documents enter the title classification in parentheses.

Block 5. Funding Numbers. To include contract and grant numbers; may include program element number(s), project number(s), task number(s), and work unit number(s). Use the following labels:

| | |
|----------------------|------------------------------|
| C - Contract | PR - Project |
| G - Grant | TA - Task |
| PE - Program Element | WU - Work Unit Accession No. |

Block 6. Author(s). Name(s) of person(s) responsible for writing the report, performing the research, or credited with the content of the report. If editor or compiler, this should follow the name(s).

Block 7. Performing Organization Name(s) and Address(es). Self-explanatory.

Block 8. Performing Organization Report Number. Enter the unique alphanumeric report number(s) assigned by the organization performing the report.

Block 9. Sponsoring/Monitoring Agency Name(s) and Address(es). Self-explanatory.

Block 10. Sponsoring/Monitoring Agency Report Number. (If known)

Block 11. Supplementary Notes. Enter information not included elsewhere such as: Prepared in cooperation with...; Trans. of...; To be published in.... When a report is revised, include a statement whether the new report supersedes or supplements the older report.

Block 12a. Distribution/Availability Statement.

Denotes public availability or limitations. Cite any availability to the public. Enter additional limitations or special markings in all capitals (e.g. NOFORN, REL, ITAR).

DOD - See DoDD 5230.24, "Distribution Statements on Technical Documents."

DOE - See authorities.

NASA - See Handbook NHB 2200.2.

NTIS - Leave blank.

Block 12b. Distribution Code.

DOD - Leave blank.

DOE - Enter DOE distribution categories from the Standard Distribution for Unclassified Scientific and Technical Reports.

NASA - Leave blank.

NTIS - Leave blank.

Block 13. Abstract. Include a brief (*Maximum 200 words*) factual summary of the most significant information contained in the report.

Block 14. Subject Terms. Keywords or phrases identifying major subjects in the report.

Block 15. Number of Pages. Enter the total number of pages.

Block 16. Price Code. Enter appropriate price code (*NTIS only*).

Blocks 17. - 19. Security Classifications. Self-explanatory. Enter U.S. Security Classification in accordance with U.S. Security Regulations (i.e., UNCLASSIFIED). If form contains classified information, stamp classification on the top and bottom of the page.

Block 20. Limitation of Abstract. This block must be completed to assign a limitation to the abstract. Enter either UL (unlimited) or SAR (same as report). An entry in this block is necessary if the abstract is to be limited. If blank, the abstract is assumed to be unlimited.

EXECUTIVE SUMMARY

A. OBJECTIVE

The objective of this effort is to understand the load deformation behavior of a soil element reinforced with synthetic inclusions when the element is subjected to high strain rate loading from a chemical explosion within the soil mass.

B. BACKGROUND

Conventional reinforced concrete protective structures are currently used by the United States Air Force to shelter aircraft, munitions, command and control facilities and other critical warfighting functions from conventional weapons attack. The advantages of reinforced concrete as a construction material include its ability to be designed to a specific strength, ability to be placed in any size or shape, and well known blast response characteristics. Some disadvantages to reinforced concrete include its high cost, long construction time, reliance on large amounts of quality construction materials, and the need for skilled labor. Therefore, reinforced concrete is not well suited for use where modern construction techniques and support are not available, or when expedient construction is required.

Alternatively, particulate media such as soil may be used for the construction of protective shelters when reinforced with synthetic inclusions. Thin stackable concrete panels are used to form the walls of the shelter. The synthetic reinforcement material is tied to the panels and the entire structure is buried with soil. Previous research in this area has focused on relating peak ground shock pressures and accelerations to the response of the structure, however this approach has been unsuccessful. To fully understand the dynamics of the interaction between the various materials within the time domain, a fundamentally based approach is necessary.

C. SCOPE

In order to achieve research objectives, a five-phased technical approach was developed as follows: 1) conduct a literature review for (a) response of reinforced soil, and its components to high strain rate loading, (b) numerical codes for evaluating reinforced soil response to ground shock, and (c) physical model testing of reinforced soil systems; 2) develop a test plan and designs for full-scale explosive tests of reinforced soil retaining walls; 3) construct and test walls, collect and reduce data; 4) estimate residual displacements of full and small-scale wall panels via a single degree of freedom model; and 5) use the simple model to conduct a parametric study of the influence of specific design variables on wall panel response.

19950425 072

D. METHODOLOGY

A single degree of freedom model was modified to characterize the response of particulate media with synthetic inclusions to high strains caused by chemical explosions within the media. A series of six full-scale tests were conducted to provide data for model validation, and data from scaled centrifuge tests were used as an independent test of the model. The model is then used to predict system displacements to the high strain rate loads and these predictions are then compared to measured test data.

E. TEST DESCRIPTION

Four reinforced soil walls were constructed with a granular media reinforced with a high density polyethylene inclusions. The face of the wall was confined with thin concrete panels tied into the inclusions. Five hundred pound Mark-82 bombs were detonated within the media and test measurements included dynamic stresses within the soil mass, strains on the reinforcement, and accelerations of the concrete facing panels.

F. CONCLUSIONS

A successful series of six explosive tests were performed on four geogrid reinforced soil walls. Since this type of instrumented test series had never been successfully performed before, this research has created a unique data base on the response of reinforced soil walls to free-field blast pressures. This research suggests two loading mechanisms are present when an explosion takes place in a granular media with synthetic inclusions. First is the high amplitude, short duration blast pressure wave. This is followed by the inertial or plastic stress wave, which has two components. The first component is the loading that takes place while the entire soil mass from the crater/soil interface to the wall panel is in compression. This is the mass movement resisted by the mass of the soil and the energy absorbed by the soil mass. Once the inertial wave decays and the entire mass is not in compression, stresses on the concrete elements are transferred to the reinforcement and boundary frictional forces, and the resistance of the inclusion becomes mobilized. Research over the past two decades has attempted to relate residual displacements to the peak free-field blast pressures and accelerations. The results of this research suggest the inertial pressure wave, and not the blast pressure wave, is the load mechanism that results in the most significant response of the system. The single degree of freedom model was validated using full and small-scale test data and provided consistent results across scales. This research suggests this model may be appropriate for evaluating system response to both blast pressure and inertial wave loading. Using measured test data, prediction of displacements for the full-scale tests yielded order of magnitude results. For the scaled tests, the model predicted displacements within 20 percent of measured. Finally, comparison of full and scaled tests show the centrifuge studies provide reasonable models of full-scale tests.

G. RECOMMENDATIONS

A predictive model for the amplitude and duration of inertial stresses from explosions in particulate media has not been developed. The development of such a model would provide a means of quantifying the inertial stress waves for a range of explosive weights and particulate media. Incorporation of this type of model would provide a forcing function for use in the single degree of freedom model used in this research, resulting in a valuable tool that could be applied in optimization of designs.

| | |
|--------------------|-------------------------------------|
| Accession For | |
| NTIS GRA&I | <input checked="" type="checkbox"/> |
| DTIC TAB | <input type="checkbox"/> |
| Unannounced | <input type="checkbox"/> |
| Justification | |
| By _____ | |
| Distribution/ | |
| Availability Codes | |
| Dist | Avail and/or Special |
| R | |

CONVENTIONAL WEAPONS EFFECTS ON REINFORCED SOIL WALLS

A Thesis
Presented to
The Academic Faculty

by

Richard Alan Reid

In Partial Fulfillment
of the Requirements for the Degree
Doctor of Philosophy in Civil Engineering

Georgia Institute of Technology
March 1995

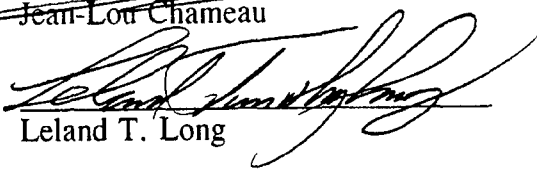
Copyright c 1995 by Richard A. Reid

CONVENTIONAL WEAPONS EFFECTS ON REINFORCED SOIL WALLS

Approved:


Glenn J. Rix, Chairman


Jean-Lou Chameau


Leland T. Long

Date Approved 3/10/95

Dedicated to my wife Kathy and our children, Lindsey, Timothy and Rebecca;
my parents, Wallace and Virginia Reid; and in loving memory
of my sister, Deidre Reid Nelson

Acknowledgements

In the eight years it has taken to complete this degree, many people have worked on my behalf towards the achievement of this elusive goal. I mention those whose efforts were significant, knowing full well that many others made important contributions but whom are too numerous to mention specifically.

I would like to thank Dr. Jean-Lou Chameau for his singular efforts while I was a student in absentia. Without his interest and influence, obtaining this degree would not have been. Dr. Glenn J. Rix had the difficult task of assisting in the development of this thesis and ensuring the requirements of the college were met. His adherence to standards of academic excellence motivated me to reach beyond my limitations and better prepare me for my future. Also, Dr. Leland T. Long, who influenced me to develop a greater understanding of wave behavior, which played an important role in the analysis of my research. Dr. Robert C. Bachus, who for over ten years has been my teacher, colleague, and mentor. He has assisted me in so many ways over my academic and professional career that he has my eternal gratitude and respect. Finally, Dr. J. David Frost, for his constructive contributions toward this thesis and preparing me for entering academia.

MSgt John Pigg, USAF, Charlie Smith, Don Kirchman, Fred LaLuzerne, Ed Lockard, Bennie Burdett, and Jim Jones of the USAF Civil Engineering Laboratory, Tyndall AFB, FL, provided the intense labor necessary for construction of the test walls in the oppressive Florida heat and humidity. Their motivation came not from just doing their job, but a unselfish and sincere desire to do whatever necessary to help me complete this research. TSgt Scott Kortum, USAF and Bill Naylor provided all data collection instrumentation support. Mr. Carl Hollopeter, made significant contributions toward the development of the procedures used to install strain gages on geogrid as well as assist with test instrumentation. Mr. Mike Purcell, provided test photography and video support, assisted with his vast experience in the handling of explosives, and technical input on the behavior and data collection on explosions in soils. Mike is my strongest ally, and I value his constant support and friendship. Dr. Doug Merkle, whose engineering expertise, friendship and guidance have helped me on this and other research projects. He made his vast personal technical library available to me and has contributed greatly to my professional development. Also, Mr. Steve Butler and Ms. Michelle Newsome, for preparation of many of the figures. Finally, Dr. Jim Collin, whose generous support guidance were critical to this research.

I would also like to recognize Lt. Col. Steve Boyce, USAF for research support from the USAF Office of Scientific Research, Washington, DC. His personal interest in my obtaining a Ph.D. provided me with an introduction to Dr. Chameau and funding for this research. I am indebted to him for his unselfish efforts that led to the resurrection my degree program.

Fellow students Wes Spang and Dr. Roger Meier who assisted in my return to college and shared a common pursuit of midlife career change. Seph Scott, the department machinist, for lots of coffee and conversation, and to Ken Thomas, CE department, for 10 years of friendship and support.

My parents, Wallace and Virginia Reid, who taught me the virtues of hard work and perseverance that are two necessary elements in both completing a Ph.D. and being successful in life. It is said that parents are so busy trying to give their children what they didn't have, that they forget to give us what they did have. They gave me both. Their love, support, teachings and guidance are the greatest gifts a child can receive.

Finally, and most importantly, my wife Kathy and our children, Lindsey, Timothy and Rebecca. The sacrifices you have made out of your love for me were significant and unselfish. Many times you were my only source of hope and motivation, especially during that bleak year of 1994. I love you forever.

TABLE OF CONTENTS

| | |
|--|-------|
| DEDICATION | iii |
| ACKNOWLEDGEMENTS | iv |
| TABLE OF CONTENTS | vii |
| LIST OF TABLES | xiv |
| LIST OF FIGURES | xvii |
| SUMMARY | xxvii |
| CHAPTER | |
| I. INTRODUCTION | 1 |
| Objective | 1 |
| Background | 2 |
| United States Air Force Relevance | 7 |
| Scope | 11 |
| Applications | 11 |
| Organization | 12 |
| II. EXPLOSIONS IN SOIL | 15 |
| Introduction | 15 |
| Explosions in Soil | 15 |
| Terminology | 17 |
| Estimation of Free-field Pressure | 18 |
| Crater Formation | 22 |
| Inertial Pressures | 24 |
| Partition of Wave Energy at Boundaries | 26 |

TABLE OF CONTENTS (CONT.)

CHAPTER

| | |
|---|-----------|
| III. EARTH BERMS AND REINFORCED SOIL IN BLAST-RESISTANT STRUCTURES | 30 |
| Introduction | 30 |
| Soil Berms | 30 |
| Reinforced Soil Systems | 32 |
| Explosive Testing of Reinforced Soil Structures | 34 |
| Full-Scale Tests | 35 |
| Physical Model Tests | 43 |
| Comparison of Model and Full-Scale Materials | 43 |
| Phase I Tests | 45 |
| Phase II Tests | 48 |
| Evaluation of Centrifuge Test Data for Further Analysis | 52 |
| Numerical Models | 53 |
| Evaluation of Previous Research | 57 |
| IV. EQUATION OF MOTION | 61 |
| Introduction | 61 |
| Development of The Equation of Motion | 63 |
| Validity For Reinforced Concrete Walls | 67 |
| Application to Reinforced Soil Walls | 68 |
| V. FULL-SCALE TEST DESIGN | 69 |
| Introduction | 69 |
| Type of Reinforcement | 70 |
| Selection of Geogrid Type | 72 |
| Type of Facing Panel | 74 |
| Test Structure Dimensions | 74 |
| Soil Type and Properties | 76 |
| Number of Tests | 78 |
| Weapon Size | 78 |
| Weapon Location | 79 |

TABLE OF CONTENTS (CONT.)

CHAPTER

| | |
|---|-----|
| Weapon Placement | 80 |
| Data Collection | 81 |
| Data Acquisition System | 81 |
| Firing System | 82 |
| Gages | 83 |
| Soil Pressure Interface Gages | 84 |
| Accelerometers | 88 |
| Strain Gages | 89 |
| Free-Field Pressure Gages | 92 |
| High Speed Camera | 93 |
| Reinforced Soil Wall Design | 94 |
| Test Wall Construction | 95 |
| VI. TEST DATA AND DATA REDUCTION | 97 |
| Introduction | 97 |
| Overview of Test Parameters | 97 |
| Overall Instrumentation Success | 100 |
| Test Data | 103 |
| High Speed Film | 113 |
| Effect of Reinforcement Stiffness | 118 |
| Ground Shock Coupling Factor | 121 |
| Failure Mechanisms | 123 |
| Data Reduction | 125 |
| Wall Panel Peak Velocities and Displacements | 125 |
| Panel Impulse Loads | 126 |
| Prediction of Compressive Wave Stress Within the Retained Backfill | 129 |
| Attenuation Coefficient | 129 |
| Predicted Versus Measured Free-Field Pressure | 132 |
| Estimation of Free-Field Stresses | 135 |
| Free-Field Pressure at Gage Locations | 135 |
| Geogrid Strains | 139 |
| Strain of UX 1400HT Geogrid | 140 |

TABLE OF CONTENTS (CONT.)

CHAPTER

| | |
|---|------------|
| Strain of UX 1500HT Geogrid | 142 |
| Summary | 142 |
| VII. MODEL VALIDATION USING FULL AND SMALL-SCALE PRESSURE WAVE DATA | 144 |
| Introduction | 144 |
| Determination of Stiffness Per Unit Area | 145 |
| Numerical Integration | 145 |
| Numerical Loading Function | 148 |
| System Stiffness of Full-Scale Walls | 150 |
| Independent Model Test Using Scaled Test Data | 161 |
| Stiffness Per Unit Area for Centrifuge Tests | 162 |
| Solution of the Equation of Motion for Scaled Tests and Blast Pressure Wave | 162 |
| Summary | 166 |
| VIII. EVALUATION OF INERTIAL LOADING AND RESPONSE MECHANISMS | 168 |
| Introduction | 168 |
| Organization | 168 |
| Inertial Wave Loading Mechanisms | 169 |
| Application of the Model to Inertial Loading | 171 |
| Prediction of Displacement Due to Mass Movement | 177 |
| Prediction of Displacement Due to Pullout Loading | 182 |
| Response of Scaled Tests to Inertial Wave Loading | 185 |
| Centrifuge Test Number 27 | 186 |
| Centrifuge Test Number 20 | 187 |
| Centrifuge Test Number 26 | 187 |
| Centrifuge Test Number 28 | 188 |
| Centrifuge Test Number 29 and 32 | 188 |
| Pullout Resistance of Nylon Mesh Reinforcing Material | 188 |
| Results of Numerical Integration | 190 |

TABLE OF CONTENTS (CONT.)

CHAPTER

| | |
|--|------------|
| Discussion of Centrifuge Evaluation | 190 |
| Application to Full-Scale Tests | 197 |
| Dynamic Pullout Resistance Function of Geogrid Reinforcement | 198 |
| Prediction of Displacement - Panel 2, Test 5 | 201 |
| Prediction of Displacement - Panel 1, Test 5 | 202 |
| Prediction of Displacement - Panel 2, Test 6 | 202 |
| Sources of Error | 203 |
| Approximation of Boundary Friction | 205 |
| Discussion of Full-Scale Test Evaluation | 207 |
| | |
| IX. INFLUENCE OF DESIGN PARAMETERS ON WALL DISPLACEMENT | 210 |
| Introduction | 210 |
| Evaluation Matrix | 210 |
| Results of Evaluation, Test Five | 211 |
| Results of Evaluation, Test Six | 213 |
| Comparison of Evaluations | 215 |
| Methods to Reduce Wall Panel Displacement | 219 |
| Decreasing Forcing Function Amplitude | 220 |
| Backfill Minimization | 220 |
| Predetonation Screens | 220 |
| Overlay Systems | 220 |
| Increasing Resistance of Structure | 221 |
| Top Restraint | 221 |
| Increase in Backfill Unit Weight | 221 |
| Vertical Reinforcement | 222 |
| Soil Stabilization | 222 |
| Increase Pullout Resistance | 223 |
| | |
| X. CONCLUSIONS AND RECOMMENDATIONS | 224 |
| Introduction | 224 |
| Summary of Conclusions | 225 |

TABLE OF CONTENTS (CONT.)

CHAPTER

| | |
|---|------------|
| Recommendations | 229 |
| APPENDIX A - INSTALLATION OF STRAIN GAGES | 231 |
| Introduction | 231 |
| Materials | 231 |
| Surface Preparation | 232 |
| Attachment | 233 |
| Protective Coating | 234 |
| Deviations and Additions to This Procedure | 235 |
| Protection of the Leadwires | 235 |
| Tie-Down of the Leadwires | 236 |
| Protection of the Strain Gages | 236 |
| Results of Test One | 237 |
| Modification of Strain Gage Installation Procedures | 237 |
| Addition of Bondable Terminals | 237 |
| Use of Low Temperature Solder | 238 |
| Reinforcement of the Geogrid Ribs | 238 |
| Strain Gage Protective Coating | 239 |
| Success Rate | 239 |
| APPENDIX B - TEST WALL CONSTRUCTION | 240 |
| Introduction | 240 |
| Test Site | 240 |
| Fabrication of Wall Panels | 241 |
| Leveling Pad and Site Preparation | 243 |
| Wall Construction | 244 |
| Introduction | 244 |
| Base Row Panels | 245 |
| Placement of Backfill | 246 |
| Placement of Geogrid Reinforcement | 247 |
| Second Row of Panels | 248 |
| Minimum Geogrid Embedment Length | 251 |

TABLE OF CONTENTS (CONT.)

CHAPTER

| | |
|--------------------------------|------------|
| APPENDIX C - DATA PLOTS | 253 |
| BIBLIOGRAPHY | 351 |
| VITA | 358 |

LIST OF TABLES

| Table | Title | |
|-------|--|-------|
| 2.1 | Typical Soil Properties For the Drake-Little Equation (Drake, et al., 1989) | 21 |
| 3.1 | Summary of Full-Scale Explosive Tests on Reinforced Soil Walls | 36-38 |
| 3.2 | Replica Scaling Relationships (Scott & Morgan, 1977) | 44 |
| 3.3 | Phase I Centrifuge Test Matrix | 46 |
| 3.4 | Phase II Centrifuge Test Matrix | 49 |
| 3.5 | Centrifuge Test Parameters - Prototype Scale | 53 |
| 3.6 | Numerical Evaluation Test Matrix | 55 |
| 5.1 | Properties of Geogrid Reinforcement (Tensar Earth Technologies, Inc., 1992) | 73 |
| 5.2 | Summary of Backfill Densities and Moisture Contents | 96 |
| 6.1 | Test Summary | 99 |
| 6.2 | Summary of Gage Operability, All Tests | 101 |
| 6.3 | Summary of Average Wavespeeds | 103 |
| 6.4 | Wall One, Test One Data | 108 |
| 6.5 | Wall Two, Test Two Data | 109 |

LIST OF TABLES (CONT.)

| Table | Title | |
|-------|---|-----|
| 6.6 | Wall Two, Test Three Data | 110 |
| 6.7 | Wall Three, Test Four Data | 111 |
| 6.8 | Wall Three, Test Five Data | 112 |
| 6.9 | Peak Panel Accelerations, Velocities, & Displacements, All Tests | 127 |
| 6.10 | Summary of Interface Pressure and Impulse | 128 |
| 6.11 | Attenuation Coefficients | 131 |
| 6.12 | Free-field Pressures, Predicted and Measured | 133 |
| 6.13 | Calculated Peak Free-field Pressures (in psi) at the Center of Each Instrumented Panel | 136 |
| 6.14 | Calculated Free-Field Pressures at Each Strain Gage Location and Peak Compressive Strain | 137 |
| 7.1 | Free-Field Stress Decay Constant | 149 |
| 7.2 | Integration for Stiffness Per Unit Area, Test 5, Panel No. 2 | 153 |
| 7.3 | Attenuation and Decay Coefficients - Centrifuge Tests 20, 26-29, 32 | 164 |
| 8.1 | Predicted and Measured Displacements - Scaled Tests | 190 |
| 8.2 | Predicted and Observed Displacements - Full-Scale Tests | 203 |

LIST OF TABLES (CONT.)

| Table | Title | |
|--------------|---|------------|
| 8.3 | Summary of Predicted Displacements With and Without Friction | 208 |
| 9.1 | Model Evaluation Matrix | 211 |
| 9.2 | Evaluation Matrix Results - 25 Foot Standoff | 212 |
| 9.3 | Evaluation Matrix Results - 20 Foot Standoff | 214 |

LIST OF FIGURES

| Figure | Title | |
|--------|---|----|
| 1.1 | Aerodynamic Deflection (Ferritto, et al, 1988) | 5 |
| 1.2 | Schematic of Wrapped Face Geotextile Wall (Koerner, 1990) | 6 |
| 1.3 | Example of Protective Soil Berm (Drake, et al, 1989) | 8 |
| 1.4 | Reinforced Soil Bunker (Reid, 1991) | 9 |
| 2.1 | Typical Half Crater Profile (Headquarters, Department of the Army, 1986) | 17 |
| 2.2 | Inertial Pressure Wave (Lower Plot) Time History (Davies and Williams, 1990) | 26 |
| 3.1 | 1990 Test Structure, Negev Desert, Israel | 40 |
| 3.2 | Plan & Profile of Wall Panel Deflections, 1990 Test Structure (Eytan and Reid, 1993) | 41 |
| 3.3 | Typical Centrifuge Test Wall | 50 |
| 4.1 | Free Body Diagram of Wall Panel With Wave Interaction (Drake, et al, 1987) | 65 |
| 5.1 | Georgia Stabilized Earth Panel | 75 |
| 5.2 | Grain Size Curve, Sky X Soil | 77 |
| 5.3 | Schematic of Test Wall Design | 85 |

LIST OF FIGURES (CONT.)

| Figure | Title | |
|--------|--|-----|
| 5.4 | Position of Strain Gages, Tests 2 and 3 | 90 |
| 5.5 | Position of Strain Gages, Tests 4 and 5 | 91 |
| 6.1 | Typical Test Wall | 98 |
| 6.2 | Plan and Profile of Weapon Location | 99 |
| 6.3 | Typical Acceleration Record | 104 |
| 6.4 | Typical Soil/Panel Interface Pressure Record | 105 |
| 6.5 | Typical Free-field Pressure Record | 106 |
| 6.6 | Typical Strain Gage Record | 107 |
| 6.7 | Pressure & Impulse From Blast Wave and Inertial Wave Loading, Centrifuge Test Data | 116 |
| 6.8 | Acceleration, Velocity and Displacement From Blast & Inertial Wave, Centrifuge Test Data | 117 |
| 6.9 | Test Two (Posttest) 30 ft Standoff, UX 1400 HT | 119 |
| 6.10 | Test Four (Posttest), 30 ft Standoff, UX 1500 HT | 119 |
| 6.11 | Test Three (Posttest) 25 ft Standoff, UX 1400 HT | 120 |
| 6.12 | Test Five (Posttest) 25 ft Standoff, UX 1500 HT | 120 |
| 6.13 | Test One (Posttest) 20 ft Standoff, UX 1400 HT | 122 |
| 6.14 | Test Six (Posttest) 20 ft Standoff, UX 1500 HT | 122 |

LIST OF FIGURES (CONT.)

| Figure | Title | |
|--------|---|-----|
| 6.15 | Ground Shock Coupling Factor as a Function of Scaled Depth of Burst for Air, Soil, and Concrete (Drake, et al, 1989) | 124 |
| 6.16 | Plot of Calculated vs. Measured Free-Field Pressure | 134 |
| 6.17 | Free-Field Pressure vs. Geogrid Compressive Strain, Tests 2-5 | 138 |
| 7.1 | Trapezoidal Rule of Integration (Al-Khafaji and Tooley, 1986) | 147 |
| 7.2 | Measured and Predicted Free-Field Stress vs. Time, Test 5, Gage F1 | 151 |
| 7.3 | Measured and Predicted Free-Field Stress vs. Time, Test 4, Gage F1 | 152 |
| 7.4 | k vs. Displacement, Test 5, Panel 2 | 154 |
| 7.5 | log k vs. log Displacement, Test 5, Panel 2 | 155 |
| 7.6 | Log k vs. Log Displacement, Tests 1-5 | 156 |
| 7.7 | Measured and Predicted Free-Field Stresses vs. Time, Test 1, Gage F2 | 158 |
| 7.8 | Log k vs. Log Displacement, Tests 2-5 | 159 |
| 7.9 | Scaled Test Panel Numbering System (Olen, et al, 1993) | 163 |
| 7.10 | Stiffness vs. Displacement, Full-Scale and Centrifuge Tests | 165 |

LIST OF FIGURES (CONT.)

| Figure | Title | |
|--------|--|-----|
| 8.1 | Free-Field Pressure, Scaled Test 27, Gage P5 | 170 |
| 8.2 | Schematic of Free-Field Pressure Wave Loading | 172 |
| 8.3 | Schematic of Mass Movement Loading | 173 |
| 8.4 | Schematic of Pullout Loading | 174 |
| 8.5 | Typical Acceleration Plot From Centrifuge Tests | 176 |
| 8.6 | Free-Field Pressure Time History - Scaled Test 26 | 194 |
| 8.7 | Free-Field Pressure Time History - Scaled Test 28 | 195 |
| 8.8 | Dynamic Pullout Response of Tensar UX 1500HT Geogrid (Yuan, et al, 1993) | 199 |
| 9.1 | Pullout Resistance as a Function of Geogrid Stiffness (Juran and Chen, 1988) | 218 |
| B.1 | Detail of Clamps and Wooden Wedges | 250 |
| C.1 | Free-Field Pressure Gage F1, Test 1 | 254 |
| C.2 | Free-Field Pressure Gage F2, Test 1 | 255 |
| C.3 | Free-Field Pressure Gage F3, Test 1 | 256 |
| C.4 | Soil Pressure Interface Gage P2, Test 1 | 257 |
| C.5 | Soil Pressure Interface Gage P3, Test 1 | 258 |
| C.6 | Soil Pressure Interface Gage P4, Test 1 | 259 |

LIST OF FIGURES (CONT.)

| Figure | Title | |
|---------------|---|-----|
| C.7 | Soil Pressure Interface Gage P5, Test 1 | 260 |
| C.8 | Soil Pressure Interface Gage P6, Test 1 | 261 |
| C.9 | Accelerometer A1, Test 1 | 262 |
| C.10 | Accelerometer A2, Test 1 | 263 |
| C.11 | Accelerometer A3, Test 1 | 264 |
| C.12 | Accelerometer A4, Test 1 | 265 |
| C.13 | Accelerometer A5, Test 1 | 266 |
| C.14 | Accelerometer A6, Test 1 | 267 |
| C.15 | Free-Field Pressure Gage F2, Test 2 | 268 |
| C.16 | Soil Pressure Interface Gage P1, Test 2 | 269 |
| C.17 | Soil Pressure Interface Gage P3, Test 2 | 270 |
| C.18 | Soil Pressure Interface Gage P4, Test 2 | 271 |
| C.19 | Soil Pressure Interface Gage P5, Test 2 | 272 |
| C.20 | Soil Pressure Interface Gage P6, Test 2 | 273 |
| C.21 | Accelerometer A1, Test 2 | 274 |
| C.22 | Accelerometer A2, Test 2 | 275 |
| C.23 | Accelerometer A3, Test 2 | 276 |

LIST OF FIGURES (CONT.)

| Figure | Title | |
|---------------|---|-----|
| C.24 | Accelerometer A4, Test 2 | 277 |
| C.25 | Accelerometer A5, Test 2 | 278 |
| C.26 | Strain Gage S7, Test 2 | 279 |
| C.27 | Strain Gage S8, Test 2 | 280 |
| C.28 | Strain Gage S9, Test 2 | 281 |
| C.29 | Strain Gage S11, Test 2 | 282 |
| C.30 | Strain Gage S12, Test 2 | 283 |
| C.31 | Free-Field Pressure Gage F1, Test 3 | 284 |
| C.32 | Free-Field Pressure Gage F2, Test 3 | 285 |
| C.33 | Free-Field Pressure Gage F3, Test 3 | 286 |
| C.34 | Soil Pressure Interface Gage P2, Test 3 | 287 |
| C.35 | Soil Pressure Interface Gage P3, Test 3 | 288 |
| C.36 | Soil Pressure Interface Gage P4, Test 3 | 289 |
| C.37 | Soil Pressure Interface Gage P5, Test 3 | 290 |
| C.38 | Soil Pressure Interface Gage P6, Test 3 | 291 |
| C.39 | Accelerometer A1, Test 3 | 292 |

LIST OF FIGURES (CONT.)

| Figure | Title | |
|---------------|---|-----|
| C.40 | Accelerometer A2, Test 3 | 293 |
| C.41 | Accelerometer A3, Test 3 | 294 |
| C.42 | Accelerometer A4, Test 3 | 295 |
| C.43 | Accelerometer A5, Test 3 | 296 |
| C.44 | Accelerometer A6, Test 3 | 297 |
| C.45 | Strain Gage S7, Test 3 | 298 |
| C.46 | Strain Gage S8, Test 3 | 299 |
| C.47 | Strain Gage S9, Test 3 | 300 |
| C.48 | Strain Gage S10, Test 3 | 301 |
| C.49 | Strain Gage S11, Test 3 | 302 |
| C.50 | Free-Field Pressure F1, Test 4 | 303 |
| C.51 | Free-Field Pressure F2, Test 4 | 304 |
| C.52 | Free-Field Pressure F3, Test 4 | 305 |
| C.53 | Soil Pressure Interface Gage P1, Test 4 | 306 |
| C.54 | Soil Pressure Interface Gage P2, Test 4 | 307 |
| C.55 | Soil Pressure Interface Gage P3, Test 4 | 308 |
| C.56 | Soil Pressure Interface Gage P4, Test 4 | 309 |

LIST OF FIGURES (CONT.)

| Figure | Title | |
|---------------|---|-----|
| C.57 | Soil Pressure Interface Gage P5, Test 4 | 310 |
| C.58 | Soil Pressure Interface Gage P6, Test 4 | 311 |
| C.59 | Accelerometer A1, Test 4 | 312 |
| C.60 | Accelerometer A2, Test 4 | 313 |
| C.61 | Accelerometer A3, Test 4 | 314 |
| C.62 | Accelerometer A4, Test 4 | 315 |
| C.63 | Accelerometer A5, Test 4 | 316 |
| C.64 | Accelerometer A6, Test 4 | 317 |
| C.65 | Strain Gage S1, Test 4 | 318 |
| C.66 | Strain Gage S2, Test 4 | 319 |
| C.67 | Strain Gage S3, Test 4 | 320 |
| C.68 | Strain Gage S4, Test 4 | 321 |
| C.69 | Strain Gage S5, Test 4 | 322 |
| C.70 | Strain Gage S6, Test 4 | 323 |
| C.71 | Strain Gage S7, Test 4 | 324 |
| C.72 | Strain Gage S8, Test 4 | 325 |
| C.73 | Strain Gage S11, Test 4 | 326 |

LIST OF FIGURES (CONT.)

| Figure | Title | |
|--------|---|-----|
| C.74 | Strain Gage S12, Test 4 | 327 |
| C.75 | Free-Field Gage F1, Test 5 | 328 |
| C.76 | Free-Field Gage F2, Test 5 | 329 |
| C.77 | Free-Field Gage F3, Test 5 | 330 |
| C.78 | Soil Pressure Interface Gage P1, Test 5 | 331 |
| C.79 | Soil Pressure Interface Gage P2, Test 5 | 332 |
| C.80 | Soil Pressure Interface Gage P3, Test 5 | 333 |
| C.81 | Soil Pressure Interface Gage P4, Test 5 | 334 |
| C.82 | Soil Pressure Interface Gage P5, Test 5 | 335 |
| C.83 | Soil Pressure Interface Gage P6, Test 5 | 336 |
| C.84 | Accelerometer A1, Test 5 | 337 |
| C.85 | Accelerometer A2, Test 5 | 338 |
| C.86 | Accelerometer A3, Test 5 | 339 |
| C.87 | Accelerometer A4, Test 5 | 340 |
| C.88 | Accelerometer A5, Test 5 | 341 |
| C.89 | Accelerometer A6, Test 5 | 342 |
| C.90 | Strain Gage S1, Test 5 | 343 |

LIST OF FIGURES (CONT.)

| Figure | Title | |
|---------------|-------------------------|-----|
| C.91 | Strain Gage S2, Test 5 | 344 |
| C.92 | Strain Gage S3, Test 5 | 345 |
| C.93 | Strain Gage S4, Test 5 | 346 |
| C.94 | Strain Gage S5, Test 5 | 347 |
| C.95 | Strain Gage S8, Test 5 | 348 |
| C.96 | Strain Gage S11, Test 5 | 349 |
| C.97 | Strain Gage S12, Test 5 | 350 |

SUMMARY

A more quantitative understanding of the response of reinforced soil walls to explosions in the retained fill was developed via a single degree of freedom model developed by Drake, et al (1987). A series of full-scale tests were conducted to investigate the response of the walls to free-field blast pressures, and detailed analysis of the test data suggested inertial stresses generated during the crater formation process, not blast pressures, were the governing loading condition. Using full and small-scale test data, the validity of the model is demonstrated through a consistent relationship between system stiffness and displacement. The consistency of the stiffness/displacement relationship for full and scaled tests suggest the centrifuge provides reasonable models of full-scale reinforced soil walls.

Application of the test data to the model yields order of magnitude results in prediction of ultimate wall panel displacements. The approach and results of this study provides a significant departure from previous research by identifying the loading mechanisms that govern response, the influence of the engineering properties of the materials, and validation of a model that provides a quantitative description of the physical response of the reinforced soil wall.

CHAPTER I

INTRODUCTION

Objective

The objective of this research was to develop a methodology for evaluating the response of reinforced soil walls with concrete facing panels to ground shock pressures from buried explosions. Previous research has qualitatively demonstrated that reinforced soil resists ground shock pressures, however, a fundamentally based approach to the identification of loading mechanisms or the respective influence of design variables has not been presented. To achieve this objective, a single degree of freedom model for a yielding wall which assumes continuity of stresses and displacements at the soil/wall interface will be developed. The model will be validated using full and small-scale test data from reinforced soil walls subjected to explosions in the retained backfill. This methodology for the evaluation of walls to resist ground shock and the influence of various design parameters will be used to demonstrate the practical applications of this research.

Background

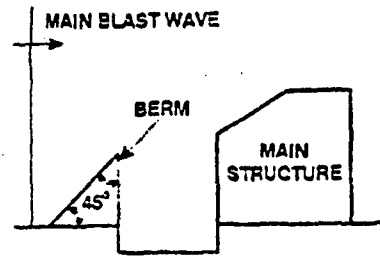
The United States (US) Air Force enjoys a degree of mobility unmatched by any other Air Force in history. Since World War II, the United States has typically conducted warfighting operations from a network of main and satellite operating bases located across the world. However, the end of the Cold War and reduction in threat of global war has lead to the closing of many overseas US Air Force Bases. At the same time, US participation in regional conflicts outside the sphere of influence of remaining US bases, coupled with a growing reluctance on the part of many nations to allow establishment of foreign military bases on their soil, requires the ability to rapidly build a warfighting airbase, typically called a "bare base". The expedient nature of these bases necessitates the use of temporary construction methods: tents, wood frame structures, or lightweight metal buildings. Although functional, these structures provide little protection from blast overpressure or small arms fire. Structural hardening may be beyond the capabilities of the logistical trial and engineering forces. The rapid construction of blast and fragment resistant barriers or shelters is necessary at bare bases to ensure survivability from enemy attack.

Throughout history, a wide variety of materials and designs have been used to protect communities, trading posts, and other strategic assets. Natural

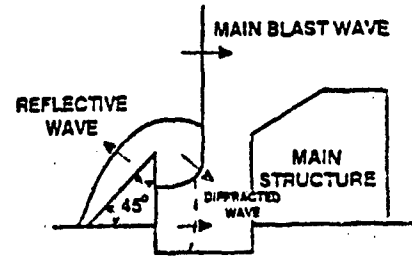
materials, such as soil and rock, trees, barriers created by terrain or water, and naturally formed tunnels and ravines were used for centuries. As the science of civil engineering progressed, new materials became available for construction: mortar, brick, concrete, reinforced concrete, steel, and a variety of synthetic materials. These construction techniques, although efficient and effective, require some major manufacturing process to create the necessary materials, heavy equipment to move and install the materials, and a suite of skilled labor for construction. Building protective shelters in a bare base environment requires minimizing dependence on highly skilled labor and manufactured materials. This can be achieved through the use of geologic materials. These materials have many advantages to the engineer: worldwide availability, relative low cost, simple construction techniques, and the ability to modify their engineering properties. For these reasons, reinforced soil systems may provide a means for rapid construction of protective shelters worldwide.

Soil is one of the least expensive, simplest, most widely used, effective, and oldest means of protection against military and terrorist attacks. To protect an above ground building or an aircraft with soil requires building a high soil barrier or berm. These berms require large soil quantities because of the angle of repose of the soil. Berms can also create blowing dust and debris as well as create a problem due to erosion. Despite these drawbacks, extensive testing

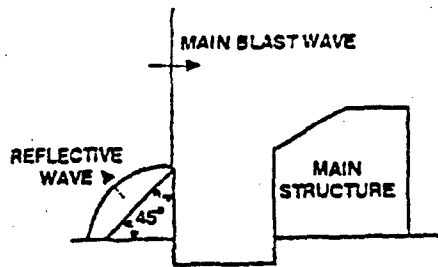
has proved soil berms are effective in reducing both leeward airblast pressures and fragment penetration (US Office of Civil Defense, 1941; Hyndman, et al, 1987; Hyde, 1989; Sues, et al, 1991). Air pressure reduction comes from the aerodynamic reflection of shock waves, as shown in Fig. 1.1. However, if the detonation occurs in the soil mass it creates ground shock pressures approximately seven times greater than the same explosion in air (Drake, et al, 1989). Therefore, the design analysis must attempt to maximize the air space between the explosion and the target, yet maintain enough soil cover to prevent fragmentation penetration. The larger the soil mass around the target, the greater probability of detonation occurring within the soil, resulting in large ground shock pressures transmitted to the target. The utility of soil berms could be increased through a reduction in the volume of the berm and increased control of the dust and erosion by replacing one of the berm slopes with a vertical wall. One method for reducing soil berm volume as well as dust and erosion problems is to build a wall of reinforced soil. Reinforced soil is a composite material consisting of soil and high tensile strength materials such as steel strips or geosynthetics. A single face of a reinforced soil berm can be constructed to approximately vertical with or without facing panels. This greatly reduces the amount of soil and therefore the space needed. If a typical berm has side slopes of 2 ft. in the horizontal dimension for every ft. of height



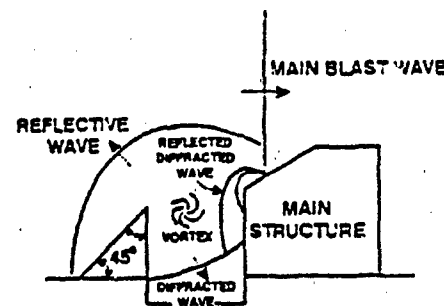
(A) SHOCK WAVE BEFORE REACHING
BERM OBSTRUCTION.



(C) FORMATION OF DIFFRACTED WAVE.



(B) FORMATION OF REFLECTED WAVE.



(D) PARTIAL ENVELOPMENT OF STRUCTURE BY
REFLECTED DIFFRACTED WAVE.

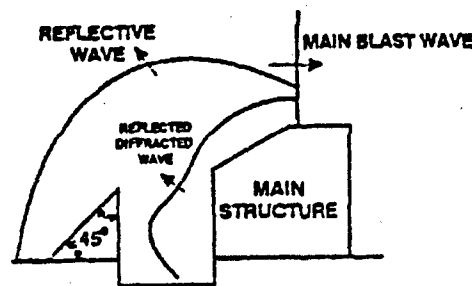


Figure 1.1 Aerodynamic Deflection (Ferritto, et al, 1988)

(2H:1V), then a free standing, symmetrical berm 12 ft. high would be 48 ft. wide at its base. By comparison, a reinforced soil retaining wall with concrete panel facing and 12 ft. reinforcement embedment depth would be 36 ft. wide at its base. This allows for 12 ft. of depth required for reinforcement embedment, and 24 ft. of depth on the back slope. Thus, reinforced soil walls require less soil to construct and may present a smaller target to a hostile force. The use of facing panels or "wrap-around" (Fig. 1.2) confinement also reduces dust and erosion relative to a free standing earth berm. One unknown is the ground shock transmission properties of reinforced soil.

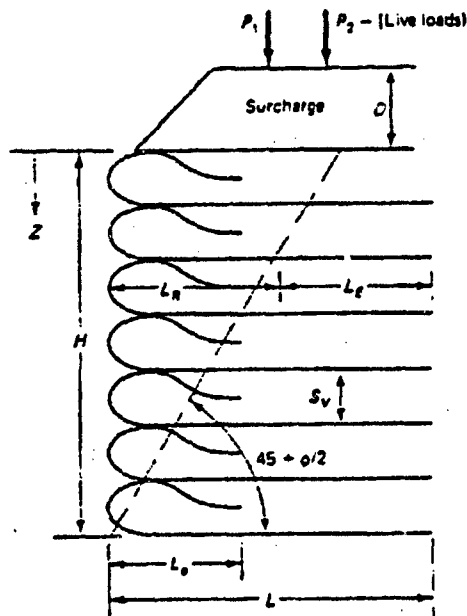


Figure 1.2 Schematic of Wrapped Face Geotextile Wall (Koerner, 1990)

Due to the demonstrated effectiveness of unreinforced soil berms in reducing leeward airblast pressures, it was hypothesized that reinforced soil structures could provide similar protection from blast loads. It is proposed that instead of building a structure and then protecting it with an earth berm as shown in Fig. 1.3, an entire structure could be built with reinforced soil, i.e. effectively closing in an area with reinforced soil. An example of this alternative design concept is shown in Fig. 1.4. In this case the facing material would serve as the interior wall, surrounded by the soil backfill. The response of reinforced soil embankments to airblast is conservatively assumed to equal that of unreinforced berms, however, the response of these structures to explosions in the soil backfill has yet to be determined. In order to develop design methodologies for reinforced soil subjected to blast loads, the response of these systems to such loading must be established. The full-scale explosive testing of reinforced soil systems, coupled with previous physical model tests and numerical analysis will establish the response of these systems to groundshock loading.

United States Air Force Relevance

This research is a key element in the larger effort to develop a design methodology for the use of reinforced soil in protective shelters. This would

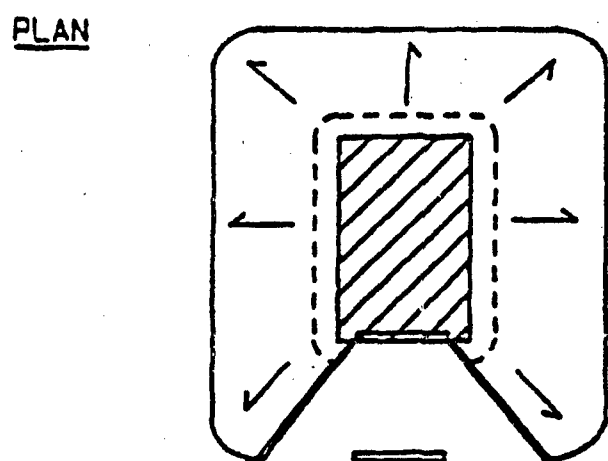
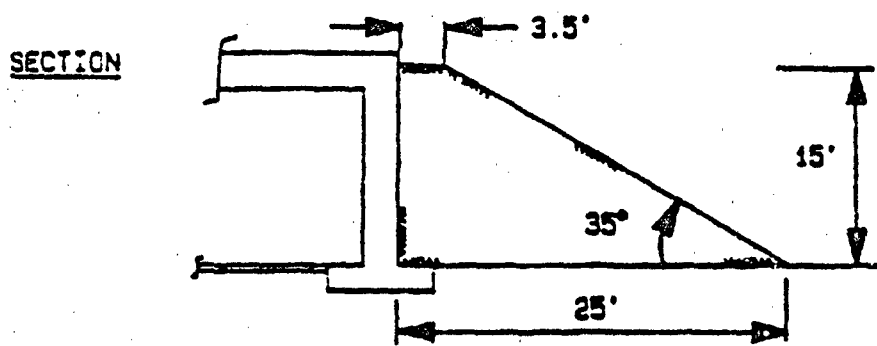


Figure 1.3 Example of Protective Soil Berm (Drake, et al, 1989)

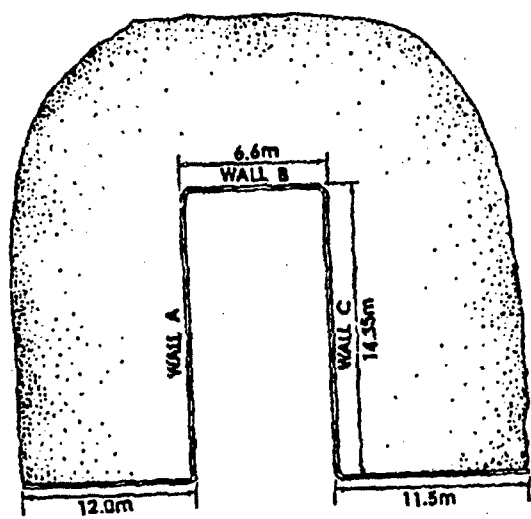
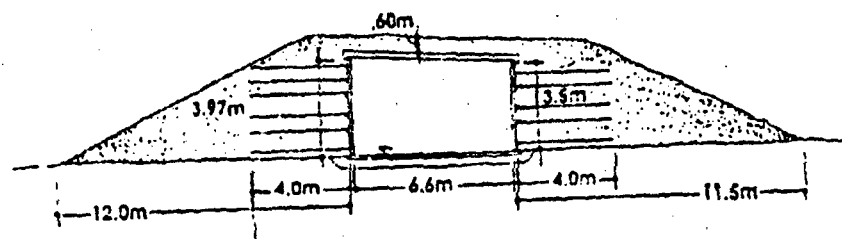


Figure 1.4 Reinforced Soil Bunker (Reid, 1991)

provide a cost effective alternative to reinforced concrete shelter designs currently preferred. With the maturation of this technology, it would be possible to use this design methodology for construction of permanent protective structures at bare and main operating bases. It is proposed that reinforced soil construction would provide the following advantages to reinforced concrete construction:

- maximizes use of in-situ materials
- utilizes existing Air Force civil engineering manpower, equipment and skills
- more rapid construction
- commercially available technology
- decreased cost
- can withstand greater deformations
- requires much less steel and concrete
- can absorb significant amounts of energy

Finally, reinforced concrete protective construction is not used at bare bases because of cost, time, and constructability constraints. Therefore there is no protective shelter construction at bare bases, only expedient means such as sandbags and revetments are used. The use of reinforced soil systems for shelters at bare bases would fill this existing void.

Scope

In order to achieve the previously stated research objectives, a scope of work was developed. This scope specified the five-phased technical approach as follows:

- conduct a literature review for: (1) response of reinforced soil, and its components to explosive loading, (2) numerical codes for evaluating reinforced soil response to explosive ground shock, and (3) physical model testing of reinforced soil systems;
- develop a test plan and designs for full-scale explosive tests of reinforced soil retaining walls;
- construct and test walls, collect and reduce data;
- estimate residual displacements of full and small-scale wall panels via a single degree of freedom model;
- use the simple model to conduct parametric study of the influence of specific design variables on wall panel response.

Applications

Although the focus of this research was toward the use of reinforced soil structures for military use, this concept does have some commercial applications. Reinforced soil has been used for construction of containment

dikes around petrochemical storage and liquid natural gas facilities for both spill containment and resilience to explosive damage. Heike, et al (1991) gives an example of such a design used around an oil tank farm. The qualities reinforced soil possesses for these applications include resistance to explosion, flooding/liquid attack, thermal shock, and fire (Reinforced Earth Company, undated). Also, reinforced soil can be used to surround large areas to protect against terrorist attack.

Organization

The remaining sections of this report are organized as follows:

Chapter II - Discusses how the energy from an explosion in soil is transferred to the soil mass and the prediction of the resulting pressures

Chapter III - Presents previous research on the full and small-scale explosive testing of unreinforced soil berms and reinforced soil walls, as well as results from numerical evaluations

Chapter IV - Details the development of a single degree of freedom model for predicting the response of yielding walls to ground shock, and the validity of this equation for reinforced concrete wall design

- Chapter V -** Details all aspects of test design including the materials selected for each component, the size and design of the structure, the type, number and installation of each data gathering device, weapon size, location and installation, soil type and properties, number of tests and weapon firing system
- Chapter VI -** Presents the data measured in each test, test observations, failure mechanisms and data reduction
- Chapter VII -** This chapter establishes the validity of the single degree of freedom model for predicting the response of the reinforced soil walls to pressure wave loading and develops the relationship between system stiffness and displacement
- Chapter VIII -** Test data are evaluated to define each loading mechanism acting upon the walls in the time domain. The data are then used to evaluate each loading mechanism and predict displacements for full and small-scale tests
- Chapter IX -** The single degree of freedom model is used to demonstrate how variations in design parameters influence ultimate wall panel displacements, as well as other methods that may improve design performance
- Chapter X -** Presents research conclusions and recommendations

Appendix A - Details the strain gage installation procedures for all tests

**Appendix B - Describes the test site and details construction methods used for
each wall, panel fabrication and installation of the leveling pad**

**Appendix C - Contains plots of each data recording made during full-scale
tests**

CHAPTER II

EXPLOSIONS IN SOIL

Introduction

As one might expect, the detonation of an explosive can have a significant impact on its surrounding media. This chapter will present how, upon detonation, the potential energy in a weapon is transferred to the surrounding media, how the materials are affected by this massive transfer of energy, and methods for predicting the magnitude of the blast-induced pressure wave.

Explosions In Soil

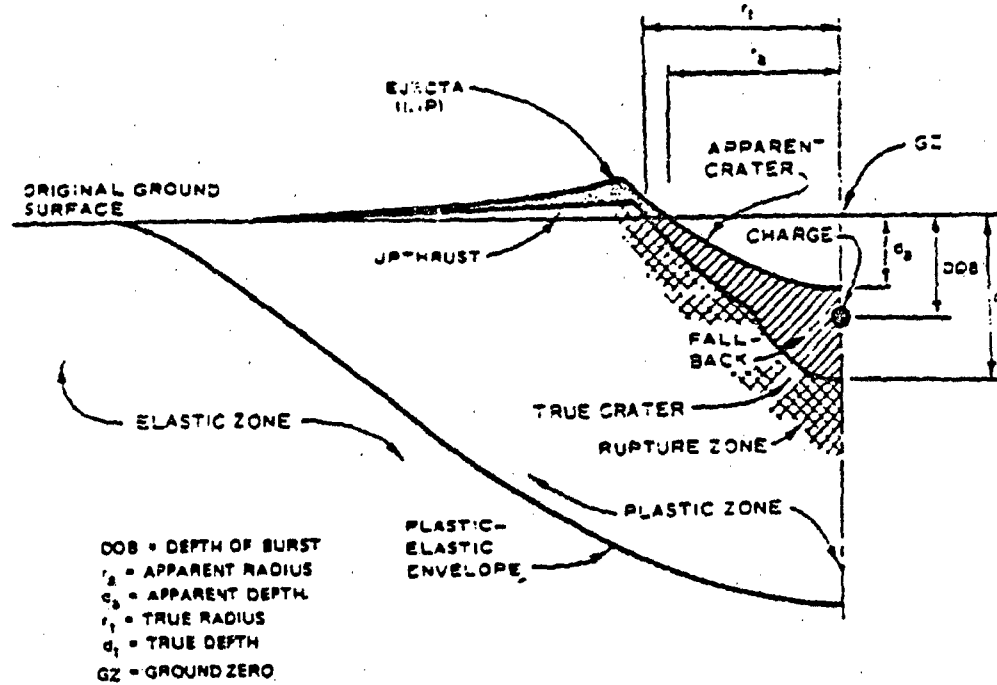
Baker (1973) defines an explosion as "a process by which a pressure wave of finite amplitude is generated in air by a rapid release of energy." In air, this pressure wave is often called the blast wave or airblast; in ground it is called ground shock.

Upon initiation of an explosion, a detonation wave propagates through the explosive at a velocity of up to 23,000 ft/sec (Baker, 1973). This velocity is so much greater than the stress wave velocity in soils that the detonation of the

explosive material is completed before the pressure wave arrives to the soil around the charge surface. The explosive pressures are thus assumed to act on the surrounding soil simultaneously. Immediately after detonation the explosive gases exist at high pressures within the explosive cavity causing crushing or large deformations of the surrounding soil. The deformation of this surrounding soil initiates a shock wave that propagates away from the source at or near supersonic speeds.

Once the explosion cavity reaches its maximum volume, the cavity will decrease in volume (collapse), decreasing the volume and increasing the gas pressure. The gases expand again and new waves are produced. This process decays rapidly, such that the second wave is negligible when compared to the first (Henrych, 1979).

As the radial distance between the pressure wave and the detonation source increases, explosive energy is dispersed over an ever increasing volume of soil (geometric attenuation), and the overpressure rapidly decreases. When the overpressure decreases below the soil strength limit, soil particle rearrangement ceases, thus changing the deformation character. Beyond this distance, soil structure will remain unchanged and the wave behavior can be evaluated via elastic theory. A typical half-crater profile is shown in Fig. 2.1.



US Army Corps of Engineers

Figure 2.1 Typical Half Crater Profile (Headquarters, Department of the Army, 1986)

Terminology

Throughout the literature, a variety of terms are used for the pressures that emanate from a subsurface explosion. Two different pressures will be discussed in this thesis; free-field and inertial pressures.

The crushing or deformation of the soil around the explosion immediately after detonation initiates a pressure wave that radiates rapidly away from the

explosive source. This wave may have velocities on the order of 1000 ft/sec, depending on the characteristics of the media as discussed later in this chapter. This high amplitude, short duration compressive pulse will be referred to as the free-field pressure or pressure wave. The amplitude is governed by charge weight and ground shock coupling factor, but may be on the order of thousands of psi for several milliseconds. In some literature this may be referred to as the ground shock or stress wave.

As the free-field pressure radiates away from the source, the soil in the proximity of the detonation is accelerated under the force of the continued expansion of the gases within the explosive crater. The response of the soil to this loading develops over a relatively longer period of time, and results in inertial pressures from the plastic movement of the soil mass, influenced primarily by charge weight and the ground shock coupling factor. This will be referred to as the inertial pressure. Davies and Williams (1992) referred to this as inertial loading.

Estimation of Free-field Pressure

A variety of methods exist for the quantitative estimation of peak free-field pressure at any point around an explosive source (Headquarters, Department of the Army, 1986; Drake, et al, 1989; Drake and Little, 1983; Westine and

Friesenhahn, 1983; Henrych, 1979). These empirical equations have been developed from both nuclear and conventional explosive tests. For conventional detonations, the solution provided by Drake and Little (1983), herein referred to as the Drake-Little equation, has been widely used and is the method presented in both US Air Force and US Army protective construction design manuals for use in practice. The primary advantage of the Drake-Little equation is that it was derived based on an extensive empirical database, is simple to use, allows for input of the variables that control peak pressure attenuation with distance from the explosive, and provides valid results. The Drake-Little equation is generally presented as:

$$P = f c \rho \frac{160}{144} \left(\frac{R}{W^{\frac{1}{3}}} \right)^{-n} \quad (2.1)$$

where: P = peak pressure in psi ρ = mass density ($\text{lb}\cdot\text{sec}^2/\text{ft}^4$)

f = ground shock coupling factor W = charge weight (lb.)

n = attenuation coefficient R = distance to explosion (ft)

c = soil compression wave velocity in ft/sec

Upon inspection of this equation it is evident that the predicted pressure is highly dependent upon the values of c and n . The other factors (ρ , f) are known or can be estimated reasonably accurately. The values of c and n can be

obtained through trial tests in the field, or through estimation using the values presented in Table 2.1. Unfortunately, to all but the most experienced users, estimation of seismic velocity and attenuation coefficient through the use of tables will only provide order of magnitude answers. However, using values of c and n obtained from field tests, the Drake-Little equation works well for most soil conditions.

The value of c is generally called the compression wave velocity and, based on the values given in Table 2.1, serves as an approximate index for ground shock prediction purposes. This parameter may also be estimated through a relationship between the stiffness and density of the soil as:

$$c = \sqrt{\frac{M}{\rho}} \quad (2.2)$$

where: M = initial tangent constrained modulus of the soil.

The constrained modulus may be obtained through resonant column tests. The resonant column test is generally used to determine the shear modulus at low strains, and in combination with Young's modulus may be used to calculate Poissons ratio. Poissons ratio and Young's modulus may then be used to determine constrained modulus as:

**Table 2.1 Typical Soil Properties For the Drake-Little Equation
(Drake et al, 1989)**

| | Dry Unit Weight γ_d (pcf) | Total Unit Weight γ (pcf) | Air-Filled Voids (%) | Seismic Velocity c (fps) | Attenuation Coefficient n |
|--|-------------------------------------|-------------------------------------|----------------------|--------------------------|---------------------------|
| Dry desert alluvium and playa, partially cemented | 87 | 93-100 | >25 | 2,000-4,200 | 3.0-3.25 |
| Loose, dry, poorly graded sand | 80 | 90 | >30 | 600 | 3.0-3.5 |
| Loose, wet, poorly graded sand with free standing water | 97 | 116 | 10 | 500-600 | 3.0 |
| Dense, dry sand, poorly graded | 90 | 104 | 32 | 900-1,300 | 2.5-2.75 |
| Dense, wet sand, poorly graded, with free standing water | 108 | 124 | 9 | 1,000 | 2.75 |
| Very dense dry sand, high relative density | 105 | 11 | 30 | 1,600 | 2.5 |
| Wet Silty-clay | 95-100 | 120-125 | 9 | 700-900 | 2.75-3.0 |
| Moist, loose, clayey sand | 100 | 122 | 5-10 | 1,000 | 2.75-3.0 |
| Wet sandy clay, above water table | 95 | 120-125 | 4 | 1,000-1,800 | 2.25 |
| Nearly saturated sand, below water table | - | - | 1-4 | 1,800-4,900 | 2.0-2.25 |
| Saturated sandy clay, below water table | 100 | 125 | <1 | 5,000-6,600 | 1.5 |
| Saturated stiff clay, saturated clay-shale | - | 120-130 | 0 | >5,000 | 1.5 |

$$\mu = \frac{E}{2G - 1} \quad (2.3)$$

and,

$$M = \frac{E(1 - \mu)}{(1 - \mu)(1 + \mu)} \quad (2.4)$$

where,

E = Young's modulus (F/L^2) M = constrained modulus (F/L^2)

μ = Poisson's ratio

Detailed discussion on the measurement and calculation of these properties for ground shock evaluations can be obtained from Das (1983).

The Drake-Little equation will be used in this research to estimate peak soil pressures at locations where pressure gages were not located (i.e. at a strain gage locations), and to validate free-field pressure measurements. Free-field pressure gages were used to measure the pressure-time response of the soil, and those data were used to establish the speed of the compressive wave in the soil (c) and the attenuation coefficient (n). This will be further discussed in Chapter VI.

Crater Formation

When a subsurface detonation occurs near a soil/air interface, the free-field pressure wave reaches the soil surface and acts as a source of surface waves.

The pressure wave is reflected from the free surface back towards the explosion cavity, and then reflects off the cavity surface in a repeating process of rapidly decreasing intensity. During this time, the soil above the cavity is continually moving upwards by the expanding gases until it is ejected from the ground, leaving behind a crater (Henrych, 1979). Discussions on the empirical estimation of pressure wave amplitudes, velocities, and crater sizes are detailed by Drake, et al (1989); Baker (1973); Crawford, et al (1971); and Headquarters, Department of the Army (1986). A more fundamental discussion of explosive-induced wave theory and crater formation is presented by Henrych (1979).

Figure 2.1 presented a schematic drawing of a typical half crater with the different zones identified. The apparent crater is defined as the crater that is visible on the surface. The true crater is the hole actually excavated by the explosion, but is normally filled with loose, disassociated material and debris (fallback) and is underlain by material that has been crushed and fractured but has not experienced significant displacement, referred to as the rupture zone. Near the true crater/rupture zone interface, shear failure has caused particle crushing and fracturing, the severity of which decreases with depth. These shear failures diminish as the rupture zone/plastic zone interface is reached. In the plastic zone, soil particles have small permanent displacements decreasing

to infinitesimal values when the transition to the elastic zone is reached (Drake, et al, 1989).

The extent of these zones varies with the type of soil and size of explosion, and prediction of the boundary locations is difficult. Vesic (1965) presented empirical equations for estimating the radius of the explosive cavity and the plastic zone. This prediction methodology, like others of its time, is based upon the data base of numerous nuclear explosions conducted under project Plowshare research, sponsored by the then Livermore Radiation Laboratory in the 1960's. Pressure measurements in the various zones are not presented, and zonal boundaries were based upon the level of disturbance observed in sand columns installed around the detonation location. Because of the differences in the charge weights between a nuclear explosion and a typical chemical explosion, these methods do not provide reasonable estimations of crater sizes and the extent of the disturbed zones for small chemical explosions.

Inertial Pressures

Inertial pressures have generally not governed the design of protective structures. Below-ground, reinforced concrete protective structures are generally designed to withstand near-miss detonations or weapons where the structure is located within the explosive crater, where relationships between

free-field pressures and structural response provide an effective means of predicting structural response. Because of this, little research has been performed on the measurement and prediction of inertial pressures.

Analytical methodologies for the prediction of inertial pressures have not been presented in the literature. Davies and Williams (1992) performed an explosive test in a geotechnical centrifuge and presented one data plot (Fig 2.2) showing the peak inertial wave amplitude of 17.1 psi, duration of 3.3 ms for a prototype 35 pound detonation in a fine sand. A polystyrene barrier of low acoustic impedance was located between the detonation and the pressure gage, and this data represents an inertial waveform. Other published data has not been identified.

Baylot (1992) modified the DYNA-3D (Whirley and Hallquist, 1991) code to model the free-field stress environment in the area immediately around the explosion. Previous models required decoupling assumptions to be made so the detonation of the charge in the soil is not included in the calculation. The Baylot model included modeling the charge, soil, and structure in the calculation. Baylot's modification then focused on predicting free-field pressures in the area within six feet of the explosion, or essentially inside the explosive crater where the soil is ejected. This model does not attempt to describe inertial pressures outside the rupture zone. Future improvements of

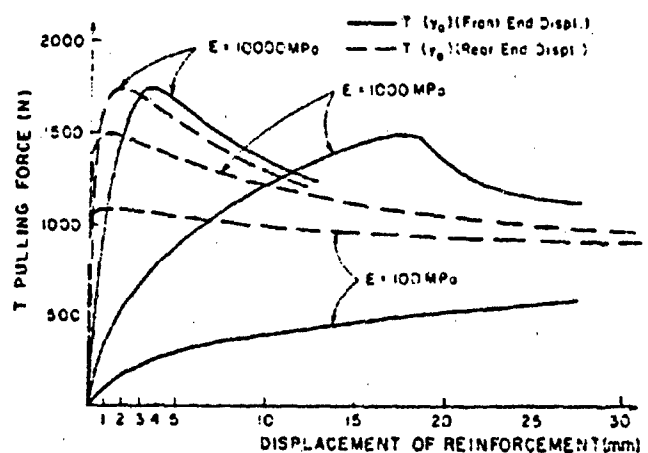


Figure 2.2 Inertial Pressure Wave (Lower Plot) Time History
(Davies and Williams, 1992)

this model and an increase in test data may provide methods for estimating inertial pressures in soil from subsurface explosions.

Partition of Wave Energy at Boundaries

The effect of boundaries between two dissimilar materials on wave propagation can be significant. An incident wave can reflect and refract at different amplitudes, angles and modes. When an explosion occurs in the backfill of a reinforced soil wall with concrete facing elements, compression

waves will propagate radially. These pressure waves will strike the soil/air interface (surface), generating surface and shear waves as well as reflected pressure waves. The pressure wave will also strike the soil/concrete boundary at the wall face. Part of this pressure wave will be transmitted into the concrete panel, and part will be reflected. The relative amplitude and direction of propagation of the waves reflected and refracted at the boundaries can be estimated utilizing relationships developed from elastic theory.

Simple relationships exist for determining the reflection coefficients of compression (P) or shear (S) waves of normal incidence, with two basic assumptions. The displacement must be continuous across the boundary (no separation) and the net stress on the boundary must be zero (Waters, 1981). Based on these assumptions the relationship between the stress wave amplitudes is:

$$A_i + A_r = A_t \quad (2.5)$$

and,

$$\rho_1 c_1 A_1 - \rho_2 c_2 A_2 = \rho_2 c_2 A_t \quad (2.6)$$

where:

A_i = amplitude of the incident stress wave

A_r = amplitude of the reflected stress wave

A_t = amplitude of the transmitted stress wave

ρ = mass density of the medium

c = compression wave velocity of the medium

Rearranging Eq. 2.6 yields:

$$\frac{A_r}{A_i} = \frac{\rho_1 c_1 - \rho_2 c_2}{\rho_1 c_1 + \rho_2 c_2} \quad (2.7)$$

By using Eq. 2.7 a relationship between A_r and A_i can be developed, assuming the mass densities and wave velocities of the respective media are known.

For example, if a soil has a mass density (ρ_1) of 3.26 lb-sec²/ft⁴, compression wave velocity (c_1) of 1000 ft/sec and concrete has a mass density (ρ_2) of 4.66 lb-sec²/ft⁴ and compression wave velocity of 10,000 ft/sec, then $A_r/A_i = -0.87$ and $0.13 A_i = A_t$. Therefore, for normal incidence the transmitted wave amplitude in the concrete is 13% of the incident wave amplitude, which is a significant reduction. This demonstrates that the partition of energy at the soil/concrete boundary must be considered when relating blast pressure wave amplitudes measured or predicted in soil to the response of the

wall. If the angle of perpendicular incidence is 90 degrees, and 0 degrees is parallel incidence, the amplitude of the transmitted wave decreases with the angle of incidence. Therefore the magnitude of the transmitted wave is at a maximum for the case of perpendicular incidence. The evaluation of test data in this report will focus on the portions of the structure subjected to compression waves of perpendicular incidence, representing the maximum transmitted stress.

CHAPTER III

EARTH BERMS AND REINFORCED SOIL IN BLAST-RESISTANT STRUCTURES

Introduction

Previous research has provided qualitative and quantitative evidence that earthen barriers can provide protection to structures from conventional weapon detonations. A review of this research is presented in this chapter to demonstrate the effectiveness of these barriers, establish the state-of-the-art, provide a basis for the design of the full-scale test series, and establish data collection requirements. This review identified previous full-scale explosive tests using unreinforced earth berms, full and small-scale (1:30) explosive tests on reinforced soil walls, and numerical analysis of reinforced soil walls subjected to explosions in the soil backfill.

Soil Berms

The effectiveness of unreinforced soil berms for mitigating leeward shock pressures led to the hypothesis that reinforced soil systems could be used for

the same purpose. A review of full-scale test data quantifies this effectiveness, but yields empirical data points, and not theoretical solutions.

In the early 1980's, the US Air Force Engineering and Services Laboratory sponsored a series of weapons effects tests on reinforced concrete walls both with and without earth berms (Coltharp, et al, 1985). The walls were 5.4 ft. in height, 13.1 ft. long, and 12.8 in. thick. In each test the reinforced concrete walls were exposed to a surface detonation of a weapon of specified threat.

The peak pressure measured on the unbermed wall was 8700 psi, and occurred 1.0 ft. up from the base of the wall. The wall was then protected with a 3.3 ft. high soil berm, and then tested with a weapon of equal size and standoff distance. The pressure at 1.0 ft. up from the base of the wall measured 589 psi, an order of magnitude pressure reduction. Consequently, the earth berm also reduced the acceleration and deflection of the concrete wall by at least 50 per cent. This effect may have been even more pronounced had the entire face of the wall been covered with the earth berm.

A variety of reports and design manuals discuss the effectiveness of earth berms, but equations for calculating pressure reductions for designs are not presented. The US Army conventional weapons design manual (Headquarters, Department of the Army, 1986) simply states "Mounded structures are essentially aboveground structures with an earth covering; however, they are

not subject to failure from the airblast of conventional weapons. Mounded structures should be checked for penetration and cratering from direct hits if the design threat includes direct hits." This is also supported by the US Air Force design manual, Section Five (Drake, et al, 1989) which concludes "In general, air-induced ground shock is not a significant threat for conventional weapons against completely buried targets."

Other references (US Office of Civil Defense, 1941; Hyndman, et al, 1987; Hyde, 1989; Sues, et al, 1991; Headquarters, Department of the Army, 1986; Coltharp, et al, 1985; and National Defense Research Committee, 1946) all show in varying levels of detail the effectiveness of earth berms for protection against airblast and fragment penetration. However, soil berms may not be effective if the explosion takes place within the soil berm.

Reinforced Soil Systems

Reinforced soil systems may provide two advantages compared to free-standing unreinforced berms: 1) they can be built at steeper slopes, thereby reducing the size of the berm and probability of weapon detonation within the soil mass; and 2) if detonation occurs within the soil mass, the reinforced soil berm may reduce the soil pressure impinged on leeward side of the berm.

Reinforced soil walls will not offer any size advantage when compared to earth berms that are placed against an existing structure, provided that structure can withstand the lateral pressures of the earth berm.

The reinforcement of soil is defined at the "inclusion of resistant elements in a soil mass to improve its mechanical properties" (Mitchell and Villet, 1987). The reinforcement of soil is analogous to the reinforcement of Portland Cement concrete. Both soil and concrete are weak in tension, but strong in compression. To exploit their strengths, and minimize their weaknesses, each is made into a composite material by adding reinforcement. This reinforcement gives the soil or concrete increased tensile strength without adversely affecting compressive strength. This reinforcement may be synthetic materials, steel, or natural fibers. In the context of this report the term "Reinforced Earth" will mean the steel strip reinforcement process as patented by the Reinforced Earth Company. "Reinforced soil" will refer to soil reinforced with any material, not to exclude steel reinforcement.

Between 1970 and 1987, over 1726 million square yards of geosynthetics representing \$3.1 billion have been used in a wide range of civil engineering applications (Koerner, 1990). Between 1991 and 1992 approximately 877 million square yards of geotextiles and geomembranes were produced worldwide (Fluet, 1993). The primary uses of these materials include landfill

liners, wall and embankment soil stabilization, drainage materials, and separation layers in pavement subgrades. As of 1990, there were over 12,000 Reinforced Earth structures in service throughout the world (Reinforced Earth Company, 1990).

As the use of reinforced soil has grown, it has become a standard construction methodology and new and innovative applications are being explored. Recently, reinforced soil has been used to construct military shelters that may be exposed to the detonation of conventional weapons. This construction has taken place despite the absence of design guidance tailored to the severe dynamic loads impinged on shelters by conventional weapons. Specific designs have been accepted on a case by case basis, but only after conducting a "pass/fail" explosive test. Specific, fundamentally sound design guidance does not exist for design and analysis that would eliminate the need for case by case pass/fail explosive acceptance testing.

Explosive Testing of Reinforced Soil Structures

Various full-scale tests, numerical and small-scale modeling efforts have taken place to investigate how high strain rate loading affects reinforced soil. This research has been done to investigate the response of reinforced soil to

explosive or earthquake loads. This early work has helped to demonstrate the effectiveness of reinforced soil under dynamic loading.

Full-Scale Tests

The response of full-scale reinforced soil walls to explosive loading has been evaluated on a number of occasions including Richardson, et al. (1977), the Central Engineering Directorate of the French Ministry of Defense 1975/1976 (Elias, 1978; Reinforced Earth Company, undated), the German Federal Office of Military Engineering and Procurement, 1979 (Reinforced Earth Company, undated), the Israeli Air Force in 1980 and 1987 (Eytan, 1988), the Directorate of Weapons Engineering, Royal Australian Air Force, 1987 (Reinforced Earth Company, undated), and the US and the Israel Air Force in 1990 (Eytan and Reid, 1993; Reid, 1990, 1991). Each of these walls used the patented Reinforced Earth construction process.

Table 3.1 summarizes some of the important parameters of each of these tests. In each of these tests, bombs were detonated in either the retained soil backfill such that the blast pressure wave impinged upon the soil side of the wall face or bombs were detonated in front of the wall face such that the exposed wall face was subjected to the blast pressure wave. Most of the tests were conducted on free-standing reinforced soil walls with concrete or metal

Table 3.1 Summary of Full-Scale Explosive Tests on Reinforced Soil Walls

| Test | Reference | Wall Type | Bomb In Backfill | Bomb In Front Of Wall Face | Wall Size (ft.) | Weapon Standoff | Weapon Size | Result |
|-----------------------|-----------------------------------|---|------------------|----------------------------|---------------------------------|-----------------|-------------|---|
| California | Richardson et al (1977) | Single Concrete Face | Yes | | 20' High 113' Long (base) | 25-50 ft. | 0.3 - 21 lb | Acceleration Max 1.5 g Vertical 1.3 g Horizontal Displacement Max: 3.8 in. Some Panel Damage |
| Meppen, Germany | Reinforced Earth Co. (Undated) | Single Metal Face | | Yes | 19.7' High 14.8' Long | 3.3 ft. | Unknown | Some Skin Rupture Some Panel Damage |
| Israel | Eytan (1988) | Single Concrete Face | Yes | | 19.7' High 55.8' Long (base) | 32.8 ft. | Classified | Some Skin Rupture Some Panel Deflection |
| | | | Yes | | | 16.4 ft. | Classified | Some Panel Deflection |
| Woomera, Australia | Reinforced Earth Co. (Undated) | Single Face 1/2 metal & 1/2 Concrete | | Yes | 13.1' High | 52.5 ft. | 8.8 tons | Some Skin Rupture Minor Skin Rupture Skin Rupture |
| | | | | Yes | 8.9' High | 32.8 ft. | 8.8 tons | |

Table 3.1 (Con't)

| Test | Reference | Wall Type | Bomb In Backfill | Bomb In Front Of Wall Face | Wall Size (ft.) | Weapon Standoff | Weapon Size | Result |
|---------------|---|--|------------------|----------------------------|-----------------------------|----------------------|-------------|--|
| Israel (1987) | Eytan (1988) | Single Concrete Face Shelter With Roof | Yes | | 9.8 ft. High 24 ft. Long | 19.7 ft. 13.1 ft. | Classified | Max Deflection: 3.4 in. Max Deflection: 2.6 ft. Wall Failed |
| Israel (1990) | Eytan and Reid (1990); Reid (1990, 1991) | Single Concrete Face Shelter With Roof | Yes | | 12.3 ft. Hgt 47 ft. Long | 19.7 ft. 16.4 ft. | Classified | Max Deflection: 2.4 in. Max Deflection: 14.5 in. Max Deflection: 27.8 in. One Panel Failed |

Table 3.1 (Con't.)

| Test | Reference | Wall Type | Bomb In Backfill | Bomb In Front Wall | Wall Size | Weapon Standoff | Weapon Size | Result |
|--------|--------------|----------------------|------------------|----------------------------------|----------------------|---|-------------|--|
| France | Elias (1978) | Single Concrete Face | Yes | 15 ft. High 40 ft. Long (top) | 3.3 ft. | 1 ton | 1 ton | Panels Damaged No Damage |
| | | Single Metal Face | Yes | 15 ft. High 35 ft. Long (top) | 13.1 ft. 32.8 ft. | 1 ton | 1 ton | Some Skin Fracture Max. Press. 50-100 tsf Max. Accel. 1.8 g Max Defl. Top 20 in. Bottom 20 in. |
| | | Double Metal Face | Yes | | 13.1 ft. | 1 ton | 1 ton | Severe Skin Fracture Max. Pressure 100 tsf Max. Defl. Top 36 in. Bottom 14 in. |
| | | | | | 9.8 ft. | 5 ton | 5 ton | Max Acceleration 22 g Complete Collapse @ Wall Center Skin Fracture |
| | | | | | 1.6 ft. | 1 ton | 1 ton | Wall Tipped Over |
| | | | | | Yes | 15 ft. High 35 ft. Long 11.5 ft. Wide | 13.1 ft. | Wall Survived, Some Skin Rupture |
| | | | | | Yes | 15 ft. Wide | 13.1 ft. | 1 ton |

facing. The most detailed information on these tests from available reference material was on the latter two tests conducted in Israel (1987, 1990).

In these U-shaped shelters the concrete facing panels formed the interior walls of the shelter, leaving an exterior exposed soil berm. The roof was cast-in-place concrete with a soil cover. Figure 3.1 shows a picture of the shelter tested in Israel in 1990. One additional detail of the 1990 Israel test not included in the table was an airblast test consisting of detonating more than 20 tons of explosives 93.5 ft. from the interior wall. This external detonation caused no measurable damage to the shelter, even though it was observed that the entire structure was within the fireball of the explosion.

One observation resulting from the 1990 Israel test was the stress concentrations present where the steel reinforcing strips anchor into the concrete facing panels. The point of connection between the reinforcing strips and the concrete panels were the first areas on the panels to fail. Even if the panel did not fail, an X-shaped crack pattern would develop between the four anchoring points. When panel failure did occur, it was initially caused by the panel cracking and separating from each of the anchor points.

Another observation was the consistent pattern of wall deformation. In each detonation in the soil backfill, the weapon was placed at the mid-height of the wall. The panels directly in front of the detonation suffered the most

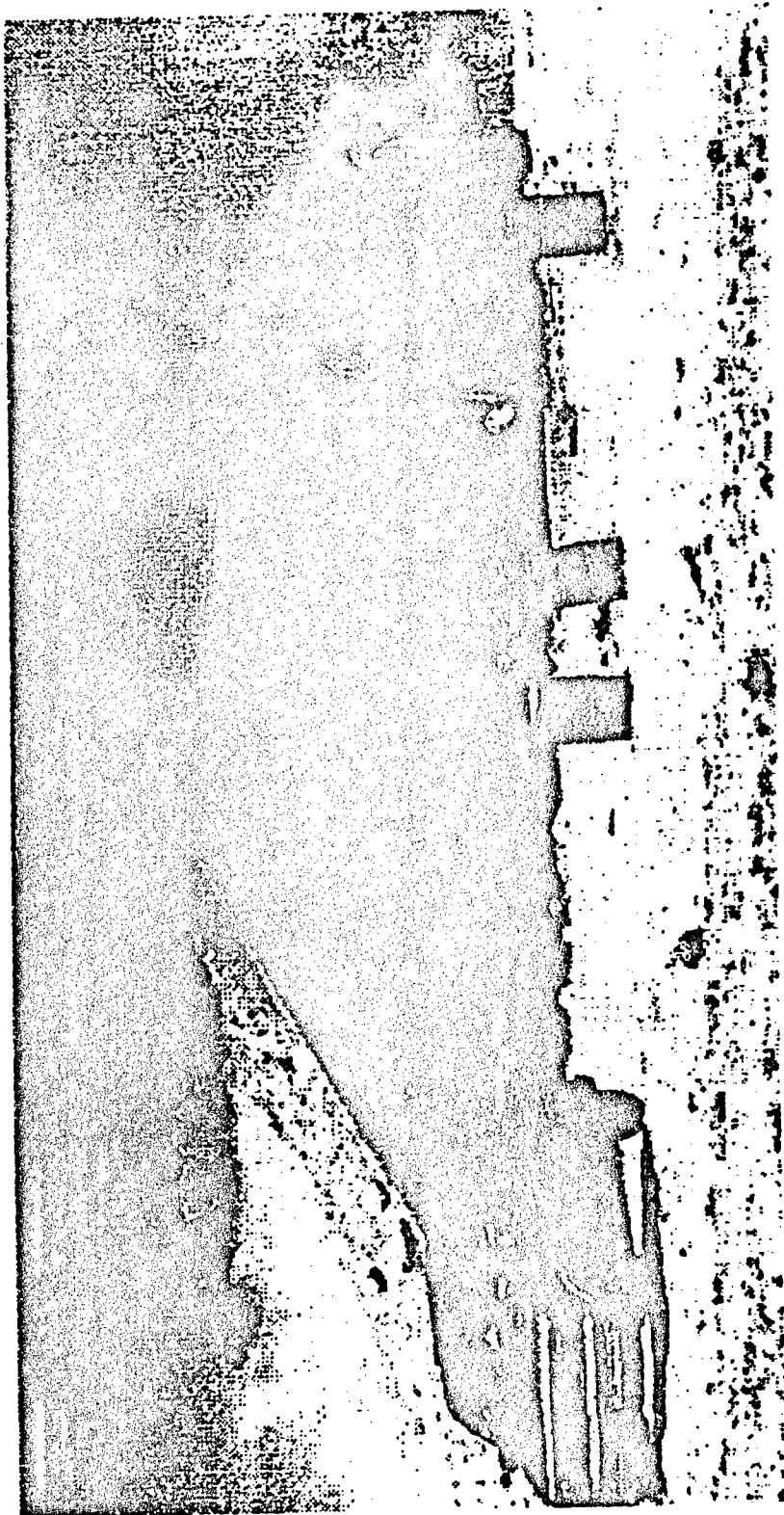


Figure 3.1 1990 Test Structure, Negev Desert, Israel

displacement, followed by each adjacent panel. The adjacent panels also exhibited rotational displacement, with displacement decreasing as distance from the detonation increased. Figure 3.2 shows the plan and profile of

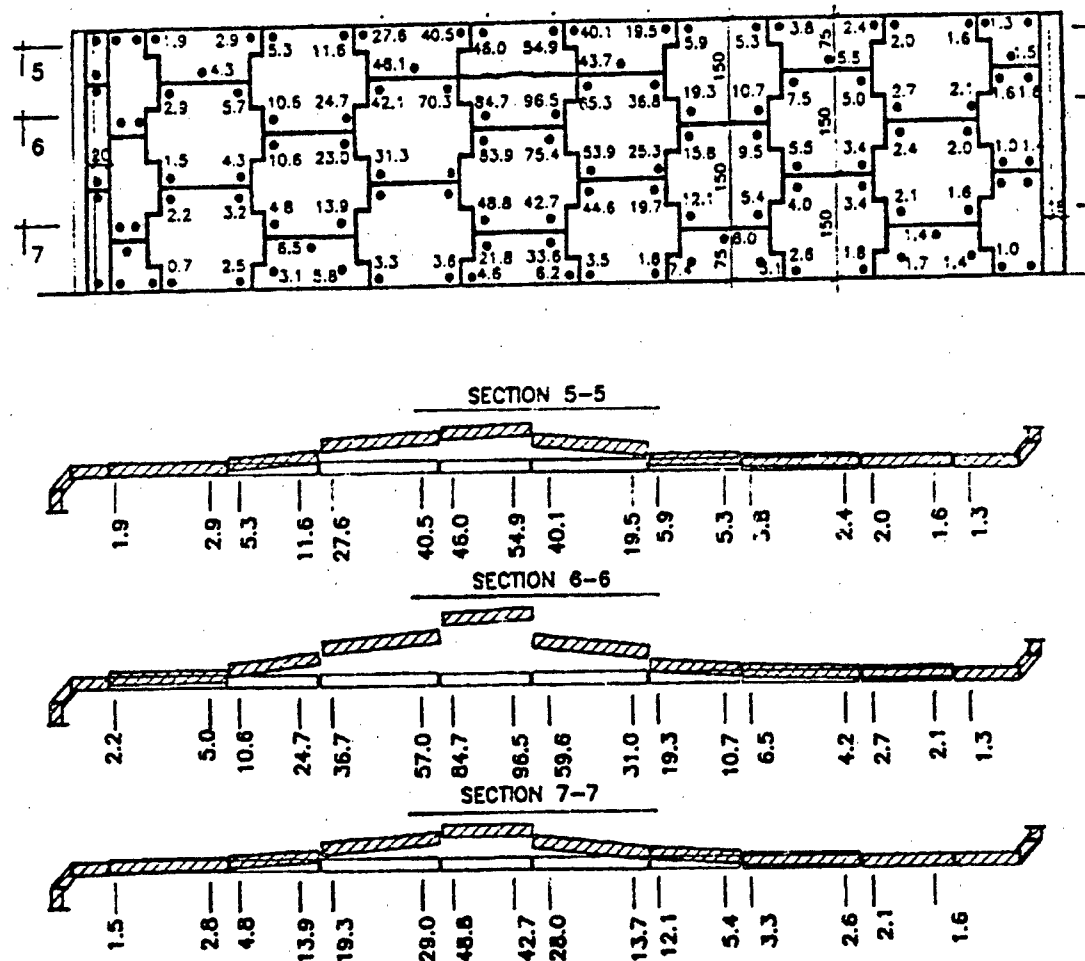


Figure 3.2 Plan and Profile of Wall Panel Deflections, 1990 Test Structure
(Eytan and Reid, 1993)

deflections (in centimeters) of each corner of the panels and each layer of panels as well as the elevation of the bomb. The radius of most significant displacement around the center of detonation is approximately 2.5 panel widths. This pattern was observed for each standoff distance used in the test series. Damage was relatively symmetrical about the point of maximum displacement. Finally, the presence of a roof or floor boundary on a panel greatly reduced the displacement of that panel when compared to panels that were only bounded by other panels.

The tests identified during this review were all conducted using the patented Reinforced Earth construction process, and many were faced with concrete panels. In these tests, little information is reported on the type, density, and moisture content of the backfill soils. Pressure, deformation and acceleration data were rarely collected. Therefore, it is difficult to ascertain what design variables affect the response of these systems to dynamic loads. The previous full-scale tests have demonstrated that the inherent flexibility of reinforced soil allows it to survive the severe loading conditions of a conventional weapon detonation, as long as the detonation does not occur too close to the wall panels. However, these tests did not assess what design variables affected the performance of these structures, nor clearly identify the loading mechanisms.

Therefore, these tests have done little to help develop an approach for the design of reinforced soil walls subjected to blast loads.

Physical Model Tests

The full-scale tests mentioned above helped demonstrate the ability of reinforced soil to withstand explosive loads. In an effort to improve the performance of these shelters, the US Air Force Civil Engineering Laboratory sponsored research projects to investigate the primary design variables that affect the dynamic response of reinforced soil (Bachus, et al, 1993; Reid, et al, 1993; Olen, et al, 1993, 1995). A series of 1:30 scale tests were conducted under a two-phase program in a geotechnical centrifuge located at the USAF Civil Engineering Laboratory at Tyndall Air Force Base (AFB), Florida.

Comparison of Model and Full-Scale Materials

In replica scaling, the scaled material properties of the model under the influence of high levels of gravity must match those of the prototype structure. The replica scaling relationships used in the design of the models are presented in Table 3.2.

The facing panels were constructed of EXTERN 625, a lightweight, high-strength, composite material made of pultruded vinyl ester resin and fiberglass reinforcement which has a unit weight of 111pcf. The scaled facing panels

were 2 in. x 2 in. which is a scaled 5 ft. square panel. To model the mass of the full-scale panel the thickness of the scaled panels was 0.253 in, which is a scaled 7.59 in. panel. This thickness does not match the 5.5 in. thickness of a typical full-scale panel, however modeling the mass of the panel was of greater importance than modeling panel thickness (Olen, et al, 1993). The reinforcement used in the scaled test was a nylon mesh material of ultimate static tensile strength of 3480 lb/in. This compares well to Tensar UX1500

Table 3.2 Replica Scaling Relationships (Scott & Morgan, 1977)

| Quantity | Full-Scale (Prototype) | Model (at g level n) |
|------------------|------------------------|----------------------|
| Linear Dimension | 1 | $1/n$ |
| Area | 1 | $1/n^2$ |
| Volume | 1 | $1/n^3$ |
| Time | 1 | $1/n$ |
| Velocity | 1 | 1 |
| Acceleration | 1 | n |
| Mass | 1 | $1/n^3$ |
| Force | 1 | $1/n^2$ |
| Energy | 1 | $1/n^3$ |
| Stress | 1 | 1 |
| Strain | 1 | 1 |
| Density | 1 | 1 |
| Frequency | 1 | n |

geogrid which has an ultimate static tensile strength of 3653 lb/in. The modulus of the nylon mesh material was not presented.

Phase I Tests. These tests consisted of constructing 1:30 scale reinforced soil walls and measuring their response to explosive detonations in the soil backfill. The objectives of the Phase I test series (Bachus, et al, 1993; Reid et al, 1993) were: 1) to investigate and compare the responses of various reinforced soil wall systems subjected to dynamic loading; 2) to obtain data which could be compared to results gathered from numerical modeling methods and full-scale tests; 3) to provide guidance for further full-scale tests; and 4) to validate the use of the centrifuge as a viable means of studying dynamically loaded geotechnical structures. A total of nine centrifuge tests were conducted under this test phase.

Bachus, et al (1993) provide a detailed discussion of the scaling technique, test equipment, test instrumentation, data collection, model materials and sample construction. The parameters evaluated in these scale tests included the reinforcement type, length, and width, use of restraint at the top of the wall, and variations in the location of the explosive detonation. Two replicate geogrid walls were tested to evaluate the reproducibility of test results.

After each test, the displacement of each of the 2 in. by 2 in. wall panels was measured. This was done by taking the average of the measured displacements at each of the four corners of the individual panels. Average total wall displacement (ATWD) was determined as average displacements of all 31 panels. The results of these tests are summarized in Table 3.3.

Pressure, acceleration and deformation measurements were made on the center column of panels as part of each test. The free-field pressure data were reported to match the values predicted by ConWep (Hyde, 1988), while the measured accelerations did not show any trend nor did they match predictions. This was primarily attributed to the presence of a layer of high density

Table 3.3 Phase I Centrifuge Test Matrix

| Study | Test No. | Variation | Average Total Wall Displacement |
|-----------------------------|----------|----------------------------------|---------------------------------|
| Effects of Embedment Length | 6 | 8 in. Geogrid | 0.24 in. |
| | 1 | 6 in. Geogrid | 0.22 in. |
| | 5 | 4.2 in. Geogrid | 0.31 in. |
| Type of Reinforcement | 2 | 0.0063 in. Steel Strip | 0.45 in. |
| | 4 | 0.0126 in. Steel Strip | 0.32 in. |
| Model Geometry | 3 | Top Restraint | Decreased 90% |
| Weapon Placement | 9 | 6 in. Standoff | Wall Failed |
| Repeatability | 7 | 10 in. Standoff, & 6 in. Geogrid | 0.26 in. |
| | 8 | | 0.22 in. |

polyethylene placed on the back face, which was used to attach the reinforcement to the panel. Impulse, or the area under the pressure vs. time plots, was not reported.

When the failure of any of the wall panels occurred, it was due to excessive deflection. Wall panels would move forward relative to the plane of the wall, and, without any underlying support, collapse. No rupture of the reinforcement or pullout of reinforcement from the soil was reported.

When wall panels deflected, they did so due to the deformation of the backfill soil. The soil, reinforcement and wall panels were reported to move as one under the influence of the explosion. Deformation due to pullout or relative motion between the reinforcement and confining soil was not observed.

Some of the conclusions reported in this study were:

- Horizontal distance between the weapon and the wall was a significant parameter.
- Significant increases in displacement occurred when the roof was removed.
- Above a minimum length for static stability, reinforcement length was not a factor in wall response.
- Reinforcement width and type were significant factors in wall response.

- Based on limited testing, the centrifuge is an appropriate tool for investigation of the response of reinforced soil walls subjected to blast loads.
- Rupture of the reinforcement did not occur.
- In each test, the pattern of panel displacement was similar.

Phase II Tests. Based on the success of the first test series, a second phase of testing (Olen, et al, 1993, 1995) was initiated with the following objectives:

- 1) to conduct a series of reliability tests on the centrifuge to quantify the limits of random variation of wall response on nominally identical test samples, and
- 2) to conduct a parametric study of reinforced soil wall system components in order to identify key parameters which contribute to the most stable wall system. The Phase II centrifuge test matrix consisted of 16 production tests as shown in Table 3.4.

Tests 6-16 were conducted to quantify the statistical variation of identical models. These tests quantified variations in displacements, pressures, accelerations and wave speeds due to random variation in model construction, test conditions, instrumentation, etc. For each test a 1:30 scale model reinforced soil wall 6 in. high by 20 in. long was constructed, instrumented and subjected to the effects of an explosive charge buried in the backfill. The test

samples were accelerated in a centrifuge to 30 g's simulating a 20 ft. high by 50 ft. long reinforced soil wall subjected to a buried blast from a MK-82 (500 lb) general purpose bomb 21.1 ft. from the back face of the wall (Fig. 3.3).

Table 3.4 Phase II Centrifuge Test Matrix

| Study | Test No. | Variation From Baseline | Average Total Wall Displacement |
|--|----------|--|---------------------------------|
| Effects of Reinforcement Coverage Area | 22 | 4.2 in. Embedment | 0.369 in. |
| | 23 | 3 Reinforcing Strips/Panel | 0.324 in. |
| | 24 | 1 Reinforcing Strip/Panel | 0.414 in. |
| | 28 | 15 in. Embedment | 0.251 in. |
| Effects of Facing Panel Geometry | 17 | 4 in. x 2 in. Panels | 0.345 in. |
| | 30 | 4 in. x 1 in. Panels | 0.315 in. |
| | 31 | 2 in. x 1 in. Panels | 0.361 in. |
| Effects of Soil Type & Density | 18 | 89 pcf Tyndall Sand | 0.462 in. |
| | 20 | 90 pcf Sky X Sand | 0.477 in. |
| | 26 | 95 pcf Tyndall Sand | 0.377 in. |
| | 27 | 98 pcf Wet Sky X Sand | 0.376 in. |
| Effects of Overall Model Geometry | 19 | Includes Roof | 0.277 in. |
| | 21 | 6.5 in. Weapon Standoff | 0.598 in. |
| | 25 | Decreased Coupling | 0.286 in. |
| Effect of Reinforcement Strength | 29 | Reduced Tensile Strength | 0.389 in. |
| | 32 | Include Shear Resistance Between Reinforcing Strips | 0.389 in. |
| Baseline | - | 6 in. Embedment 103 pcf Tyndall Sand 8.1 in. Weapon Standoff | 0.324 in. |

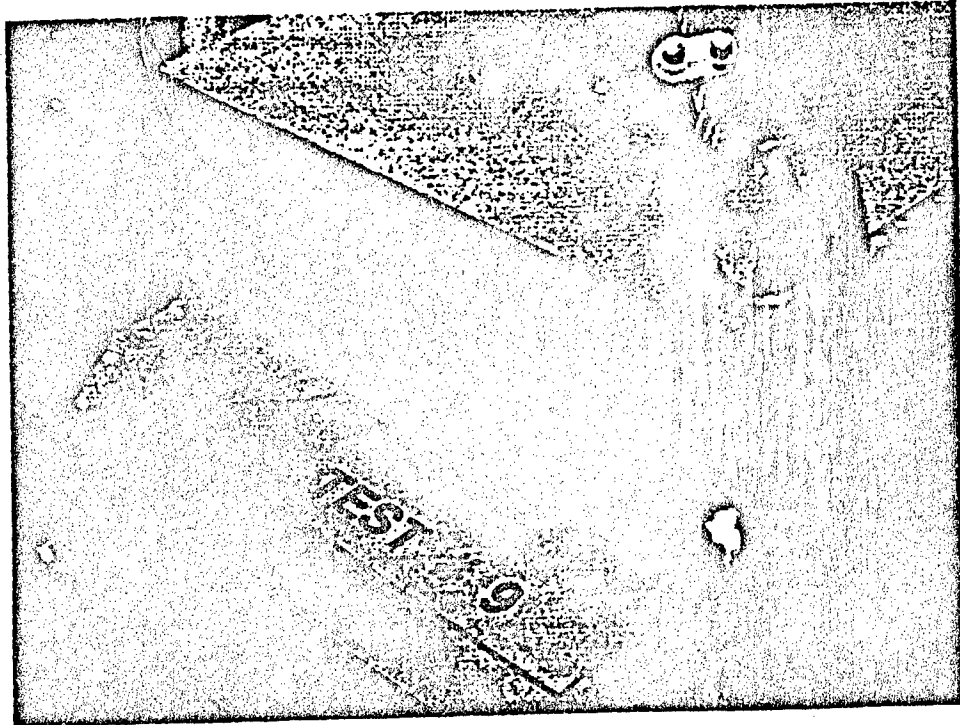


Figure 3.3 Typical Centrifuge Test Wall

Some of the conclusions of the Phase II centrifuge study are as follows:

- Soil density was the most significant factor influencing wall response.
As soil density increased, wall displacements decreased.
- Reducing standoff distance by 2 in. (5 ft. at full-scale)
significantly increases wall residual displacements, peak pressures and accelerations, and wave speeds.

- Reducing reinforcement tensile strength significantly increased wall residual displacement at the sides of the wall, but not as much as should be expected for a large reduction in reinforcement strength.
- Two soil types with slight property differences produce different results. Although wall residual displacements were similar, peak pressures and accelerations measured in Sky X sand were significantly lower than those in the Tyndall Beach sand at similar densities.
- Using one continuous sheet of soil reinforcement, as opposed to several strips, significantly increases wall residual displacements at the sides of the walls, but did not reduce them at the wall center.
- Facing panel geometry does not significantly affect wall response.
- The amount of reinforcing used in the wall does not significantly affect wall response (provided the minimum amount of soil reinforcement is used to maintain static stability).
- The roof structure significantly reduces panel residual displacements in the top row of panels only.
- A reduction in coupling factor reduces wall panel residual displacements.

Evaluation of Centrifuge Test Data for Further Analysis

Each of the individual acceleration, soil pressure interface, and free field pressure data records from the 16 centrifuge tests were evaluated for use in this research. In 10 of the tests, residual displacements of panel No. 2 (closest to the detonation), were within \pm 1.5 in. of each other at prototype scale (0.05 in. at 1:30 scale). Tests with larger residual displacements were sought out to provide data well outside the range of statistical variations. From the data set, six centrifuge tests were selected for evaluation. The design parameters for each of these tests are presented in Table 3.5. Tests 20 and 27 were models of full-scale Tests 5 and 6 conducted as part of this research and detailed in Chapter V. Tests 26 and 28 were constructed with a different backfill material, allowing for evaluation of test data with respect to changes in the material properties of the backfill. Also, the difference in measured displacements between Tests 26 and 28, at full-scale, was over 0.39 ft. Finally, Tests 29 and 32 provided clear data records of the measurements necessary for the evaluation, and are included in the evaluation. Test 29 was constructed with geogrid of reduced tensile strength, and in Test 32 one each geogrid layer was installed as a continuous sheet connected to each panel, rather than individual strips.

Table 3.5 Centrifuge Test Parameters - Prototype Scale

| Test Number | Soil Type | ρ (lb-sec ² /ft ⁴) | Weapon Standoff (ft.) | Variable | Ultimate Displacement, Center Panel (ft.) |
|-------------|--------------|--|-----------------------|--------------------------|---|
| 20 | Sky X | 2.80 | 21.1 | Full-Scale Model | 2.33 |
| 26 | Tyndall Sand | 2.95 | 21.1 | Reduced Unit Weight | 1.76 |
| 27 | Sky X | 3.0 | 25 | Full-Scale Model | 1.63 |
| 28 | Tyndall Sand | 3.2 | 21.1 | 37.5 ft. Grid Embedment | 1.37 |
| 29 | Tyndall Sand | 3.2 | 21.1 | Reduced Tensile Strength | 1.67 |
| 32 | Tyndall Sand | 3.2 | 21.1 | Continuous Reinforcement | 1.56 |

Numerical Models

The development of numerical models to predict the behavior of reinforced soil to dynamic loads has primarily focused on the seismic response of these systems (Yogendrakumar, et al, 1992). These models have used the full-scale test data presented by Richardson, et al (1977) to evaluate model output data. In order to model the response of reinforced soil to a large explosion in the soil backfill, a new model or modified model would be necessary.

Bachus, et al (1993) present an effort to modify the computer model DYNA-3D (Whirley & Hallquist, 1991) to address the response of geogrid-reinforced soils to explosions in the soil backfill. This model was tested through previous full-scale test data and explosive centrifuge tests presented by Bachus, et al (1993). Once operational, a series of 14 analyses were conducted to evaluate the effect of various parameters on the performance of a geogrid reinforced wall. The test matrix is shown in Table 3.6.

The standard analysis used in the test matrix was a model wall 14.8 ft. high with six layers of Tensar UX 1600 geogrid, 14.8 ft. long. Each layer of geogrid is attached to the center of a concrete facing panel 2.46 ft. high and 0.48 ft. thick. The prototype soil used for the wall and foundation was a clean sand with a friction angle of 35 degrees. To reduce the computer time needed and therefore expand the parametric analysis, a two-dimensional, plane-strain model was used. The explosive charge was initiated at selected distances behind the wall face and 7.38 ft. below the ground surface. The charge weight was 197 pounds of TNT and assumed to be fully coupled with the ground.

The loading resulting from the explosive detonation within the soil was modeled by describing the horizontal component of the velocity-time history for selected nodes in the finite element mesh. The velocity-time histories were calculated using equations from Drake, et al (1989), which estimates particle

Table 3.6 Numerical Evaluation Test Matrix (Bachus, et al, 1993)

| Test | Test Variable |
|-------|--|
| PS1 | Standard Analysis |
| PS2 | Reinforcement stiffness decreased by two orders of magnitude |
| PS3 | Reinforcement stiffness increased by two orders of magnitude |
| PS4 | Length of reinforcement reduced |
| PS5 | Standard analysis without roof |
| PS6 | Standard weapon 20 ft. from boundary |
| PS7 | Large 500 lb. weapon 10 ft. from boundary |
| PS8 | Large weapon 20 ft. from boundary |
| PS9 | Large weapon 40 ft. from boundary |
| PS1B | Standard weapon located at base of wall |
| PS1S | Standard analysis with soil/reinforcement interface friction coefficient reduced from 0.9 to 0.7 |
| PS1W | Standard analysis w/soil stiffness decreased by a factor of 10 |
| P1PHI | Standard analysis with ϕ increased from 35 to 40 degrees |
| PS1N | Standard analysis without gravity initialization |

velocity from the free-field blast pressure wave, but does not include prediction of inertial wave particle velocities.

The conclusions of this parametric study are summarized as follows:

- Weapon size and distance are critical parameters which influenced wall behavior much more than any other parameter.
- Wall panel motions decrease as soil strength and stiffness increase. This effect appears to be more important than reinforcement stiffness.
- Wall panel displacement decreases with increasing reinforcement stiffness in a nonlinear fashion. An increase of four orders of magnitude in reinforcement stiffness leads to approximately a 40 percent decrease in average peak displacement of the wall facing.
- Increasing the relative compaction of the soil will lead to enhanced performance.
- Within the range investigated, reinforcement length has little effect on the behavior of the reinforced system, provided the length meets static design criteria.
- The reinforcement is subject to very high compressive stresses as the blast wave passes through the system.
- Dynamic tensile stresses do not develop until after the blast wave has reached the facing.

- Dynamic tensile stresses develop relatively slowly in the reinforcement.

Rise times of tens of milliseconds are predicted by the numerical code.

- Reinforcement rupture and excessive deflection were the only observed failure mechanisms. Very little relative movement between the reinforcement and the soil (pullout) was observed.

The version of DYNA-3D used for that research program was effective for general parametric evaluations, however further refinements were necessary for quantitative analysis, as detailed by Bachus, et al (1993).

Evaluation of Previous Research

The dynamic response of reinforced soil systems has been evaluated in full and small-scale testing programs, and through numerical analysis. These testing and analysis programs were reviewed as part of this research in order to: 1) evaluate how previous research could be applied to this program; 2) develop a clear understanding of what additional research contributions could be made to further the state-of-the-art; 3) identify potential failure mechanisms; and, 4) provide a basis for design of this research test.

The previous full-scale tests have shown reinforced soil can contain and survive explosions: 1) in the backfill; 2) in front of the wall face; and 3) behind the soil berm. However, each of these tests have had little or no data

collected. The most comprehensive data from a full-scale test is the deflection data presented by Eytan and Reid (1993). This test also showed the steel reinforcement strips tended to cause stress concentrations at the point where they anchor into the facing panels, causing the panels to break apart. Their report also provides a detailed presentation of wall panel displacements. Full-scale pressure and acceleration data are almost non-existent, and in each of these tests no measured soil properties are presented. This lack of full-scale test data provides little information of use in the validation of numerical or small-scale models. All previous full-scale tests have been performed on steel strip reinforced walls. No full-scale test data exists for the response of geogrid reinforced soil walls to explosive loads.

The small-scale (1:30) test results have demonstrated what design parameters have the most effect on the response of reinforced soil walls. Soil properties, location of the weapon, and type of reinforcement were three parameters that significantly affect wall response. Once enough reinforcement exists for static stability, increasing the length, coverage area, or number of layers of reinforcement had little effect on the response of scaled walls. Also the assumed failure modes, reinforcement rupture and pullout, were not observed. The effects of the three primary design variables, soil properties,

weapon location, and reinforcement type on wall response needs to be validated through full-scale tests.

The DYNA-3D code, specifically altered to address the dynamic response of reinforced soil, confirmed many of the conclusions of the 1:30 scale test. This included confirming that the reinforcement, reinforcement length, reinforcement, weapon size and location, and soil properties had the most significant effect on system response. Also, reinforcement length (over that required for static stability) and soil/reinforcement interface friction had little effect on wall response. The numerical model did show rupture of reinforcement is a potential failure mode, however this was not observed in the 1:30 scale tests. The primary failure mode observed in the numerical model was excessive deflection of the wall facing panels. Finally, the model shows an explosion in the reinforced backfill causes the reinforcement to be subjected to compression before tension. The data generated by this model requires validation via a full-scale test.

The information discovered through the literature review has shown a need for a full-scale test of a reinforced soil wall subjected to an explosive detonation in the soil backfill, coupled with the development of a fundamentally based approach for relating loading mechanisms and the engineering properties of the materials to the residual behavior of the walls. Previous research has helped develop potential failure modes and a better understanding of the physical

response of the structure, which is valuable in developing a design for the proposed test program. However, the influence of specific design variables are based solely on post-test measurements, and not fundamentally sound relationships. The coupling of a fundamental equation of motion with detailed pressure, acceleration, strain and displacement data collected from full-scale testing is necessary to further develop our understanding of dynamic response of reinforced soil.

CHAPTER IV

EQUATION OF MOTION

Introduction

The design of structures to resist the effects of groundshock from conventional weapons is often founded on design methods developed for nuclear weapons threats. The nature of nuclear-generated load pulses are such that structural loads have small spatial gradients and are not greatly affected by structural deformations (Drake, et al, 1987).

The conventional weapons used in this research yield loads that are spatially variable across the dimensions of the test structure, change significantly at soil structure boundaries, and are affected by the deformation of the structure. Therefore, a model for reinforced soil walls must consider motion of the system in response to the imposed stresses.

Early design approaches considered buried concrete walls to be unyielding, and therefore designed to withstand stresses that are twice that of the free-field stresses. Drake, et al (1987), developed a more rational approach for the solution of a yielding wall by considering displacement boundary conditions.

For buried reinforced concrete walls, this approach determined that the groundshock stresses transmitted to the structure were less than the free-field soil stresses at the soil/structure interface. Newmark and Haltiwanger (1962) made the general statement that observed structure loads were usually less than free-field loads because of an "arching" phenomena. To the geotechnical engineer, these differences in structural loads are analogous to the difference between at rest earth pressure (K_0) and active earth pressure (K_a). That is, small amounts of structural yielding can result in significant pressure relief. The equations developed by Drake, et al (1987) are increasing in use in the design of reinforced concrete shelters over the highly conservative unyielding wall design method.

The unyielding design approach was not considered to be appropriate for a reinforced soil wall because individual reinforced soil wall elements have neither the mass nor displacement-controlled boundary conditions that would resist panel motion. If the boundaries of the wall elements were fixed, the lack of reinforcing steel and small section thickness would result in failure of the concrete panels under the imposed blast stresses. Reinforced soil is recognized as a flexible system, as stated by Christopher, et al (1990):

One of the greatest advantages of mechanically stabilized soil structures is their flexibility and capability to absorb deformations due to poor subsoil conditions in the foundations. Also, based on observations in seismically active zones, reinforced soil structures have demonstrated a higher resistance to seismic loading than rigid concrete structures.

It will be shown that an equation of motion based on the work by Drake, et al (1987) can be adapted to model the response of a reinforced soil wall with concrete panel facing to blast pressure loads. The ultimate objective of this application is a methodology to evaluate wall panel behavior based on the applied pressures.

Development of The Equation of Motion

The basic physical principles of wave propagation through elastic solids are applied to the partition of energy across the boundary of two media (Waters, 1981). The boundary conditions assume continuity of both stress and displacement between the soil and the structure. These conditions can be stated as

$$\sigma_z = \sigma_{ff} + \sigma_s \quad (4.1)$$

where σ_i is the interface stress, σ_r is the stress reflected from the structure and σ_n is the free-field incident stress produced by the explosion. Continuity of displacements requires that

$$\dot{u}_{ff} - \dot{u}_r = \dot{u} \quad (4.2)$$

where \dot{u}_{ff} is the particle velocity associated with σ_{ff} , \dot{u}_r is the particle velocity of the reflected wave and \dot{u} is the velocity of the structure. Particle velocity and stress can be related by the impedance of the media via the relationship

(Bangash, 1993):

$$\sigma_r = \rho c_L \dot{u} \quad (4.3)$$

where ρ is the mass density of the soil and c_L is the longitudinal wavespeed of the soil.

Combining Eqs. 4.3 and 4.1 yields

$$\sigma_i = \sigma_{ff} + \rho c_L \dot{u}_r \quad (4.4)$$

and combining Eqs. 4.2 and 4.4 gives

$$\sigma_i = \sigma_{ff} + \rho c_L (\dot{u}_{ff} - \dot{u}) \quad (4.5)$$

Figure 4.1 shows a free body diagram of the structure with wave interaction and cross sectional area (A).

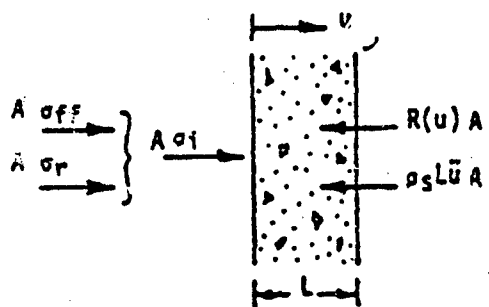


Figure 4.1 Free Body Diagram of Wall Panel With Wave Interaction
(Drake, et al, 1987)

Summation of the horizontal forces in the free body diagram results in

$$\sigma_I = \rho_s L \ddot{u} + R(u) \quad (4.6)$$

where ρ_s is the mass density of the structure, L is the thickness of the structure, and $R(u)$ is the resistance per unit area of the structure.

From Eqs. 4.5 and 4.6,

$$\rho_s L \ddot{u} - \rho c_L (\dot{u}_{ff} - \dot{u}) + R(u) = \sigma_{ff} \quad (4.7)$$

which is the equation of motion for the structure that includes the interaction effect. Applying the assumptions used in Eq. 4.3, it can also be shown that

$$\sigma_{ff} = \rho c_L \dot{u}_{ff} \quad (4.8)$$

and substituting Eq. 4.8 into Eq. 4.7 yields

$$\rho_s L \ddot{u} + \rho c_L \dot{u} + R(u) = 2 \sigma_{ff} \quad (4.9)$$

the final equation of motion.

This equation is of the form of a single degree of freedom system and assumes continuity of both stress and displacement between the soil and the wall. The equation resembles that of a single degree of freedom system with damping, however the damping term is the result of satisfying the boundary conditions and is not related to viscous or frictional damping effects. The resistance function represents the resistance of the structure per unit area, and is dependent upon the displacement of the wall (Drake, et al, 1987).

Validity For Reinforced Concrete Walls

The validity of the equation of motion for predicting the deflection of buried concrete structures subjected to buried explosions was also presented by Drake, et al (1987). The test case was modeled as a one way slab with fixed ends. Drake, et al (1989) presented tables for calculating the resistance function for various types of beams and slabs based upon the moment capacities and shear capacities of the appropriate elements. In the test case, the peak free-field stress exceeds the calculated resistance of the structure by a factor of nine. The model predicted the maximum deflection within ± 30 percent of measured values. The model tended to underestimate peak deflections and permanent deflections. Drake attributed these differences to the overprediction of stiffness.

using the handbook methods and that, in the validation test, the entire structure translated before the peak deflection occurred, further reducing interface loads.

Application to Reinforced Soil Walls

The equation will be adapted for use in subsequent chapters to evaluate the response of the wall panels to the free-field and inertial pressures. The adaptation will require modification of the resistance function to appropriately model the resistance of reinforced soil walls, and will be discussed in detail in Chapters VII and VIII.

To apply the equation of motion to reinforced soil walls requires validation through test data. Chapters V and VI will discuss the development and results of a full-scale test program to measure the response of reinforced soil walls to blast pressure wave.

CHAPTER V

FULL-SCALE TEST DESIGN

Introduction

Based upon the literature review and the needs of the research sponsor, a research program was developed to evaluate the response of a series of full-scale geogrid-reinforced soil walls to explosive detonations in the retained backfill. The research program test parameters considers two of the primary design variables identified in previous small-scale and numerical analysis research programs while balancing overall research objectives against the constraints of time, budget, and capability. This chapter will discuss how the information derived from the literature review affected the test parameters, selection and sizing of materials, weapon size and placement, test instrumentation, and design of the test walls.

Type of Reinforcement

The selection of the reinforcement material was based on three factors: the needs of the research sponsor, the advancement of research, and elimination of a potential failure mode. First of all, the research sponsor ultimately is to use the results of this research to help develop a design methodology for protective shelters built of reinforced soil. These shelters must be rapidly erectable in remote areas of the world. In choosing between inextensible (metal strip) and extensible (geosynthetic) reinforcement, logistical requirements are of paramount concern. The components of the reinforced soil structure may have to be stored for many years and then on short notice be shipped to a location for use. The design for this shelter would be done as needed, although some non-site-specific pre-design may be possible in advance. It is likely, however, that soil conditions will not be known at the time the shelter components are procured; therefore maximum flexibility is imperative.

The inability to perform design before procurement of materials means reinforcement must be cut to length in the field. Geosynthetic materials can be cut to any length during the installation process, and waste is minimized. Steel strip reinforcement may be shortened in the field, however that wastes the

excess reinforcement. It is difficult to lengthen steel strip reinforcement in the field.

Steel strip reinforcement is generally recommended in frictional soils, preferably sands and gravels (Christopher, et al, 1990), whereas geogrid type materials can be used in both clays and sands. Also, if facing panels are not available, geogrid reinforcement can be used to construct a wall with a "wrap around" face as long as some liner material is available to contain the soil.

Also, steel strip reinforcement generally is connected to the facing panels at four anchors. As shown in the 1990 tests (Eytan and Reid, 1993), these anchor points are susceptible to failure. The transfer of load from the panel to the reinforcement should take place over a larger area to reduce stress concentrations and reduce the occurrence of this potential failure mode.

Geogrid reinforcement can be embedded into the concrete facing panel over the entire roll width which distributes the reinforcement stress over a larger area of panel. Finally, steel is subject to corrosion.

It was also noted in the literature review that all previous full-scale tests had been performed on steel strip reinforced walls, but that no pressure or acceleration data was collected. The scaled test walls were reinforced primarily with geogrids, but did not have appropriate full-scale test data for data

validation. Because of these considerations, geogrid reinforcement was chosen for use in this test program.

Selection of Geogrid Type

The first constraint that affected the selection of geogrid material was the requirement to embed the geogrid into the concrete facing panel. Some geogrid materials are made of coated polyester which has been shown to degrade when embedded in portland cement concrete. High-density polyethylene (HDPE) is resistant to degradation (hydrolysis) in the alkaline environment created by the concrete panel and has excellent stiffness properties under rapid loading (Reid and Collin, 1995).

The two HDPE geogrids selected for this test series were Tensar Earth Technology, Inc. UX 1400HT and UX 1500HT. A summary of the properties of these grids is shown in Table 5.1. As Table 5.1 shows, the two geogrids are very similar in many respects. The key differences are in tensile modulus and strength. The difference in tensile modulus at 2% strain is a factor of two. The creep-limited strength of UX 1500HT is 1.7 times that of the UX 1400HT. Because these materials are similar except for tensile modulus and strength, they were chosen for use in this test. For two equal tests, the performance difference in wall deflection could then be primarily attributed to the tensile

stiffness or strength of the reinforcement. However, as shown in Chapter III, the deformation of the walls in scaled tests were not significantly affected by changes in reinforcement strength. This suggests that if the geogrid does not rupture, differences in displacements may be affected more by reinforcement stiffness than strength. By using these geogrids data would be available to compare to the conclusion drawn from the numerical analysis that reinforcement stiffness is a primary factor affecting wall deflection.

**Table 5.1 Properties of Geogrid Reinforcement
(Tensar Earth Technologies, Inc., 1992)**

| Property | Test Method | UX 1400 HT | UX 1500 HT |
|------------------------------|---------------|--------------|---------------|
| Apertures: Along Roll Length | Calipers | 9.5 in. | 9.5 in. |
| Apertures: Along Roll Width | Calipers | 0.66 in. | 0.66 in. |
| Rib Thickness | ASTM D1777-64 | 0.03 in. | 0.055 in. |
| Junction Thickness | ASTM D1777-64 | 0.10 in. | 0.16 in. |
| Creep Limited Strength | ASTM D5262 | 1,600 lb/ft | 2,700 lb/ft |
| Tensile Modulus | GRI GG1-87 | 50,000 lb/ft | 100,000 lb/ft |
| Roll Length | | 98 ft. | 98 ft. |
| Roll Width | | 4.3 ft. | 4.3 ft. |
| Roll Weight | | 38 lbs. | 55 lbs. |

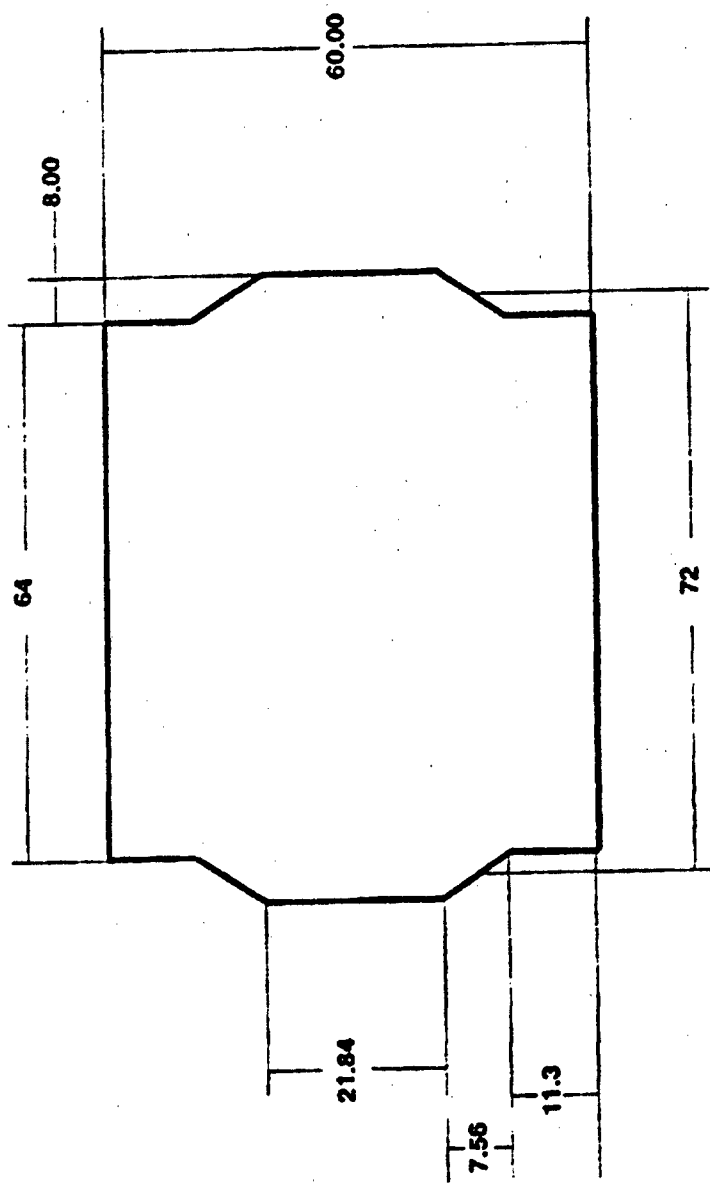
Type of Facing Panel

Numerous facing panel shapes are used in reinforced soil wall construction: cruciform, Georgia Stabilized Earth, Modular Block, full height tilt-up panels, modular block and others. A Georgia Stabilized Earth panel shape (Fig. 5.1) was selected since a local contractor had experience in their fabrication and could fabricate them on site within the test schedule.

Test Structure Dimensions

Design of the test wall was based upon ensuring the walls were long enough to capture the full effect of the blast loads, with maximum displacements at the centerline, and negligible displacements at the edges of the wall face. The wall height was based upon compatibility with previous research.

As shown in Fig. 3.2, the most significant deflections occur within a zone approximately five panel widths wide, centered about the load source. To capture this damage on the planned tests, the wall face should be five panels wide. The face of the wall should also be 30 ft. wide, to ensure it is wider than the explosive crater. Therefore, the center full section of wall was designed to be five panels wide, with each panel 6 ft. wide. The height of the test wall should be compatible with previous tests. The 1990 full-scale test used walls approximately 12.3 ft. in height. The 1:30 scale model tests



PANEL THICKNESS 5.5"
REINFORCING NO. 4's @ 12"

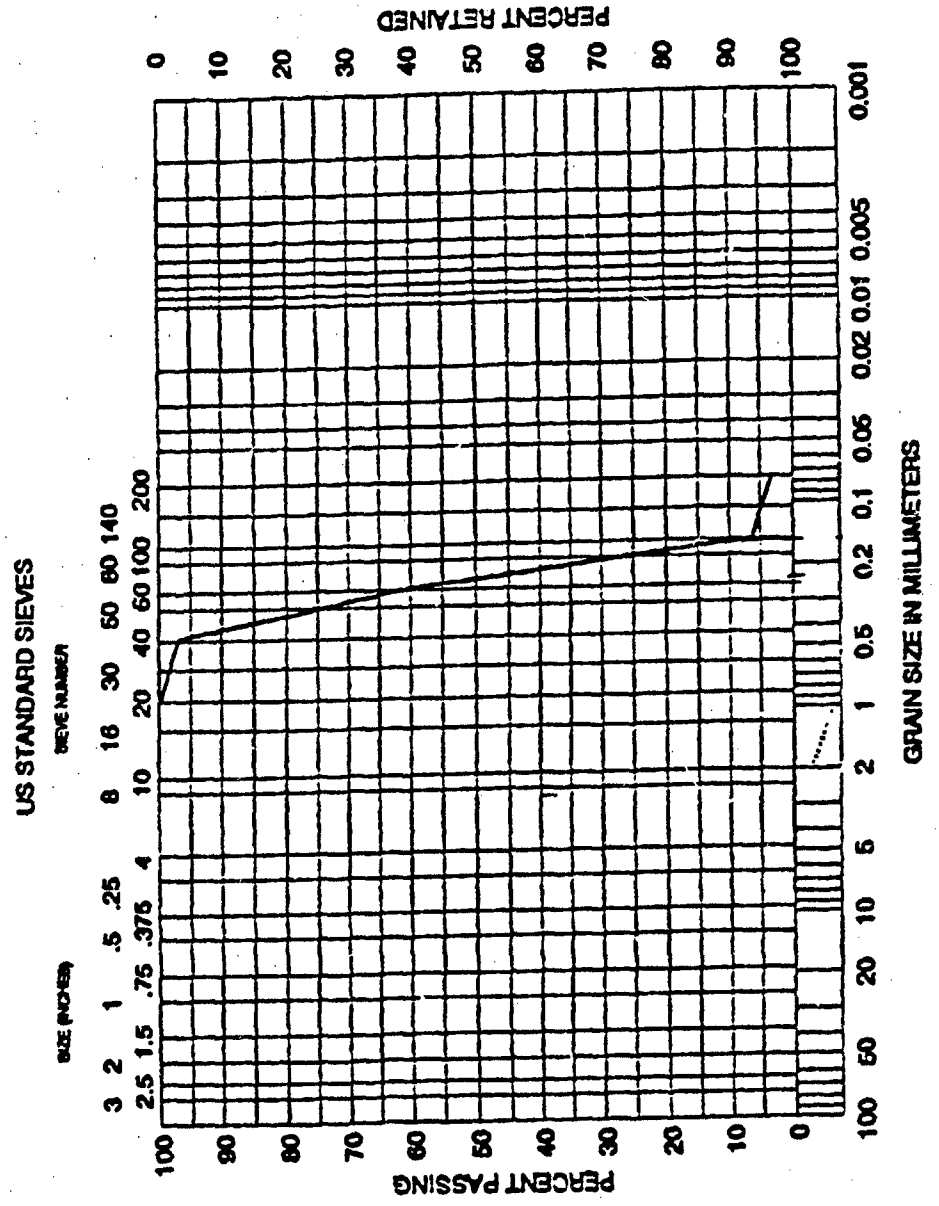
Figure 5.1 Georgia Stabilized Earth Panel
(All Dimensions in Inches)

discussed by Bachus, et al (1993) and Olen, et al (1993), were scaled 15 ft. high walls. Because of the large amount of scaled test data, and the ability to do more scaled testing as needed, the full-scale test wall height of 15 ft. was acceptable. To provide a symmetrical wall face, each panel should be 5 ft. in height and 6 ft. wide, making the overall wall approximately 79 ft. at its base and 16.5 ft. high (this includes 1.5 ft. embedment depth).

Soil Type and Properties

After the wall size was determined, earthwork for construction had to be considered. Based on the overall dimensions of the test wall, at least 1400 yd³ of backfill would be needed. Because of the amount of soil needed and the limited budget, a local sand was chosen as the backfill material. The sand is referred to as Sky X (Sky Ten) sand, a SP-SM sand whose name derives from the test range where the tests were conducted.

The grain size distribution is shown in Fig. 5.2. The coefficient of uniformity is $C_u = 1.63$ and $D_{50} = 0.24$ mm categorizing this as a uniform fine sand. Based on the results of modified Proctor tests on the backfill soil, the maximum dry unit weight was 101.8pcf at 11.3% water content. Finally, based on consolidated drained triaxial tests at confining pressures of 50 to 300 psi, the angle of internal friction of the sand was 33 degrees.



ADA293552

Figure 5.2 Grain Size Curve, Sky X Soil

Number of Tests

It has been established that three of the primary design variables that affect the design of a reinforced soil wall subjected to explosive loads are: 1) soil properties; 2) reinforcement stiffness; and, 3) weapon size and placement. Due to research program limitations, it was decided to evaluate only two of these variables: the stiffness of the reinforcement and the weapon size and placement. To maximize the usage of each wall, a two-stage test was performed. In the first of two stages, the weapon standoff was chosen to hopefully cause only minor deflections. Following this first test the bomb crater was repaired and a second bomb was placed closer to the wall in order to cause moderate displacements of the wall panels. At this point, the wall sustained enough damage to make it unusable for future tests. A duplicate wall was constructed and the weapon located such that it caused heavy damage.

After these tests, two more walls were built to the same specifications but with a much stiffer reinforcement material. Tests were then conducted with weapons at the same standoff distances.

Weapon Size

Many previous explosive tests on hardened reinforced concrete shelters and reinforced soil used 500 lb. cased general purpose bombs (GP) as an explosive source. These bombs are referred to as Mark-82 or MK-82 bombs. The 1:30

scale tests also used a scaled explosive designed to model the MK-82. To maintain continuity between these tests, and because of ready access to the necessary number of MK-82 bombs, this weapon was chosen for use in this test series. The MK-82 bomb is an aerodynamic, low-drag cast iron bomb designed to be carried and delivered from under the wing of supersonic aircraft, however it has also been delivered from the bomb bay of larger bombers. The MK-82 contains approximately 192 pounds of explosive H-6 filler, which is the explosive equivalent to 264 lbs. of TNT (Dobratz and Crawford, 1985). The 192 pounds of explosive is referred to the Net Explosive Weight (NEW) of H-6 in the weapon. The remaining weight of the weapon comes from the cast iron casing.

Weapon Location

The distance between the explosive source and the retaining wall has a significant impact on the response of the wall. In the first of two tests on a wall, the weapon had to be close enough to cause the pressure gages to react and for the wall panels to move. Conversely, the weapon had to be far enough away in order to prevent catastrophic failure of the wall. Based on the review of previous full and small-scale test data, a weapon standoff distance of 20 ft. was selected for the first test. If this distance caused minor damage, then subsequent tests would use standoff distances of 15 and 10 ft. If the 20-ft.

standoff caused moderate damage, tests would be conducted at 25 and 15 ft. Finally, if the 20-ft. standoff caused major damage, further tests would use 30 and 25-ft. standoffs.

Weapon Placement

The placement of the bomb required a methodology allowing for placing the weapon after construction was complete, while providing control over the location of the explosive. Safety restrictions prevented placing the bomb in the backfill until the date of testing.

After completion of construction, a small hole was excavated at the required distance behind the wall to a depth of ten ft. Since the bombs are five ft. in length, if the nose of the bomb rests at a depth of ten ft. then the center of the bomb will be 7.5 ft. from the top of the wall. This places the center of the bomb directly in line with the soil pressure interface gage on the centermost panel. A PVC pipe, referred to as the "bomb tube", 12 ft. long and approximately 18 in. in diameter was set in the center of the excavation. Backfill material was replaced in the excavation and compacted.

On the day of each test, the bomb was delivered to site and charged. A crane would then pick the bomb up and then lower it into the tube. Once the bomb was in place, the bomb tube was lifted out of the ground.

The rationale behind this process was to simulate how an air delivered weapon might impact the soil. An air delivered weapon would penetrate the soil, loose soil would collapse in over the hole made by the bomb, and the bomb would detonate. This method was devised to simulate that process, while still providing complete control over the weapon location.

Data Collection

To further understand of the response of the wall to the test loads, pressure, acceleration, strain and displacement measurements were collected during testing. The data collection design was developed to provide pressure and acceleration data similar to that collected in the scaled tests. Also, geogrid strains were measured to determine the response of the geogrid to blast pressures. This section will discuss the specific types of gages, data collection system, firing system, and some miscellaneous components of the instrumentation.

Data Acquisition System

A Pacific Instruments Portable Data Acquisition System Model 5700 was used to record the data during each test. With the slave enclosure this system is a 32 channel fully programmable transient recorder that can record samples at rates of up to 1,000,000 samples per second per channel. The digitized data

is recorded in a solid state non-volatile memory with a capacity of 256,000 data points. To prepare the data acquisition system requires preprogramming each data channel for each test. This programming required the input of each gage's characteristics into the computer. The gages were connected directly to the data acquisition system via instrumentation cable from Alpha Corporation, Type-L, which was a four strand shielded cable. This data acquisition system was connected to the firing system.

The 32 channels are divided into 4 groups of 8 channels each. One channel in each group was reserved for input of the firing pulse. This gave each group a signal for "zero time"; the time the firing pulse was sent to detonate the bomb. Normally, one channel for the entire system is needed for firing pulse input, but any failure for this information to be transmitted between groups makes it impossible to determine when each gage reads the blast load with respect detonation time, preventing time dependent comparisons between groups. To be conservative, one zero time channel was reserved per group. Using four channels for zero time left 28 channels for recording test data.

Firing System

A Reynolds Industries Systems Incorporated FS-17 firing system was used in this test. This key-operated firing system consists of a control module which inputs 28 volts DC into a firing module containing a high voltage discharge

capacitor that emits a nominal 2000V DC signal to the exploding bridge wire ordinance. The exploding bridge initiates the explosion of the detcord, which in turn detonates C-4 explosive in the bomb fuse well, which in turn detonated the bomb. When the firing module capacitor builds up enough charge (2000V) a fire signal is sent to the high speed camera. The camera would turn on, and once the film reached the proper speed it sends a signal to the control module which in turn signals the firing module to discharge the capacitor. The capacitor then discharges, sending 2000V to the exploding bridge wire which initiates the blast.

Gages

Four different gage types were used to measure test data: 1) soil interface pressure gages; 2) free-field soil pressure gages; 3) accelerometers; and, 4) strain gages.

The soil interface pressure gages were produced by the Kulite Corporation, Model number VM-750 with pressure ranges up to 200 psi. Free-field soil pressure gages were manufactured by the Kulite Corporation, Model number LQ-090U with a range of 200 psi. The accelerometers were manufactured by the Endevco Corporation. These piezoresistive gages, Model number 2262 CA had ranges up to 1000 g's. The strain gages were Type EP-08-250BG-120,

manufactured by Measurements Group, Inc. All gages were calibrated prior to use in any of the tests.

Without other full-scale test data to use as a comparison, gage sizing was based primarily on the Phase I centrifuge test program data. The peak acceleration measured during that test series was approximately 350 g's at prototype scale. Using a factor of safety of two, the initial gage size selected for the full-scale tests was 1,000 g's.

Soil pressure gages were located on the order of 20 ft. from the detonation, and in the centrifuge the pressures measured at that range were on the order of 100 psi. Applying a factor of safety of two, 200 psi free-field and soil pressure interface gages were selected. Gage measurements were evaluated after each test to determine if the gage ranges were appropriate to collect the most significant data.

Soil Pressure Interface Gages. Soil interface pressure gages were used to measure the ground shock transmitted to the back side of the wall panels. Because the gages are expensive and due to limits on the number of channels of data that could be collected, six panels were fitted with these gages. The panels subjected to the highest levels of stress were fitted with these pressure gages.

The gages were numbered P1-P6 corresponding to panels numbered 1-6 in Fig. 5.3. The blast wave and pressures were assumed to be symmetrical about the center of the wall. Also, most of the deflection, based on previous tests,

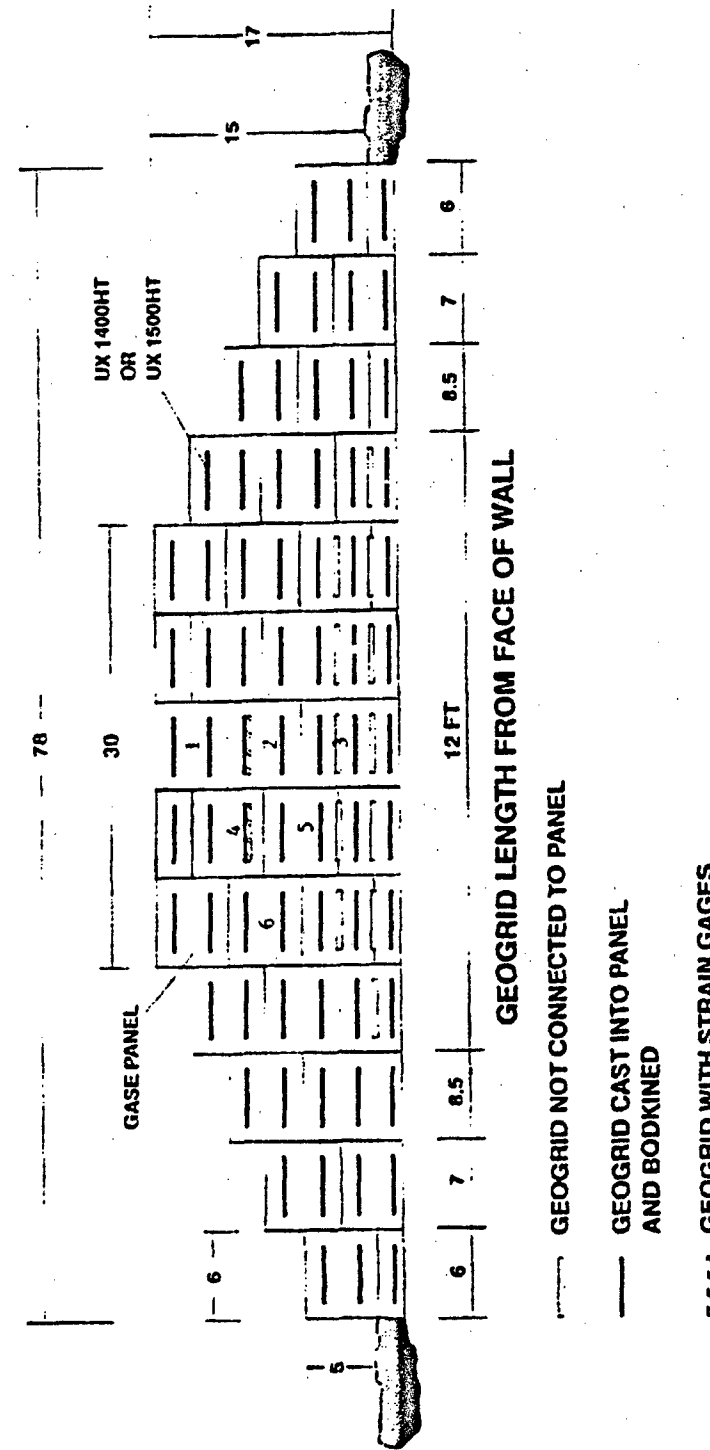


**Figure 5.3 Schematic of Test Wall Design
(All Dimensions in Ft.)**

should be contained within two and one half panel widths of the centerline.

Therefore, these six gages should collect the most significant data.

In order to measure the blast pressure on the soil side of the wall panels, soil pressure interface gages had to be mounted such that the gage face was flush with the soil side of the panel. It was decided to install the gages after construction, as opposed to casting the gages into the panels or placing them during construction. Installing the gages during construction has four disadvantages. First, these expensive gages would be subjected to construction damage due to shoveling, heavy equipment, and exposure. Secondly, some of the walls were to be tested more than once. If large variations exist in the predicted stress between the two tests, then the gage has to be sized to the larger stress level. This can make reading of the small stress levels less accurate. Third, if a gage fails between installation and test time (which may be many weeks), or between tests, then the gage is lost. Finally, casting gages into the panels or installing during construction would make it extremely difficult to retrieve gages after each test. Therefore, it was desired that a gage mount system be developed that allowed for installation of the soil pressure interface gages after construction and just prior to testing, and their subsequent removal after each test.

A gage mount was designed for the soil pressure interface gages. The gage mounts were 5 1/2 in. long, 3 1/2 in. diameter steel cylinders. The mounts

were capped at one end, with a 3/4 in. hole in the center of the cap. On the outside of the mount, a 1 1/2 in. diameter, 1/4 in. thick nylon lining was countersunk into the cap. Centered in the nylon lining is a 3/4 in. diameter hole that aligned with the hole in the end cap. Using a pair of forceps, a soil pressure interface gage could be pushed into the hole into the end cap, and the face of the gage would be flush with the end cap, which in turn was flush with the back face of the wall panel. Two, 3 in. diameter plates, one nylon and the other steel, with 3/4 in. diameter holes in the center slide into the gage mount and over the gage. With four screws, these plates and tightened against the end cap and gage, providing a rigid mount for the gage. The gage was held in place by the nylon inserts on both sides, which would minimize any ringing effects from the steel cylinder. Twenty-four of these gage mounts were cast into panels for use in the test series. The mounts were covered with duct tape during casting to prevent concrete from entering the gage mount. This tape was removed prior to construction.

To ensure the gage was bearing against soil, a 3/4 in. diameter tamping rod was fabricated. Prior to gage installation, additional sand was forced into the hole in the end cap and compacted with the tamping rod. The pressure gage would be installed and removed. Upon removal, the gage face would be inspected, and if soil residue covered the gage face, then the gage would be installed into the gage mount. If soil residue did not cover the gage face,

additional soil was tamped into the hole until satisfactory results were achieved.

Accelerometers. In order to develop load-deformation relationships on the panels, the movement of each panel fitted with a soil pressure interface gage was measured. An accelerometer was placed on the exposed surface on each of those panels, and numbered A1-A6. Hence, six accelerometers were used in each test.

The accelerometers were installed on the face of the concrete panels, adjacent to the location of the soil pressure interface gages. Accelerometers could not be affixed to the concrete directly because the gages could easily separate from the concrete. To provide a rigid and uniform bearing surface for the accelerometers, gage mounts were cast into the panels that also had the soil pressure interface gages cast into them. The accelerometer mounts were 2 in. by 2 in. steel plates with 10-32 National Fine (NF) threads tapped into the center of the plate. Four-two in. pieces of threaded rod were welded onto the corner of each plate. These rods, when cast into the panels, would ensure the accelerometer plate remained a rigid part of the panel. The plates were placed face down into the panel forms next to the soil pressure gage mounts, with the rods extending into the panel. The threaded hole was covered on both sides with aluminum tape to prevent concrete from filling the threads. Concrete was then carefully poured into the forms. Prior to testing, the protective tape was

removed from the accelerometer plate and the accelerometer was then screwed into the plate.

Strain Gages. One objective of this test was to understand loading and failure mechanisms within the reinforced soil mass. It was not understood how much relative motion would occur between the soil and the reinforcement, or if the motion of the panels would cause an elastic or plastic response in the reinforcement. It was of interest to try to measure the strain in the reinforcement with respect to distance behind the panel as well as distance from the centerline. Because strain gages are inexpensive, and because of the potential high failure rate (due to the fragility of the gages and possible construction damage) twelve strain gages would be attached to the reinforcement on each test. Strain gages are identified as gages S1 through S12.

The strain gages were placed on the layer of geogrid above and closest to the vertical center of the wall and identified in Fig. 5.3. The gages would be placed in line on the upper layer of grid on the center panel. Three gages would be placed along the centerline of the grid layer, and three at the edge of center piece of grid, three ribs in from the edge. Three more gages would be placed in line at three ribs in from the edge of the grid layer adjacent to the center, and three more along the centerline of the grid adjacent to the center piece, as detailed in Figs. 5.4 and 5.5. The attachment of the strain gages to

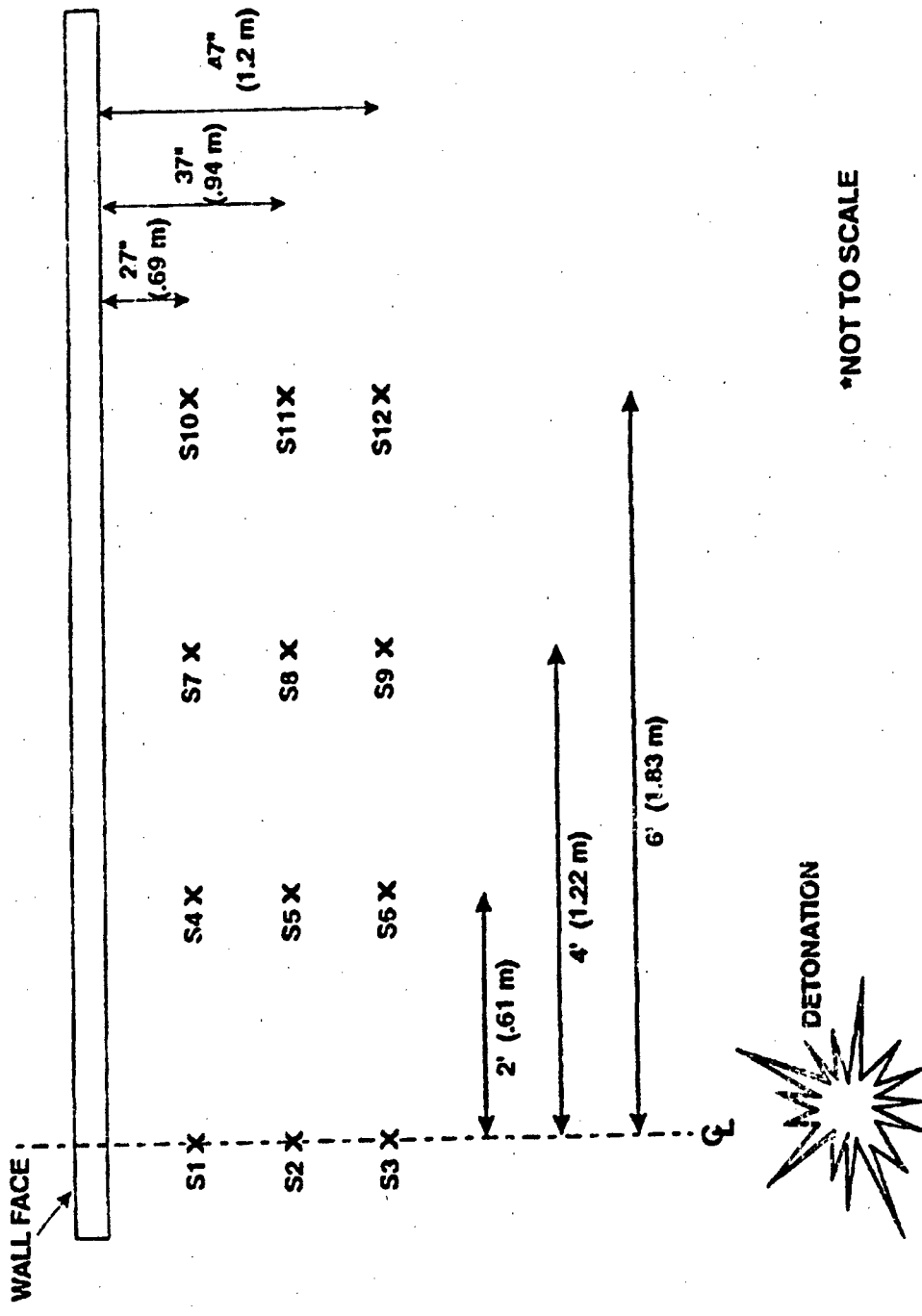


Figure 5.4 Position of Strain Gages, Tests 2 and 3

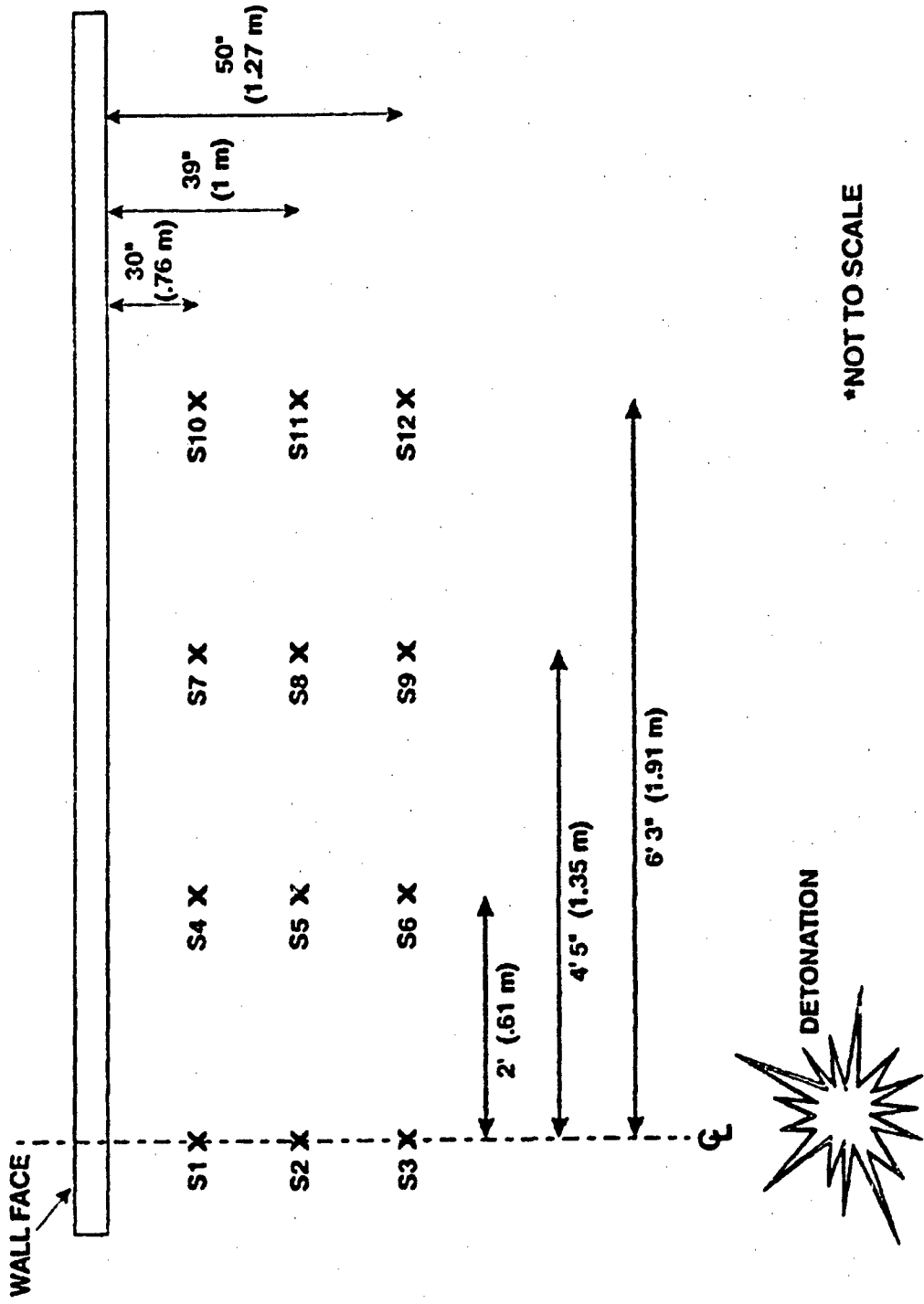


Figure 5.5 Position of Strain Gages, Tests 4 and 5

the geogrid is a difficult problem. This has been successfully done for laboratory creep and extension tests (Oglesby, 1992), and those methods were used (Appendix A).

Once the strain gages were installed onto the geogrid in the lab, the gaged grid was transported to site and installed. The protected lead wires were fed between gaps in the wall panels so they could be accessed from the wall face. Each gage was then hand covered with soil to protect against construction damage. When construction of the first wall was complete, a circuit test on each strain gage was performed through the leadwires. These tests showed a break in every circuit. This failure was suspected to be in the connection between the lead wires and the strain gages.

Before the second wall was constructed, modifications to the strain gage mounting process were made, and the survival rate of the gages increased significantly. The modified procedures used for installing the strain gages for each subsequent test are also detailed in Appendix A.

Free-field Pressure Gages. Three free-field pressure gages were placed within the soil backfill to measure the groundshock in the area where strain gages were attached to the geogrid. The gages were placed directly in line between the explosive source and the wall adjacent to strain gages S1-S3 (Figs. 5.4 and 5.5). These gages were numbered F1-F3.

Because the free-field gages were placed in the soil backfill, they had to be installed during construction. After the backfill had been compacted to 4 to 6 in. above the elevation of the gages, construction was halted. Holes were hand dug through the soil at the location of the free-field gages. The gages were then pushed into the compacted soil, and the soil was filled in over the gage and recompacted. Gage wires were run through a narrow trench to the back of the wall and fed through the gap between two panels, making the gage wire accessible from the wall face. The wires were protected with additional fabric shielding wrapped around the wires where they passed between the panels.

High Speed Camera

The high speed camera was a Photec, Inc. 16mm high speed motion picture camera with a capacity of 400 ft. of triacetate base film or 450 ft. of polyester based film. The film speed is variable from 100 to 10,000 frames per second or 400 to 40,000 pictures per second. The lens used was a 45mm F/2.8 Mamiya M645 lens. Power to the camera was supplied by portable rechargeable batteries. The camera was linked to the data acquisition system and firing system via instrumentation cable.

Reinforced Soil Wall Design

With selection of the soil, geosynthetic reinforcement, wall panel type, and instrumentation complete, the embedment lengths of the reinforcement were selected using procedures outlined by Christopher, et al (1990). Based on this design, the maximum embedment length of the geogrid was 8.25 ft., with seven layers of reinforcement. Tensar Earth Technology, Inc., located in Atlanta, GA was providing the geogrid for this test. To take advantage of their expertise in working with their own materials, they were invited to evaluate the design for this problem. Using the Tensar Geogrid Reinforced Retaining Wall Analysis program called 'TENSWAL' (Version 3.1), they recommended a design embedment length of 12 ft., with nine layers of reinforcement. This embedment length was shortened on the tapered ends of the wall, and two of the layers of reinforcement were not embedded into the wall panels. The overall design is detailed in Fig. 5.3. Although the TENSWAL design was more conservative, it was selected for use in this test. Due to the unique nature of the test, degree of uncertainty, and lack of data on the response of geogrid reinforced walls to explosive loading, the conservative design was deemed most appropriate.

Test Wall Construction

Standard procedures for the construction of the walls were used for each wall. Details of the test site and procedures used for fabrication of the wall panels, leveling pad and wall construction are detailed in Appendix B.

During construction of each wall, soil density and moisture content tests were performed using a nuclear density gage. A summary of these measurements is presented in Table 5.2. The standard deviation of the unit weight and water content measurements from Test One are inconsistent with the other tests. This may be due to the extended periods of rain that were experienced during construction that may have affected the moisture content and unit weight of some lifts. Also, inexperience with construction may also be a cause since Wall One was the first wall constructed by this particular work crew.

Field unit weights exceed those of the Proctor tests, suggesting the compactive effort in the field differed from that in the laboratory tests.

Table 5.2 Summary of Backfill Densities and Moisture Contents

| | Test 1 | Test 2 | Test 3 | Test 4 | Test 5 | Test 6 |
|--------------------|-----------|-----------|-----------|-----------|-----------|-----------|
| No. of Samples | 42 | 21 | 21 | 8 | 8 | 33 |
| Average Unit Wgt. | 108.8 pcf | 108.0 pcf | 108.0 pcf | 105.7 pcf | 105.7 pcf | 104.9 pcf |
| Standard Deviation | 5.1 | 2.0 | 2.0 | 2.4 | 2.4 | 2.4 |
| Average Water % | 11.3 % | 9.6% | 9.6% | 7.5% | 7.5% | 4.4% |
| Standard Deviation | 6.1 | 0.9 | 0.9 | 0.9 | 0.9 | 0.9 |

Note: $\gamma_{dry, \max} = 101.8 \text{ pcf}$ $w_{optimum} = 11.3\%$

CHAPTER VI

TEST DATA AND DATA REDUCTION

Introduction

A total of six full-scale explosive tests were conducted on four geogrid reinforced soil walls between February 17th and August 4th, 1993. Figure 6.1 shows a typical test wall. This chapter includes a summary of test design parameters, instrumentation types, success of data collection efforts, all collected test data and test observations, and initial data reduction. Test data are summarized in tables and individual time history plots of gage recordings are presented in the Appendix C.

Overview of Test Parameters

The only variations in the constructed walls were the weapon standoff distance and reinforcement stiffness as summarized in Table 6.1. The standoff distance is also identified by the variable x , which is also used in Figure 6.2 to show the weapon location for each test. The final overall condition of the wall, or residual condition, is identified under the result column of Table 6.1.

Figure 6.1 Typical Test Wall

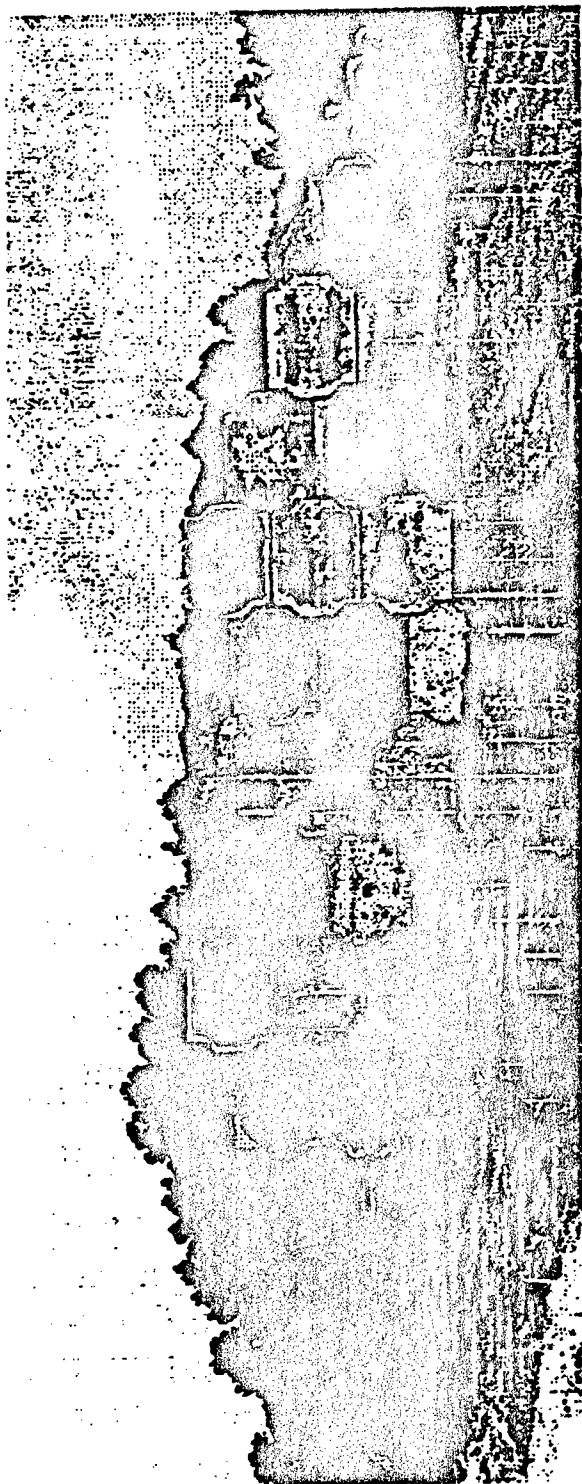


Table 6.1 Test Summary

| | TEST NUMBER | GEOGRID | WEAPON STANDOFF (X) | RESULT |
|------------|-------------|----------|---------------------|----------------|
| WALL ONE | 1 | UX1400HT | 20 ft. | WALL FAILED |
| WALL TWO | 2 | UX1400HT | 30 ft. | WALL SURVIVED |
| WALL TWO | 3 | UX1400HT | 25 ft. | WALL FAILED |
| WALL THREE | 4 | UX1500HT | 30 ft. | WALL SURVIVED |
| WALL THREE | 5 | UX1500HT | 25 ft. | WALL SURVIVED |
| WALL FOUR | 6 | UX1500HT | 20 ft. | 1 PANEL FAILED |

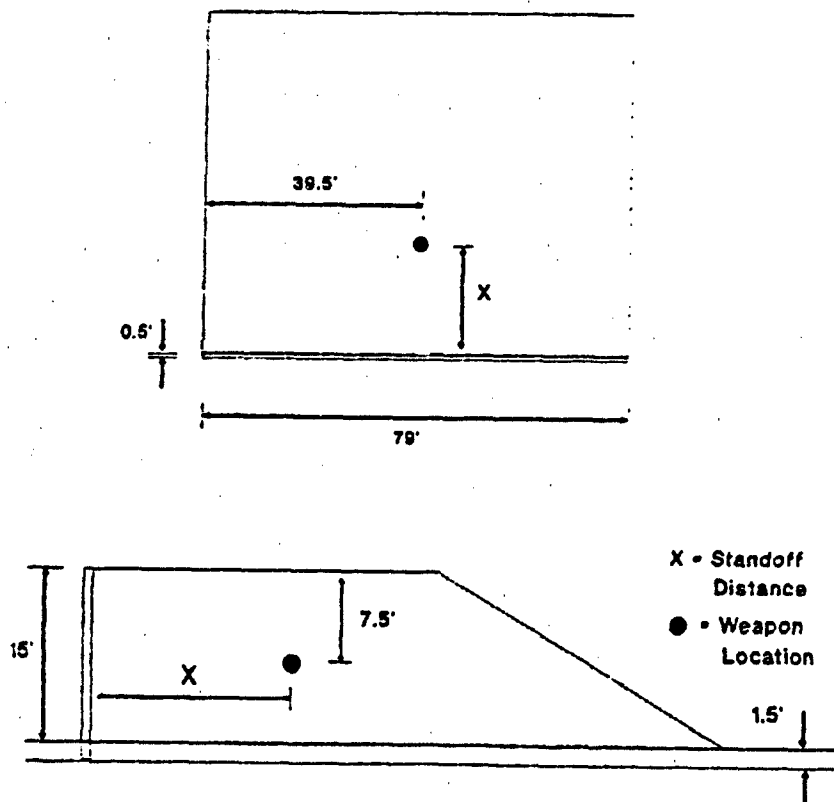


Figure 6.2 Plan and Profile of Weapon Location

Overall Instrumentation Success

Wall panel accelerations, soil/panel interface pressures, geogrid strains and free-field soil pressure gages were used in each test as detailed in Chapter V. Table 6.2 summarizes, for each test and gage, which gages were functional during the tests and if usable data was obtained. A blank cell in Table 6.2 indicates the gage did not work, X denotes gage worked, and X* denotes gage worked but, in the author's judgement, the data was invalid. The prefix designations are as follows:

F = Free-field Pressure Gage A = Accelerometer

S = Strain Gage P = Soil Pressure Interface Gage

After construction of the first wall, and prior to testing, a check of the wires leading to each of the twelve strain gages determined each circuit was broken. Therefore, no strain measurements could be taken during this test. These failures were attributed to construction damage and strain gage installation procedures for subsequent tests were changed as discussed in Appendix A.

The difference between the number of strain gages that survived construction and the number of gages that provided usable data can not be completely accounted for. However, two possible reasons for this difference are proposed. First, there may have been an error in the programming of the data recording system that created an incompatibility between the output of the

Table 6.2 Summary of Gage Operability, All Tests

| | Test 1 | Test 2 | Test 3 | Test 4 | Test 5 | Test 6 |
|-----|--------|--------|--------|--------|--------|--------|
| P1 | X* | X | X | X | X | X* |
| P2 | X | X* | X | X | X | X* |
| P3 | X | X | X | X | X | X* |
| P4 | X | X | X | X | X | X* |
| P5 | X | X | X | X | X | X* |
| P6 | X | X | X | X | X | X* |
| A1 | X | X | X | X | X | X* |
| A2 | X | X | X | X | X | X* |
| A3 | X | X | X | X | X | X* |
| A4 | X | X | X | X | X | X* |
| A5 | X | X | X | X | X | X* |
| A6 | X | X* | X | X | X | X* |
| F1 | X* | X* | X | X | X | X* |
| F2 | X | X | X | X | X | X* |
| F3 | X | X* | X* | X | X | X* |
| S1 | | X* | X* | X | X | X* |
| S2 | | X* | X* | X | X | X* |
| S3 | | X* | X* | X | X | X* |
| S4 | | X* | X* | X | X | |
| S5 | | | X* | X | X | X* |
| S6 | | X* | | X | X* | X* |
| S7 | | X | X | X | | X* |
| S8 | | X | X | X | X | X* |
| S9 | | X | X | | | X* |
| S10 | | X* | X | | | X* |
| S11 | | X | X | X | X | |
| S12 | | X | | X | X | X* |

gage and the recording system. This should not be a problem, but is a potential source of error. Another reason may be complete or partial debonding of the strain gage from the geogrid. In this case, the gage would measure a complete circuit with the appropriate resistance when tested, however it would not measure any geogrid strain.

The number of strain gages providing usable data improved dramatically in Tests 4 and 5. This may be due to two factors: 1) improvement in gage installation quality with experience; and 2) the stiffer UX 1500HT geogrid used in Tests 4 and 5 did not flex as much as the UX 1400HT. A more flexible geogrid may be more prone to separate from the strain gage during installation and handling yet still test as a complete circuit. Also, increasing geogrid flexibility may increase its tendency to distort during installation, and the electrical connections to the strain gages may have broken under this movement.

In either case, careful handling of geogrid mounted with strain gages during installation and construction is important, as is becoming familiar and competent in the procedures of properly installing strain gages on geogrid. In the case of this test, the strain gage installation procedures resulted in an improvement from 0 percent gage survival to over 80 percent gage survival.

In almost every case, the gages that collected unusable data recorded a haphazard arrangement of lines that were clearly distinct from the other gages.

Only two gages that collected unusable data, F1 from Test 1 and F3 from Test 2, recorded clean plots. However, the magnitude of the peak pressures were so great that the data was not considered valid. In Test 6, no usable data was collected due to a major system error in the data recorder.

Test Data

Figures 6.3 through 6.6 show typical data plots for acceleration, soil/panel interface pressure, free-field pressure, and geogrid strain. The data collected from Tests 1 through 5 is summarized in Tables 6.3 through 6.8, respectively. Table 6.3 summarizes the average of the wavespeed measurements in each test. These wavespeeds were used in the Drake-Little equation to predict ground shock pressures at all gage locations within the backfill (Chapter VII).

Table 6.3 Summary of Average Wavespeeds

| | Test 1 | Test 2 | Test 3 | Test 4 | Test 5 | Test 6 |
|-----------------------------|--------|--------|--------|--------|--------|---------|
| Average Wavespeed (ft/sec) | 1065.8 | 1000.4 | 935.3 | 1084.7 | 935.6 | No Data |
| Standard Deviation (ft/sec) | 131.1 | 132.2 | 126.1 | 181.7 | 171.6 | No Data |

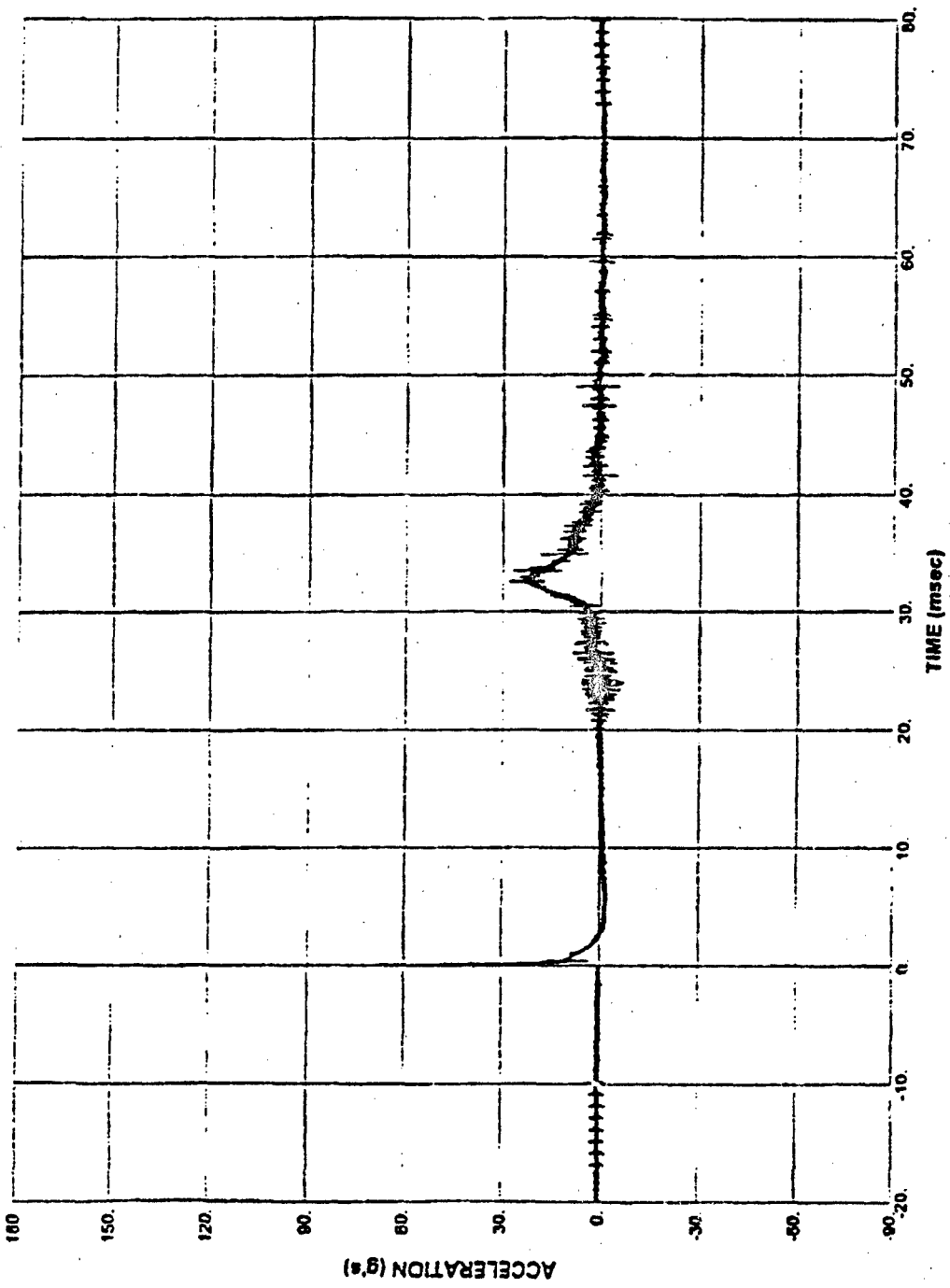


Figure 6.3 Typical Acceleration Record

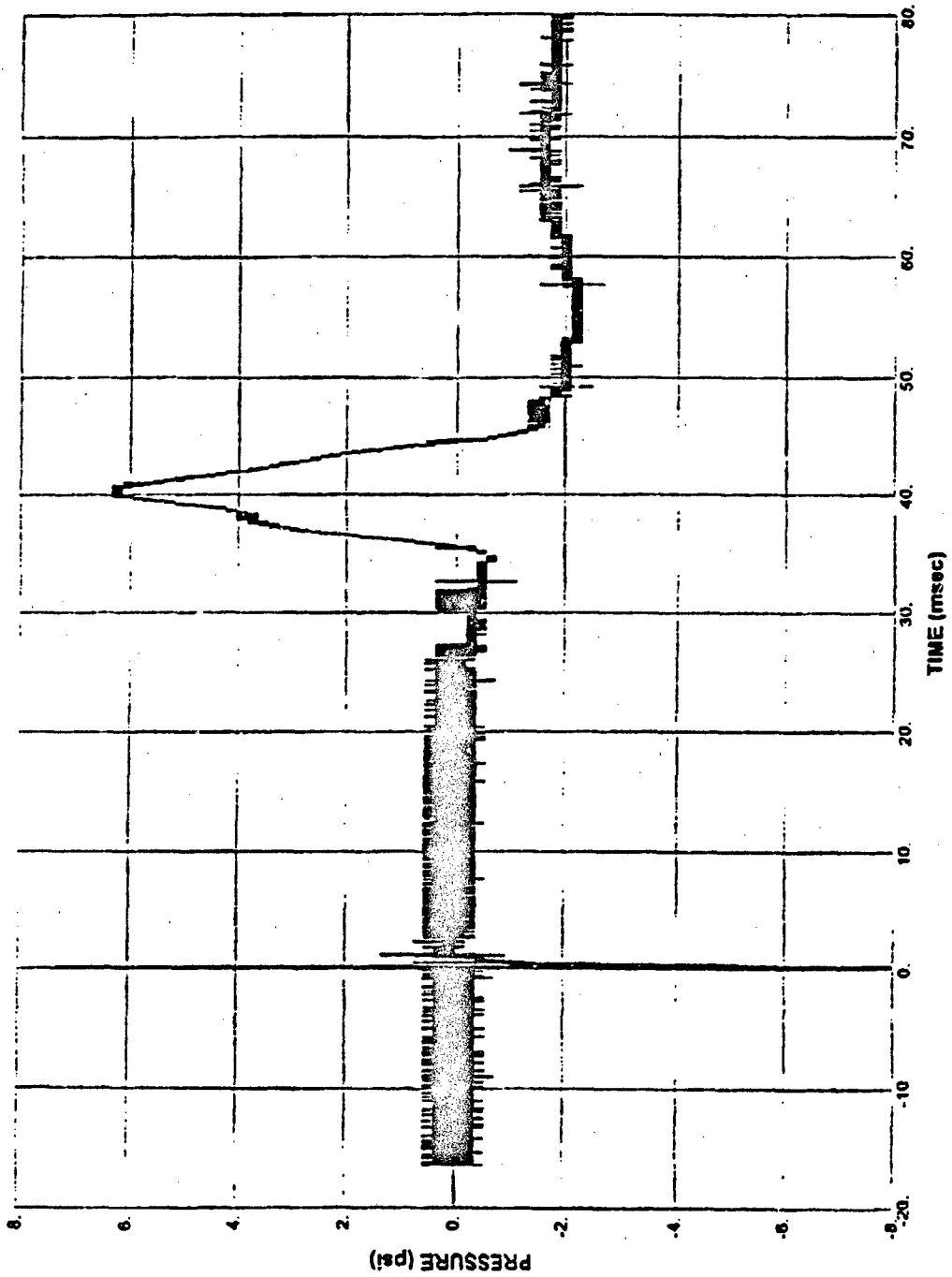


Figure 6.4 Typical Soil/Panel Interface Pressure Record

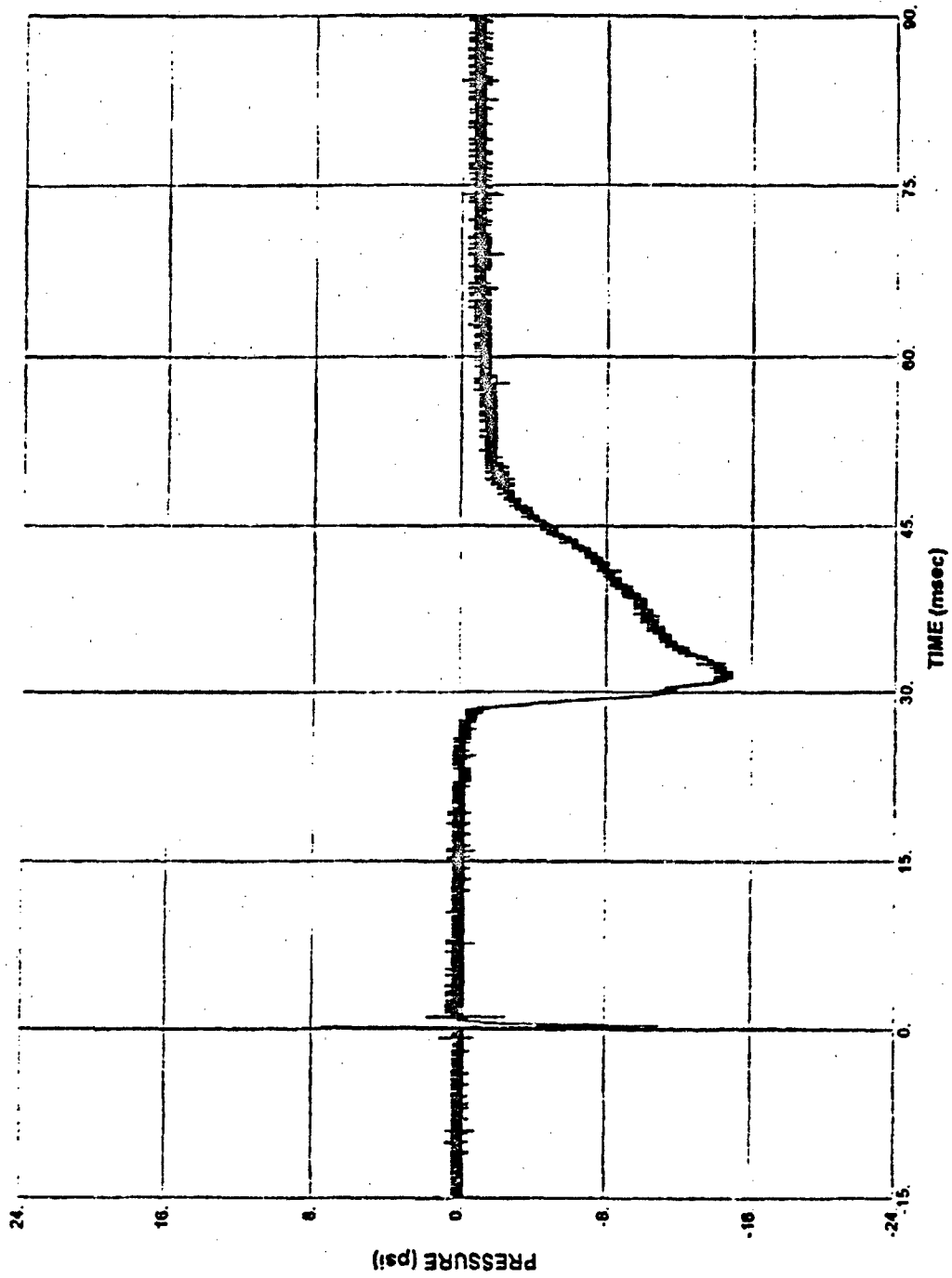


Figure 6.5 Typical Free-field Pressure Record

106

ADA293552

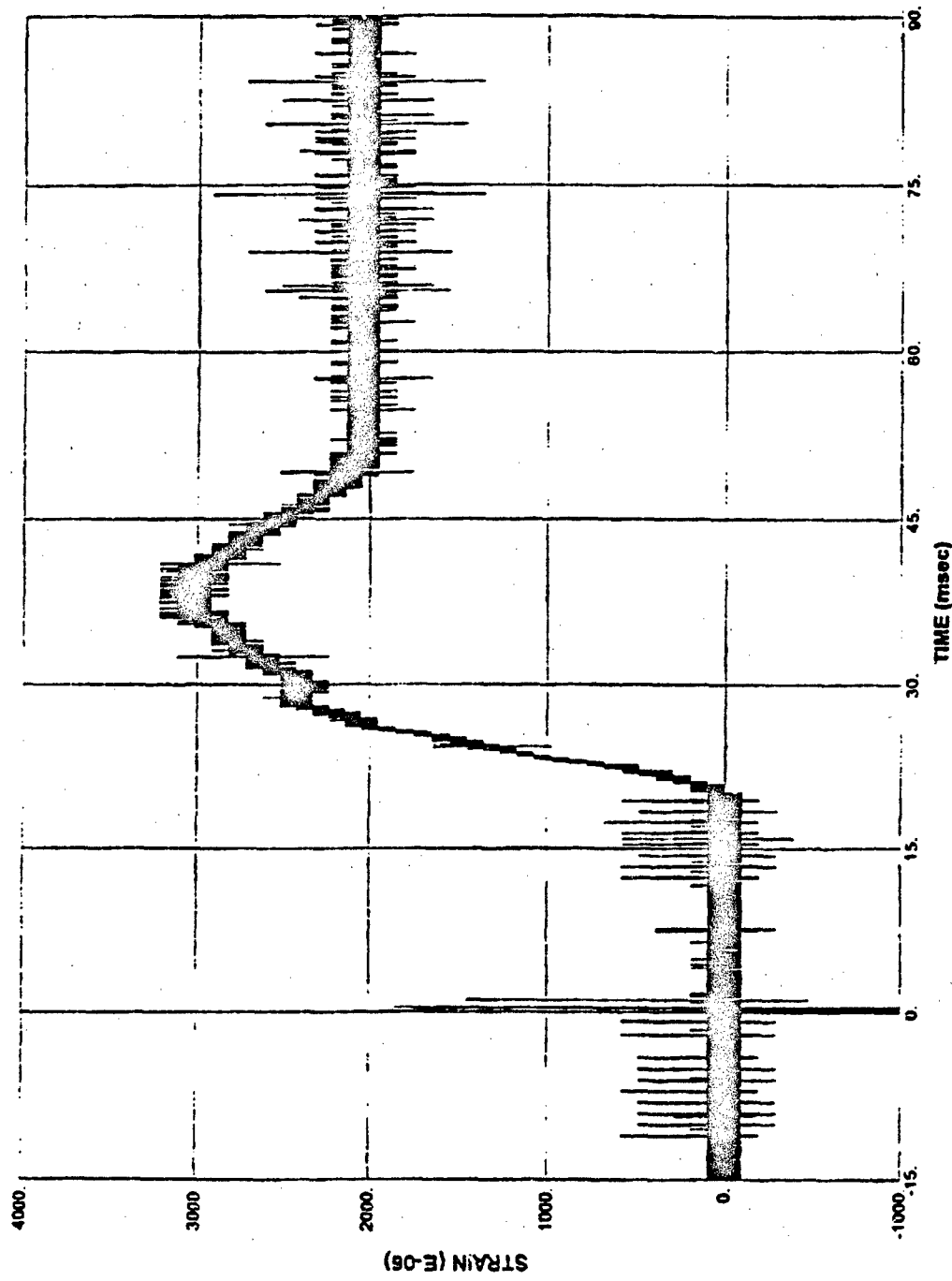


Figure 6.6 Typical Strain Gage Record

Table 6.4 Wall One, Test One Data

| Gage Number | Distance From Explosion (ft) | Peak Pressure (psi) | Arrival Time (ms) | Wavespeed (ft/sec) |
|-------------|------------------------------|---------------------|-------------------|--------------------|
| P1 | 20.6 | No data | No data | No data |
| P2 | 20.0 | 4.8 | 20.7 | 966.2 |
| P3 | 20.6 | 7.2 | 18.5 | 1113.5 |
| P4 | 21.0 | 3.4 | 24.0 | 875.0 |
| P5 | 21.0 | 37.9 | 19.7 | 1066.0 |
| P6 | 23.3 | 2.0 | 25.0 | 932.0 |
| F1 | 17.6 | 99.5 | 14.1 | 1248.2 |
| F2 | 16.6 | 174.3 | 13.0 | 1276.9 |
| F3 | 15.9 | 409.6 | 12.0 | 1325.0 |

| Gage Number | Distance From Explosion (ft) | Peak Acceleration (g's) | Arrival Time (ms) | Wavespeed (ft/sec) |
|-------------|------------------------------|-------------------------|-------------------|--------------------|
| A1 | 20.6 | 28 | 21.1 | 976.3 |
| A2 | 20.0 | 40 | 19.0 | 1052.6 |
| A3 | 20.6 | 90 | 18.5 | 1113.5 |
| A4 | 21.0 | 26 | 21.7 | 967.7 |
| A5 | 21.0 | 88 | 20.4 | 1029.4 |
| A6 | 23.3 | 20 | 23.8 | 979.0 |

Table 6.5 Wall Two, Test Two Data

| Gage Number | Distance From Explosion (ft) | Peak Pressure (psi) | Arrival Time (ms) | Wavespeed (ft/sec) |
|-------------|------------------------------|---------------------|-------------------|--------------------|
| P1 | 30.4 | 7.1 | 32.9 | 924.0 |
| P2 | 30.0 | No Data | No Data | No Data |
| P3 | 30.4 | 2.9 | 32.6 | 932.5 |
| P4 | 30.7 | 0.61 | 38.6 | 795.3 |
| P5 | 30.7 | 1.27 | 32.7 | 938.8 |
| P6 | 32.3 | 7.0 | 35.1 | 920.2 |
| F1 | 25.0 | 88,520 | 28.4 | 880.3 |
| F2 | 26.0 | 17.9 | 25.3 | 1027.7 |
| F3 | 27.5 | No Data | No Data | No Data |

| Gage Number | Distance From Explosion (ft) | Peak Acceleration (g's) | Arrival Time (ms) | Wavespeed (ft/sec) |
|-------------|------------------------------|-------------------------|-------------------|--------------------|
| A1 | 30.4 | 20 | 29.7 | 1023.6 |
| A2 | 30.0 | 6 | 31.6 | 949.4 |
| A3 | 30.4 | 4.5 | 32.1 | 947.0 |
| A4 | 30.7 | 15.8 | 33.2 | 924.7 |
| A5 | 30.7 | 16 | 33.5 | 916.4 |
| A6 | 32.3 | No Data | No Data | No Data |

| Gage Number | Distance From Explosion (ft) | Compressive Strain (μS) | Net Strain (μS) | Arrival Time (ms) | Wavespeed (ft/sec) |
|-------------|------------------------------|--------------------------------------|------------------------------|-------------------|--------------------|
| S1-6, 10 | No Data | No Data | No Data | No Data | No Data |
| S7 | 27.9 | 4089.3 | 2434.1 | 20.7 | 1347.8 |
| S8 | 27.1 | 4332.7 | 4332.7 | 24.4 | 1110.7 |
| S9 | 26.2 | 2434.1 | 1849.9 | 26.2 | 1000.0 |
| S11 | 27.5 | 3991.9 | 3699.8 | 23.0 | 1195.7 |
| S12 | 26.6 | 2774.8 | 2774.8 | 22.7 | 1171.8 |

Table 6.6 Wall Two, Test Three Data

| Gage Number | Distance From Explosion (ft) | Peak Pressure (psi) | Arrival Time (ms) | Wavespeed (ft/sec) |
|-------------|------------------------------|---------------------|-------------------|--------------------|
| P1 | 25.5 | 1.7 | 31.2 | 817.3 |
| P2 | 25.0 | 10.2 | 34.2 | 731.0 |
| P3 | 25.5 | 42.7 | 30.0 | 850.0 |
| P4 | 25.8 | 15.8 | 37.7 | 684.4 |
| P5 | 25.8 | 11.6 | 31.7 | 813.9 |
| P6 | 27.7 | 13.0 | 29.3 | 945.4 |
| F1 | 22.5 | 14.1 | 25.9 | 868.7 |
| F2 | 21.0 | 20.4 | 22.0 | 954.6 |
| F3 | 20.0 | No Data | No Data | No Data |

| Gage Number | Distance From Explosion (ft) | Peak Acceleration (g's) | Arrival Time (ms) | Wavespeed (ft/sec) |
|-------------|------------------------------|-------------------------|-------------------|--------------------|
| A1 | 25.5 | 3.5 | 27.0 | 944.4 |
| A2 | 25.0 | 10.2 | 27.7 | 902.5 |
| A3 | 25.5 | 20.0 | 22.8 | 1118.4 |
| A4 | 25.8 | 12.1 | 28.9 | 892.7 |
| A5 | 25.8 | 22.3 | 27.0 | 955.6 |
| A6 | 27.7 | 20.7 | 31.1 | 890.7 |

| Gage Number | Distance From Explosion (ft) | Compressive Strain (μ S) | Net Strain (μ S) | Arrival Time (ms) | Wavespeed (ft/sec) |
|-------------|------------------------------|-------------------------------|-----------------------|-------------------|--------------------|
| S1-6, 12 | No Data | No Data | No Data | No Data | No Data |
| S7 | 23.0 | 4186.8 | 4186.8 | 21.5 | 1069.8 |
| S8 | 22.2 | 5355.0 | 4478.8 | 19.8 | 1121.2 |
| S9 | 21.3 | 6523.4 | 4478.8 | 18.5 | 1151.4 |
| S10 | 23.4 | 5841.9 | 5160.3 | 23.1 | 1013.0 |
| S11 | 22.7 | 5257.7 | 4673.5 | 21.7 | 1046.1 |

Table 6.7 Wall Three, Test Four Data

| Gage Number | Distance From Explosion (ft) | Peak Pressure (psi) | Arrival Time (ms) | Wavespeed (ft/sec) |
|-------------|------------------------------|---------------------|-------------------|--------------------|
| P1 | 30.4 | 1.3 | 38.0 | 800.0 |
| P2 | 30.0 | 8.6 | 31.5 | 952.4 |
| P3 | 30.4 | 34.3 | 31.3 | 971.3 |
| P4 | 30.7 | 6.7 | 34.7 | 884.7 |
| P5 | 30.7 | 6.9 | 34.7 | 884.7 |
| P6 | 32.3 | 5.4 | 33.6 | 961.3 |
| F1 | 27.8 | 14.1 | 28.4 | 978.9 |
| F2 | 25.6 | 15.4 | 25.8 | 992.2 |
| F3 | 25.0 | 21.6 | 23.9 | 1046.0 |

| Gage Number | Distance From Explosion (ft) | Compressive Strain (μS) | Net Strain (μS) | Arrival Time (ms) | Wavespeed (ft/sec) |
|-------------|------------------------------|--------------------------------------|------------------------------|-------------------|--------------------|
| S9-10 | No Data | No Data | No Data | No Data | No Data |
| S1 | 27.8 | 2190.6 | 924.9 | 21.5 | 1293.0 |
| S2 | 27.0 | 3115.7 | 2142.0 | 20.3 | 1330.1 |
| S3 | 26.1 | 4284.0 | 2920.9 | 18.9 | 1381.0 |
| S4 | 27.9 | 2385.4 | 1898.6 | 21.6 | 1291.7 |
| S5 | 27.0 | 2969.3 | 2093.0 | 20.5 | 1317.1 |
| S6 | 26.2 | 3894.6 | 2628.8 | 20.1 | 1303.5 |
| S7 | 28.1 | 1654.9 | 1265.4 | 23.8 | 1180.7 |
| S8 | 27.2 | 2921.2 | 2142.2 | 21.7 | 1253.4 |
| S11 | 27.6 | 2433.5 | 1703.9 | 21.4 | 1289.7 |
| S12 | 26.8 | 3213.0 | 2044.7 | 20.6 | 1301.0 |

| Gage Number | Distance From Explosion (ft) | Peak Acceleration (g's) | Arrival Time (ms) | Wavespeed (ft/sec) |
|-------------|------------------------------|-------------------------|-------------------|--------------------|
| A1 | 30.4 | 4.4 | 32.0 | 950.0 |
| A2 | 30.0 | 9.3 | 32.2 | 931.7 |
| A3 | 30.4 | 14.6 | 28.2 | 1078.0 |
| A4 | 30.7 | 13.1 | 36.0 | 852.8 |
| A5 | 30.7 | 34.9 | 31.7 | 968.5 |
| A6 | 32.3 | 12.5 | 35.0 | 922.9 |

Table 6.8 Wall Three, Test Five Data

| Gage Number | Distance From Explosion (ft) | Peak Pressure (psi) | Arrival Time (ms) | Wavespeed (ft/sec) |
|-------------|------------------------------|---------------------|-------------------|--------------------|
| P1 | 25.5 | 2.2 | 37.0 | 689.2 |
| P2 | 25.0 | 4.8 | 34.0 | 735.3 |
| P3 | 25.5 | 45.7 | 26.7 | 955.1 |
| P4 | 25.8 | 2.5 | 40.4 | 638.6 |
| P5 | 25.8 | 9.0 | 31.0 | 832.3 |
| P6 | 27.7 | 4.8 | 37.3 | 742.6 |
| F1 | 22.8 | 21.5 | 25.4 | 897.6 |
| F2 | 20.6 | 37.0 | 23.0 | 895.6 |
| F3 | 20.2 | 49.7 | 19.2 | 1047.7 |

| Gage Number | Distance From Explosion (ft) | Peak Acceleration (g's) | Arrival Time (ms) | Wavespeed (ft/sec) |
|-------------|------------------------------|-------------------------|-------------------|--------------------|
| A1 | 25.5 | 16.0 | 34.3 | 743.4 |
| A2 | 25.0 | 8.4 | 28.8 | 868.1 |
| A3 | 25.5 | 31.4 | 24.5 | 1040.8 |
| A4 | 25.8 | 9.1 | 36.2 | 712.7 |
| A5 | 25.8 | 49.6 | 28.3 | 911.7 |
| A6 | 27.7 | 12.3 | 31.2 | 887.8 |

| Gage Number | Distance From Explosion (ft) | Compressive Strain (μ S) | Tensile Strain (μ S) | Net Strain (μ S) | Arrival Time (ms) | Wavespeed (ft/sec) |
|-------------|------------------------------|-------------------------------|---------------------------|-----------------------|-------------------|--------------------|
| S6-7,9-10 | No Data | No Data | No Data | No Data | No Data | No Data |
| S1 | 22.8 | 2823.1 | 7107.5 | -476.7 | 20.2 | 1128.7 |
| S2 | 22.0 | 5647.2 | 0 | 3213.1 | 18.5 | 1189.2 |
| S3 | 21.1 | 4673.5 | 0 | 4673.5 | 17.4 | 1212.7 |
| S4 | 22.9 | 4235.4 | 6036.6 | -1605.5 | 20.5 | 1117.1 |
| S5 | 20.0 | 584.2 | 876.3 | 0 | 22.1 | 905.0 |
| S8 | 22.3 | 4868.2 | 0 | 3213.0 | 19.3 | 1155.4 |
| S11 | 22.8 | 4040.6 | 0 | 2385.4 | 20.4 | 1117.7 |
| S12 | 22.0 | 3310.4 | 0 | 2142.0 | 20.0 | 1100.0 |

High Speed Film

All tests were filmed with a high speed camera as discussed in Chapter V.

The film from Test 1 was overexposed, and therefore only video recordings of the test were obtained. The Test 1 high speed film was overexposed due to a change in the natural lighting between the time the camera settings were made and detonation. Setting of the camera aperture had to be completed before final arming of the weapon, and in this case some cloud cover cleared prior to the test event.

Review of the high speed film from Tests 2 through 5, in concert with a review of the other test data lead to an interesting discovery. The information presented from previous full and model-scale tests suggests wall displacements were caused by the blast pressure wave. Based on an assumed soil wavespeed of 1000 ft/sec, it was anticipated the pressure wave data would be collected starting at 20 to 30 milliseconds after detonation, depending upon standoff distance. Therefore, the data recording system was set to receive data for 105 ms after detonation, providing a factor of safety of three to four for receiving the pressure wave data. Gage data collected shows pressures, accelerations and strains all being received in that time span and the gage readings return to zero before the data recorders shut down. Based on the data collected and post-test visual observations, the residual wall displacements were assumed to have been

caused by the pressure wave. However, the high speed film proves that assumption to be incorrect.

When viewing the high speed film, a timing light flashes on the screen every millisecond. Careful review of the film from Tests 2 through 5 and observation of the timing light, it was noted that even after 100 milliseconds no observable wall motion had taken place. Even though the pressure wave had passed and the wall panel accelerations were as large as 90 g's, wall motion was not evident. It was not until more than 200 milliseconds after detonation that wall motion began. This simple observation leads the author to suggest that two loading mechanisms act on the wall from an explosion.

The first loading mechanism is suggested to be the pressure wave generated by the explosion in the backfill. The second is the pressure caused by the expanding cavity or cratering of the soil. This cavity expansion can be thought of as a crater formed in two directions, vertical and lateral. The bombs were covered with 7.5 ft. of soil, and in the lateral dimension, 20, 25, or 30 ft. of soil separated the bomb from the wall face. The cavity expansion pressure followed the path of least resistance, and therefore the main crater was formed above the bomb. However, the wall face was close enough to the bomb such that the cratering forces also impinged on the wall face. Based on post-test observations, the two tests conducted at a 30-ft. standoff distance caused little

deformation of the wall face, so this two dimensional cratering effect was most pronounced at standoff distances less than 30 ft.

In general terms, the explosive pressure wave moves through the soil at approximately 1000 ft/sec and impacts the wall. While this is taking place the explosive crater is still not fully developed. In relative terms the crater develops slowly (Henrych, 1979). However, the expanding gases forming the surface crater also displace the soil in the lateral direction, and this causes the soil, geogrid reinforcement and wall panels to move laterally.

Therefore, the data presented in this chapter characterize the response of the test walls to the explosive pressure wave, and the more significant pressure caused by the expanding gas cavity will be evaluated via scaled test data in Chapter VIII. Scaled test data provides an example of the relationship between acceleration, velocity and displacement, as well as pressure and impulse from the respective loading mechanisms as shown in Figs. 6.7 and 6.8. As may be seen from the centrifuge data in Fig. 6.7, initial inertial pressures arrive at approximately 3 ms after detonation. Since time scales as $1/n$ in the centrifuge, at 30 g's this arrival time corresponds to 90 ms at prototype scale. Impulse pressures increase significantly at 4 to 5 ms, which is 120 to 150 ms at prototype scale. Significant motion of the wall panels was observed on the high speed film at a time of approximately 200 ms after detonation, which corresponds well with the centrifuge gage data. This level of agreement

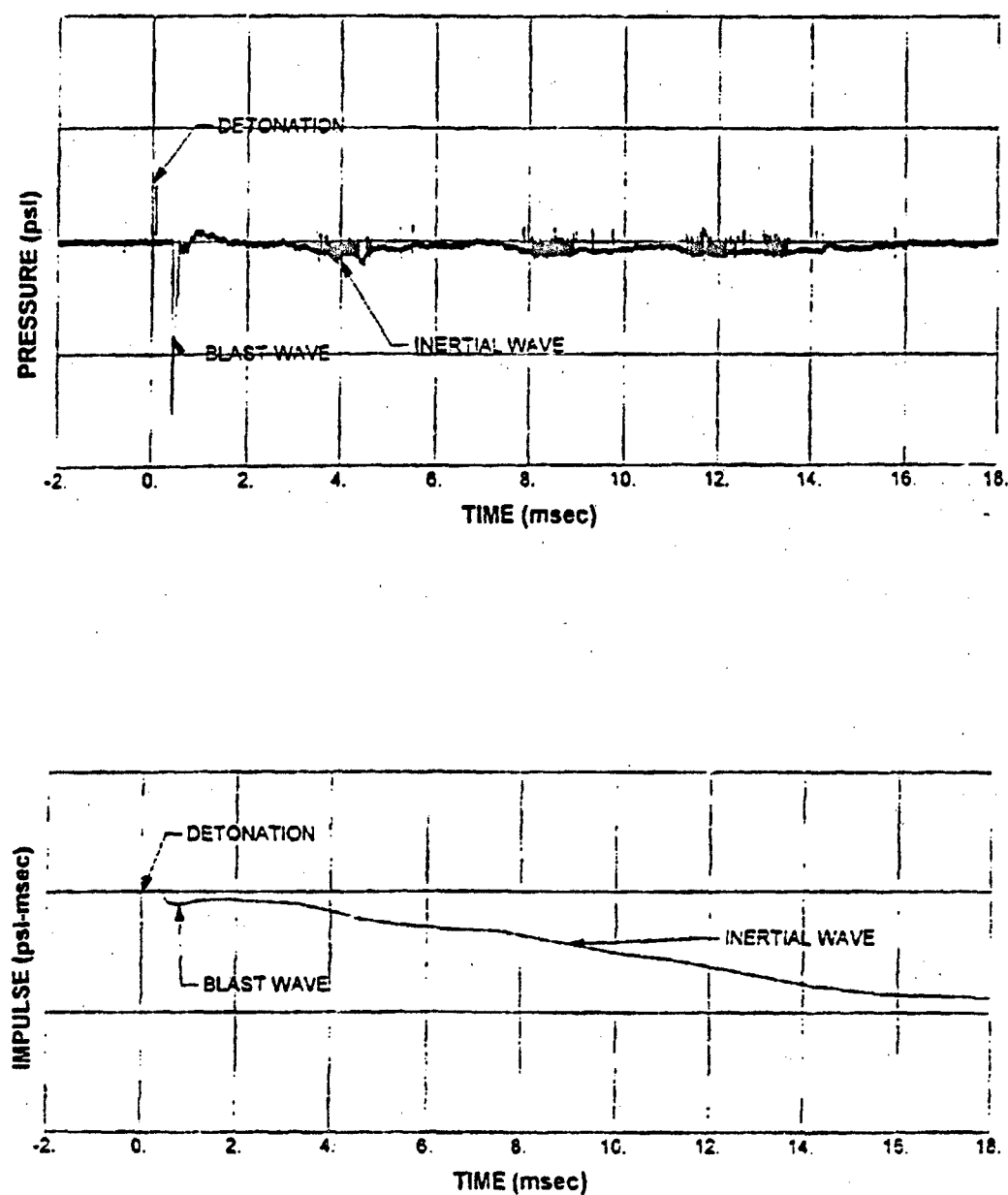


Figure 6.7 Pressure and Impulse From Blast Wave and Inertial Wave Loading,
Centrifuge Test Data

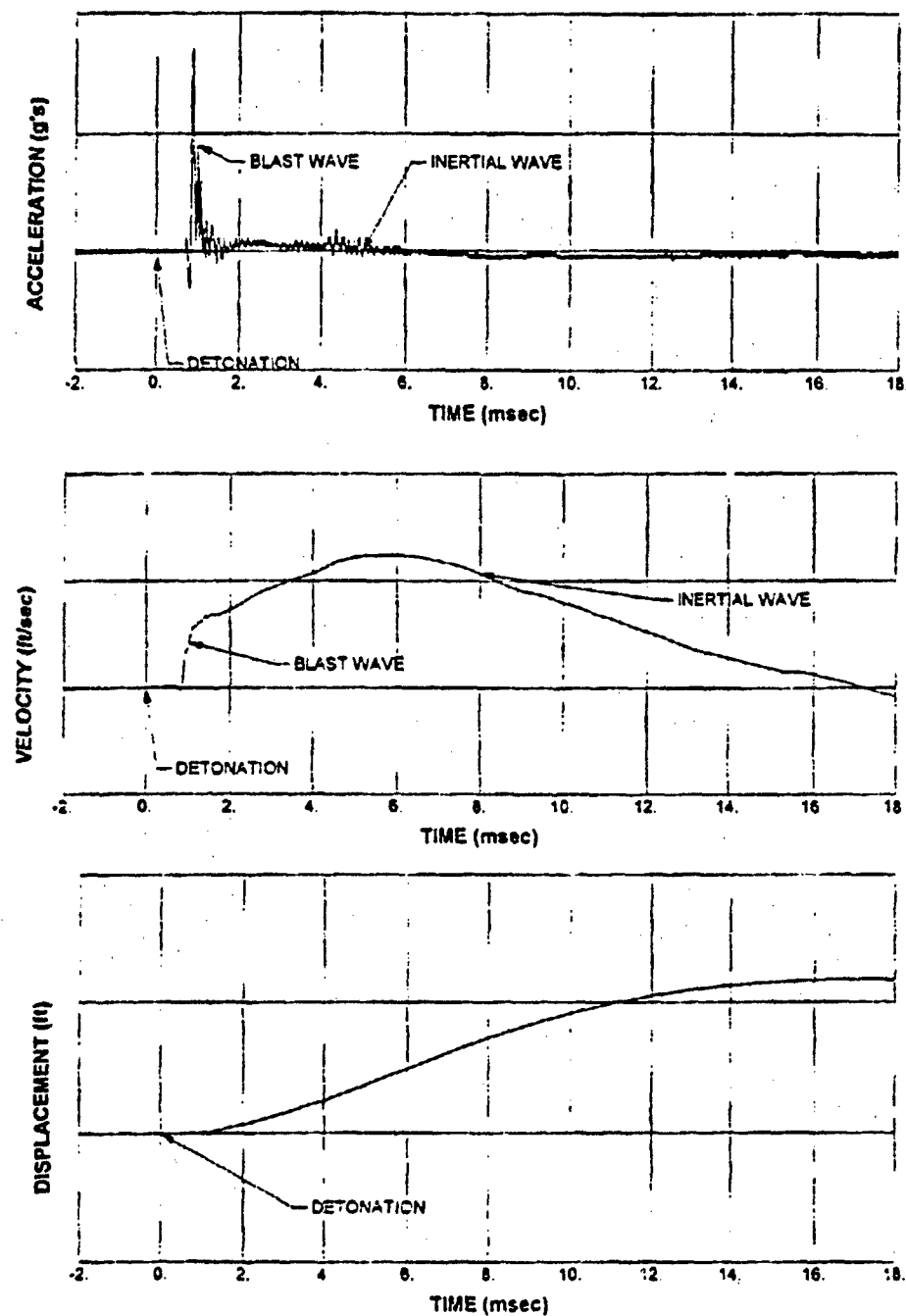


Figure 6.8 Acceleration, Velocity and Displacement From Blast and Inertial Wave, Centrifuge Test Data

suggests the scaled data may have measured the response of the walls to the inertial pressure wave.

Effect of Reinforcement Stiffness

One of the primary objectives of this test series was to evaluate how changes in geogrid reinforcement stiffness affect wall panel displacements. Prior to testing it was assumed residual displacements were caused by the incident pressure wave. After reviewing the test data and high speed film, it is evident that the movement of the wall panels is caused by the lateral movement of the soil during the explosive crater cavity expansion. Since the data were not collected for a long enough period of time, no data exists to quantify the change in wall panel displacements as a function of reinforcement stiffness.

Lacking quantitative data, some qualitative observations can be made based on post-test photographs. Figures 6.9 and 6.10 are post-test photographs of Tests 2 and 4, respectively. Both walls were tested at 30 ft. explosion standoff distances, one reinforced with UX 1400HT geogrid (Fig. 6.9), the other with UX 1500HT geogrid. In both tests, little residual displacement was observed.

Figures 6.11 and 6.12 are post-test photographs of Tests 3 and 5, respectively. Both were tested at a weapon standoff of 25 ft. The wall reinforced with the UX 1400HT (Fig. 6.11) geogrid completely failed and only

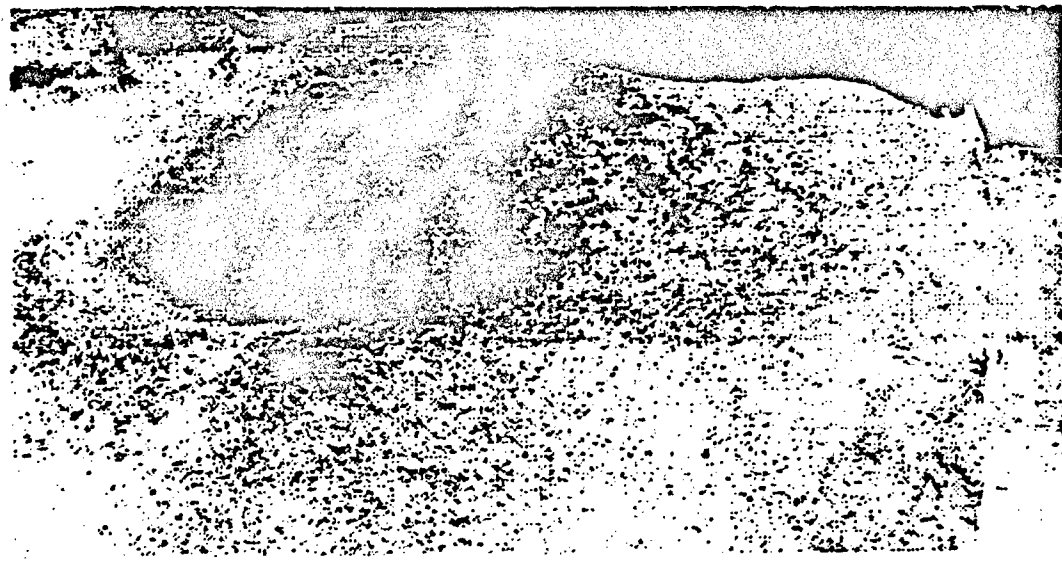


Figure 6.9 Test Two (Post-test) 30 ft Standoff, UX 1400 HT



Figure 6.10 Test Four (Post-test) 30 ft Standoff, UX 1500 HT



Figure 6.11 Test Three (Post-test) 25 ft Standoff, UX 1400 HT

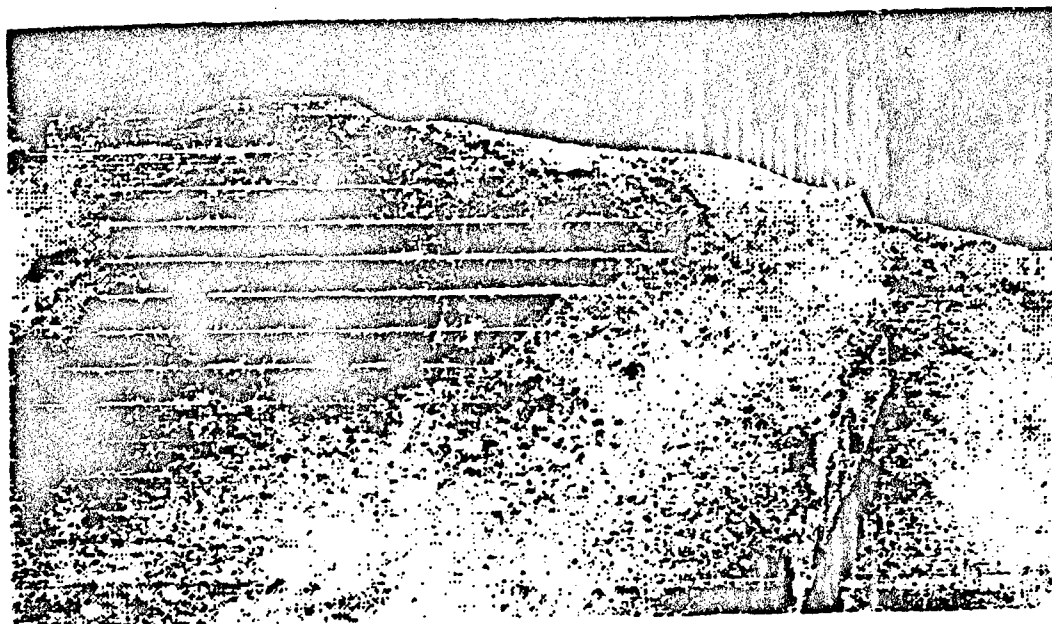


Figure 6.12 Test Five (Post-test) 25 ft Standoff, UX 1500 HT

portions of the wing walls remained standing. At the same standoff distance, the wall reinforced with the UX 1500HT geogrid remained standing, although lateral displacements of Panel One were observed to be approximately one ft.

Figures 6.13 and 6.14 show post-test photographs for Tests 1 and 6, respectively. At a standoff distance of 20 ft, the wall reinforced with UX 1400HT geogrid (Fig. 6.13) failed. The wing walls remained in place, but the center section was completely failed. With the UX 1500HT geogrid, only one wall panel failed. Panel One failed when the top layer of geogrid lost its confining soil. The lower layer of geogrid remained in place, so the panel rotated 180 degrees and came to rest face to face with Panel Two, hanging by one layer of geogrid.

Based on these observations, the hypothesis that wall panel displacement is reduced when geogrid stiffness is increased, all other factors being equal, is qualitatively shown to be valid.

Ground Shock Coupling Factor

The preceding sections have summarized all measurements made during this test series. Other necessary data necessary for data analysis include the ground shock coupling factor and charge weight.



Figure 6.13 Test One (Post-test) 20 ft Standoff, UX 1400 HT



Figure 6.14 Test Six (Post-test) 20 ft Standoff, UX 1500 HT

The magnitude of ground motions and stresses initiated by an explosion is enhanced as the weapon penetrates more deeply into the soil. The coupling factor f is defined as the ratio of the ground shock magnitude from a partially buried or shallow-buried weapon (near surface burst), to that from a fully buried weapon (contained burst) in the same medium (Drake, et al., 1989). This parameter is used as a reduction factor applied to ground shock for a contained detonation to account for the effects of a shallow weapon detonation depth. Figure 6.15 shows the ground shock coupling factor as a function of scaled depth of explosion for air, soil and concrete. For this test series, the depth of explosion (d) is 7.5 ft. and the weight of charge (W) is 192 lbs. From Fig. 6.15 this yields a ground shock coupling factor of 0.99 for all tests, or that the maximum ground shock magnitude will be generated. In Chapter VII both the charge weight and ground shock coupling factor will be necessary for the estimation of free-field soil pressures.

Failure Mechanisms

In Tests 1 and 3, complete failure of numerous wall panels was observed, but geogrid rupture was not observed in either test. The soil, geogrid and wall panels all appeared to move as one unit under the influence of the cavity expansion pressure. However, as shown in the post-test photographs, the wall

panels exhibited differential lateral displacement relative to one another. In each of the cases where failure was observed, the panels at the base of the wall (especially Panel Three) moved outward. The panels above the lower panels did not move out as much, and the upper panels to lose their underlying support. The backfill began to spill out, causing the geogrid to lose its confining soil and, in concert with the loss of support from the lower panels, caused failure of the walls. Further detail on loading and failure mechanisms are discussed in Chapter VIII.

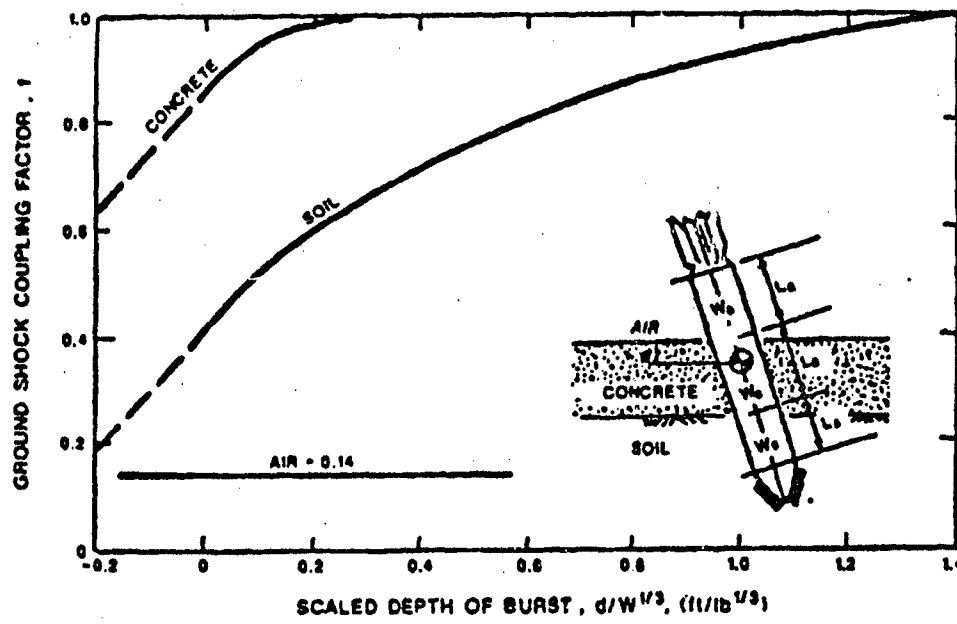


Figure 6.15 Ground Shock Coupling Factor as a Function of Scaled Depth of Burst for Air, Soil and Concrete (Drake, et al, 1989)

Data Reduction

From the data obtained in this test series, the wall panel velocities, displacements and impulses will be established for free-field blast pressures. Free-field pressure data are used to determine the attenuation coefficient of the backfill soil, which in turn is applied to calculate the free-field pressure environment at any point in the retained backfill. These data are then reviewed for consistency and to determine if any unique relationships exist between any of the categories of data. Following that initial investigation, these data are applied in Chapter VII toward the validation of an equation of motion for the walls in this test series.

Wall Panel Peak Velocities and Displacements

In each test the acceleration as a function of time was recorded for six wall panels. Acceleration data were recorded for approximately 100 ms, capturing panel acceleration caused by the pressure wave. Initial wall panel acceleration occurred between 18.5 to 36 ms after detonation, depending upon weapon standoff distance and soil wavespeed, and typically returned to zero within approximately 15 ms after the initial arrival. Through integration of this portion of the curve, maximum panel velocity is obtained. Maximum velocity occurs when the acceleration returns to zero; therefore peak acceleration and

maximum velocity do not occur simultaneously. Double integration of the acceleration curve yields an estimation of wall panel displacement from the blast pressure wave. The integrations were performed using the computer program DPLOT/W (Hyde, undated), and are summarized in Table 6.9.

Displacement values are very small, but are consistent and within an order of magnitude of each other. Double integration of acceleration provides approximate displacements but their very small values suggests failure was not a result of the blast pressure wave loading. These displacements were also too small to be observed from the high speed film.

Panel Impulse Loads

Soil pressure interface gages measured the transmitted stress to Panels No. 1-6 for each of the tests. The panel numbering was detailed in Fig. 5.3. The area under the pressure time history curve is defined as impulse, and Table 6.10 shows the results of the integration of each soil interface pressure curve. Determination of impulse allows for consideration of both load amplitude and duration. Since it appears the free-field blast pressure wave caused only minimal displacements of the wall panels, the interface stress values will not be used in subsequent analysis.

Table 6.9 Peak Panel Accelerations, Velocities, and Displacements, All Tests

| Test Number | Gage Number | Peak Acceleration (g's) | Velocity (ft/sec) | Displacement (in) |
|-------------|-------------|----------------------------|----------------------|-------------------|
| 1 | A1 | 28 | 0.172 | 0.017 |
| 1 | A2 | 40 | 0.0727 | 0.007 |
| 1 | A3 | 90 | 0.2087 | 0.0053 |
| 1 | A4 | 26 | 0.1319 | 0.0073 |
| 1 | A5 | 88 | 0.1390 | 0.003 |
| 1 | A6 | 20 | 0.0557 | 0.0016 |
| 2 | A1 | 20 | 0.1092 | 0.0082 |
| 2 | A2 | 6 | 0.0419 | 0.0046 |
| 2 | A3 | 4.5 | 0.0174 | 0.0005 |
| 2 | A4 | 15.8 | 0.0747 | 0.0048 |
| 2 | A5 | 16 | 0.0675 | 0.0053 |
| 3 | A1 | 3.5 | 0.0088 | 0.0015 |
| 3 | A2 | 10.2 | 0.1006 | 0.0088 |
| 3 | A3 | 20.0 | 0.0839 | 0.0010 |
| 3 | A4 | 12.1 | 0.0711 | 0.0039 |
| 3 | A5 | 22.3 | 0.1127 | 0.0078 |
| 3 | A6 | 20.7 | 0.0892 | 0.0044 |
| 4 | A1 | 4.4 | 0.0363 | 0.0005 |
| 4 | A2 | 9.3 | 0.0589 | 0.0037 |
| 4 | A3 | 15.1 | 0.0930 | 0.0074 |
| 4 | A4 | 13.1 | 0.0872 | 0.0056 |
| 4 | A5 | 34.9 | 0.2108 | 0.0123 |
| 4 | A6 | 12.5 | 0.0664 | 0.0045 |
| 5 | A1 | 16 | 0.0402 | 0.0247 |
| 5 | A2 | 8.4 | 0.0650 | 0.0244 |
| 5 | A3 | 31.4 | 0.1369 | 0.0158 |
| 5 | A4 | 9.1 | 0.0504 | 0.0245 |
| 5 | A5 | 49.6 | 0.1889 | 0.0068 |
| 5 | A6 | 12.3 | 0.0504 | 0.0056 |

Table 6.10 Summary of Interface Pressure and Impulse

| Test Number | Gage Number | Peak Pressure (psi) | Impulse (psi-sec) |
|-------------|-------------|------------------------|----------------------|
| 1 | P2 | 4.8 | 0.0125 |
| 1 | P3 | 7.2 | 0.0161 |
| 1 | P4 | 3.4 | 0.0039 |
| 1 | P5 | 37.9 | 0.0910 |
| 2 | P1 | 7.1 | 0.0235 |
| 2 | P3 | 2.9 | 0.0106 |
| 2 | P4 | 0.61 | 0.0018 |
| 2 | P6 | 7.0 | 0.0234 |
| 3 | P1 | 1.7 | 0.0126 |
| 3 | P2 | 10.2 | 0.0466 |
| 3 | P3 | 42.7 | 0.3310 |
| 3 | P4 | 15.8 | 0.0502 |
| 3 | P5 | 11.6 | 0.0485 |
| 3 | P6 | 13.0 | 0.0927 |
| 4 | P1 | 1.3 | 0.0162 |
| 4 | P2 | 8.6 | 0.0454 |
| 4 | P3 | 34.3 | 0.1613 |
| 4 | P4 | 6.7 | 0.0368 |
| 4 | P5 | 6.9 | 0.0206 |
| 4 | P6 | 5.4 | 0.0217 |
| 5 | P1 | 2.2 | 0.029 |
| 5 | P2 | 4.8 | 0.0217 |
| 5 | P3 | 45.7 | 0.2891 |
| 5 | P4 | 2.5 | 0.0088 |
| 5 | P5 | 9.0 | 0.0334 |
| 5 | P6 | 4.8 | 0.0138 |

Prediction of Compressive Wave Stress Within the Retained Backfill

Because there was a limit on the total number of gages that could be used in each test, free-field pressure measurements could not be made at every wall panel or at every strain gage location. The following sections will present how free-field pressures may be estimated at any point in the soil backfill. In each test, three free-field gages measured the stress-history of the compressive wave in the backfill. These measurements will be used to backcalculate soil compressive wave speed and the attenuation coefficient (n) via Eq. 2.1. Once the attenuation coefficient is established for each test, it will be used in Eq. 2.1 with the average wavespeed from all gage measurements to estimate free-field pressure at each free-field pressure gage location. These calculated and measured values of free-field pressure will be compared to establish the viability of this method for free-field stress predictions. Equation 2.1 will then be used to predict free-field pressures at every instrumented panel and strain gage location.

Attenuation Coefficient

The Drake-Little equation (Eq. 2.1) can be used to establish the attenuation coefficient for the soil in each test. Equation 2.1 can be rearranged in the following manner to determine the attenuation coefficient (n):

$$\log P - \log \rho c f \frac{160}{144} = -n \log \frac{R}{W^{\frac{1}{3}}} \quad (6.1)$$

To determine the attenuation coefficient for each test, a plot of $\log (P) - \log \rho c f (160/144)$ vs. $\log (R/W^{1/3})$ was made using the data from each free-field gage. The slope of this curve yields a representative value of attenuation coefficient for that data set. When these plots were made, the values of n were highly inconsistent with those obtained from independent determinations of n for each gage. This was attributed to the close spacings of the gages (R). For this method to be effective the gages must be spread over a greater distance to limit scatter of the data points. Therefore, the representative values of n for each test were taken as the average of the individual measurements for each test. These individual measurements represent the attenuation coefficient from the source to the receiver for each gage. Table 6.11 contains the individual values of n calculated for each gage and average n values for each test. In calculating n , the wavespeed from that particular gage, and not the wavespeed from the average of all measurements, was used.

Comparing the average attenuation coefficients from this test data with those presented in Table 2.1 shows the attenuation coefficients in Table 6.11 to be greater than any of the values presented in Table 2.1. From Table 2.1 a representative value of n for a poorly graded dense sand should be

Table 6.11 Attenuation Coefficients

| Test | F1 (psi) | F2 (psi) | F3 (psi) | n1 | n2 | n3 | Average n |
|------|----------|----------|----------|---------|------|---------|-----------|
| 1 | 99.5 | 174.3 | No Data | 3.45 | 3.13 | No Data | 3.29 |
| 2 | No Data | 17.9 | No Data | No Data | 3.56 | No Data | 3.56 |
| 3 | 14.1 | 20.4 | No Data | 3.99 | 3.99 | No Data | 3.99 |
| 4 | 14.1 | 15.4 | 21.6 | 3.51 | 3.66 | 3.52 | 3.56 |
| 5 | 21.5 | 37.0 | 49.7 | 3.65 | 3.55 | 3.48 | 3.56 |

approximately 2.5 - 2.75, compared to values of 3.29 - 3.99 obtained from this test data. This was also noted by Olen, et al (1993) who identified two possible reasons for this difference. First, was the presence of the silt fraction of the Sky X sand, although the small percent of fines would not be expected to make that large a difference. A second reason was based upon observations of the Sky X sand under a scanning electron microscope (SEM). The sand particles were coated by a non-quartz (possibly organic) coating that would reduce the interparticle friction and increase attenuation in this soil. Therefore, the n values presented in Table 6.11 are considered valid. As previously stated in this report, using n values from Table 2.1 in the Drake-Little equation only provides an order of magnitude estimation of free-field pressure due to the

difficulty in estimating n . To increase the accuracy of the equation, field measured values of n are necessary.

Predicted Versus Measured Free-Field Pressure

With the attenuation coefficient for each test thus established, Eq. 2.1 was used to predict the peak free-field soil pressure at each free-field gage location. In the previous section, specific values of c and n were established for each free-field gage. In this section, the average wavespeeds for all measurements as summarized in Table 6.3 and the average n values from Table 6.11 will be used to predict free-field pressure. A summary of these calculations is shown in Table 6.12, and Fig. 6.16 presents a plot of calculated vs. measured free-field pressures. This was done to evaluate how well free-field pressures calculated using average c and n values in Eq. 2.1 varied from using values specific to that gage. These calculations provide an indication of how well the equation predicts free-field blast compressive stresses at any point in the soil mass. From these data, the standard error of the estimated free-field pressure is 8.5 psi. The range of values of the calculated free-field stress was

Table 6.12 Free-field Pressures, Predicted and Measured

| Test | Gage | c (ft/sec) | ρ (lb- sec ² /ft) | R (ft) | n | Calculated Free-field Pressure (psi) | Measured Free-field Pressure(psi) |
|------|------|---------------|--------------------------------------|--------|------|---|---|
| 1 | F2 | 1065.8 | 3.379 | 17.6 | 3.29 | 101.0 | 99.5 |
| 1 | F3 | 1065.8 | 3.379 | 16.6 | 3.29 | 122.4 | 174.3 |
| 2 | F2 | 1000.4 | 3.354 | 26.0 | 3.56 | 17.4 | 17.9 |
| 3 | F1 | 935.3 | 3.354 | 22.5 | 3.99 | 15.1 | 14.1 |
| 3 | F2 | 935.3 | 3.354 | 21.0 | 3.99 | 19.9 | 20.4 |
| 4 | F1 | 1084.7 | 3.283 | 27.8 | 3.56 | 14.5 | 14.1 |
| 4 | F2 | 1084.7 | 3.283 | 25.6 | 3.56 | 19.5 | 15.4 |
| 4 | F3 | 1084.7 | 3.283 | 25.0 | 3.56 | 21.2 | 21.6 |
| 5 | F1 | 935.6 | 3.283 | 22.8 | 3.56 | 25.4 | 21.5 |
| 5 | F2 | 935.6 | 3.283 | 20.6 | 3.56 | 36.4 | 37.0 |
| 5 | F3 | 935.6 | 3.283 | 20.0 | 3.56 | 40.4 | 49.7 |

14.1 - 174.3 psi. If the data from Test 1, gage F3 is eliminated from the data set, the standard error is reduced to 3.8 psi. Based on this agreement between calculated and measured pressures, the average n and c values from each test can be used in Eq. 2.1 to predict free-field stresses within any point within the soil mass.

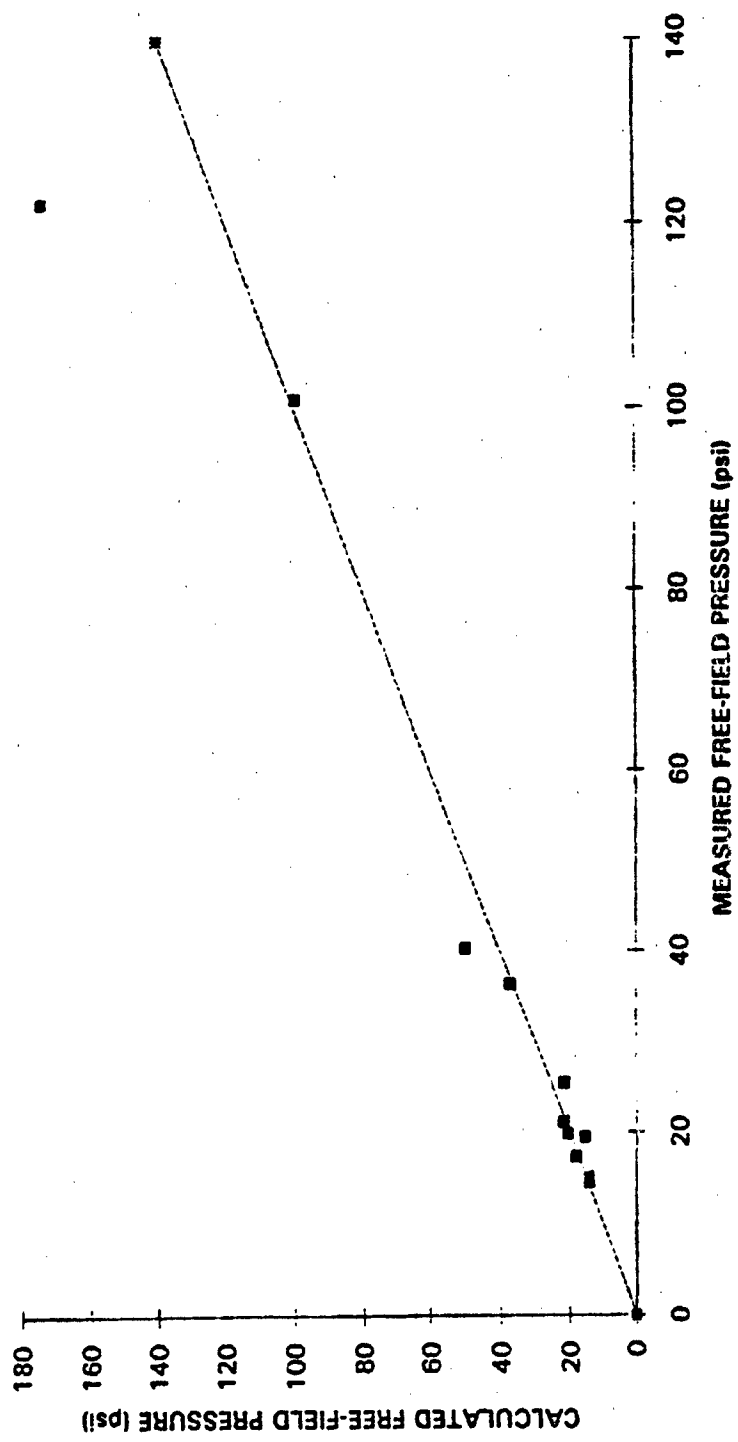


Figure 6.16 Plot of Calculated vs. Measured Free-Field Pressure

Estimation of Free-Field Stresses

The measurements obtained in these tests quantified the response of the wall and geogrid to the free field blast pressures. Pressures will be estimated via Eq. 2.1 and then related to the measured strains, accelerations, velocities and displacements. Values of c , ρ , and n are given in Table 6.12, and the R distance for each gage is listed in Tables 6.4 through 6.8.

Free-Field Pressure at Gage Locations

Table 6.13 lists the calculated free-field pressures at the center of each instrumented wall panel, corresponding to the locations of both the soil interface pressure gages and accelerometers. Table 6.14 lists the calculated free-field pressures at each strain gage location, and Fig. 6.17 presents a plot of peak stress vs. geogrid strain. It was initially anticipated that free-field pressures at each panel could be related to other test measurements. These analysis yielded no direct relationship between the values in Table 6.13 and individual test measurements of interface stress and acceleration.

As was observed in the scaled tests, the magnitude of the individual pressure and acceleration measurements did not show any observable trends within a test. For instance, in Test 2 the panel furthest from the detonation recorded pressure in excess or equal to all other panels within that test. Acceleration measurements also followed the same type of scatter. As expected, when

weapon standoff distance decreased (all other factors being equal), measured pressure and acceleration tended to increase. This being the case, a more fundamental approach to relating test data to measured response was required, as will be discussed in Chapter VIII.

Table 6.13 Calculated Peak Free Field Pressures (in psi) at the Center of Each Instrumented Panel

| Panel | Test 1 | Test 2 | Test 3 | Test 4 | Test 5 |
|-------|--------|--------|--------|--------|--------|
| 1 | 60.2 | 10.0 | 9.2 | 10.6 | 17.0 |
| 2 | 66.3 | 10.4 | 9.9 | 11.1 | 18.3 |
| 3 | 60.2 | 10.0 | 9.2 | 10.6 | 17.0 |
| 4 | 56.5 | 9.6 | 8.8 | 10.2 | 16.3 |
| 5 | 56.5 | 9.6 | 8.8 | 10.2 | 16.3 |
| 6 | 40.1 | 8.0 | 6.6 | 8.5 | 12.7 |

**Table 6.14 Calculated Free-Field Pressures at Each Strain Gage Location
and Peak Compressive Strain**

| Test | Gage | Calculated Free-field Pressure (psi) | Compressive Strain (μ Strain) |
|------|------|--------------------------------------|------------------------------------|
| 2 | S7 | 13.5 | 4089.3 |
| 2 | S8 | 15.0 | 4332.7 |
| 2 | S9 | 16.9 | 2434.1 |
| 2 | S11 | 14.2 | 3991.9 |
| 2 | S12 | 16.0 | 2774.8 |
| 3 | S7 | 13.9 | 4186.8 |
| 3 | S8 | 16.0 | 5355.0 |
| 3 | S9 | 18.8 | 6523.4 |
| 3 | S10 | 12.9 | 5841.9 |
| 3 | S11 | 14.6 | 5257.7 |
| 4 | S1 | 14.5 | 2190.6 |
| 4 | S2 | 16.1 | 3115.7 |
| 4 | S3 | 18.2 | 4284.0 |
| 4 | S4 | 14.3 | 2385.4 |
| 4 | S5 | 16.1 | 2969.3 |
| 4 | S6 | 17.9 | 3894.6 |
| 4 | S7 | 14.0 | 1654.9 |
| 4 | S8 | 15.7 | 2921.2 |
| 4 | S11 | 14.9 | 2433.5 |
| 4 | S12 | 16.5 | 3213.0 |
| 5 | S1 | 25.4 | 2823.1 |
| 5 | S2 | 28.8 | 5647.2 |
| 5 | S3 | 33.4 | 4673.5 |
| 5 | S4 | 25.0 | 4235.4 |
| 5 | S5 | 40.4 | 584.2 |
| 5 | S8 | 27.4 | 4868.2 |
| 5 | S11 | 25.4 | 4040.6 |
| 5 | S12 | 28.8 | 3310.4 |

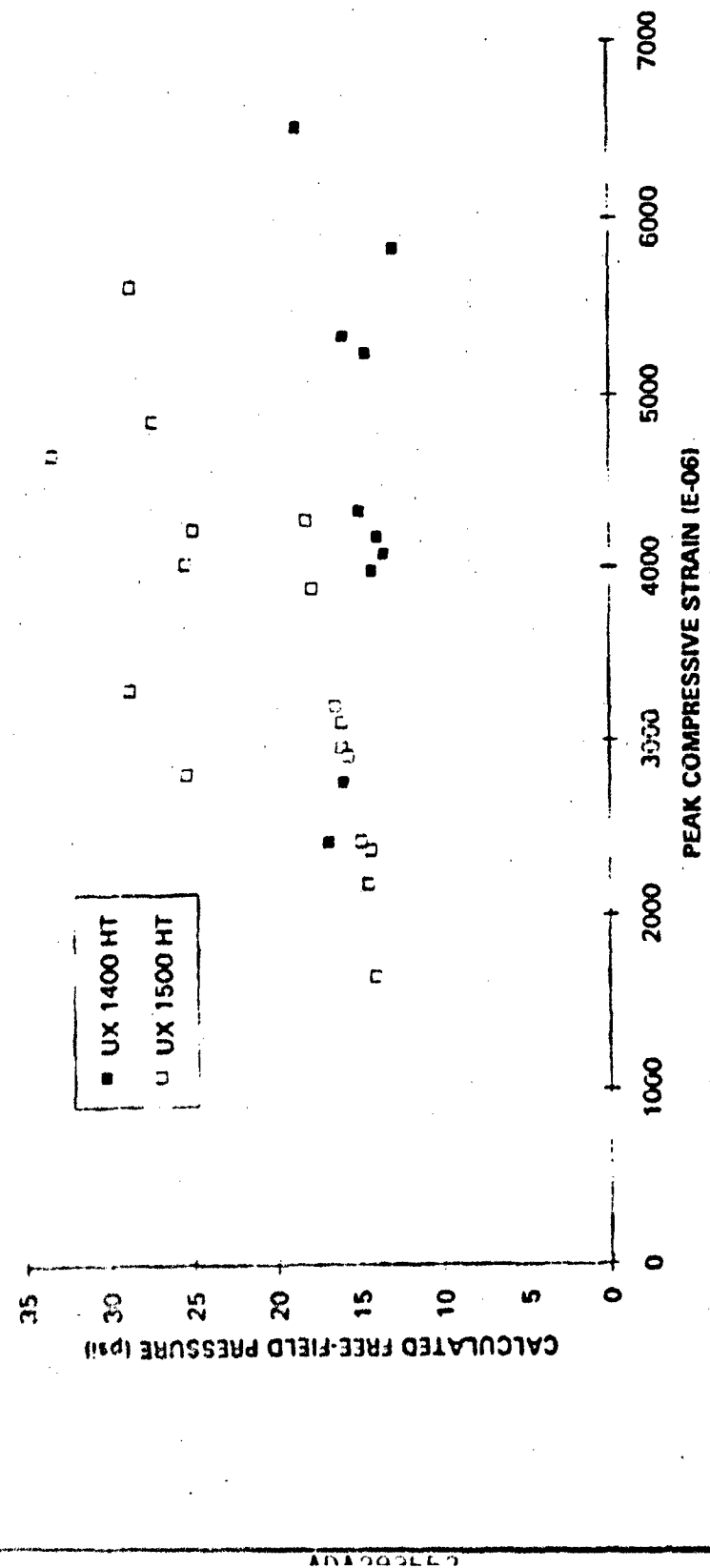


Figure 6.17 Free-Field Pressure vs. Geogrid Compressive Strain, Tests 2-5

Geogrid Strains

The motivation for measuring strains on the geogrid was the assumption that tensile strains in the geogrid would be observed and then related to the movement of the wall panels. However, as discussed previously, data collection had ceased by the time significant wall panel motion occurred. Therefore, with two exceptions, only compressive strain was measured as the compression wave moved through the backfill. The estimated free-field blast pressure was determined for each gage location, but the actual stress applied to the geogrid is unknown. The level of uncertainty in establishing the stresses applied to the reinforcement and the confined compressive modulus of the geogrid present numerous uncertainties that prevent a more detailed evaluation of the strain gage data. However, a qualitative discussion of the measurements will be presented based upon the estimated free-field blast pressure and measured strains. The measurement of compressive strains in the geogrids confirms the conclusions presented by Bachus, et al. (1993) that the reinforcement is subjected to compression during the blast wave loading.

The compressive strain of the UX 1500HT geogrid behaves as expected. As shown in Fig. 6.17, compressive strain increases with increasing free-field stress. Also, the UX 1500HT grid requires higher levels of free-field stress to achieve the same compressive strains measured in the UX 1400HT geogrid.

The behavior of the UX 1400HT grid is not as straightforward. Figure 6.17

shows that the strain associated with 15 psi free-field stress varies from 2500 - 6500 (E-06). This does not match the expectation that increases in strain require some commensurate increase in stress.

The strain gage data also exhibits some scatter, and this may be attributed to the effects of placement and compaction of the soil around the area of the reinforcement that was instrumented. After compaction of the backfill, each portion of geogrid mounted with a strain gage may not be in the same initial orientation. This may cause the geogrid to flex upward or downward, in addition to some twisting of the geogrid. The strain response of the geogrid could be affected by the initial position of the grid in relation to the location of the explosion.

Of the 28 strain gage recordings made in four tests, only three gages recorded any tensile strain, and only two gages of these recorded any net tensile strain. All tensile strains were recorded during Test 5, and the magnitude of the tensile strains were not directly related to position or free-field stress level. No clear rationale for this observation can be made based on either the test measurements or observations.

Strain of UX 1400HT Geogrid. Relating the predicted free-field pressures to the geogrid strains assumes that the direction or orientation of the load (i.e. pressure wave), with respect to each gage, is the same for all strain gages.

Figure 5.4 shows the position of the strain gages in relation to the explosion.

In Test 2 (standoff distance = 30 ft) strain measurements were obtained from gages S7-S9 and S11-S12, in Test 3 (standoff distance = 25 ft), gages S7-S11. All of these gages are on the layer of grid that is not directly between the explosion and the wall. Rather, the position of these gages is such that the free-field pressure impinges the gages at some angle. Because of this, the free-field stresses presented in Fig. 6.17 for the UX 1400HT geogrid may be greater than the stresses that were applied parallel to the strain gage.

For Test 2, Table 6.14 supports this conclusion. The gages closest to the detonation recorded lower values of strain than the gages further away. One potential cause for this is that the gages further away were more in line with the orientation of the pressure wave. The peak pressures do not vary significantly because the gages are spaced about 10 in. apart, and the effect of orientation was greater than the pressure decay over this short distance. An unsuccessful attempt was made to correct these stresses by calculating the free-field stress vector parallel to the strain gages. Since the calculated stresses at each strain gage were relatively equal, and since the strain gages were closely spaced, the stress vector parallel to each strain gages also remained approximately equal.

For Test 3, the stresses presented in Fig. 6.17 may also be greater than the stresses actually applied parallel to the strain gage. With the exception of one gage, the strain gage set that recorded data for Test 3 was the same as Test 2. However, as shown in Table 6.14, the Test 3 strain gages closest to the weapon

recorded the greatest strains. This is the reverse of the trend observed in Test 2. This was the second test of this wall, and the residual displacement caused by Test 2 may have put the geogrid in tension, and that tension may have affected the compressive strain response recorded in Test 3.

Strain of UX 1500HT Geogrid. In Test 4 strain gages S1-S8 and S11-S12 recorded data; for Test 5, gages S1-S5, S8, and S11-S12. In these tests, referring to Fig. 5.5, these strain gages are generally located between the explosion and the wall. Therefore, the pressures in Fig 6.14 may generally be assumed to be representative of the actual pressures that were parallel to the strain gage. For that reason, the data follows the expected trend of increasing strain with increasing compressive stress.

Summary

The full-scale test series has generated an extensive data base of accelerations, pressures, and geogrid strains measuring the response of a geogrid reinforced soil wall to blast wave pressures. Also, original methods were developed for installing strain gages on uniaxial geogrid that survives both construction damage and ground shock pressures. The significance of the inertial pressure wave on the response of the walls has been qualitatively established, however these pressures were not measured in the full-scale tests.

The full-scale test data provides the necessary input to develop a simplified model of the response of a reinforced soil wall to pressure wave loading based on the work of Drake, et al (1987). This model is discussed in Chapter VII. As an independent test, the scaled test data will also be applied to the model. This model provides a qualitative methodology for relating how well the scaled tests model the full-scale tests. The relationship between full and small-scale test data must be established before the more extensive scaled data base can be used to evaluate the response of reinforced soil walls to inertial pressures in Chapter VIII.

CHAPTER VII

MODEL VALIDATION USING FULL AND SMALL-SCALE PRESSURE WAVE DATA

Introduction

The full-scale tests provide extensive data on the response of the walls to free-field pressures. However, the high speed film indicated that the blast pressure is not the only loading mechanism acting on the wall, and that other loading mechanisms may be governing response. Previous empirical research has been unsatisfactory in describing the loading mechanisms and why specific design variables affect residual displacements (Bachus, et al, 1993, Olen, et al, 1993, Eytan and Reid, 1993). Therefore, a more rational approach to evaluating the load mechanisms and influence of design variables is necessary. The yielding wall model proposed by Drake, et al (1987) and discussed in Chapter IV appears to provide a good model for the dynamic response of reinforced soil walls. For consistency, the model, or the framework of the model, will be used to provide a more complete description of the loading mechanisms and their relationship with respect to time, and how the properties

of the materials considered in the model affect the response of the wall to each load mechanism.

In this chapter, the yielding wall model will be adapted to reinforced soil walls to evaluate the stiffness per unit area of full and small-scale reinforced soil walls. The consistency of this model within an individual test and from test to test provides a qualitative method for evaluating the validity of the model for blast pressure wave loading.

Determination of Stiffness Per Unit Area

Numerical Integration

The mass densities of the materials and acceleration and pressure time histories obtained in the full-scale tests provide the necessary input to evaluate the stiffness per unit area for pressure wave loading. The equation of motion for a yielding wall was previously presented as:

$$\rho_s L \ddot{u}(t) + \rho c_L \dot{u}(t) + R(u) = 2\sigma_{ff}(t) \quad (7.1)$$

The resistance function is given an assumed form of:

$$R(u) = ku(t) \quad (7.2)$$

in which k (F/L^3) is the stiffness per unit area, similar to a coefficient of subgrade reaction.

At a discrete time interval $i+1$, the equation may then be rewritten as:

$$\rho_s L \ddot{u}_{i+1} + \rho c_L \dot{u}_{i+1} + k u_{i+1} = 2\sigma_{eff,i+1} \quad (7.3)$$

Using the trapezoidal rule (Fig. 7.1), the known accelerations at time i and $i+1$ are used to solve for velocity at time $i+1$ during a time step h by:

$$\dot{u}_{i+1} = \dot{u}_i + \frac{h}{2} (\ddot{u}_i + \ddot{u}_{i+1}) \quad (7.4)$$

In turn, displacement at time $i+1$ is evaluated as:

$$u_{i+1} = u_i + h \dot{u}_i + \frac{h^2}{4} (\ddot{u}_i + \ddot{u}_{i+1}) \quad (7.5)$$

Substituting Eqs. 7.5 and 7.4 into Eq. 7.3 yields:

$$\rho_s L \ddot{u}_{i+1} + \rho c_L \left(\dot{u}_i + \frac{h}{2} \ddot{u}_i + \frac{h}{2} \ddot{u}_{i+1} \right) + k \left(u_i + h \dot{u}_i + \frac{h^2}{4} \ddot{u}_i + \frac{h^2}{4} \ddot{u}_{i+1} \right) = 2\sigma_{eff,i+1}$$

(7.6)

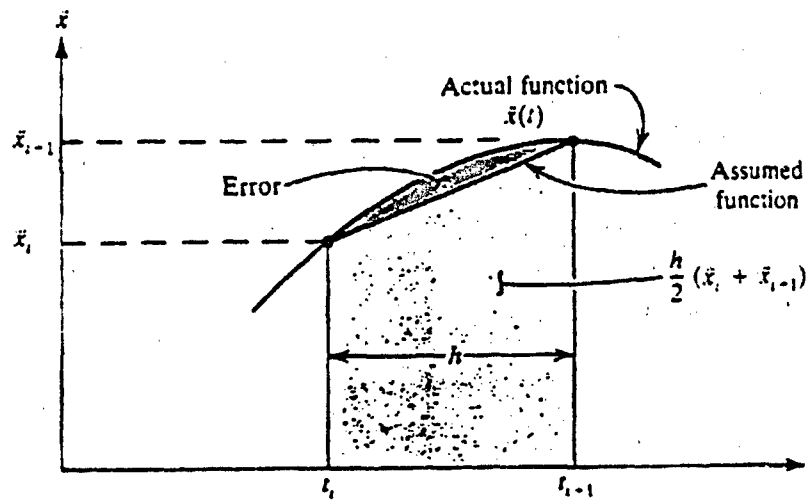


Figure 7.1 Trapezoidal Rule of Integration (Al-Khafaji and Tooley, 1986)

Finally, Eq. 7.6 is rearranged to solve for k.

$$k = \frac{2\sigma_{xx_{i+1}}(t) - \rho_c L \ddot{u}_{i+1}(t) - \rho c_L (\dot{u}_i(t) + \frac{h}{2} \ddot{u}_i(t) + \frac{h}{2} \ddot{u}_{i+1}(t))}{u_i(t) + h \dot{u}_i(t) + \frac{h^2}{4} \ddot{u}_i(t) + \frac{h^2}{4} \ddot{u}_{i+1}(t)} \quad (7.7)$$

The resistance function, R(u) may be calculated by multiplying displacement by the coefficient k.

An example of the numerical solution is as follows:

Given: $\ddot{u}_i, \ddot{u}_{i+n}, P_i, P_{i+n}, \dot{u}_i, u_i$

For time $t=i$

a. Solve Eq. 7.7 for k_i

b. Solve Eq. 7.2 for R_i

For time $t=i+1$

a. Solve Eq. 7.4 for \dot{u}_{i+1}

b. Solve Eq. 7.5 for u_{i+1}

c. Solve Eq. 7.7 for k_{i+1}

d. Solve Eq. 7.2 for R_{i+1}

e. $i=i+1$, return to step a and repeat at intervals (0.001 sec)

over entire time period of interest

Numerical Loading Function

The free-field stress can be characterized by an exponentially decaying pulse having an immediate rise to peak stress (Headquarters, Dept. of the Army, 1986) in the form:

$$\sigma_{ff}(t) = \sigma_0 e^{-st} \quad (7.8)$$

where σ_0 is the peak free-field stress, α is the decay constant and t is the elapsed time after arrival. Equation 7.8 may be rearranged as:

$$\ln \frac{\sigma_{ff}}{\sigma_0} = -\alpha t \quad (7.9)$$

Plotting the $\ln \sigma_{ff}/\sigma_0$ versus time yields a curve whose slope is equal to $-\alpha$.

Peak free-field pressures for each panel location were presented in Chapter VI. In each test, free-field pressure gages were located within two ft. of the wall, not at the wall panel/soil interface. From these data, a representative decay constant for each test is calculated and then applied to the predicted peak free-field stress at the panel locations for use in the equation of motion.

Table 7.1 presents a summary of the decay constants for full-scale Tests 1-5 from the gage located closest to the wall (Gage No. F1). Typical plots comparing measured free-field stresses and those predicted using Eq. 7.6 and

Table 7.1 Free-Field Stress Decay Constant

| Test | 1 | 2 | 3 | 4 | 5 |
|------------------|-------|------|-------|------|-------|
| α (1/sec) | 152.3 | 86.2 | 114.2 | 92.5 | 161.7 |

the decay constants from Table 7.1 are presented in Figs. 7.2 and 7.3. These plots assume an immediate rise time to peak stress, followed by an exponential decay.

System Stiffness of Full-Scale Test Walls

Twenty seven acceleration time histories from the five full-scale tests with their associated free-field loading functions were evaluated numerically using the approach detailed above. Figure 6.3 presented a typical acceleration time history, and all others are found in Appendix C. Table 7.2 shows a detailed example of the integration of the data from wall panel No. 2, Test 5. Figure 7.4 shows how system stiffness decreases with displacement, and Fig. 7.5 shows log k vs. log u. As expected, the calculated stiffness initially assumes a very high value and rapidly decays. This is a result of the almost instantaneous rise of free-field pressures to peak values, while peak acceleration is not achieved until a few milliseconds later. As the acceleration, velocity and displacement of the yielding wall increases, the stiffness and pressures decrease.

Figure 7.6 demonstrates the level of consistency between the full-scale test data. The data from nine accelerometers did not fall within the grouping, including all from Test 1. Test 1 data do plot relationships of the same form as the others in Fig. 7.6, however they do not fall completely within the rest of the data group. Since the entire data set from Test 1 does not match the

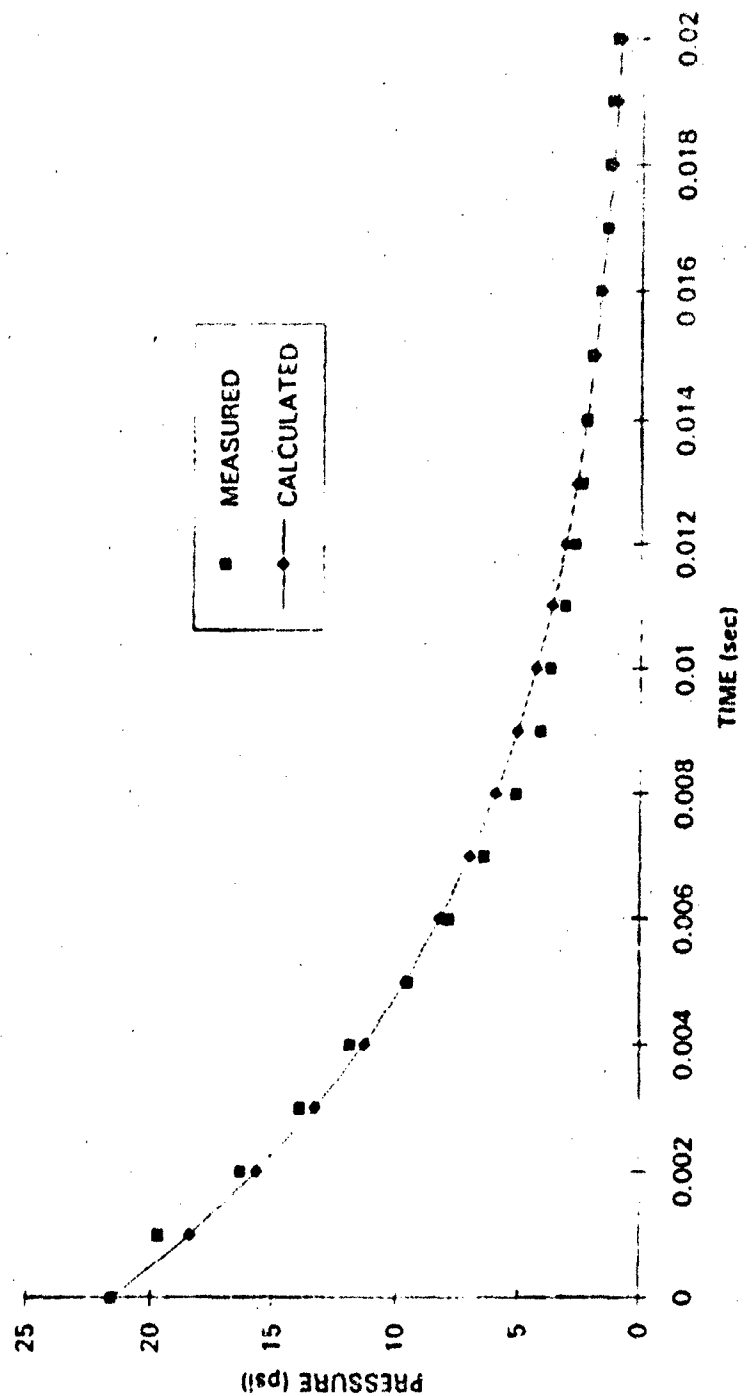


Figure 7.2 Measured and Predicted Free-field Stress vs. Time, Test 5, Gage F1

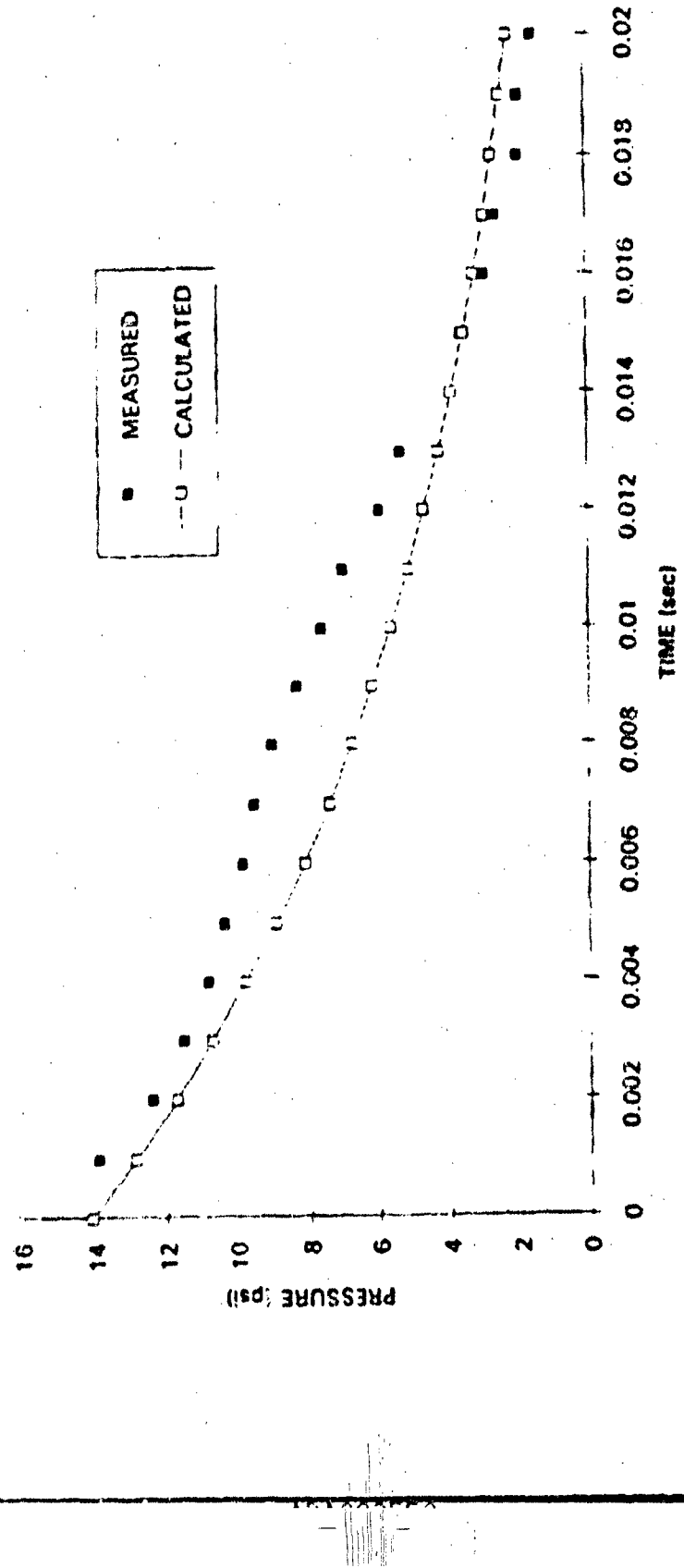


Figure 7.3 Measured and Predicted Free-field Stress vs. Time, Test 4, Gage F1

Table 7.2 Integration for Stiffness Per Unit Area, Test 5, Panel No. 2

| TIME msec | ACCELERATION g's | PRESSURE psf | VELOCITY ft/sec | DISPLACEMENT ft | K lb·ft ⁻³ | RESISTANCE psf |
|--------------|---------------------|-----------------|--------------------|--------------------|--------------------------|-------------------|
| 0 | 0 | 0 | 0 | 0 | 0 | 0 |
| 1 | 0.84 | 2635.2 | 3.40E-04 | 1.40E-07 | 4.70E+09 | 658 |
| 2 | 1.05 | 2241.8 | 1.29E-03 | 9.53E-07 | 1.35E+09 | 1290 |
| 3 | 1.26 | 1907.1 | 2.44E-03 | 1.01E-06 | 7.96E+08 | 800 |
| 4 | 1.26 | 1622.3 | 3.70E-03 | 2.92E-06 | 4.41E+08 | 1287 |
| 5 | -2.53 | 1380.1 | 3.07E-03 | 5.04E-06 | 3.41E+08 | 1723 |
| 6 | -2.11 | 1174.1 | 7.45E-04 | 7.58E-06 | 2.33E+08 | 1769 |
| 7 | 2.95 | 998.8 | 1.17E-03 | 1.09E-05 | 1.21E+08 | 1311 |
| 8 | 4.84 | 849.6 | 4.95E-03 | 1.35E-05 | 6.83E+07 | 922 |
| 9 | 5.47 | 722.8 | 1.00E-02 | 1.72E-05 | 4.15E+07 | 714 |
| 10 | 4.64 | 614.9 | 1.51E-02 | 2.47E-05 | 2.51E+07 | 619 |
| 11 | 5.9 | 513.1 | 2.03E-02 | 3.73E-05 | 1.55E+07 | 577 |
| 12 | 3.79 | 445 | 2.52E-02 | 5.48E-05 | 9.85E+06 | 540 |
| 13 | 5.08 | 378.5 | 2.96E-02 | 7.74E-05 | 6.49E+06 | 502 |
| 14 | 4.64 | 322 | 3.45E-02 | 1.05E-04 | 4.47E+06 | 469 |
| 15 | 3.79 | 273.9 | 3.87E-02 | 1.37E-04 | 3.22E+06 | 440 |
| 16 | 2.53 | 233 | 4.18E-02 | 1.73E-04 | 2.41E+06 | 415 |
| 17 | 0.84 | 198.3 | 4.35E-02 | 2.12E-04 | 1.83E+06 | 388 |
| 18 | 0.42 | 148.7 | 4.42E-02 | 2.54E-04 | 1.40E+06 | 355 |
| 19 | 1.26 | 115 | 4.50E-02 | 2.98E-04 | 1.08E+06 | 322 |
| 20 | 2.53 | 121 | 4.69E-02 | 3.43E-04 | 8.73E+05 | 300 |
| 21 | 1.69 | 103 | 4.80E-02 | 3.89E-04 | 7.32E+05 | 285 |
| 22 | 0.84 | 88.3 | 5.03E-02 | 4.37E-04 | 6.25E+05 | 273 |
| 23 | -0.42 | 75.1 | 5.05E-02 | 4.86E-04 | 5.25E+05 | 255 |
| 24 | 0.42 | 63.9 | 5.05E-02 | 5.36E-04 | 4.40E+05 | 238 |
| 25 | 1.26 | 54.4 | 5.13E-02 | 5.87E-04 | 3.81E+05 | 224 |
| 26 | 1.26 | 46.3 | 5.26E-02 | 6.38E-04 | 3.38E+05 | 216 |
| 27 | 1.23 | 39.4 | 5.38E-02 | 6.90E-04 | 3.07E+05 | 212 |
| 28 | 0.42 | 33.5 | 5.47E-02 | 7.43E-04 | 2.83E+05 | 210 |
| 29 | -0.42 | 28.5 | 5.7E-02 | 7.97E-04 | 2.55E+05 | 203 |
| 30 | 0 | 24.2 | 5.45E-02 | 8.52E-04 | 2.27E+05 | 183 |
| 31 | 0.84 | 20.6 | 5.49E-02 | 9.07E-04 | 2.07E+05 | 188 |
| 32 | 0.84 | 17.8 | 5.5E-02 | 9.61E-04 | 1.85E+05 | 187 |
| 33 | 0.42 | 14.9 | 5.64E-02 | 1.02E-03 | 1.64E+05 | 187 |
| 34 | 0 | 12.7 | 5.66E-02 | 1.07E-03 | 1.73E+05 | 186 |
| 35 | 0 | 10.6 | 5.66E-02 | 1.13E-03 | 1.63E+05 | 184 |
| 36 | -0.42 | 9.2 | 5.64E-02 | 1.19E-03 | 1.52E+05 | 181 |
| 37 | 0 | 7.8 | 5.61E-02 | 1.24E-03 | 1.42E+05 | 176 |
| 38 | 0.42 | 6.6 | 5.64E-02 | 1.30E-03 | 1.32E+05 | 175 |
| 39 | 0.42 | 5.7 | 5.68E-02 | 1.36E-03 | 1.30E+05 | 175 |
| 40 | 0 | 4.8 | 5.70E-02 | 1.41E-03 | 1.25E+05 | 176 |
| 41 | 0 | 4.1 | 5.70E-02 | 1.47E-03 | 1.19E+05 | 175 |

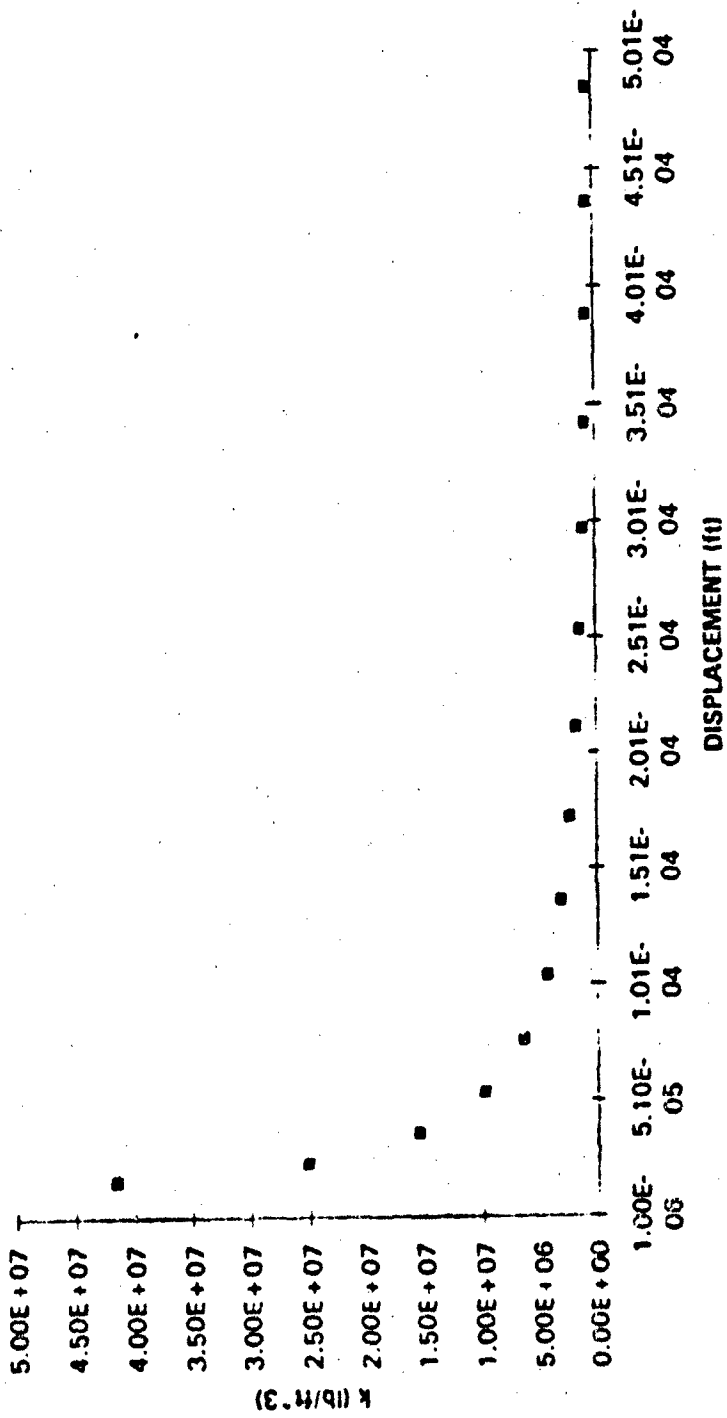


Figure 7.4 k vs. Displacement, Test 5, Panel 2

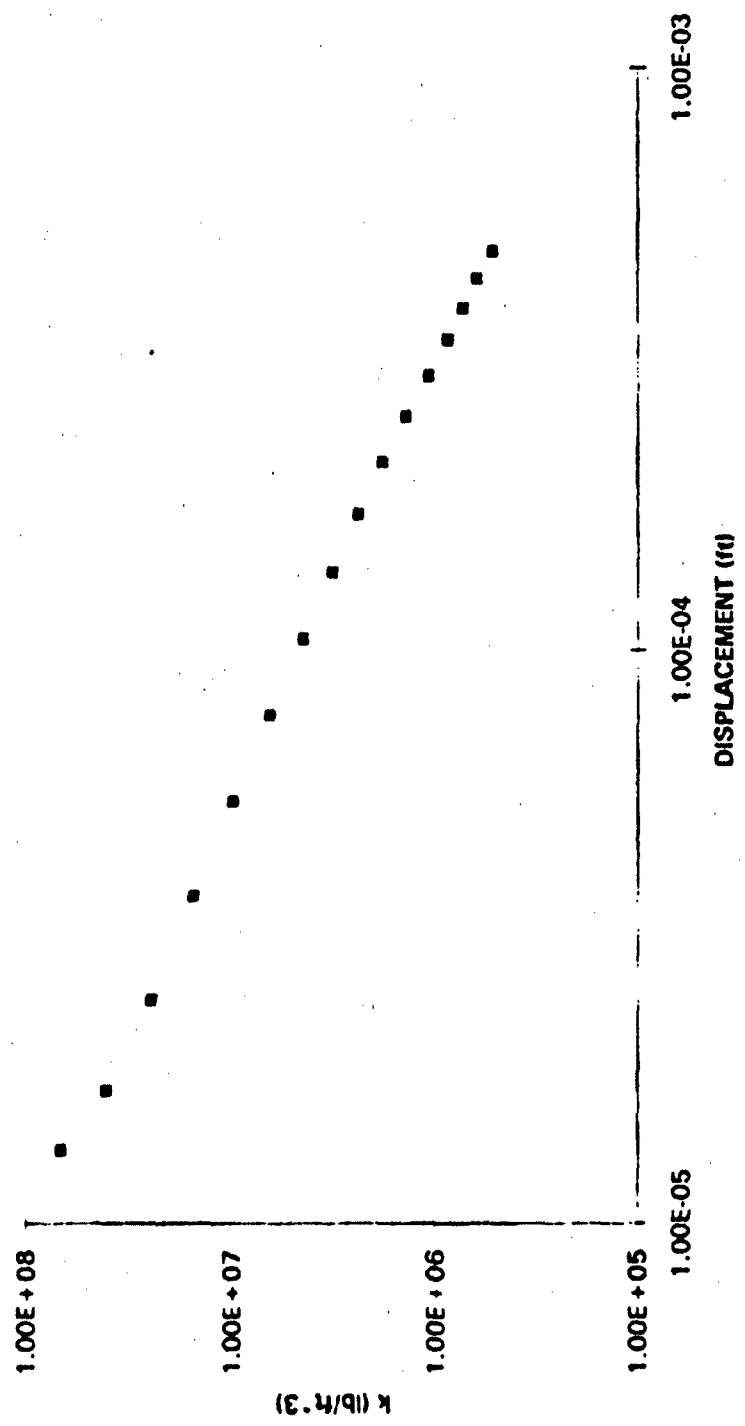


Figure 7.5 log k vs. log Displacement, Test 5, Panel 2

155

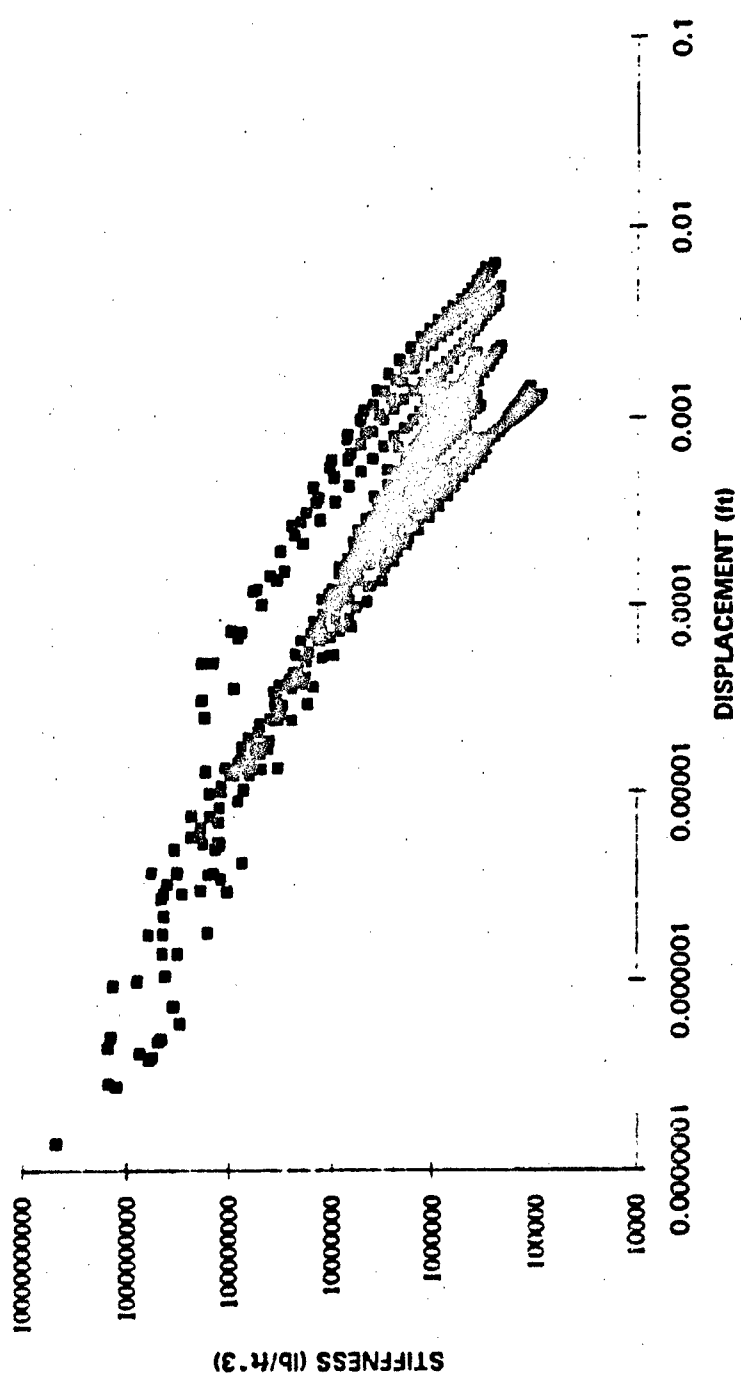


Figure 7.6 Log k vs. Log Displacement, Tests 1-5

behavior of the other data, rather than just select gages, the most likely source of this deviation is attributed to an inconsistency in the numerical forcing function and the actual forcing function, as shown in Fig. 7.7. From a review of the test data no specific rationale for the behavior of the measured free-field pressures in Test 1 can be made. The revised log k vs. log displacement plot for Tests 2-5 is shown in Fig. 7.8.

The data presented in Fig. 7.8 was investigated for any trends that may be responsible for the spread in the data. These included level of excitation, or weapon standoff distance, relative panel location to investigate effects related to boundary conditions, and the unit weight of the backfill. Of the four sets of scaled test data included in Fig. 7.8, two are from tests with weapon standoff distances of 20 ft., the other two were at 25 ft., and the unit weights of the soils were within 5 percent of each other. This analysis showed no discernable trend related to the relative position of the individual data plots using the above criteria. Based on the test data as plotted on a log-log scale, the stiffness does not appear to be significantly effected by changes in these parameters.

As previously stated, the resistance function is equal to the product of stiffness and displacement. From Fig. 7.8 this value is on the order of 1000 psf. The concrete panels used in these tests resisted at their top and bottom by the friction of the other panels, and had free boundaries along their sides,

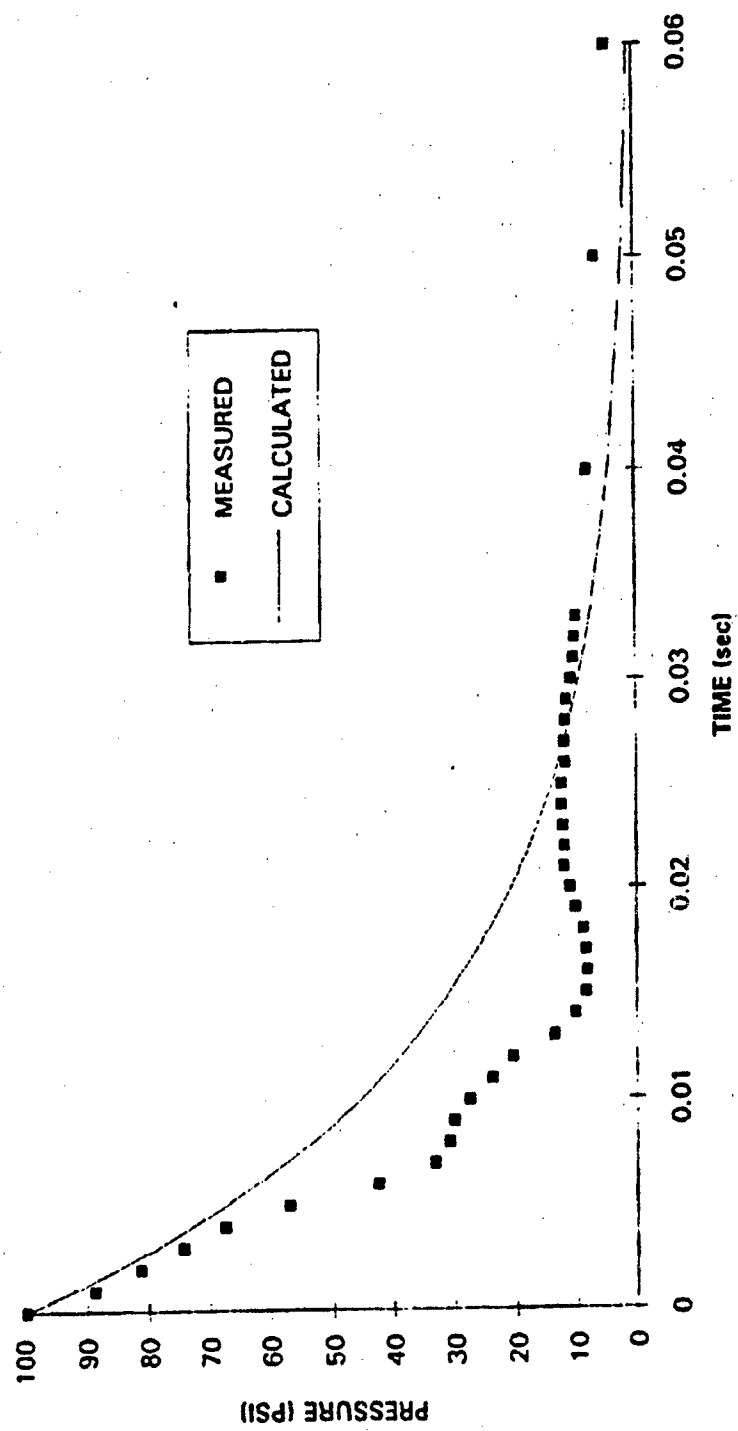


Figure 7.7 Measured and Predicted Free-field Stresses vs. Time, Test 1, Gage F2

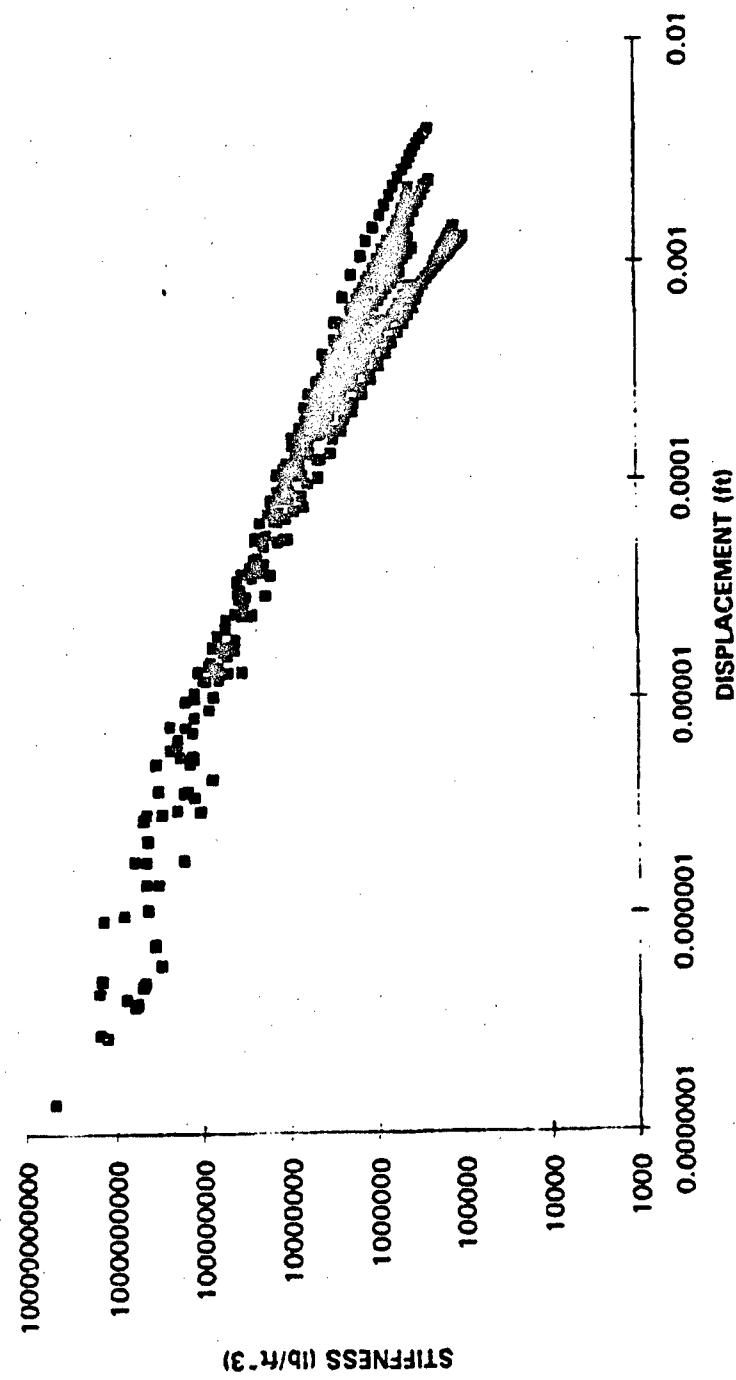


Figure 7.8 Log k vs. Log Displacement, Tests 2-5

suggesting these panels best represent a one-way slab. The one-way action may be assumed as long as the displacements are small and displacement at the boundaries does not occur. Calculating the resistance of a one-way slab from the tables presented by Drake, et al (1989) and using the design parameters of the panels yielded a resistance function of 1224 psf. This suggests the test data provides a value of resistance of the same order of magnitude as those estimated by Drake, et al (1989) for a concrete slab. At the small displacements caused by the free-field blast pressure wave, the measured response of the system is that of the wall panel, and not a composite system.

This analysis has provided the first evidence that the resistance function provides a relationship between free-field blast pressures and wall panel accelerations and displacements. Previous research (Bachus, et al, 1993; Olen, et al, 1993) had attempted to establish correlations between peak values of pressure, acceleration, and displacement. These correlations proved unreliable. The approach presented herein suggests that the data is reliable and reproducible, but must be evaluated in the time domain. Based on this analysis of the model using test data, the model appears to be valid for the range of data and systems tested in this study.

Independent Model Test Using Scaled Test Data

The centrifuge test data, identified in Chapter III, provide an independent data set for testing the validity of the model. The six centrifuge tests selected include two that model the full-scale tests, and four that were constructed with a different backfill soil. This test will determine if the stiffness vs. displacement relationship established for the model is consistent when applied to tests conducted at different scales and soil types.

This evaluation required discretization of the free-field pressure data to determine the decay constant of the free-field pressure. Also, the attenuation coefficient of the soil was determined from the free-field pressure data as detailed in Chapter VI. The attenuation coefficient was then used in Eq. 2.1 to solve for peak stress at the wall panel location. These data were necessary for the numerical loading function in the equation of motion. Next, the acceleration time history of the wall panel of interest was discretized to provide the necessary input data for the equation of motion. With this data and the material property data, the equation of motion was solved numerically to establish the relationship between stiffness and displacement. This process provides an independent test of the model, and if successful, provides a basis for establishing the validity of the centrifuge tests.

Stiffness Per Unit Area for Centrifuge Tests

In the centrifuge tests, three panels were instrumented in each test to establish panel acceleration; these panels are numbered 6, 16 and 27 as shown in Fig. 7.9, corresponding to panels 1, 2 and 3 in the full-scale test. These panels will be referred to as panel 1, 2 and 3 within this text for continuity.

Soil pressure interface gages were located directly behind these three panels and free-field pressure gages were located within the soil backfill or attached to the centrifuge container wall.

Solution of the Equation of Motion for Scaled Tests and Blast Pressure Wave

The attenuation coefficient of each of the centrifuge tests and the decay constant of the free-field blast pressure wave are shown in Table 7.3. In Test 20, the free-field pressure wave gages show an immediate rise to a value of peak stress, but did not decay due to unknown disturbance. These data could be used to obtain peak stress and arrival time for calculating the attenuation coefficient, but a decay constant could not be established. As an approximation, the decay constant from Test 27 will be used for Test 20, since both tests used the same sized weapon and soil type.

The attenuation coefficients for Tests 20 and 27 using the Sky X sand, are within the range of values measured in the full-scale tests (Table 6.11), which

| 10 | 9 | 8 | 7 | 6 | 5 | 4 | 3 | 2 | 1 |
|----|----|----|----|----|----|----|----|----|----|
| 21 | 20 | 19 | 18 | 17 | 16 | 15 | 14 | 13 | 12 |
| 31 | 30 | 29 | 28 | 27 | 26 | 25 | 24 | 23 | 22 |

Figure 7.9 Scaled Test Panel Numbering System (Olen, et al, 1993)

were 3.29 to 3.99. The values for Tyndall Beach Sand, used in Tests 26, 28, 29 and 32 compares well with the value of 3.5 for sands in Table 2.1. The decay constants for Tests 26 and 28 are also in the range of values measured in the full-scale tests (Table 7.1). For Tests 29 and 32, the decay of the free-field blast pressure wave was best represented by a linear function instead of an exponential function. The linear decay equations for these tests are shown in Table 7.3. At the present time, no clear rationale for the linear decay observed in these two tests can be established.

The results of the numerical solution of the equation of motion for the full-scale tests and centrifuge tests are plotted as stiffness vs. displacement as shown in Fig. 7.10. For Tests 20 and 27, the full and small-scale test data provide

similar results when compared to the stiffness vs. displacement plot for the full-scale tests. The data obtained from Tests 26, 28, 29 and 32 consistently have a higher stiffness for a given level of displacement. The model appears to be consistent across scales as demonstrated by the agreement between the full-scale and model-scale data for the Sky X sand. Also, the difference between the material properties of the wall panels used at full and small-scale is accounted

Table 7.3 Attenuation and Decay Coefficients - Centrifuge Tests 20, 26-29, 32

| Test Number | Attenuation Coefficient | Decay Constant (1/T) |
|-------------|-------------------------|--------------------------------|
| 20 | 3.8 | 137.95 |
| 26 | 3.02 | 163.17 |
| 27 | 3.74 | 137.95* |
| 28 | 3.32 | 100.45 |
| 29 | 3.38 | 99.4-8517.34(Δt)** |
| 32 | 3.26 | 107.23-9595.52(Δt)** |

* assumed equal to decay constant for Test 20.

** linear decay provided better fit than exponential

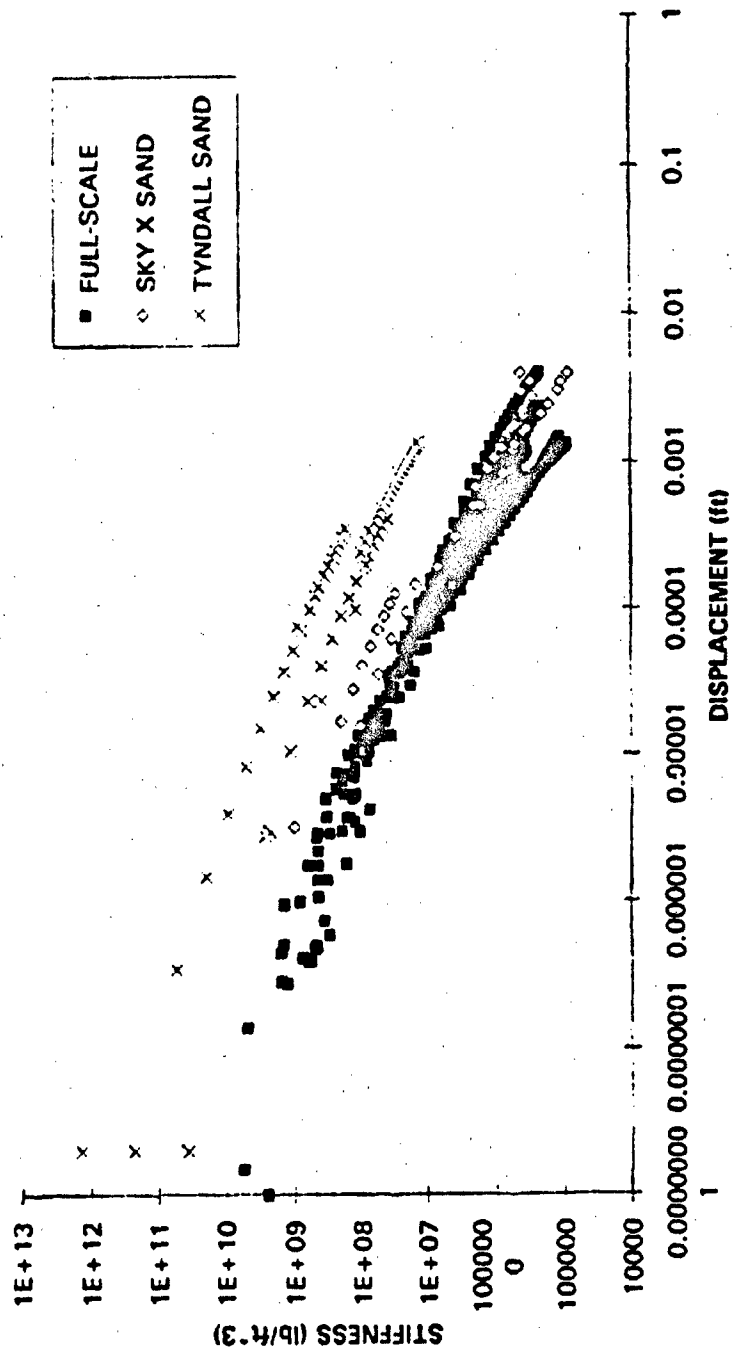


Figure 7.10 Stiffness vs. Displacement, Full-Scale and Centrifuge Tests

for in the model, and did not effect the consistency of the results of Tests 20 and 27 when compared to full-scale. As the material properties of the wall panel are accounted for in the first term of the equation of motion, the soil properties are accounted for in the second term. The model also addresses different levels of excitation through the stress term, and for the Sky X sand was consistent at both full and small scale.

The data from Tests 26, 28, 29 and 32 appear to be representative when compared to the peak values of stress and acceleration obtained in similar scaled tests. Finally, the form of the curve for these tests is consistent with the others, except that it lies above the rest of the group. With test data available for only two soil types, it is unclear as to whether this represents a trend based on soil type, or if this represents test scatter.

The use of the scaled data in the model provides an independent test of the validity of the equation. Since this equation has never been applied in this manner, it was necessary to test the relationship with multiple data sets.

Summary

The yielding wall model also provides a means of relating test pressures, accelerations and velocities on a fundamental basis, as opposed to simply comparing peak values of test measurements. The application of the model to

data from full-scale and model-scale tests on reinforced soil walls has resulted in a consistent relationship between wall stiffness and displacement. As a result, the model is considered valid for the small displacements caused by the blast pressure wave. Further investigation is required to determine if the relationship between stiffness and displacement is sensitive to changes in soil type. Based on the agreement of the full and small-scale data, the model provides a basis for moving forward and addressing the more critical issue of the inertial wave loading.

CHAPTER VIII

EVALUATION OF INERTIAL LOADING AND RESPONSE MECHANISMS

Introduction

Olen, et al (1993) present test data from a series of 1:30 scale explosive tests on geogrid reinforced soil walls in a geotechnical centrifuge. Two of the tests within this scaled test program simulated full-scale tests conducted in this research program, as well as fourteen others using a similar sand. The data from selected tests will be evaluated within the framework of the equation of motion to study the response of the walls to the inertial loading mechanisms and evaluate the design variables that most affect wall displacements.

Organization

The data necessary to solve the equation of motion for each loading mechanism is not available from any single test, so data from various tests must be sequentially evaluated to assemble the necessary values for analysis. The free-field pressure wave displacements were evaluated in Chapter VII, and this Chapter will estimate the response to the inertial wave loading within the

framework of the equation of motion. Centrifuge tests that modeled the full-scale tests provide data on the inertial loading that was not obtained in the full-scale test series. These data will be applied to the full-scale test structures to predict the wall panel displacements. The results of the evaluation will be discussed and the relative influence of the design parameters for each loading mechanism will be established.

Inertial Wave Loading Mechanisms

The displacement of the wall panels under the influence of the inertial wave can be separated into two components: 1) mass movement and, 2) geogrid pullout. In this analysis, these effects will be evaluated independently and then superimposed.

Free-field soil pressure gages were located in the retained fill of the centrifuge tests. Data from one such gage from Test 27 is shown in Fig. 8.1. This gage is 15 ft. from the detonation at prototype scale. These data shows the inertial wave arrives 45 ms at prototype scale after detonation and has a duration of 135 ms at prototype scale, therefore it is traveling at a velocity of 333 ft/sec. Assuming a crater radius of 10 ft., and using Fig. 8.1 as a

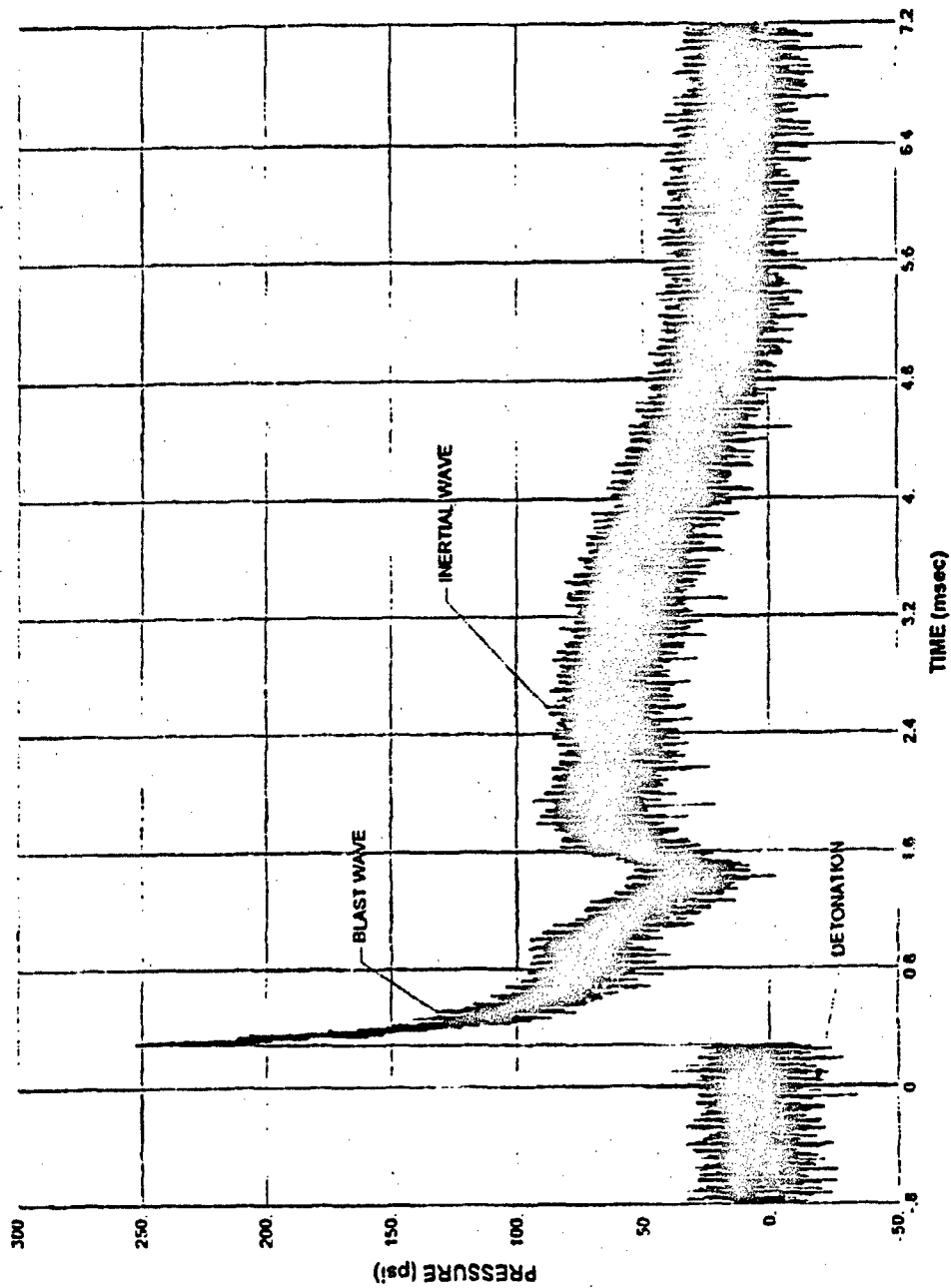


Figure 8.1 Free-field Pressure, Scaled Test 27, Gage P5

170

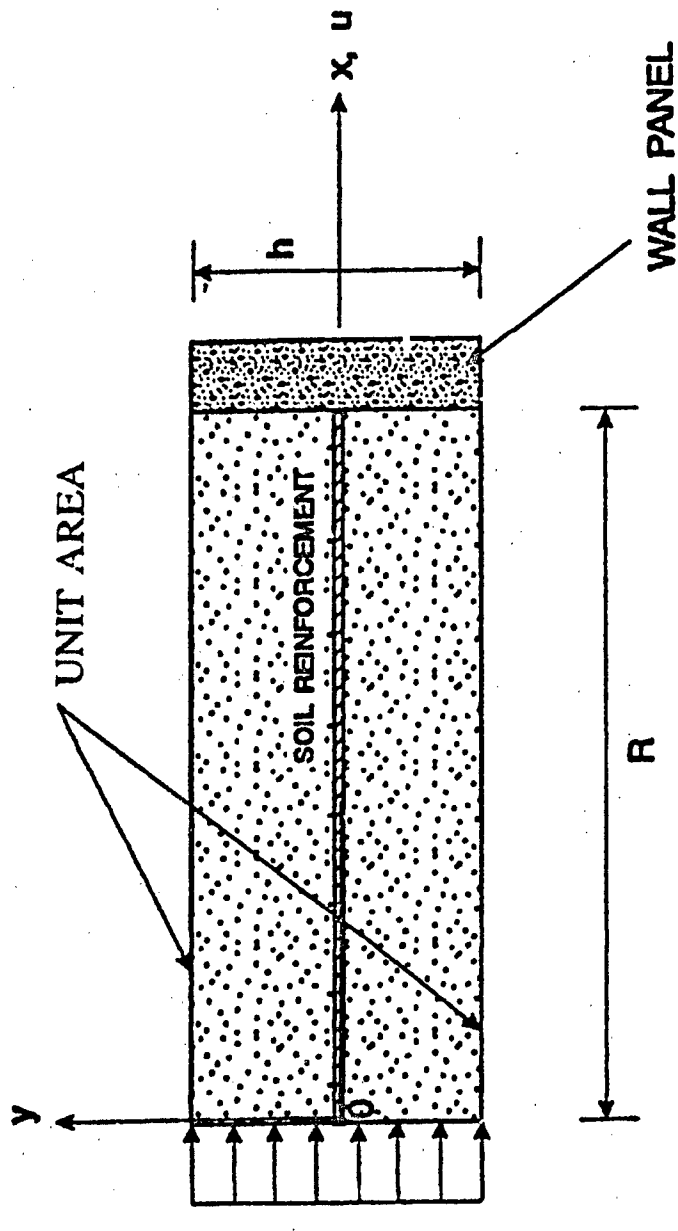
ADA293552

representative pressure time history, the mass of soil between the crater/soil interface and wall panel is being compressed for a period of 135 ms. During this time period, the soil mass is assumed to be accelerated as a uniform block, resisted only by the mass of the soil. This component of the inertial wave loading will be referred to as mass movement.

Once the inertial pressure wave at the crater/soil interface decays to zero, the soil in that area returns to a static state. Up until this time, stresses on the wall panels could not be resisted by load transfer to the geogrid because the geogrid was moving with the entire mass. Once the soil around the geogrid closest to the crater returns to a static state, the geogrid provides resistance to the pressures on the wall panel. At this time, pressures on the wall panel are transferred to the geogrid which now becomes engaged and the pullout resistance of the geogrid is mobilized. This component of the inertial wave loading is referred to as the pullout loading. Figures 8.2 through 8.4 show respectively the free-field, mass movement and pullout loading mechanisms.

Application of the Model to Inertial Loading

Ideally, the Drake, et al (1987) model could be used to predict the response of the soil mass to inertial wave loading using measured wall panel



$$\sigma_x(t) = \sigma_0 e^{-\alpha t}$$

PLANE
SHOCK WAVE

Figure 8.2 Schematic of Free-Field Pressure Wave Loading

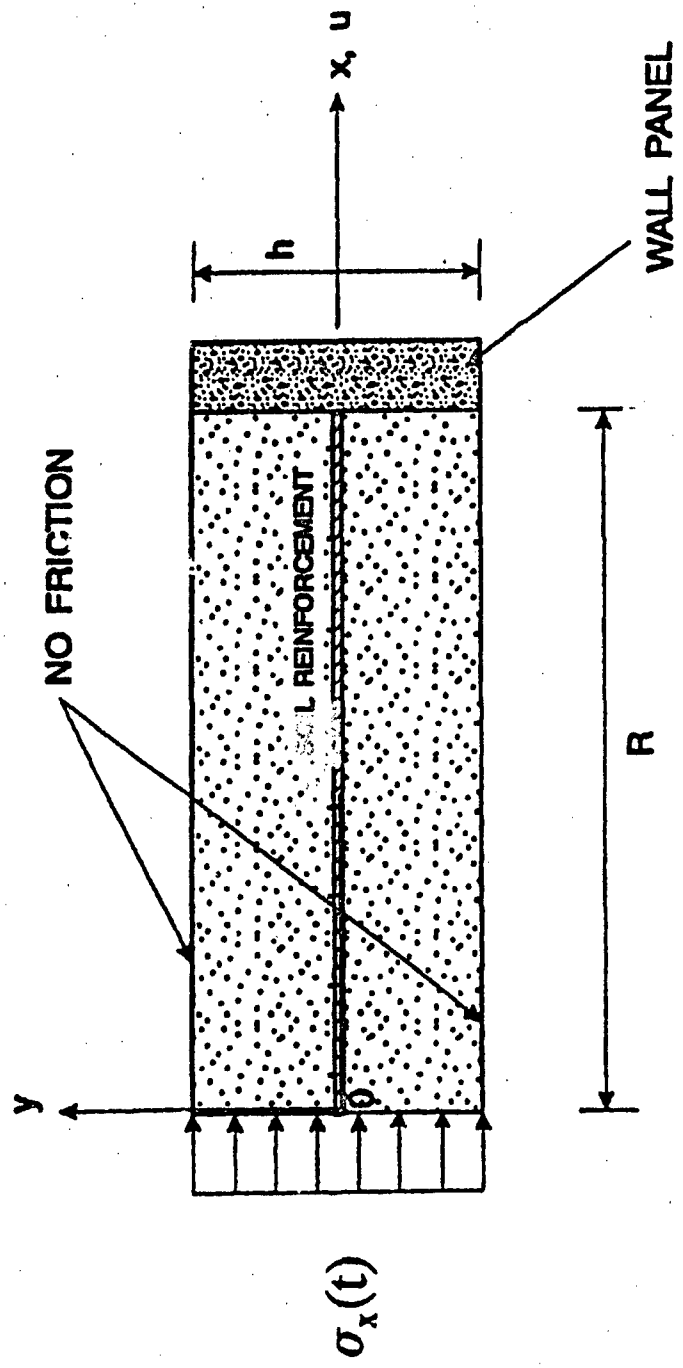


Figure 8.3 Schematic of Mass Movement Loading

173

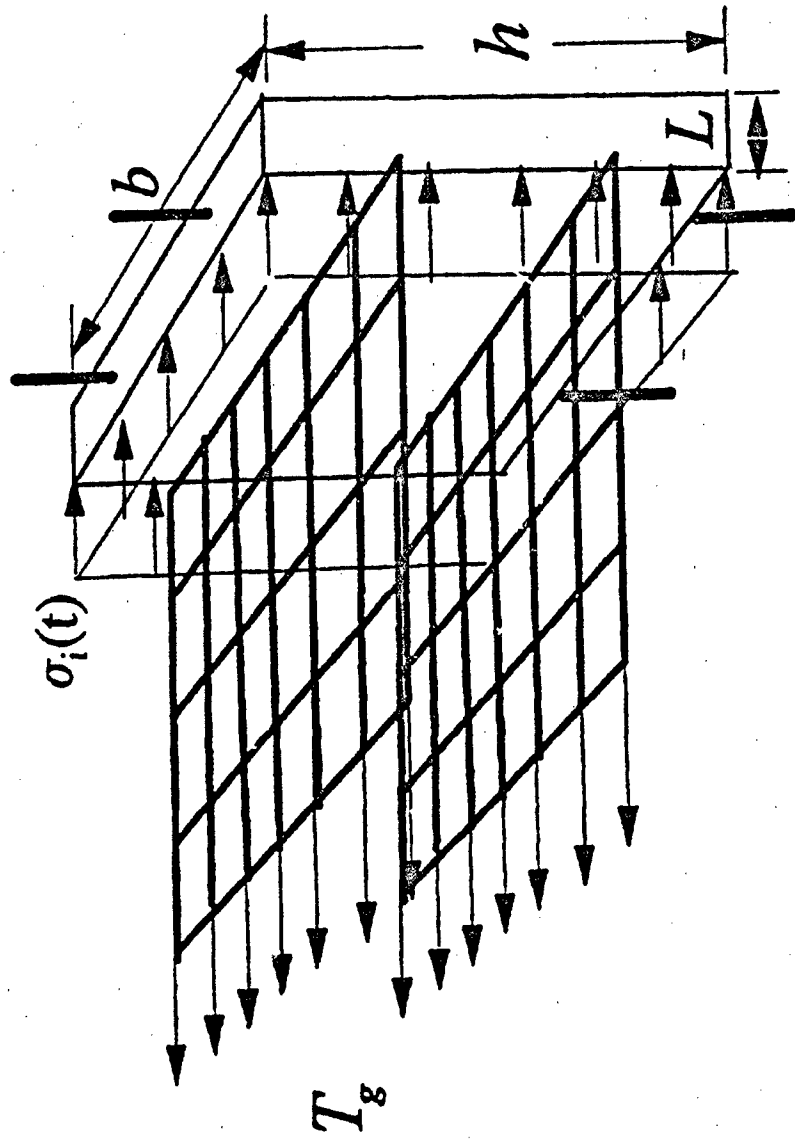


Figure 8.4 Schematic of Pullout Loading

174

accelerations and pressures. However, limitations in the test data prevent full exploitation of the model due to the significant noise (Fig. 8.5) in the acceleration gage data after the arrival of the blast pressure wave and a lack of agreement between measured displacements and those obtained via integration. After arrival of the blast wave, severe noise is observed throughout the rest of the acceleration time history. The primary source of this is attributed to reflections from the sides and bottom of the steel centrifuge containment vessel. The test wall was in direct contact with the sides and base of the steel containment vessel, and the contact area between the wall and bucket were sealed with caulk to prevent sand leakage. The level of noise causes significant fluctuations in both the positive and negative direction, effectively obscuring the true acceleration signal. Secondly, double integration of the acceleration time histories provides estimates of displacement that are an order of magnitude below those obtained from post-test measurements. The level of control exercised over the measurement of the displacements after each test suggests that they are more representative than those obtained from integration.

Alternatively, pressure gages provided comparatively clear measurements of pressure with respect to time. Their response did not have the significant fluctuations or noise as observed in the acceleration plots. These gages were located on the back face of the facing panels, suggesting the surrounding soil

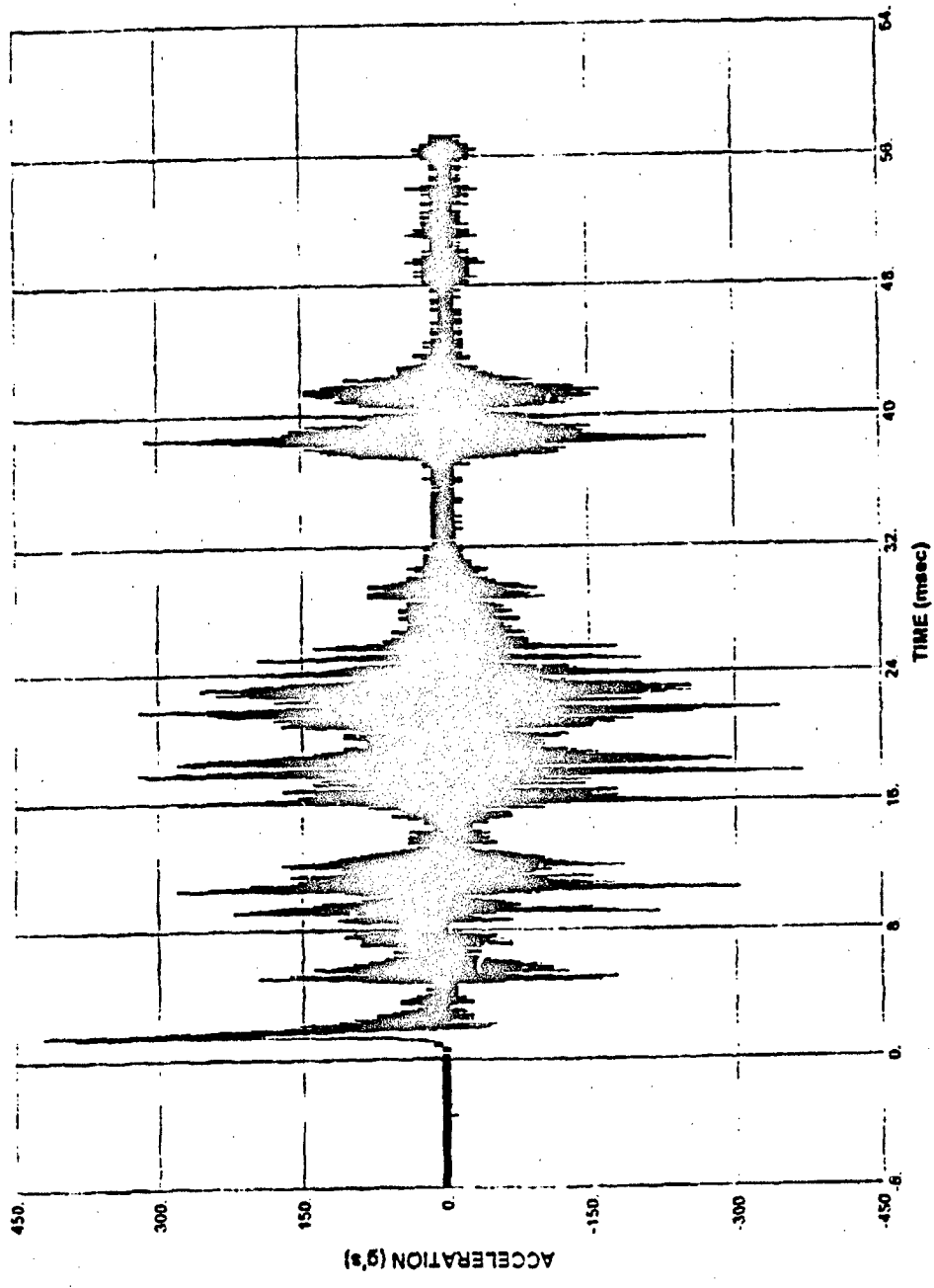


Figure 8.5 Typical Acceleration Plot From Centrifuge Tests

176

ADA293552

provided an element of damping from the vibrations that resulted in the significant noise recorded by the accelerometers.

Therefore, the model will be evaluated using measured pressures to estimate accelerations, which in turn are used to estimate velocities and displacements. The following sections are devoted to the prediction of the wall panel displacements due to inertial loading, first for the scaled tests, then for the full-scale tests. Each component of the inertial loading is evaluated independently and superimposed. The framework of the Drake model will be solved numerically for each component of the displacement for both full and small-scale test data.

Prediction of Displacement Due to Mass Movement

The equation of motion is adapted for evaluation of the mass movement of the soil/wall system. In Chapter IV, Eq. 4.6 shows that:

$$\sigma_i(t) = m_{block} \ddot{u}_{block}(t) + R(u) \quad (8.1)$$

In Eq. 8.1, $\sigma_i(t)$ is the free-field inertial stress, $\ddot{u}(t)$ is the acceleration of the all of the soil between the crater and wall and m is its mass. The resistance term represents the friction resisting the mass movement. However, the entire

embankment is assumed to be moving as a uniform block, as observed from the high speed film of full-scale tests. The boundary resistance will be assumed to be zero, an assumption that is most valid in the area between the explosion and the center area of the wall. The frictional effects increase with distance from the wall centerline, so study of Panel 2, the centermost panel, will be least affected by boundary (i.e. interslice) friction. Assuming negligible boundary resistance, the resistance term drops out of Eq. 8.1 yielding:

$$\ddot{u}(t)_{block} = \frac{\sigma_i(t)}{m_{block}} \quad (8.2)$$

where:

$\ddot{u}_{block}(t)$ = acceleration of soil/reinforcement/wall Panel System

$\sigma_i(t)$ = load on Soil/reinforcement/wall Panel System

m_{block} = mass of soil/reinforcement/wall Panel System

Alternatively, this may be expressed in terms of the impulse-momentum relationship:

$$\dot{u}_{block}(t) = \frac{1}{m_{block}} \int_0^t \sigma(t) dt \quad (8.3)$$

and evaluated over the time of duration of the plastic stress wave on the crater soil interface as determined from the gage data.

In this form, the equation of motion provides a means for estimating the displacement of the reinforced soil wall and the retained fill between the explosion and the wall during the period of time the entire mass is subjected to a dynamic compressive stress. The centrifuge test data includes a free-field pressure gage located at a distance that corresponds to the approximate center of the mass of soil between the explosion cavity and the wall face. The gages with clear data traces record both the free-field pressure wave and the inertial pressure wave. This form of pressure time history is used as the forcing function for the mass movement analysis. For this analysis, the mass of soil will be treated as a rigid block, assigned a unit area directly between the weapon and the center of wall Panel 2. This element best represents the one-dimensional behavior of the model. The equation of motion is solved numerically, based upon the assumptions that the mass of soil between the explosion and the wall moves as a single mass under the influence of the inertial pressure wave, and that the pressure measured at the center of the sliding block is a representative pressure for the entire block. Numerical evaluation of this equation using measured pressures over the time of pressure

application provides an acceleration time history, and velocity and displacements are determined by integration over small time steps.

To solve the equation numerically using measured inertial pressures, the size of the sliding block must be established. The evaluation is on a per unit area basis, however the length of the block must be established by estimating the size of the explosion cavity.

The true crater diameter is the diameter of the cylindrical soil mass that is ejected during the explosion. This value will differ from post-test measurements of crater diameter, referred to as the apparent crater. The apparent crater diameter differs from the true crater because of the amount of ejected soil that falls back into the crater, as well as changes in the diameter due to slope stability failures that occur after the decay of the explosive pressures. Henrych (1979) presents an empirical method with experimentally determined constants for estimation of the radius of the cavity created during the detonation. For a cylindrical charge the explosive cavity will have a cylindrical shape (except at the terminal regions) whose radius is:

$$R_{vd} = K_{vd} \sqrt{W} \quad (8.4)$$

where:

R_{vd} = cavity radius in m

K_{vd} = constant $\approx .35 \text{ m/ kg}^4$ for sandy soils

W = charge weight in kg

For the 192 pound cylindrical charges used in the full and small-scale test series, Eq. 8.4 predicts a cavity radius of 10.7 ft. Post-test measurements from the full-scale tests of apparent crater radius at the crater lip were approximately 17 to 18 ft. and of 12 ft. depth. The average apparent crater radii from the scaled tests were 16.3 ft. at prototype scale. Estimation of true crater radius from post-test measurements of the full-scale tests were in the range of 8.5 - 13.5 ft. The value estimated from Eq. 8.4 provides a representative value for true crater radius.

The length of the sliding block is estimated by subtracting the true crater radius from the distance between the weapon and the wall. The mass of the block is obtained from the product of the length of the block and mass density of the soil.

The velocity of the block at time $t = i+1$ is determined by:

$$\dot{u}_{i+1} = \dot{u}_i + \frac{1}{m_{block}} \left(\frac{h}{2} (\ddot{u}_i + \ddot{u}_{i+1}) \right) \quad (8.5)$$

Displacement at time $t = i+1$ is estimated by:

$$u_{i+1} = u_i + \frac{h}{2} (\dot{u}_i + \dot{u}_{i+1}) \quad (8.6)$$

The evaluation is repeated over the length of time that the inertial pressure was measured at 0.006 ms time steps. After the inertial pressure at the cavity surface decays to zero, it is assumed the soil returns to a static state and further deformation of the wall panels is resisted by the transfer of stress from the wall panel to the geogrid reinforcement.

Prediction of Displacement Due to Pullout Loading

During the first component of inertial loading, the resistance was assumed to be zero. However, during the pullout component of inertial loading the geogrid is now embedded in static soil, therefore the resistance will now assume a value determined from the pullout resistance of the geogrid. The mass term now becomes the wall panel mass per unit area, the interface stress

is the measured stress at the soil/panel interface, and the acceleration is the acceleration of the wall panel.

As presented in Chapter IV and repeated again, the equation of motion for the interface stress on a moving wall panel is:

$$\sigma_i(t) = m_{panel}\ddot{u}(t) + R(u) \quad (8.7)$$

where:

$\sigma_i(t)$ = interface stress at the soil/panel interface

m_{panel} = wall panel mass per unit area

$\ddot{u}(t)$ = acceleration of the wall panel

$R(u)$ = resistance provided by the geogrid

In the centrifuge tests, the interface stress was measured by gages attached to the wall panels at the soil/wall panel interface. The resistance of the wall panel is assumed to be primarily based upon the pullout resistance of the geogrid reinforcement. The pullout resistance of the geogrid, which is developed by wall displacement, is established as a function of displacement. The resistance of the geogrid for the applied normal stress must be converted to a resistance per unit area for use in the equation. This requires multiplying the

pullout resistance of the geogrid times the width of the geogrid attached to each panel. This gives the pullout resistance in terms of force. Dividing the pullout force by the cross sectional area of the panel yields the resistance per unit area.

Dividing the pullout resistance per unit area by the amount of displacement required to achieve full resistance gives the slope of the resistance function for pullout vs. displacement curve. The resistance function in Eq. 8.7 becomes $ku(t)$, where k is the slope of the resistance function for pullout curve and $u(t)$ is the displacement. Once enough displacement is achieved to develop full pullout resistance, the pullout resistance assumes a constant value (R_{max}), where u_e is defined as the displacement required to achieve R_{max} .

Numerical solution of Eq. 8.7 yields the wall panel displacement after sliding block motion has ceased. The acceleration of the wall panel at time step $t = i+1$ is calculated by:

$$\ddot{u}_{i+1} = \frac{1}{m_{panel}} (a_{i+1} - R(u)) \quad (8.8)$$

Velocity is then calculated by:

$$\dot{u}_{i+1} = \dot{u}_i + \frac{h}{2} (\ddot{u}_{i+1} + \ddot{u}_i) \quad (8.9)$$

where: $u_i < u_u$ $R(u) = ku_i$

$u_i > u_u$ $R(u) = R_{max}$

Displacement is calculated as:

$$u_{i+1} = u_i + \frac{h}{2} (\dot{u}_{i+1} + \dot{u}_i) \quad (8.10)$$

Solving the above equations using the pressure time history for the inertial stress from the soil pressure interface gage on the wall panel and the pullout resistance of the geogrid over the time of loading yields the displacement due to the transfer of stress from the wall panel to the geogrid reinforcement.

Response of Scaled Tests to Inertial Wave Loading

In this section, each of the six centrifuge test data sets will be individually evaluated using the equation of motion to predict residual displacement. The unique parameters of each test and evaluation will be discussed individually, followed by a summary of the results of the model calculations.

Centrifuge Test Number 27

Centrifuge Test 27 was a scaled test of full-scale Test 5. The backfill material was the Sky X sand compacted to a total unit weight of 107.8pcf at 10 percent water content. In full-scale Test 5, the unit weight of the backfill was 105.7pcf at 7.5 percent water content.

As previously established, the equivalent full-scale radius of the explosion cavity was 10.7 ft. The distance between the weapon and wall was 24.9 ft, so the length of the soil mass between the cavity and wall is 14.2 ft. For a section with unit area, the mass of the block equal to 47.54 lb-sec²/ft and the mass of the facing panel is 2.18 lb-sec²/ft, making the total mass of the block 49.72 lb-sec²/ft.

In this test, a free field pressure gage was located 15 ft. at prototype scale from the detonation. The center of the block is 17.8 ft. from the detonation. The inertial wave pressure time history for this gage will be assumed to be a representative pressure for the block, and these pressure values will be used as the forcing function for the sliding block. Using this mass of block and the pressure time history, the sliding block model was solved numerically over the time of inertial wave load duration, which was 135 ms at full-scale.

Centrifuge Test Number 20

Centrifuge Test 20 used the same soil as Test 27, however the weapon standoff distance was reduced to 21.1 ft. and the unit weight of the backfill was reduced to 90pcf.

In this test, the mass of the sliding block will be lower than that of Test 27 because the explosion standoff distance is reduced by almost 4 ft. In this case, the length of the sliding block is 10.4 ft. and the mass of the block and panel is 31.3 lb-sec²/ft. Also, the free-field pressure gage in the backfill did not record a clear trace of the inertial pressure wave. As an approximate solution, the inertial pressure data from Test 27 will be used as the forcing function for this test. This pressure was recorded 15 ft. from the detonation, and the center of the sliding block in this test is 16 ft. from the detonation.

Centrifuge Test Number 26

In centrifuge Test 26 the backfill material was a dry Tyndall Beach Sand, a poorly graded fine sand. The unit weight was 95 pcf, and the weapon standoff distance was 21.1 ft. The length of the sliding block is 10.4 ft., and the mass of the block is 32.9 lb-sec²/ft. The free-field inertial pressures measured for this test at the approximate center of the sliding block was used as the forcing function in this analysis.

Centrifuge Test Number 28

Centrifuge Test 28 also used the Tyndall Beach Sand at a unit weight of 107.8 pcf and a weapon standoff distance of 21.1 ft. In this test, the reinforcement length was increased from 15 ft. to 37.5 ft. This increase in embedment length had a negligible effect on the wall panel displacements and crater sizes when compared to the control tests, therefore the increase in length will not be factored into this analysis. The length of the sliding block is 10.4 ft., and the mass is 37.0 lb-sec²/ft.

Centrifuge Tests Number 29 and 32

Centrifuge Tests 29 and 32 were of the same overall design as Test 28 with one exception. In Test 29 the reinforcement tensile strength was reduced by punching holes in the geogrid reinforcement across both its length and width. In Test 32 each layer of geogrid consisted of one continuous sheet across the entire width of the wall instead of individual sheets attached to each panel. For Tests 29 and 32 these changes in design had little effect on the displacement of the center panel. Since the mass of the soil and explosion size was identical to Test 28, the length of the sliding block is 10.4 ft., and the mass is 37.0 lb-sec²/ft.

Pullout Resistance of the Nylon Mesh Reinforcing Material. The pullout resistance of the nylon mesh material used in the centrifuge tests was not

known. Attempts were made to determine this value in the laboratory, however in a 1 g environment the material would rupture at all but the lowest values of normal stress due to excessive stresses at the mesh/clamp interface. In the absence of a reliable measured value, the pullout capacity of the nylon mesh was estimated to be 1320 lb/ft. This value is a credible value for pullout resistance of some geogrid materials. Yuan, et al (1993) and Bachus, et al (1993) present the dynamic pullout resistance of various geogrids at normal stresses similar to those in this centrifuge model. The estimated pullout capacity of the nylon mesh is within the range of 1000-3000 lb/ft presented in these sources. Approximately 0.19 ft. of displacement was required to achieve full pullout resistance.

Because this approach used an assumed pullout capacity of the nylon mesh material, the predictions based on this one test may not be entirely representative of actual response. However, using this pullout resistance in other evaluations of the centrifuge data with differing forcing functions and soil type and comparing predicted vs. measured displacements will provide tests of this model and its ability to predict the approximate magnitude of the resistance, whose individual components are still unknown.

Results of Numerical Evaluation

The results of each of the evaluations are presented in Table 8.1. The displacements from the centrifuge tests are converted to full-scale.

Table 8.1 Predicted and Measured Displacements - Scaled Tests

| Test Number | Pressure Wave Displacement (ft) | Predicted Sliding Block Displacement (ft) | Predicted Pullout Displacement (ft) | Total Displacement Predicted By Model (ft) | Measured Displacement (ft) |
|-------------|---------------------------------|---|-------------------------------------|--|----------------------------|
| 20 | 0.01 | 1.41 | 0.64 | 2.06 | 2.33 |
| 26 | 0.01 | 1.17 | 0.20 | 1.38 | 1.78 |
| 27 | 0.01 | 0.75 | 0.66 | 1.42 | 1.63 |
| 28 | 0.01 | 0.78 | 0.39 | 1.18 | 1.37 |
| 29 | 0.01 | 0.89 | 0.35 | 1.24 | 1.67 |
| 32 | 0.01 | 1.20 | 0.18 | 1.38 | 1.56 |

Discussion of Centrifuge Evaluation

Evaluation of the model results provides further insight into the effect of various design parameters on the wall panel displacements. These predictions provide excellent results when compared to those obtained by post-test measurements, and also show trends that compare well with those obtained by empirical testing.

Based upon this evaluation and data used, expected trends are present in the results. In Test 20 the weapon standoff distance was 5 ft. closer than Test 27, and the unit weight of the soil in Test 20 was 13 pcf lower than that of Test 27. As expected, the decrease in weapon standoff distance resulted in increased wall panel displacement. The combination of the increase in the forcing function and decrease in soil unit weight cause the mass movement of Test 20 to be almost twice that of Test 27. The difference in pullout displacement also follows the same trend. The decrease in weapon standoff distance significantly affects both displacement mechanisms. The peak interface pressures for Test 20 are approximately 1000 psi, while the peak interface pressures for Test 27 are approximately 500 psi. Displacement due to pullout is controlled first by the peak stresses that exceed the pullout resistance, coupled with the length of time these stresses are applied.

Tests 26 and 28 were constructed with Tyndall Beach Sand and the unit weight of Test 26 was 13 pcf lower than that of Test 28 while the weapon standoff distance was constant for both tests. The displacement due to mass movement was greater for the test with lower unit weight (Test 26), yet its pullout displacement was less than that of the soil of greater unit weight (Test 28). This may have been caused by interaction between the wall panels.

The edges of each panel were keyed, providing a certain amount of interlock. The center row of panels was bounded by panels on all four sides, while the top row was bounded on three sides, and therefore had less boundary resistance. When exposed to the same pressures under mass movement, the top row of panels will displace further than the center row. In Test 26 the reduced unit weight caused more mass movement, and the top panel may have moved the center panel with it due to the interlock at their boundary, providing pressure relief to the center panel. The pressure data from these tests may support this analysis. The area under the inertial pressure time history curve from Test 26 is almost twice that of Test 28. However the peak interface stresses of Test 26 never exceed 5 psi, whereas the peak interface stresses of Test 28 are as high as 12 psi. This mechanism of pressure relief be responsible for the difference in pullout response. The small changes in unit weight of a specific soil type increases the mass of the block and may cause subtle changes in the engineering properties of the soil. This change may either reduce displacement through increased mass or because the increased unit weight alters the form of the inertial pressure wave.

Tests 26 and 28 were conducted on the same soil type at unit weights of 95 and 103 pcf respectively. Free-field pressure measurements were made in each test at the same distance from the detonation. The peak values of the inertial

stress wave were 56 and 66 psi for Tests 26 and 28, respectively, as shown in Figs. 8.6 and 8.7. The area under the inertial pressure time curves, defined as impulse, are also similar. The impulses are 74 and 82 psi-msec for Tests 26 and 28. This evidence suggests that the inertial stress wave magnitude and durations are not significantly effected by an approximate 8 percent change in unit weight, for a given soil type, and therefore increase in soil unit weight serves mainly to decrease accelerations during the mass movement of the soil block.

The results of Tests 29 and 32 should be of the same order as Test 28 since each parameter was constant except for the reinforcement strength. Post-test measurements show the reinforcement strength had little effect on ultimate displacements, therefore model predictions should be similar. The results from Test 29 are very close to Test 28, and although the ultimate displacement of Test 32 is similar to Tests 28 and 29, the amount of displacement predicted from each component of the inertial wave differs for Test 32. The inertial pressures of Test 32 measured on the gage located within the soil mass was of slightly lower amplitude and longer duration than those of Tests 28 and 29, and this longer duration would cause more mass movement. The difference in the pressure wave for this test cannot be accounted for since the explosion and soil properties were equal for each test.

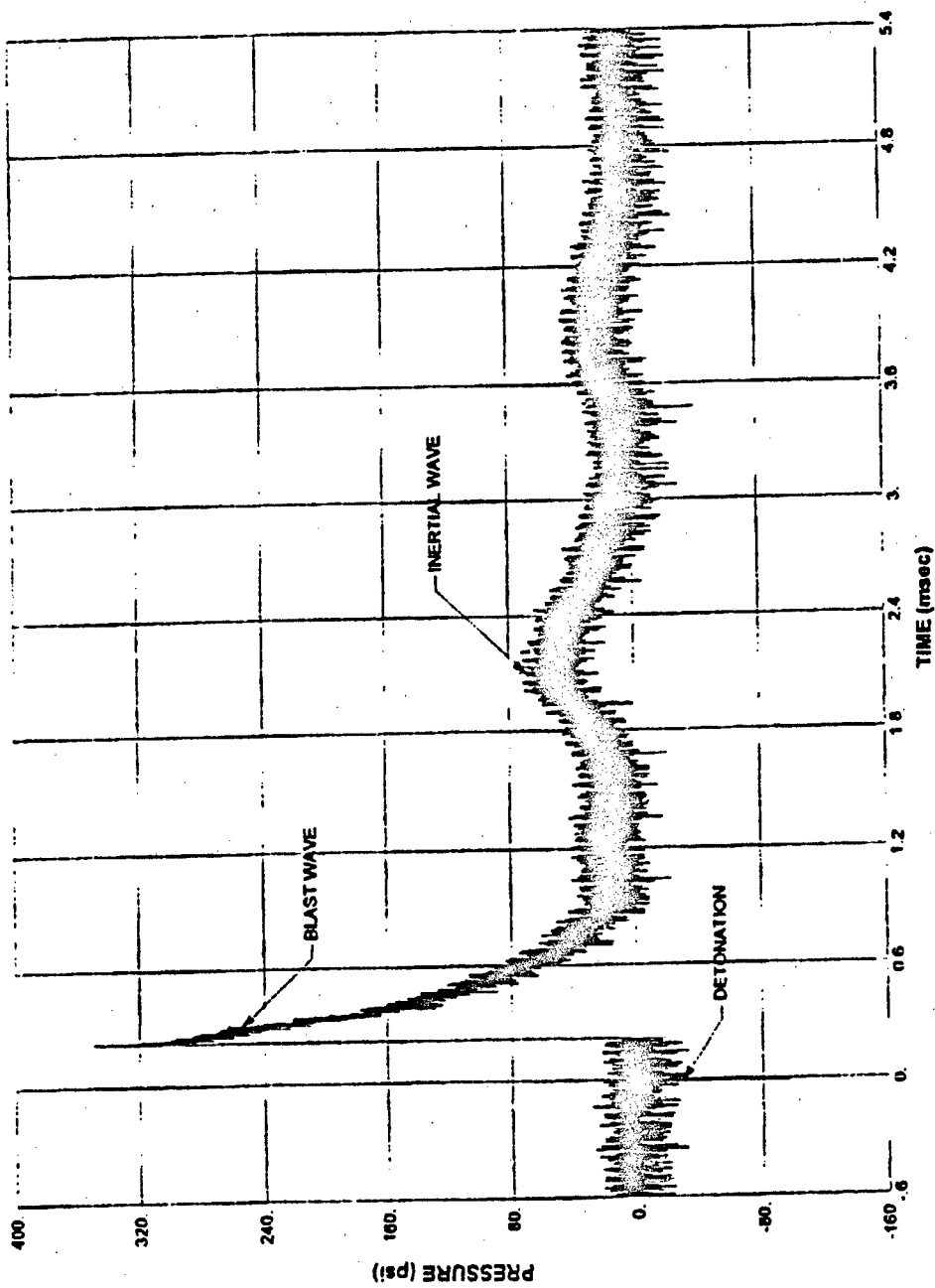


Figure 8.6 Free-field Pressure Time History - Scaled Test 26

194

ADA293552

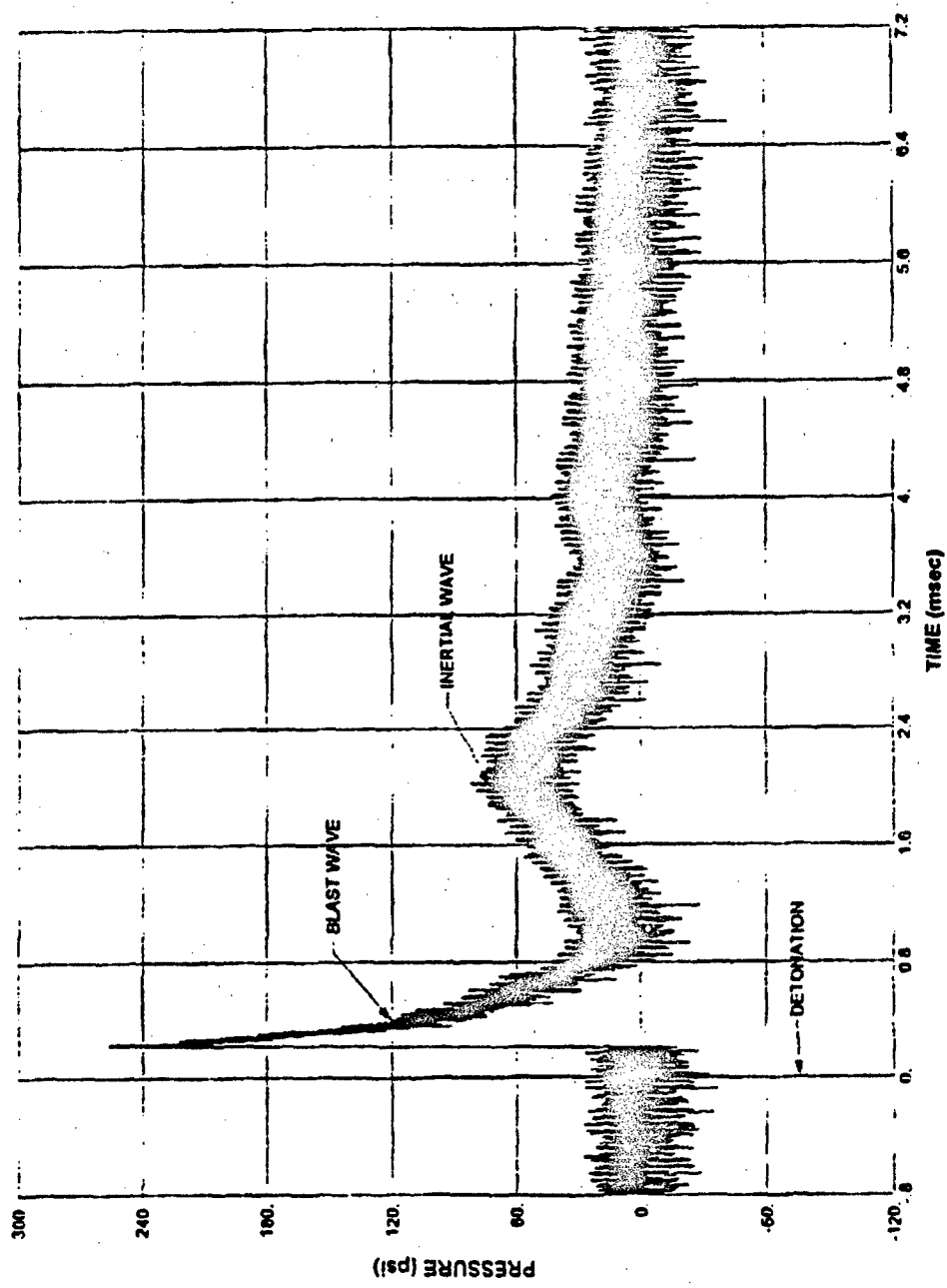


Figure 8.7 Free-field Pressure Time History - Scaled Test 28

195

ADA293552

In each case, the model underpredicted displacement. The accelerations predicted by the model are generally less than 100 g's, however in some cases accelerations jumped to values between 100-200 g's, and in one case, 500 g's. The higher accelerations were observed during spikes in pressures and generally lasted for 1 to 2 ms. The high accelerations may be a result of inadequate consideration of resisting forces. One such force is the structural resistance of the wall. The scaled test wall panels had lap joints around their boundaries providing some interlock between the panels. At the ends of the wall, the panels were sealed against the containment bucket with caulk. These boundary conditions may have prevented the wall panels from acting independently, and therefore some structural resistance is likely to exist.

As best as could be estimated from the acceleration plots, accelerations during inertial wave loading reach peak values of 30 - 100 g's. This is of the same order of magnitude as the accelerations calculated by the model, with the model exceeding those estimated from test data by as much as a factor of two. This evaluation was made after filtering out high-frequency noise in the 100 to 200 kHz range.

An increase in resistance from the forces not accounted for would decrease accelerations and displacements. However, the model is currently underpredicting displacements by 10 to 20 percent. The measured centrifuge

displacements that were used for comparison may also contain some error. When the centrifuge bucket containing the test wall was accelerated, the test walls rotated from a vertical orientation to horizontal. While in flight, the wall was tested, then decelerated back to vertical. The rotation of the wall in the bucket during deceleration may have caused increases in displacement. This possibility was also supported by the centrifuge operator (Purcell, 1995), however qualitative measurements were not made.

Results of previous scaled tests and numerical analysis concluded the unit weight of soil, size and location of the explosion, and geogrid stiffness were the three parameters having the most significant effect on wall panel displacement. Evaluation of the centrifuge data has shown decreases in unit weight primarily affect the response of the wall to mass movement, and explosion location affect both the mass movement and pullout loading mechanisms. Geogrid stiffness was not evaluated in the scaled tests, therefore this parameter could not be specifically addressed. This simple analysis is in agreement with the trends observed in the scaled tests.

Application to Full-Scale Tests

The scaled tests provided the necessary data for use in this model, with the exception of the pullout resistance of the nylon mesh material. In the full-scale

test, the pullout resistance of the reinforcing material is known, but the inertial pressures are not. In this section, the equation of motion will be used to predict panel displacements using a known pullout resistance and the inertial pressures from the replica tests.

The model has provided a means of evaluating the deformations of the scaled test walls. This same analysis technique will be used to predict the displacement of full-scale Tests 5 and 6, which are full-scale versions of centrifuge Tests 27 and 20. The only difference between these tests is the scale and the pullout resistance of the reinforcing material. To achieve this, the equation of motion was solved using the resistance of the geogrid as the resistance function for the pullout loading.

Dynamic Pullout Resistance Function of Geogrid Reinforcement

The dynamic pullout resistance of Tensar UX1500HT geogrid in Sky X sand was determined by Yuan, et al (1993) via procedures detailed by Bachus, et al (1993). Results of these tests for various normal stresses are shown in Fig. 8.8. These data will be used to establish the resistance function for the equation of motion when evaluating the response to pullout loading.

Using the unit weight of the soil from Test 5, the normal stress for each geogrid layer is established, and pullout resistance is obtained from Fig. 8.8.

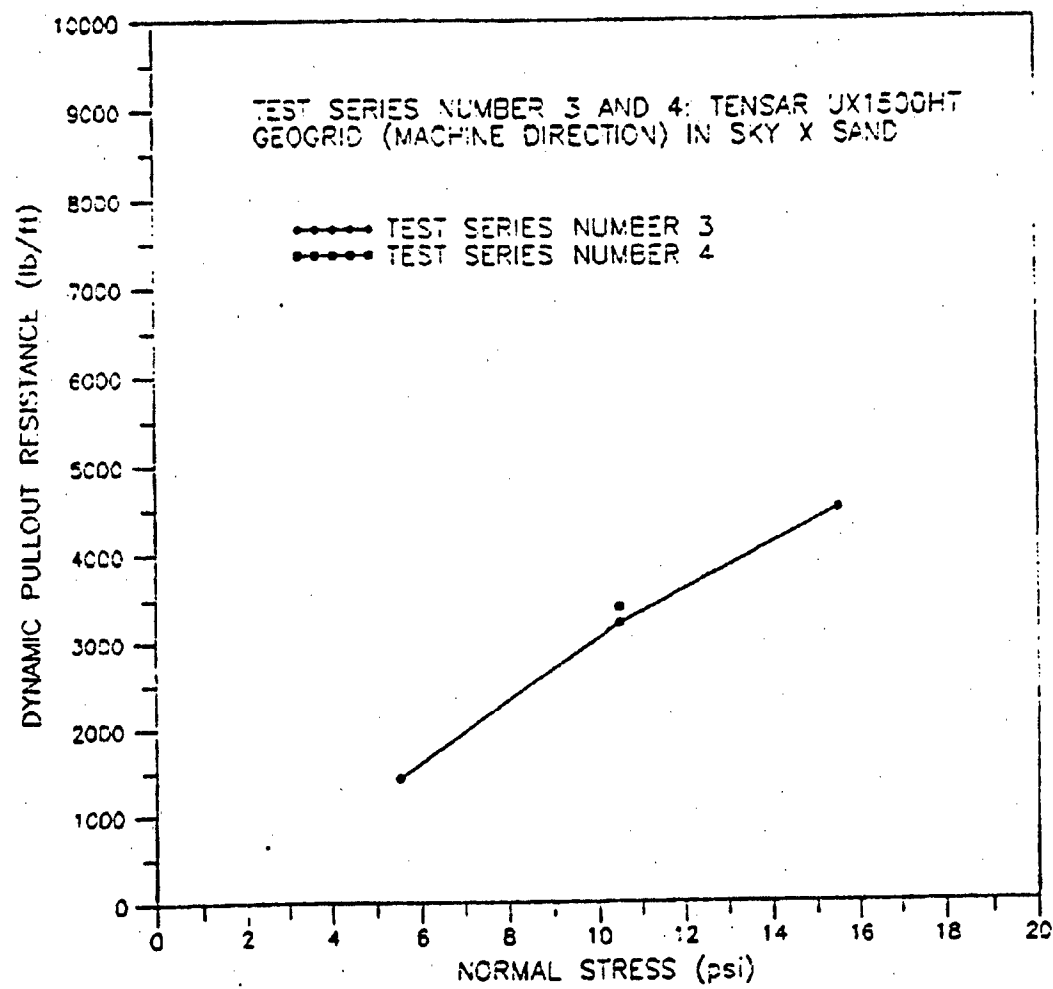


Figure 8.8 Dynamic Pullout Response of Tensar UX 1500 HT Geogrid
(Yuan, et al, 1993)

Extrapolation will be used for normal stresses below those plotted on the curve. The embedded width of each geogrid layer was 4.3 ft., and ultimate pullout force is obtained by multiplying the total width of grid by its respective pullout resistance. Resistance per unit area is obtained by dividing the pullout force by the cross sectional area of the wall panel, which for Test 5 was 30 ft². The amount of displacement required to achieve full pullout resistance was not presented. Bachus, et al, 1993, report on pullout tests of Tensar UX 1500HT geogrid in sands. For normal stresses of 2.5-5.3 psi, the pullout-displacement curve remained approximately linear until displacements approached 0.19 ft. The pullout resistance at this displacement were 500 to 1500 lb/ft.

For Panel 2, the normal stress at the top layer of geogrid is 4.9 psi, and for the lower layer, 6.1 psi. From Fig. 8.8, the pullout resistance of the top layer of grid is 1400 lb/ft and 1600 lb/ft for the lower layer. Based on the width of each layer, the pullout force is 12,900 lbs., or 430 psf of panel. The development of full pullout resistance is assumed to increase linearly with displacement. The displacement required to achieve full pullout resistance is 0.19 ft., making the slope of the pullout resistance function/displacement curve 2263 lb/ft of displacement per unit area. If a geogrid of different pullout resistance was used, the pullout resistance function would be established in the same manner using different values for ultimate pullout resistance and the

displacement required to achieve that resistance. The relationship between pullout resistance and tensile modulus, and their effect on the pullout resistance function, are discussed in Chapter IX.

Prediction of Displacement - Panel 2, Test 5

For this test, the inertial pressures are not known. The reinforcement used in Test 5 was the UX 1500HT. The inability to characterize the inertial wave within the soil mass and the subsequent soil response required using small-scale data as the best estimate of the inertial wave stresses. Since centrifuge Test 27 was a replica model of this test, the inertial wave pressures from this test will be applied this full-scale test. For the weapon standoff distance of 25 ft. and true crater radius of 10.7 ft., the mass of the sliding block and concrete panel is 49.3 lb-sec²/ft.

Analysis of the sliding block model resulted in a predicted displacement of 0.75 ft and displacement due to pullout was 3.34 ft, for a total displacement of 4.09 feet. The displacement observed after the test for this panel was 0.67-0.83 ft., which is approximately 25 percent of what the model predicts. Based upon these results, this analysis overpredicts the displacement of the wall panel.

Prediction of Displacement, Panel 1, Test 5

In this case, the pullout resistance of the geogrid was recalculated to account for the reduction due to the decrease in normal stress. Using the inertial pressure time history from centrifuge Test 27, Panel 1 was applied to Panel 1, full-scale Test 5. The block movement of the wall is 0.75 ft. and the predicted pullout related displacement is 1.31 ft., for a total of 2.06 ft. Observed displacement of the wall panel was 1.33 - 1.5 ft. This estimate is approximately 25 percent greater than observed.

Prediction of Displacement, Panel 2, Test 6

This test had a weapon standoff distance of 20 ft., which is close to the 21-ft. standoff distance used in centrifuge Test 20. The length of the soil block used in the block analysis was 9.3 ft. with a mass of 32.5 lb-sec²/ft. The pullout resistance function will be the same as that of wall Five, Panel 2. This remains relatively unchanged because the difference in unit weight between Tests 5 and 6 was only 0.8 pcf. The sliding block displacement for this test was predicted as 1.2 feet, and pullout displacement was 0.97 feet, for a total displacement of 2.17 feet. Observed displacements for this panel were 1-1.2 ft. The prediction is approximately 50 percent greater than observed. A summary of each prediction is presented in Table 8.2.

Sources of Error

Based on the results of this first analysis using the known pullout resistance of the geogrid, four potential sources of error are identified: 1) the pressure time histories from the scaled tests are not representative of those at full-scale 2) the sliding block model, 3) frictional drag of the moving soil mass on the geogrid, and 4) boundary frictional forces.

Table 8.2 Predicted and Observed Displacements - Full-Scale Tests

| Test | Blast Pressure Wave Displacement (ft) | Predicted Sliding Block Displacement (ft) | Total Pullout Displacement (ft) | Total Predicted Displacement (ft) | Observed Displacement (ft) |
|------------|---------------------------------------|---|---------------------------------|-----------------------------------|----------------------------|
| 5 -Panel 1 | 0.03 | 0.75 | 1.31 | 2.09 | 1.33-1.5 |
| 5 -Panel 2 | 0.02 | 0.75 | 3.75 | 4.52 | 0.66-0.83 |
| 6 -Panel 2 | No Data | 1.2 | 0.97 | 2.17 | 1.0-1.17 |

One difference between the explosions in the full and small-scale tests were the boundary conditions. The centrifuge soil was confined in a metal vessel that is 20 in. x 20 in, where 20 in. equals 50 ft. at prototype scale. The detonation of the bomb was in the center of the backfill, 25 ft. away from the

sides of the vessel at prototype scale. This confinement is approximately 10 ft. from the edge of the resulting explosive crater. The expanding soil around the explosion is restricted on three sides, which may tend to increase the pressure in the direction of the yielding wall. Applying those pressures to the full scale tests may yield greater accelerations, resulting in greater displacements.

The second source of error may be attributed to prediction of the mass movement component of the inertial wave loading. The block model assumes rigid body motion of the soil between the explosion cavity and the wall face. This essentially means all of the force applied to the block directly results in acceleration of the mass. Since the soil mass is not a rigid body, some of the input forces are expended through compression of the soil. This simple model will therefore overpredict the mass movement of the soil by not accounting for this influence. The use of the inertial stress time history from the approximate center of the block may have helped reduce this error, but only serves as an approximation.

The third source of error is related to increased stresses on the geogrid due to the frictional drag of the confining soil. The inertial wave does not decay to zero over the entire soil mass at one time. Rather, it decays to zero at the cavity/soil interface, and then progresses through the soil mass as a function of the wave velocity. With some of the soil returning to a static state, and some

being compressed, the compressing soil will cause frictional drag on the geogrid, increasing the pullout force on the grid. These forces are not considered in the model, therefore the model may be underpredicting the tensile forces on the geogrid.

The fourth source of error is the contribution of panel boundary resistances. Post-test observations from full-scale tests provide some evidence that frictional forces at the panel boundaries may affect displacement. In many cases, wall panels become jammed against each other during the test. Also, the four steel alignment rods on each panel may also become engaged. In many cases, it was observed that the rods were severely bent due to the differential movement of the wall panels. Finally, frictional forces exist at the top and bottom of each panel at their contact points. When differential displacement occurs between panels, these forces may either increase or decrease the forces on the panel, depending upon the direction of relative motion. The relative contributions of these frictional forces are difficult to quantify.

Approximation of Boundary Friction

The estimation of static boundary frictions may be incorporated in this model, however the interactions between the individual panels and alignment pins change rapidly and may either increase resistance or load, depending on

the directions of relative motion. As a simple approximation of the complex mobilization of the contribution of boundary frictional forces, the analysis will be repeated using static panel contact friction added to the pullout resistance function.

In this test, wood spacers were placed at the base of each panel during construction. Panel 2 rested on two of these spacers, and Panel 1, rested on Panel 2, also separated by two spacers. Robbins and Riskowski (1990) presented a mean value of approximately 0.6 for the coefficient of static friction for wood on smooth concrete. The weight of the panels is approximately 2200 pounds, and the frictional resistance was determined by taking the normal force at the upper and lower edge of the panel and multiplying by the coefficient of static friction yielding a total frictional resistance of 3960 pounds. On a per unit area, this resistance becomes 132 psf. The resistance function for this evaluation becomes:

$$R(u) = 132 + 2263u \quad \text{for } u < 0.19 \text{ ft.}$$

$$R(u) = 132 + 2263(0.19) = 562 \text{ psf} \quad \text{for } u = > 0.19 \text{ ft.}$$

For Test 5, Panel 1, boundary friction is reduced because it has no other panels resting upon it, and the pullout resistance is reduced due to the reduction in overburden. The relationship for resistance becomes:

$$R(u) = 44 + 752.6u \quad \text{for } u < 0.19 \text{ ft.}$$

$$R(u) = 187 \text{ psf} \quad \text{for } u = > 0.19 \text{ ft.}$$

The evaluation for pullout displacement was repeated for each of the panels evaluated previously, and are the results are summarized in Table 8.3

Discussion of Full-Scale Test Evaluation

Applying the model to the full-scale test provided conservative estimations of displacements that exceed observed by 20-30 percent when friction was considered. Consideration of friction made a significant difference to reducing the displacement of Panel 2, Test 5, and a smaller influence on the other cases.

The majority of the error is suggested to be in the use of the centrifuge pressure time history and the mass movement portion of the model. However, the data trends follow the expectations that decreasing weapon standoff distance

Table 8.3 Summary of Predicted Displacements With and Without Friction

| Test | Blast Pressure Wave Displacement (ft) | Total Predicted Displacement No Friction (ft) | Total Predicted Displacement With Friction(ft) | Observed Displacement (ft) |
|-------------|---------------------------------------|---|--|----------------------------|
| 5 - Panel 1 | 0.03 | 2.09 | 1.71 | 1.33-1.5 |
| 5 - Panel 2 | 0.02 | 4.52 | 1.12 | 0.66-0.83 |
| 6 - Panel 2 | No Data | 2.17 | 1.76 | 1.0-1.17 |

increases wall panel displacements for both loading mechanisms. Comparing the results of the two panels from Test 5 shows decreasing the resistance function through decreased overburden stresses on the geogrid and decreased boundary frictional resistances greatly increases displacement due to pullout.

An extreme case of the effect of increased boundary resistances was also shown in the centrifuge tests. In centrifuge Test 19, a steel bar was placed at along the top edge of the wall and attached to the centrifuge bucket wall. This rigid frictional boundary condition reduced the displacement of the top wall panels by approximately 40 percent when compared to that of the control tests without the top restraint. The introduction of frictional resistance at the

boundaries provides reductions in displacement, both in the model predictions and as observed in testing. However, too much restraint at the panel boundaries could lead to failure of the concrete panels. This was observed in the full-scale tests on walls reinforced with inextensible reinforcement (Eytan and Reid (1993), where the presence of a frictional boundary at the top of the wall resulted in flexural panel failure.

The introduction of boundary frictional resistance provided a method for increasing the effectiveness of the model, and provided consistent results when applied to panels with variations in their frictional forces. In this analysis, the use of boundary static frictions provided a simple approximation of the complex mobilization of boundary forces. Further evaluation of the resistance forces will be discussed in Chapter IX.

CHAPTER IX

INFLUENCE OF DESIGN PARAMETERS ON WALL DISPLACEMENT

Introduction

The development of a model to evaluate the response of the full and small-scale test data provides a tool to investigate the relative influence of the design variables considered in the model on wall panel displacements. In this chapter, the results of full-scale Tests 5 and 6, wall panel two, will be used as control tests. Changes to different design variables will be made and input into the model to compare the output with that of the control test for a constant forcing function time history. The forcing function time histories from centrifuge Tests 20 and 27 will be used, provides data for 21 and 25-ft. weapon standoffs.

Evaluation Matrix

The parameters in this model that may effect wall panel displacement are the coefficient of static friction between the wall panels, μ_s , unit weight of the backfill material, and pullout resistance of the geogrid. The percent changes in each parameter are representative of the range of values available for use in

design. The evaluation matrix that will be applied to each loading function is presented in Table 9.1.

Table 9.1 Model Evaluation Matrix

| Parameter | μ_s | μ_o | Unit Wgt | Unit Wgt | Pullout Resistance | Pullout Resistance | Pullout Resistance |
|-----------|---------|---------|----------|----------|--------------------|--------------------|--------------------|
| % Change | +50% | -50% | +20% | -24% | +25% | -25% | +100% |

Results of Evaluation, Test Five

The results of the evaluation matrix for Test 5, Panel 2 are presented in Table 9.2. The evaluation of the influence of the design variables considered in this model show that increasing the unit weight of the backfill soil and significantly increasing the pullout resistance of the reinforcement have the greatest influence on reducing wall panel displacements when compared to the control test. Both of these parameters decreased displacements by 15 and 20 percent, respectively over the control test. Increases in the frictional resistance and smaller increases in pullout resistance also, to a lesser extent, reduce predicted displacements.

In terms of increasing displacement, reduction in the unit weight of the soil has a significant effect on panel displacement when compared to the control

Table 9.2 Evaluation Matrix Results - 25 Foot Standoff

| Evaluation | Parameter | μ_s | Unit Wgt (pcf) | Pullout Resistance (lb/ft) | Block Displacement (ft) | Pullout Displacement (ft) | Percent Change in Displacement |
|------------|----------------|---------|-------------------|----------------------------------|-------------------------------|---------------------------------|--------------------------------------|
| Test 5 | Control | 0.6 | 105.7 | 1500 | 0.75 | 0.43 | 0 |
| 1 | - μ_s | 0.3 | 105.7 | 1500 | 0.75 | 1.0 | +59.1 |
| 2 | + μ_s | 0.9 | 105.7 | 1500 | 0.75 | 0.29 | -4.6 |
| 3 | + 25% Pullout | 0.6 | 105.7 | 1875 | 0.75 | 0.28 | -6.4 |
| 4 | - 25% Pullout | 0.6 | 105.7 | 1125 | 0.75 | 2.16 | +164.6 |
| 5 | +100 % Pullout | 0.6 | 105.7 | 3000 | 0.75 | 0.13 | -19.8 |
| 6 | - Unit Wet | 0.6 | 80.0 | 900 | 1.03 | 5.81 | +521.8 |
| 7 | + Unit Wet | 0.6 | 125.0 | 1700 | 0.66 | 0.28 | -14.6 |

test. The reduction in unit weight is detrimental since it reduces the resistance to the mass movement of the soil when the entire mass is under compression, and, to a lesser extent, decreases the normal stresses on the geogrid, thereby decreasing its resistance to pullout. Decreasing the pullout resistance by 25 percent also lead to a significant increase in displacement. Reduction in the boundary frictional forces also increases wall panel displacements by almost 60 percent over the control test.

Coupling the results of a specific set of parameters also demonstrates a consistent trend. When resistance is increased, displacements are reduced on the order of 10 percent. When resistance is decreased, displacements increase on the order of 100 percent. This suggests this specific test wall design offered a low factor of safety, meaning the design may not be appropriate for the loading condition.

Results of Evaluation, Test Six

The results of the evaluation for Test 6, Panel 2 are presented in Table 9.3. Significant increases in pullout resistance and backfill unit weight have the greatest influence on reducing wall panel displacement, followed by increasing boundary frictional resistance and a 25 percent increase in pullout resistance.

Table 9.3 Evaluation Matrix Results - 20 Foot Standoff

| Evaluation | Parameter | μ_s | Unit Wgt (pcf) | Pullout Resistance (lb/ft) | Block Displacement (ft) | Pullout Displacement (ft) | Percent Change in Displacement |
|------------|----------------|---------|-------------------|----------------------------------|-------------------------------|---------------------------------|--------------------------------------|
| Test 6 | Control | 0.6 | 104.7 | 1500 | 1.2 | 0.56 | 0 |
| 1 | - μ_s | 0.3 | 104.7 | 1500 | 1.2 | 0.75 | +10.8 |
| 2 | + μ_s | 0.9 | 104.7 | 1500 | 1.2 | 0.42 | -8.0 |
| 3 | + 25% Pullout | 0.6 | 104.7 | 1875 | 1.2 | 0.42 | -8.0 |
| 4 | - 25% Pullout | 0.6 | 104.7 | 1125 | 1.2 | 0.80 | +13.6 |
| 5 | +100 % Pullout | 0.6 | 104.7 | 3000 | 1.2 | 0.24 | -18.2 |
| 6 | - Unit Wgt | 0.6 | 80.0 | 900 | 1.6 | 0.9 | +42.0 |
| 7 | + Unit Wgt | 0.6 | 125.0 | 1700 | 1.0 | 0.48 | -15.9 |

Again, decreasing backfill unit weight has the greatest influence on increasing wall panel displacement, followed equally by a 25 percent decrease in pullout resistance and decreasing boundary frictional resistance. When resistance was increased or decreased, displacements increased or decreased accordingly on the order of 10 percent.

Comparison of Evaluations

As expected, both evaluations provide similar conclusions as to the influence of these design parameters on increasing or decreasing wall panel displacement. When resistance was increased, the predicted displacements were reduced by 10-20 percent over their respective control tests. What is significant to note is that in the evaluation for Test 5, any decrease in resistance lead to significant increases in displacement, much more so than Test 6. This highlights the significance of the relationship between interface stress amplitude and duration of loading. In Test 5, the interface stress remains between 300 and 500 psf for periods on the order of tens of milliseconds. The reductions in resistance in this evaluation resulted in resistances that were less than the interface stress for many iterations, resulting in significant displacements. In Test 6, the pressure time history was somewhat different. The interface pressures in Test 6 during some time steps exceeds 1000 psf, and then drops to

less than 250 psf before increasing again. The reduction in resistance in Test 6 did not have as significant effect on results as Test 5 because of the differences in the pressure time histories, especially the duration of the pressure when it exceeds resistance. This example serves to highlight that in the development of techniques to estimate the magnitude and duration of the inertial stress waves, errors on the order of several milliseconds in predicting the load duration could have significant results on the prediction of system response. In the control tests for each evaluation, when the applied stress exceed the resistance by approximately 100 psf for a duration of 30 ms, an additional 0.06 ft. of displacement was predicted. This results in approximately 0.2 ft. displacement in 0.1 sec. This sensitivity suggests simple techniques to estimate amplitude and duration of the plastic stress wave may not appropriate for use in this analysis.

In terms of the unit weight of the backfill, the results of this evaluation are confirmed by empirical results. Three identical scaled tests were performed with variations in unit weight of backfill (Olen, et al 1993). At prototype scale, the displacement of wall panel two for backfill densities of 103, 95, and 89 pcf were 1.49, 1.76, and 2.49 feet respectively. Figures 8.6 and 8.7 show changes in unit weight do not seem to significantly affect inertial stress wave decay, so therefore increased unit weight does not appear to alter the forcing function.

Second, the normal stress on the geogrid is not significantly altered by small changes in unit weight, therefore decreased displacement due to increases in unit weight are not related to minor changes in the pullout resistance function. Based upon this analysis, the primary contribution of increased unit weight is to reduce displacement due to the mass movement component of the inertial wave loading.

Increasing the pullout resistance by increasing the tensile modulus of the reinforcement also reduces displacement as shown in the model evaluation and validated by the full-scale tests. Increases in pullout resistance may be achieved by decreasing the extensibility of the reinforcement through influencing the load transfer mechanisms between the reinforcement and soil (Juran and Chen, 1988). Increasing the extensibility of the reinforcement results in nonuniform stress distributions on the reinforcement, resulting in stress concentrations in the geogrid in the area near the facing panel. Alternatively, decreasing the extensibility results in more uniform stress distribution over the reinforcement. Juran and Chen (1988) report increased pullout resistance and decreased displacement with increasing tensile stiffness, all other factors being equal. In short, increasing geogrid stiffness provides increases in pullout resistance and less displacement to achieve those higher levels of resistance (Fig. 9.1). This is very important in this research program, where during the inertial wave

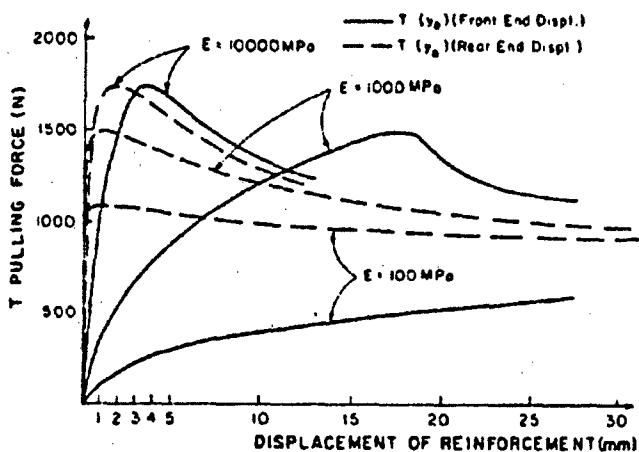


Figure 9.1 Pullout Resistance as a Function of Geogrid Stiffness
(Juran and Chen, 1988)

propagation the geogrid tail may be statically confined and the soil closer to the wall may still be in compression while stresses are being applied to the wall panel. The stiffer geogrid would reduce the opportunity for large stress concentrations occurring in the zone of soil being compressed by the inertial wave. This confirms the observations from the full-scale tests, as previously discussed, where the increase in geogrid stiffness between tests 1 and 3 and 5-6 resulted in significant reductions in wall panel displacement.

Methods to Reduce Wall Panel Displacement

The results of this research have shown that the wall, as designed for this research program, is not appropriate to completely mitigate the effects of a fully coupled explosion of a 500 lb. at distances less than 30 ft. from the wall facing. Both designs did survive detonations at 30 ft. and one survived 25 and 20 ft. standoff detonations. Therefore, for an expedient shelter, the structure may provide one time protection, but the wall panel displacements may make the structure vulnerable to subsequent explosions. If more predictable and permanent protection is required, the engineer would defer to more traditional designs using reinforced concrete.

However, since many weapons have smaller charge weights, and not every explosion takes place in the retained backfill other design parameters, some not specifically addressed in this research, may increase the level of protection offered by reinforced soil walls. This section will summarize how the design of these structures can be improved, based on the results of this research and the results of other research in related areas. The improvements fall in two categories: reducing the forcing function or increasing the resistance of the structure.

Decreasing Forcing Function Amplitude

The full-scale and centrifuge tests have shown that increasing the distance between the explosion and the wall significantly reduces the residual wall panel displacements. This same effect may be achieved by preventing the explosion from becoming fully coupled in the soil by reducing the depth of penetration an

Backfill Minimization. In these research tests, the backfill soil extended well beyond the embedment depth of the soil reinforcement. The retained fill should extend back from the wall as short a distance as possible. This decreases the chance of a weapon landing in the backfill by presenting a smaller target. In previous tests (Eytan and Reid, 1993), four 500 lb. bombs were placed on the slope of the backfill of a reinforced soil wall. This test caused no measurable displacement of the wall panels, suggesting that most of the blast energy was dissipated into the surrounding air instead of the soil mass. This is one simple method of increasing the effectiveness of a given design.

Predetonation Screens. Many weapons use contact fuses to initiate detonations. The presence of a thin concrete or steel superstructure around the target provides a method of initiating an explosion at or near the surface of the soil, serving to minimize the coupling between the explosion and the soil mass.

Overlay Systems. Another method for reducing the penetration capability of projectiles is to overlay the exposed face of the soil with rock rubble or

concrete deflection grids (Underwood and Westmoreland, 1993; Rohani, 1987; Creighton, 1982). These materials also provide a method for altering the flightpath of penetrating weapons and inducing detonation. Rock rubble overlays provide a simple and effective upgrade, especially against smaller classes of weapons.

Increasing Resistance of Structure.

For a given forcing function, methods identified as part of this research as well as from other sources provide some methods to increase the resistance of reinforced soil walls to explosion effects.

Top Restraint. As previously discussed and as detailed in other research (Olen, et al, 1994; Eytan and Reid, 1993), the presence of a displacement controlled boundary at the top of the wall greatly reduces panel displacements along the top row of panels. This is particularly beneficial because the top layer of panels have the least resistance to reinforcement pullout because of the relatively low normal stresses on the reinforcement.

Increase in Backfill Unit Weight. As discussed previously in this chapter, increases in the unit weight of the backfill also appear to reduce the displacement of the wall panels by increasing the resistance to the mass movement of the soil/wall system.

Vertical Reinforcement. Another method to decrease the inertial pressures on the wall would be to install vertical layers of geogrid between the explosion and the wall. This may present a unique challenge during installation, but research in this area demonstrates the potential of this system. Ohrt (1995) has investigated the effects of geogrid layers in reducing the size of explosive craters. Testing conducted as part of this research consisted of placing layer(s) of uniaxial or biaxial geogrid placed between the explosion and the soil surface. Preliminary results show that crater diameters are significantly reduced by placing two layers of uniaxial geogrid at perpendicular orientations in the soil above the weapon. These layers of geogrid are believed to reduce the magnitude of the propagating inertial stresses. The decrease in crater size suggests vertical reinforcement may show promise towards reducing inertial stresses propagating in the horizontal direction, just as horizontal reinforcement appears to reduce inertial stresses propagating in the vertical direction.

Soil Stabilization. One method for reducing the size of explosion craters in airfield pavements has been to provide a thick aggregate layer under the pavement surface or to stabilize the pavement base material with cement. These methods limit the propagation of the inertial stresses by increasing the strength of the soil.

Increase Pullout Resistance. As shown previously in this chapter, increasing the pullout resistance of the geogrid also reduces wall panel displacement by transferring stresses more uniformly over the geogrid towards the geogrid tail that is confined with static soil while other portions of the geogrid/soil may still be in compression.

CHAPTER X

CONCLUSIONS AND RECOMMENDATIONS

Introduction

Current methods of evaluating the design of reinforced soil walls to explosion induced groundshock are extremely limited, consisting primarily of proof testing. Previous scaled testing qualitatively identified that load magnitude, backfill unit weight, and the tensile modulus of the reinforcement were the design parameters that had the most significant effect on reducing wall panel displacements. To develop a more quantitative understanding of the parameters affecting wall response, the problem was studied within the framework of a model of yielding walls presented by Drake, et al (1987). A series of full-scale tests were conducted to investigate the response of the walls to free-field blast pressures, and detailed analysis of test data suggested inertial stresses, not blast pressures, were the governing loading condition. The Drake model was adapted to provide a more quantitative approach to understanding the phenomena of inertial wave loading in the time domain. The validity of the model was established via full-scale data, and checked with scaled data. The

validated model was then used to study the inertial wave loading. The approach and results of this study provides a significant departure from previous research by identifying the loading mechanisms that govern response, the influence of the engineering properties of the materials, and validation of a model that provides a quantitative description of the physical response of the reinforced soil wall.

In this section, a brief summary is presented of the most significant conclusions of this first test of a geogrid-reinforced soil retaining wall with concrete facing panels subjected to loads from explosions in the retained backfill. Details on the development of each conclusion are discussed throughout the text of this report. Based on the experience of this research, recommendations are suggested as to further investigations that would contribute to providing further progress in this research area.

Summary of Conclusions

1. A successful series of six explosive tests were performed on four geogrid reinforced walls. Since this type of instrumented test series had never been successfully preformed before, this research has created a unique data base on the response of the reinforced soil walls to free-field blast pressures.

2. This research suggests two loading mechanisms are present when an explosion takes place in the retained backfill. First is the high amplitude, short duration blast pressure wave. This is followed by the inertial or plastic stress wave, which has two components. First is the loading that takes place while the entire soil mass from the crater/soil interface to the wall panel is in compression. This is the mass movement resisted by the mass of the soil and energy absorbed by the compression of the soil mass. Once the inertial wave decays in the region of the geogrid tail, stresses on the facing panel are transferred to the reinforcement and boundary frictional forces, and the pullout resistance of the soil/reinforcement becomes mobilized.

3. Research conducted over the past two decades has attempted to relate residual wall displacements to the free-field blast pressures and accelerations. The results of this research have shown that the inertial pressure wave, and not the blast pressure wave, is the load mechanism that results in the most significant displacement of the wall panels.

4. The model proposed by Drake, et al (1987) was applied in this research to the three loading components to provide increased understanding of the loading mechanisms and system response. The model was validated for the pressure wave response using full and small-scale test data and provided consistent

results across scales. However, further investigation is necessary to determine the sensitivity of the model to changes in soil type. Because of limitations in test data, the model was adapted for evaluation of the inertial wave loading. However, this research suggests this model may be appropriate for evaluating wall response to both the blast pressure and inertial wave loading.

5. The equation of motion provides a means for evaluating the response of the walls to the two components of inertial wave loading. Evaluating the equation of motion in terms of interface stress provided a means of estimating the pullout related displacements of the wall panels based upon measured interface pressures and reinforcement pullout resistance. The resistance function in this equation was modified to consider both the pullout resistance of the reinforcement and the resistance offered by the boundary frictional forces. Boundary frictional forces were estimated by conventional static means. Considering the mass of soil as a rigid block, the displacement due to the mass movement of the soil was estimated via the equation of motion, resisted only by the mass of the soil and wall panel. Using measured soil pressures from the scaled tests, prediction of displacements using the equation of motion yielded order of magnitude results. For the scaled tests, the model predicted displacements within 20 percent of measured. The primary source of error for the full-scale analysis is attributed the application of the scaled test pressure

time histories to the full-scale tests. The rigid block assumption in the mass movement analysis, estimation of boundary frictional resistances and the superposition of the mass movement and pullout displacements are three additional sources of error.

6. As qualitatively shown in previous research, the unit weight of the backfill material and tensile modulus of the reinforcement are the two engineering properties that have the most significant effect on reducing wall panel displacements. For two similar sands, increasing unit weight was shown to reduce the mass movement of the soil/wall system primarily through mass, not through any significant increase in shear resistance. Empirical test results indicates increasing the tensile modulus of the geogrid reduces pullout related displacement through increased pullout resistance. The stiffer reinforcement provides more uniform stress distribution over the embedded length of geogrid, transferring the stress to the area of grid embedded in static soil, and away from the compressive zone.

7. For the materials and stresses used in this evaluation, geogrid rupture was not observed.

8. The Drake-Little equation, as used in this research to predict free-field blast wave pressures, predicted free-field stresses with a standard error of 8.5 psi,

and is therefore considered a viable method for estimating free-field stresses within a reinforced soil mass.

9. Original procedures for installing strain gages on geogrid that would survive the installation, field construction, and free-field blast and inertial pressures were developed and modified during this test series. By the final test series, the gage survival rate was 80 percent.
10. Based upon the comparison of the full and small-scale test data, the centrifuge studies provide reasonable models of full-scale tests.

Recommendations

Based on the experience of this study, recommendations for further research are presented that, in the author's opinion, would lead to further progress in the study of this subject.

1. A model that, for a given explosion in soil, characterizes the amplitude and duration of the inertial stress wave in a semi-infinite soil mass. This would provide a means of quantifying these stresses for a range of weapon sizes and standoff distances, as well as their spatial variations. Incorporation of this model with the Drake model would provide a means of further study into this research area.

2. Data from full or scaled testing that details the inertial stress wave is very limited, for either the infinite or semi infinite case. Further test data would be necessary to validate any modeling of inertial stresses.

3. Current models for soil reinforcement interaction are based upon modelling the behavior observed in standard pullout testing with various levels of success. The interaction between the soil and reinforcement when large strains in the soil mass are propagating through the reinforced zone towards the wall panel may not be represented by current models. Investigation of the effect of this loading condition on the soil/reinforcement interaction establish how laboratory pullout test results compare to this unique loading condition.

APPENDIX A

INSTALLATION OF STRAIN GAGES

Introduction

The preparation, attachment, and coating procedure for attaching strain gages to polymer geogrids described in this appendix was based on research by Oglesby, et al (1992). Much of this procedure, developed and validated for strain measurements of unconfined geogrid in laboratory tensile tests, is included herein. These procedures were used for attaching the strain gages during full-scale Test One. Based on the experience of this first test, a series of modifications were made to the procedures, greatly increasing the survival rate of the gages. These modifications are also detailed in this appendix.

Materials

- 1) Micro Measurement's (MM) EP-08-250BG-120 strain gages
- 2) MM's A-12 adhesive
- 3) non-aggressive cellophane tape, 3 strand wire (MM 326-DTV), and standard tools for strain gage work
- 4) 000 steel wool, 220 and 400 grit wet/dry sandpaper
- 5) laboratory grade alcohol for cleaning
- 6) large spring clamps

- 7) 0.25 in. thick aluminum bar stock
- 8) 0.25 in. thick medium density closed cell neoprere sponge
- 9) oven with sufficient capacity for samples, capable of holding 125 degrees Fahrenheit for four hours or longer
- 10) aluminum foil
- 11) rubber cement
- 12) TYGON tubing
- 13) GE (or similar) 35 year silicon rubber General Household Sealant

Surface Preparation

The surface preparation procedure developed uses commonly available materials. A clean, metal topped table was used as a firm surface for all preparation and gluing. Laboratory grade alcohol on gauze pads was used for cleaning the geogrid surface before and after each abrasive. The surface was wiped until no residue or discoloration showed on the gauze pad each time. A cross-hatch pattern was used with each abrasive, 45 degrees clockwise and counter-clockwise from the direction in which the grid was to be tested. 000 steel wool was the first abrasive used. Pressing hard, and being careful not to damage or peel the edge of the tensile rib, the rib surface was scoured, using the cross-hatch pattern to completely cover the surface, seven times. This number of repetitions was sufficient to completely degloss the surface. After

cleaning, 220 grit wet/dry sandpaper was used. The surface was abraded four times using the cross-hatch pattern. This produced a roughened surface without actually removing the geogrid material. After cleaning, the third and final abrasive, 400 grit wet/dry sandpaper was used. As with the 220 grit sandpaper, the surface was abraded four times using the cross-hatch pattern. The final cleaning with alcohol was very thorough. The prepared surface appears smooth, with a dull finish.

Attachment

The techniques used to glue the stain gages to the geogrid are similar to those used for attaching strain gages to other surfaces. Care was taken in handling the gages so that all surfaces stayed clean. Non-aggressive cellophane tape was used to hold the gage, and align it properly on the prepared surface. The tape was then pulled back from one end, lifting the aligned gage from the geogrid. A small amount of adhesive was then placed on the geogrid or foil strip, and the strain gage was placed back onto the prepared surface. Using a firm, smooth stroke, the tape is pressed down to spread the adhesive and remove any bubbles. Very detailed instructions for this type of gluing technique are available from strain gage manufacturers.

To apply uniform pressure while the adhesive sets required placing clamps over the strain gages. One neoprene pad was placed on the cellophane tape covering the strain gage. The two aluminum blocks were placed over each side of the geogrid rib, sandwiching the neoprene, gage, and geogrid in between. Everything was held together using a spring clamp. It is important to center the clamp so that the pressure is evenly applied. After the strain gages were glued and clamped in place, the samples were placed in a large oven, clamps attached, at 125 degrees Fahrenheit, for at least four hours. After the samples were removed from the oven, they were allowed to cool overnight before the clamps were removed. The neoprene sponges and the cellophane tape should be removed carefully to avoid damaging the gages. At this time the leadwires can be soldered to the strain gages.

Protective Coating

Six thin coats of rubber cement were applied to the entire strain gage surface, exposed leadwires, and soldered connections. Each coat was allowed to dry at least ten minutes before another coat was applied. The silicon caulk, a transparent medium which allows the glued gage to be observed, was then applied. Two long pieces of TYGON tubing were split and placed around the geogrid rib and strain gage to act as a mold and to contain the caulk. The

caulk will cure in about 24 hours at 125 degrees Fahrenheit, or in 3 to 4 days at room temperature. After the caulk was cured, the TYGON tubing "mold" was removed.

Deviations and Additions to This Procedure

Protection of the Leadwires. Because the leadwires would be covered with many feet of soil backfill, subjected to the stresses of the earth moving and compaction equipment, and had to pass through the gaps between the facing panels to be accessible, the leadwires had to have additional protection. In this case, each 12 ft. long leadwire was passed through approximately 10 ft. of 1/4 in. diameter TYGON tubing. Since passing wire through long lengths of small diameter tubing is analogous to pushing wet spaghetti through a soda straw, a procedure for feeding the wire through the tubing was developed. For all tests, the leadwire used was Micro-Measurements 326-DTV stranded tinned-copper wire, 3-conductor twisted cable, with vinyl insulation.

First, a 12 ft. piece of nylon string was obtained, and a small knot was tied on one end. One end of the 1/4 in. TYGON tubing was attached to a vacuum source and the knotted end of the string was inserted into the other end of the tubing. If the tubing was free of kinks or other defects, the string would then pass through the tubing to the end connected to the vacuum source.

The string was then attached to a 12 ft. piece of stiff wire, and the string was pulled through the tube, pulling the wire with it. Once through the tube, the wire was soldered to the strain gage lead wire, and then again pulled through the tubing. Now the leadwires were encased in a protective tubing. This process was developed through trial and error, and made best use of the materials and equipment on hand.

Tie - Down of the Leadwires. Another step added to the above procedures was the use of plastic tie downs to provide strain relief to the leadwires, and reduce the stress on the soldered connection. After the leadwires were soldered to the strain gages, a plastic tie was wrapped around the geogrid rib and encased leadwire and tightened, within an inch of the soldered connection. A second plastic tie was used a few inches further away from the soldered connection. This prevented the self weight of the wire from breaking the soldered connection.

Protection of the Strain Gages. Due to the potential for construction damage to the strain gages, the TYGON tube used on each rib to contain the silicon caulk was left in place.

Results of Test One

After completion of construction of the first test wall, a test of the strain gages determined that none of the connections between the leadwires and the strain gages had survived construction. It was hypothesized that there was a failure in the soldered connections between the leadwires and strain gages, therefore the strain gage installation procedures had to be modified to prevent a reoccurrence of this problem in subsequent tests.

Modification of Strain Gage Installation Procedures

The stiff soldered connection between the strain gages and the leadwires was breaking under construction and installation stresses. To improve the survivability of the strain gages, modifications were made to the strain gage installation procedures.

Addition of Bondable Terminals

To provide strain relief between the soldered leadwires and the strain gage, bondable terminals were epoxied to the geogrid rib adjacent to the solder tabs of the gage. These were attached to the geogrid rib using the same procedures used for the strain gages. Both the bondable terminals and the strain gages could be installed at the same time. The instrument leadwires were then

soldered to the bondable terminals adjacent to the gage, and small flexible jumper wires, curved to form strain-relief hoops, were then connected from the terminals to the gage solder tabs. The specific bondable terminals used for all subsequent tests were Micro-Measurements terminals number CTF-50-C.

Use of Low Temperature Solder

The high temperature solder used in the first test required temperatures in the 600-800 degrees F to melt the solder. To melt the solder at this temperature required long contact times to the solder and strain gage. This lead to some melting of the geogrid. To reduce the contact time between the soldering iron and the solder and strain gage, a lower temperature solder was used. The specific solder used for all subsequent tests was Micro-Measurements solder #361A-20R. This solder would melt at 361 degrees F, and greatly reduced heat transfer to the geogrid. Soldering at specific temperatures required the use of a temperature control soldering station that allowed for complete control of the temperature of the soldering iron.

Reinforcement of the Geogrid Ribs

The flexible geogrid ribs on which the strain gages were mounted tended to bend during handling, stressing the soldered connection between the leadwires and the strain gages. To help stiffen the ribs, without affecting the overall

strength of the geogrid, thin wooden sticks ("popsicle sticks") were glued to the underside of the rib using rubber cement. This helped prevent excessive bending of the geogrid ribs, without significantly affecting the strength properties of the geogrid.

Strain Gage Protective Coating

The use of six coats of rubber cement to coat the strain gages and soldered connections was time consuming and had unknown properties. To speed the process, and to provide specified performance, two coats of Micro-Measurements M-Coat D coating material was used for all subsequent tests. This material provided a hard coating capable of high elongation. This material provides a good moisture barrier and negligible electrical leakage.

Success Rate

Using these procedures with the modifications mentioned above, the survival rate for these strain gages increased to over 80 percent.

APPENDIX B

TEST WALL CONSTRUCTION

Introduction

This section will discuss the test site, fabrication of the concrete wall panels, pouring the leveling pad, and construction of the embankment.

Test Site

The test site selected for this project was the Sky X test site located in the eastern section of Tyndall Air Force Base, near Panama City, Florida. The test site is a designated research and development test area approximately 800 by 1100 ft. in size. The maximum Net Explosive Weight of explosives authorized for detonation at the site is 1000 lbs. equivalent TNT. This site was chosen because it is an approved explosive test site, and also due to its proximity to the available laborers, heavy equipment, borrow pit, instrumentation, and research offices/labs. Having this site locally available greatly reduced the project cost.

Within the test area many potential sites were evaluated for use. A site was selected near the remains of an existing hardened shelter used in an earlier research project. Only the first test wall was constructed on this site, because with each successive lift it became more difficult for the heavy equipment to get to and operate on the top of the embankment. The next three walls were constructed near the first on a location lower in elevation. This allowed the equipment easier access to the top of the embankment since it could be reached via a soil bridge constructed from the nearby higher ground.

Fabrication of Wall Panels

A commercial fabrication company was hired to fabricate the wall panels needed for this test. A contract for approximately \$29,000.00 was let to United International, Inc. of Birmingham, Alabama, to be executed by their office in Fairhope, Alabama.

A total of 160 panels were fabricated with a total area of wall facing of approximately 1093 sq. ft. per wall. This yielded a fabrication cost of approximately \$6.64 per sq. ft., fabricated on site and not including construction of the actual test wall. This cost included the necessary spacers and joint materials used in construction.

A series of 12 wooden forms were built for pouring of the panels. The standard steel forms for the panels were committed to another job, so wooden forms were used to speed delivery time. A concrete pad was poured to provide a smooth and level location for panel fabrication. After the forms were set in place they were lined with form grease and the reinforcing cages were placed into the forms on metal saddles. Two 3 ft. long pieces of the appropriate geogrid were wire tied to the reinforcing cage, one centered between the middle and the top of the panel, the other centered between the middle and the base of the panel. This would result in a 30 in. spacing of geogrid layers. Standard 4000 psi ready mix concrete was delivered to the site and poured into each of the forms. The concrete was vibrated and then hand finished.

In 24 of the full sized panels, metal soil pressure gage mounts were cast into their geometric center. Also, a 2 by 2 in. metal plate with 4 anchor legs was placed into these same 24 panels, such that the metal plate was on what would be the exposed face of the wall panel. Each plate had a small hole tapped into it for mounting of the accelerometers.

After an initial cure time of approximately 18 hours, the forms were stripped and the panels moved to temporary storage to complete curing and await for construction to begin. When the panels were moved after the initial cure time, they were lifted by the geogrid and not the lifting eyes embedded in

the panels. This was done because the concrete was too "green" and therefore not strong enough yet to prevent the lifting eyes from pulling out of the concrete. Before the panels were stacked, the edges of the panels were inspected and any excess concrete that might have squeezed through the forms was chipped off.

The concrete panels were placed in stacks of five panels or less. Wooden dunnage was placed between the panels. It was extremely important that the dunnage pieces were lined up axially. If the dunnage was randomly placed, there is a chance the lower panels could crack and break under the stresses. Finally, the panel faces could not come in direct contact with the wood dunnage, because it can cause a permanent stain on the panel face. Therefore, each piece of dunnage had plastic separators on the side exposed to the panel face.

Leveling Pad and Site Preparation

Before construction could begin, the site was cleared and leveled and a leveling pad was installed. The test site was an area of silty sand and with intermittent grassy areas. The top 6 to 12 in. of soil was removed to provide a level working table for construction. At the proposed location of the concrete facing panels, a ditch was constructed for the pouring of a leveling pad. This

ditch was 100 feet long, approximately 2 ft. deep, and 3 ft. wide at its base. The embankments of the ditch were tapered outward to allow room for working the screed boards after pouring. Metal forms were then placed in the ditch and leveled. The final pad surface had to be level to ensure the facing panels fit together properly. The forms were placed such that the leveling pad would be 1 ft. thick and 18 in. wide. No reinforcing steel was placed in the forms. The steel was not required because the pad only served to provide a level base for the facing panels to rest upon, and was not designed as a load bearing footing. Prior to pouring the concrete, a transit was used to check the level of the forms and guide the final adjustments. The concrete was poured, vibrated, and the surface was screeded smooth.

Wall Construction

Introduction

This section will generically discuss the procedures used for construction of the reinforced soil walls. Construction procedures were modeled after those performed on any commercial reinforced soil retaining wall project. With the exception of the instrumentation, no special allowances were made during the erection of these walls. Also, attention to detail was necessary to ensure the six instrumented panels on each wall were installed in their proper place nor

overlooked amid all the activity of construction. Finally, no drainage system was designed into the embankment due to the short design life of the project.

Base Row Panels

Prior to placing the first panels, a string line was established to over the length of the leveling pad to ensure proper alignment of the wall panels. The 5½ in. thick panels were to be centered on the 18 in. wide leveling pad. The string line was placed so that each panel would rest 2 in. away from it to prevent any interference between the panels and the string. A steel tape measure was used to ensure proper offset between the string and the panels.

While the string line was being established, an all terrain forklift was moving the concrete panels to the site. When picking up panels from a stack extreme care had to be taken to ensure the forklift tines did not catch on the geogrid tails sticking out of each panel. When a partial stack was to be picked up, long planks were placed between the panels such that the forklift tines would be above the geogrid, separated from the geogrid by the wooden planks.

With the stringline in place and panels at the site, placement of the panels could begin. First, two 6 ft. by 20 in. panels were lowered into place. The distance between these panels was gaged such that a 6 ft. by 40 in. high panel could fit between them. After the first two panels were set, a 6 ft. by 40 in.

panel was set between them. Each panel was separated from the adjacent panels by a $\frac{1}{2}$ in. gap. After the panels were set, the 6 ft. by 40 in. panel was clamped to the two adjacent panels. Next, another 6 ft. by 20 in. panel was set in place, spaced such that a 6 ft. by 40 in. panel could fit between them. After the second 6 ft. by 40 in. panel was set, it was clamped to the adjacent panels. This process was repeated until the entire first row of panels was in place.

Once the first row was set, each 6 ft. by 40 in. panel was restrained with wooden shoring. A clamp was placed at the top center of the panel, and a long 2 in. by 4 in. board was nailed to the clamp. The panel was then pushed toward the backfill side to provide an inward batter of approximately $\frac{1}{4}$ of an in. per ft. of panel height. The amount of batter depends upon the type of reinforcing material and backfill soil. A coarse backfill requires less batter than a fine soil, and a higher tensile modulus geogrid requires less batter than a lower tensile modulus geogrid. The shoring was then nailed to a heavy stake driven into the ground in front of the wall.

Placement of Backfill

With the first row of panels in place, soil was then placed in front of the wall to ensure the proper embedment depth, which in this case was 1.5 feet. Before backfill could be placed behind the wall, the gaps between the panels

had to be covered to prevent soil loss through the cracks. In this case, filter cloth strips were placed over the joints on the backfill side of the wall, and this material was glued directly to the backside of the panels. With the joints covered, backfill soil was then placed and compacted behind the wall up to the elevation of the first layer of geogrid. For this project, the soil was placed, leveled and compacted with a tracked John Deere TD-15 bulldozer. The bulldozer remained at least 4 ft. away from the concrete panels. This distance may increase or decrease, depending upon the size of the heavy equipment.

Once the soil was in place, the geogrid reinforcement was installed.

Placement of Geogrid Reinforcement

The geogrid roll was placed behind the first panel and connected to the geogrid tail that extended out from behind the panel. The pieces of geogrid were overlapped, and aligned so the ribs from one piece could be woven into the gaps of the other piece. A plastic Bodkin bar was then pushed between the two layers of geogrid over its entire length. The geogrid was then unrolled to the specified embedment length, and cut from the roll with a razor knife. This was repeated until the entire first layer of geogrid was in place. Once the geogrid was in place, soil could be placed over the grid starting at one end of the wall. Two long steel rods are pushed through the ends of the geogrid mesh

and driven into the soil with a sledgehammer. Workers then pulled on each rod, effectively prestressing the geogrid. The bulldozer pushed soil over the prestressed grid, starting in the area just behind the wall panels and working back. Soil was placed such that the equipment never came in contact with the geogrid. Once the first piece of grid was covered, the next piece of grid was prestressed, and the whole process repeated. The lifts of soil were placed to the level just below the horizontal gap at the top of the 20 in. high panels. The bulldozer then made repeated passes over the backfill until the necessary compaction was achieved, as confirmed by a nuclear density gage.

Second Row of Panels

The next row consisted of seven full (6 ft. by 5 ft.) panels. Two 1/2 in. spacers are placed on the top edge of the panel upon which the next panel will rest. These spacers are made of rubber for a permanent wall, however since this wall was temporary, 4 in. by 4 in. by 1/2 in. wooden shims were used. Metal alignment pins are placed in the holes on the edges of the in-place panels. The clamp is removed from the panel and the next panel is guided into the alignment pins and set into place. Once the panel is in place, and before the crane is released from the panel, the alignment of the panel is adjusted. The gap between the panels is set and the base of the panel is in line with the

panel below it. Crow bars were used to make the necessary panel adjustments. The panel is then loosely clamped to the adjacent panels. Next, the batter of the panel is adjusted. Two wooden wedges were driven into the horizontal gap between the panels until the desired batter is achieved, and then the clamps are tightened. Details of the clamps and wooden wedges are detailed in Fig. B.1. This process was repeated until the entire row of panels was installed. At this time the first layer of "loose" geogrid was installed.

The design for this wall called for two additional layers of geogrid that were not attached to the panels ('loose' grid). These grids were placed at the locations shown in Fig. 5.3. Seven pieces of geogrid were placed 2 ft. and five pieces placed 4.5 ft. up from the base of the wall on 6 ft. centers. The ends of the grid were bent up 90 degrees upward against the back of the panel. This geogrid was not prestressed.

Once in place, the filter material was glued over the gaps, and the next lifts of soil were placed until they reached the level of the next layer of grid.

Since the heavy equipment could not operate near the back face of the retaining wall, some measures had to be taken to achieve soil compaction in that area. First of all, soil placed directly behind the wall was stomped down by foot. This was continued until no further significant compaction could be observed. Secondly, large volumes of water were sprayed behind the wall for

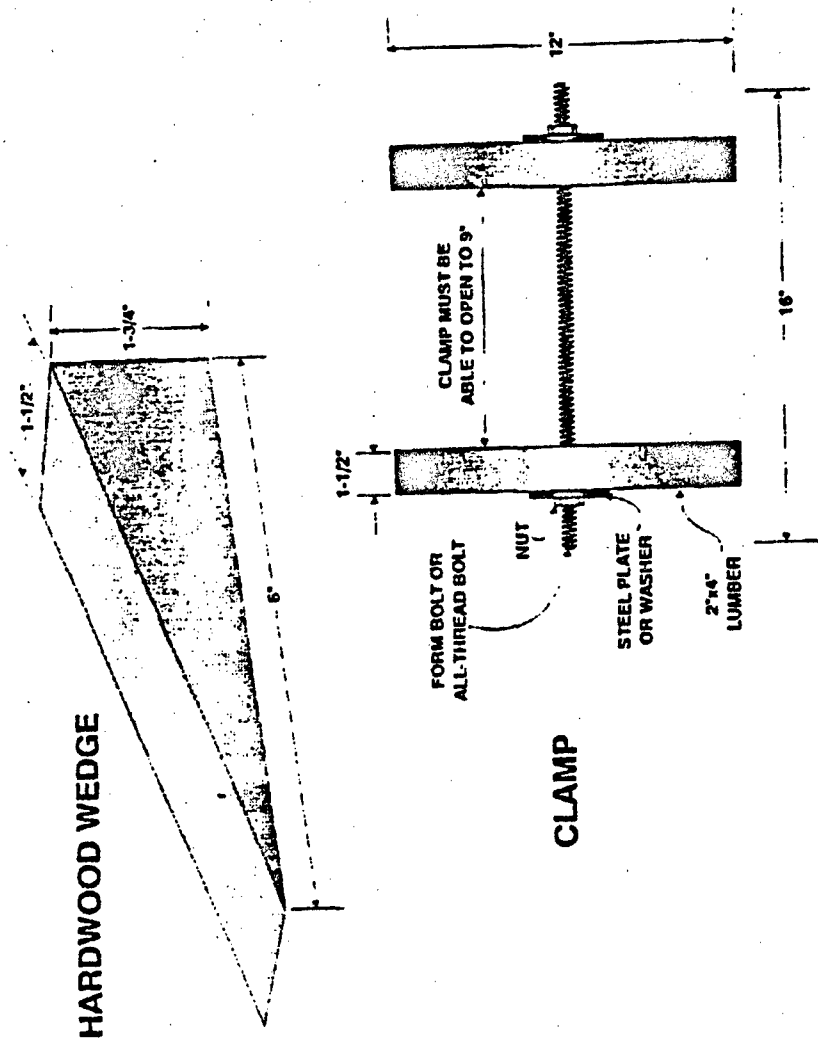


Figure B.1 Detail of Clamps and Wooden Wedges

hydraulic compaction. This was observed to work well in the silty sand.

Although these methodologies are not precise, the densities in this region were similar to the area compacted by the heavy equipment.

Before the third course of panels could be installed, the wooden shoring had to be removed. After this was done, the panel installation process was repeated until the wall was completed.

Throughout the construction process, the vertical and horizontal alignment and spacing of the panels were checked. If the alignment on the lower layers had been poor, some of the upper panels may not fit into the remaining space. Also, backfill soil density was maintained through periodic checks with a nuclear density gage. Density measurements are presented in Table 5.2.

Minimum Geogrid Embedment Length

The wall design called for embedment length to decrease with decreasing wall height. The outermost panels had design geogrid embedment lengths of 6 and 7 ft. During construction of the first wall, it was found that these short embedment lengths interfered with the construction process. When a layer of grid was placed, long metal bars were inserted through the tail of grid layer and pulled to provide some pretensioning of the geogrid. When the tail of the grid layer was this close to the wall, the heavy equipment could not place the soil

without endangering the workers pretensioning the grid or getting too close to the wall face. On all subsequent walls, the reinforcement length at the edges of the wall was increased to 8.5 ft. which allowed the heavy equipment to safely place the backfill without any interference from the workers while still maintaining a safe distance from the wall.

APPENDIX C

DATA PLOTS

253

ADA293552

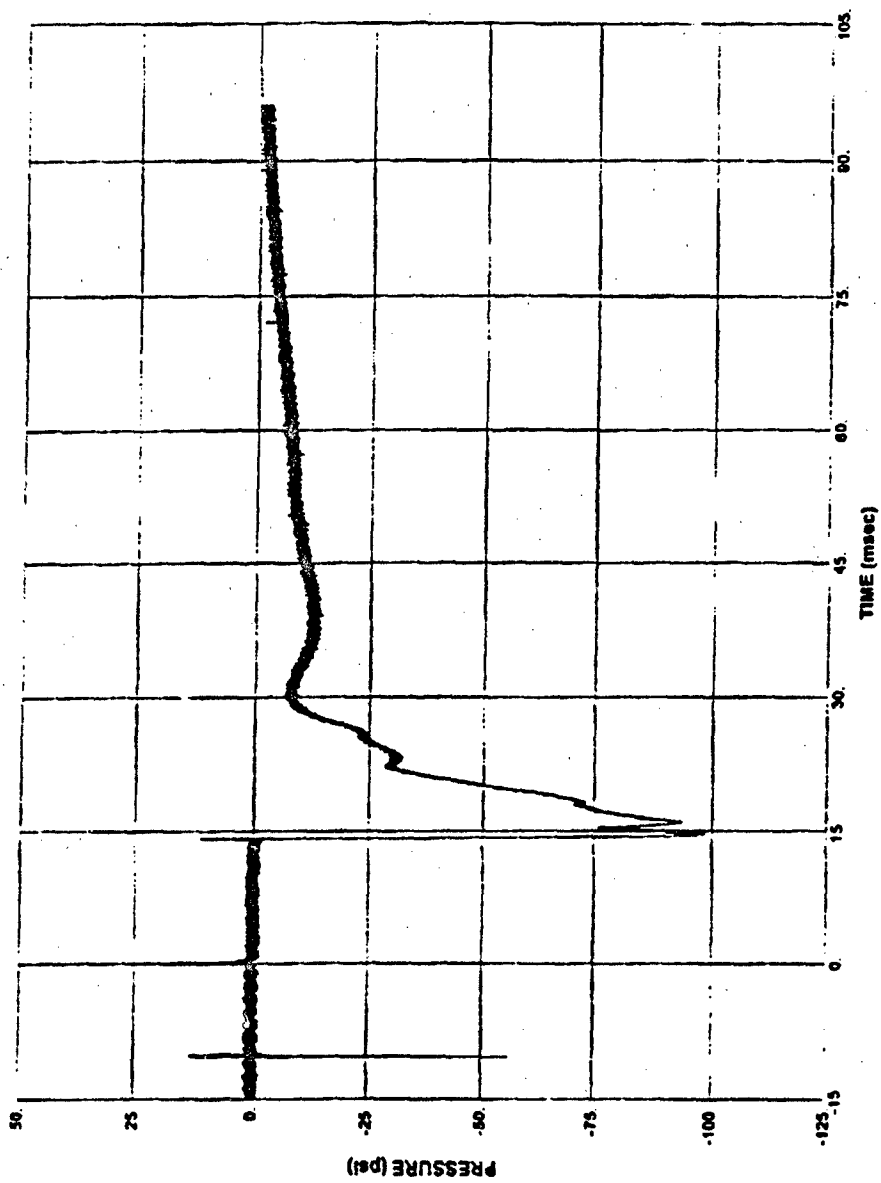


Figure C.1 Free-Field Pressure Gage F1, Test 1

254

ADA293552

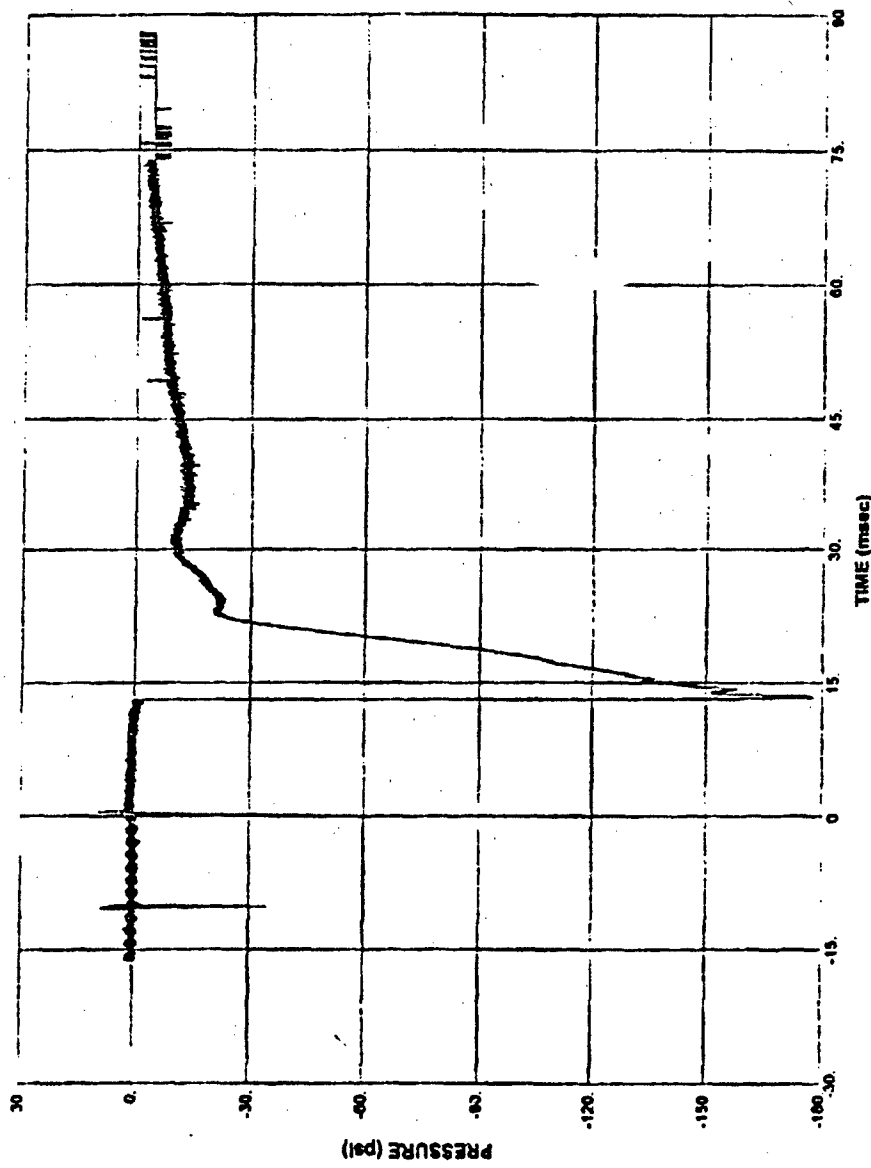


Figure C.2 Free-Field Pressure Gage F2, Test 1

265

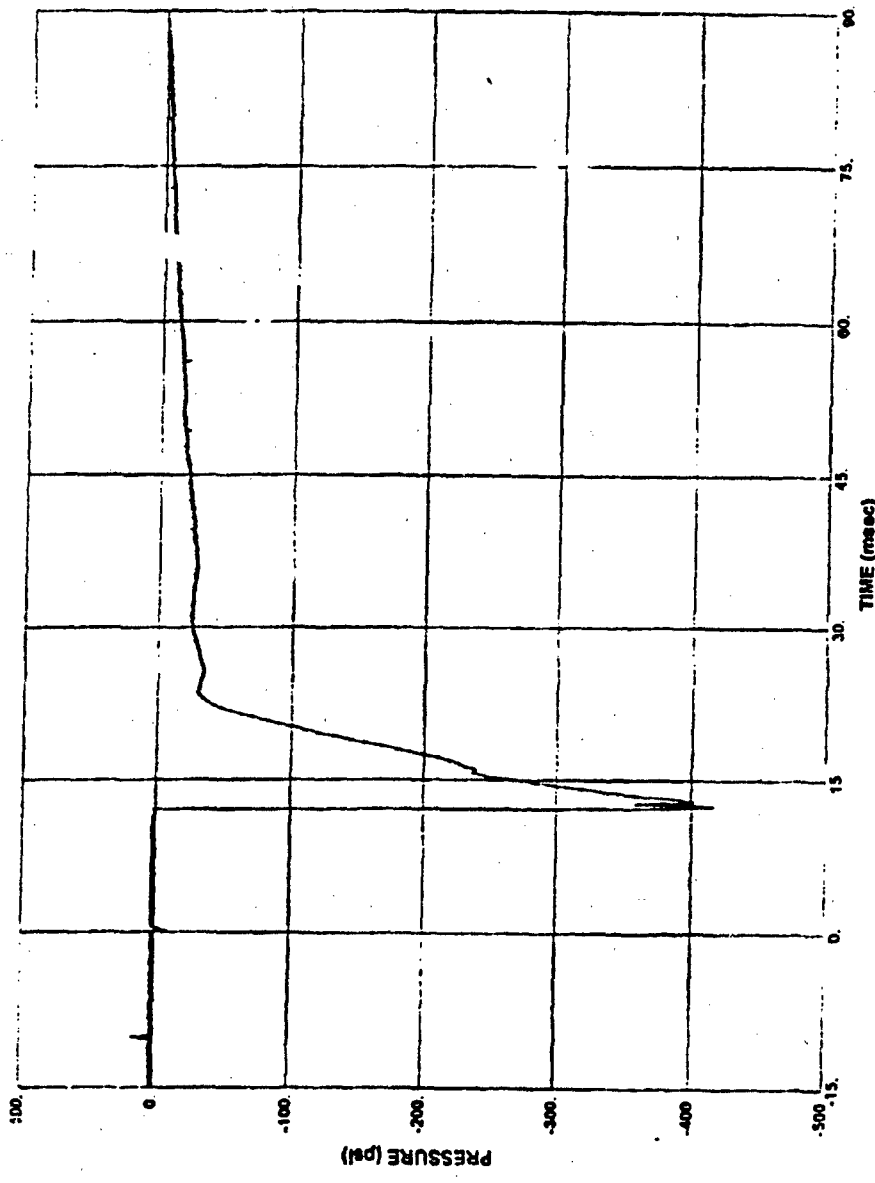


Figure C.3 Free-Field Pressure Gage F3, Test 1

256

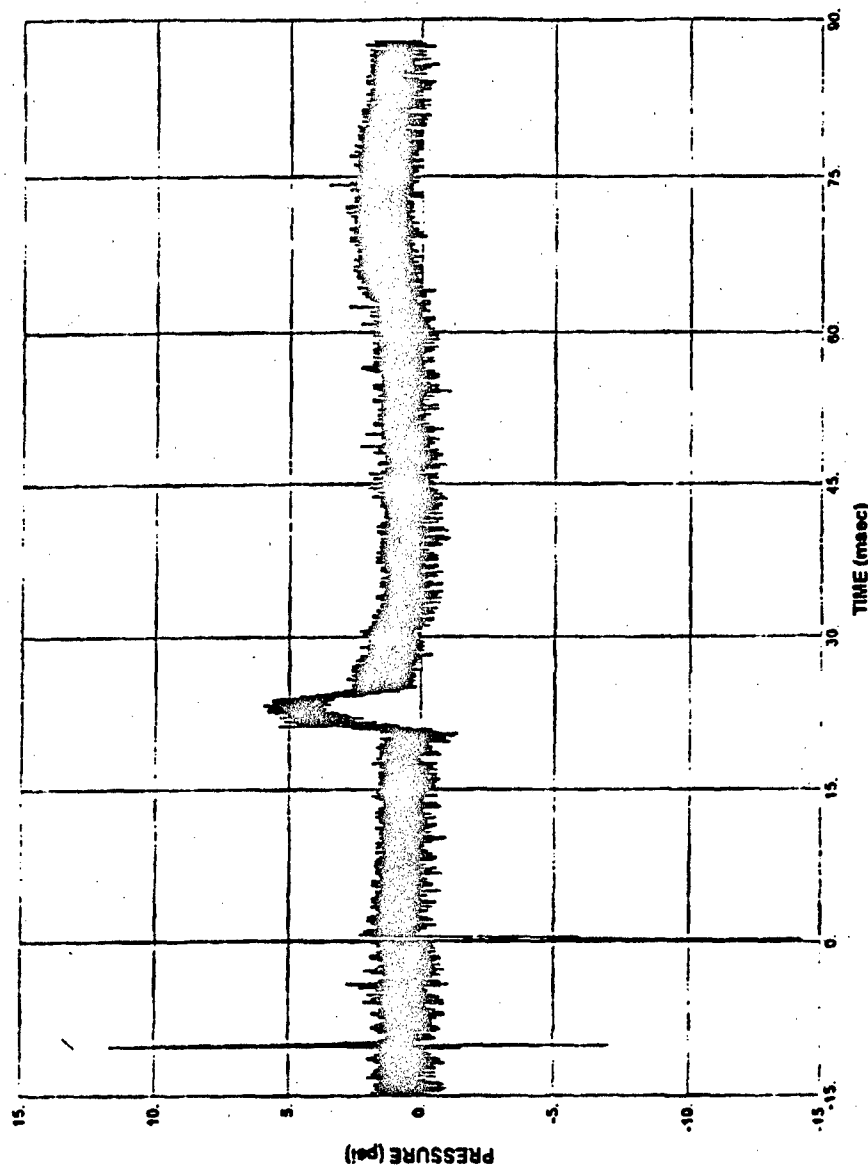


Figure C.4 Soil Pressure Interface Gage P2, Test 1

257

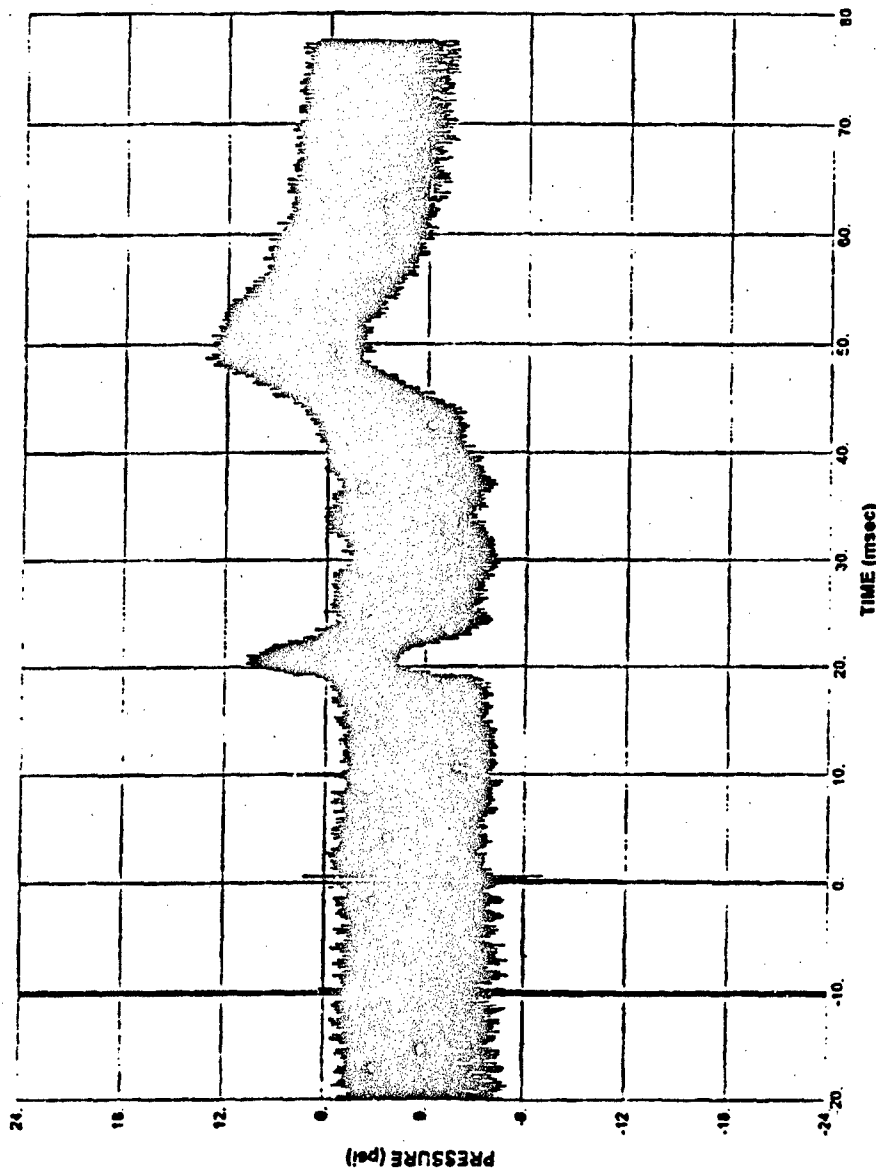


Figure C.5 Soil Pressure Interface Gage P3, Test 1

258

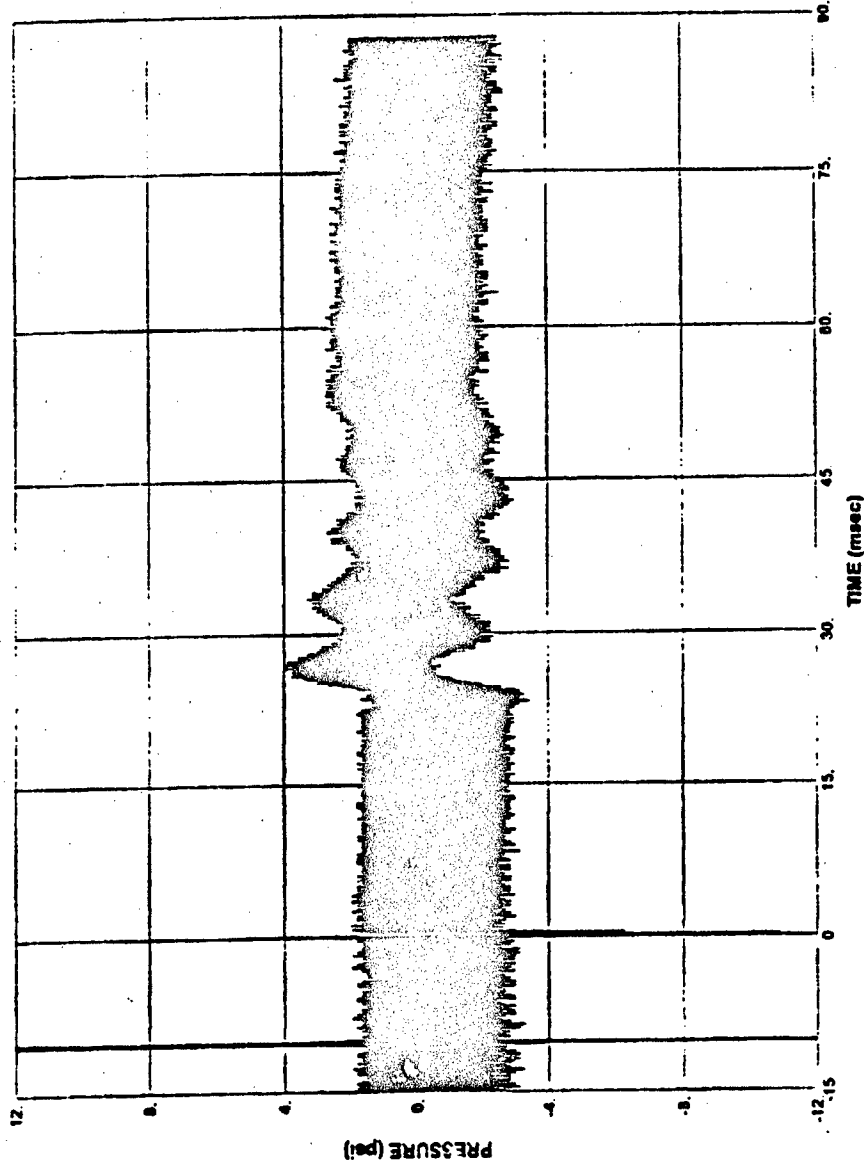


Figure C.6 Soil Pressure Interface Gage P4, Test 1

259

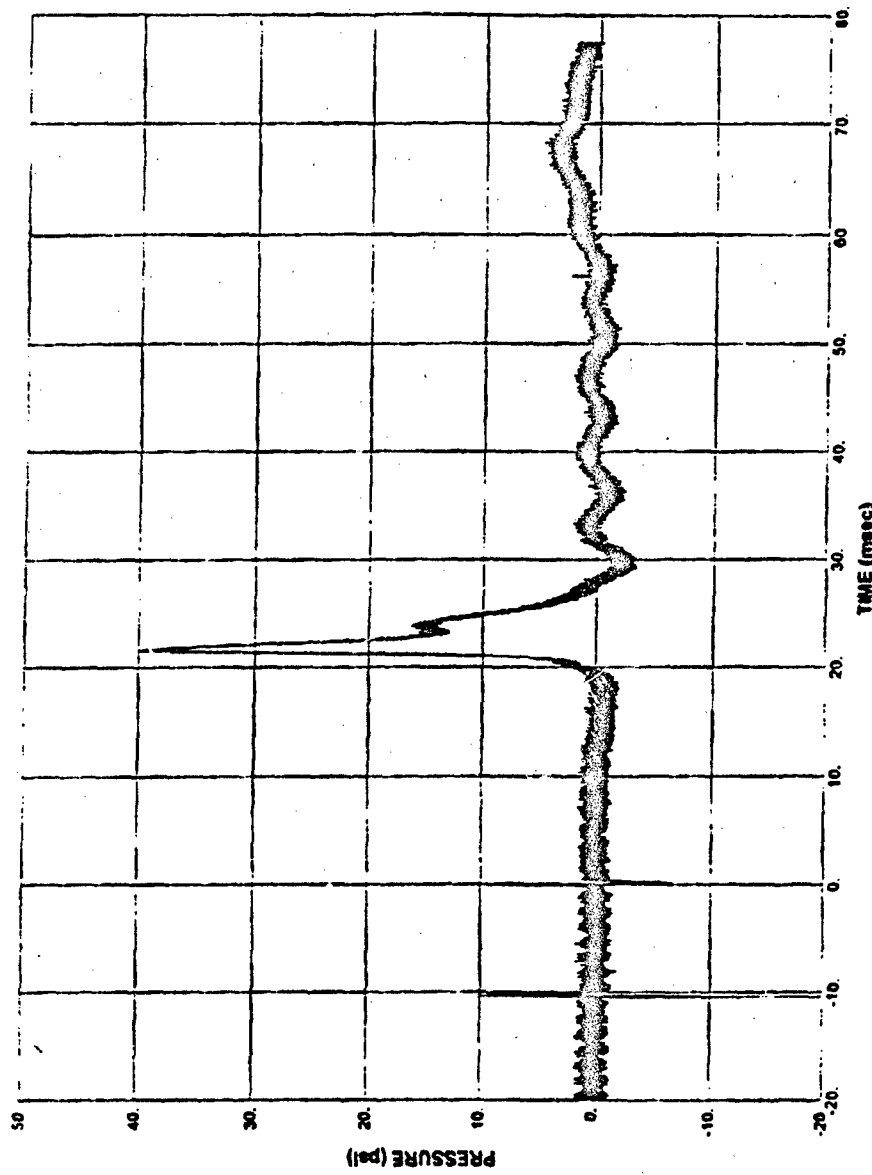


Figure C.7 Soil Pressure Interface Gage P5, Test 1

260

ADA293552

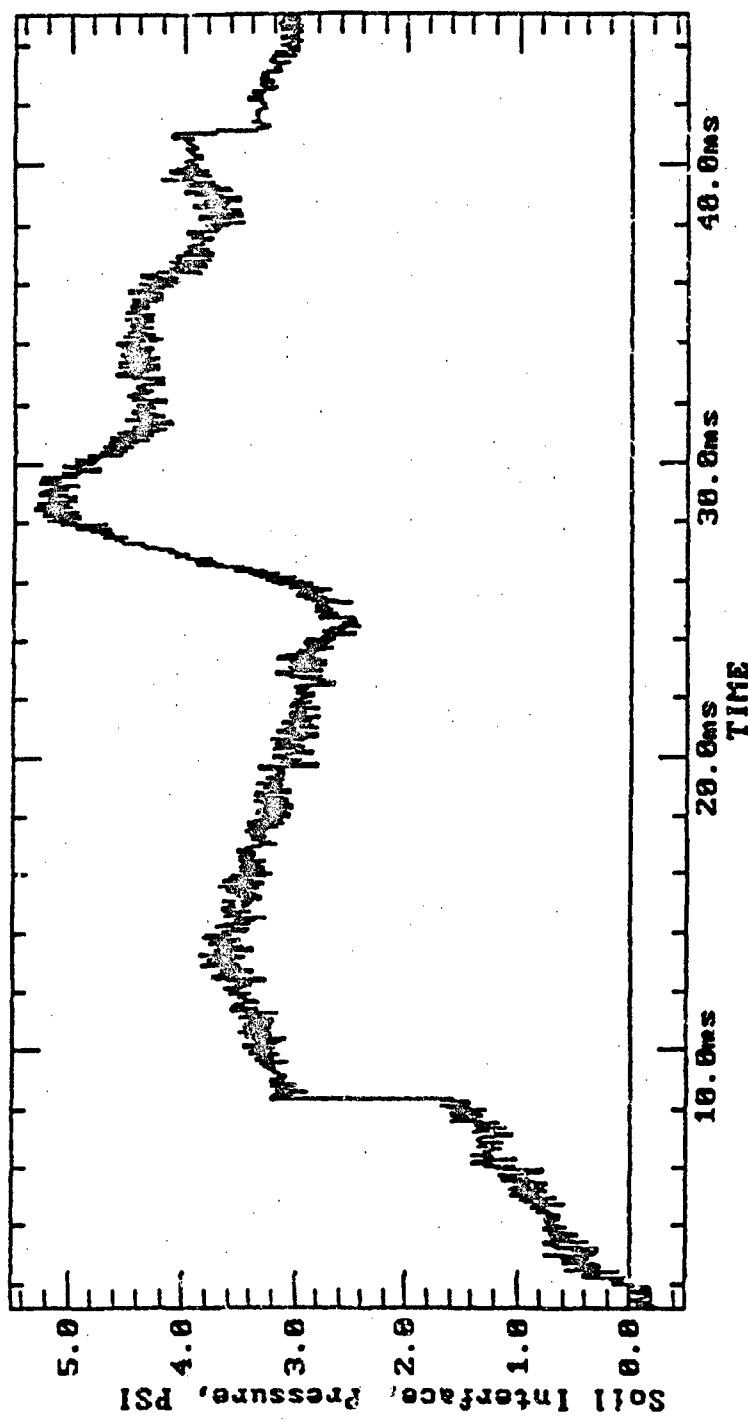


Figure C.8 Soil Pressure Interface Gage P6, Test 1

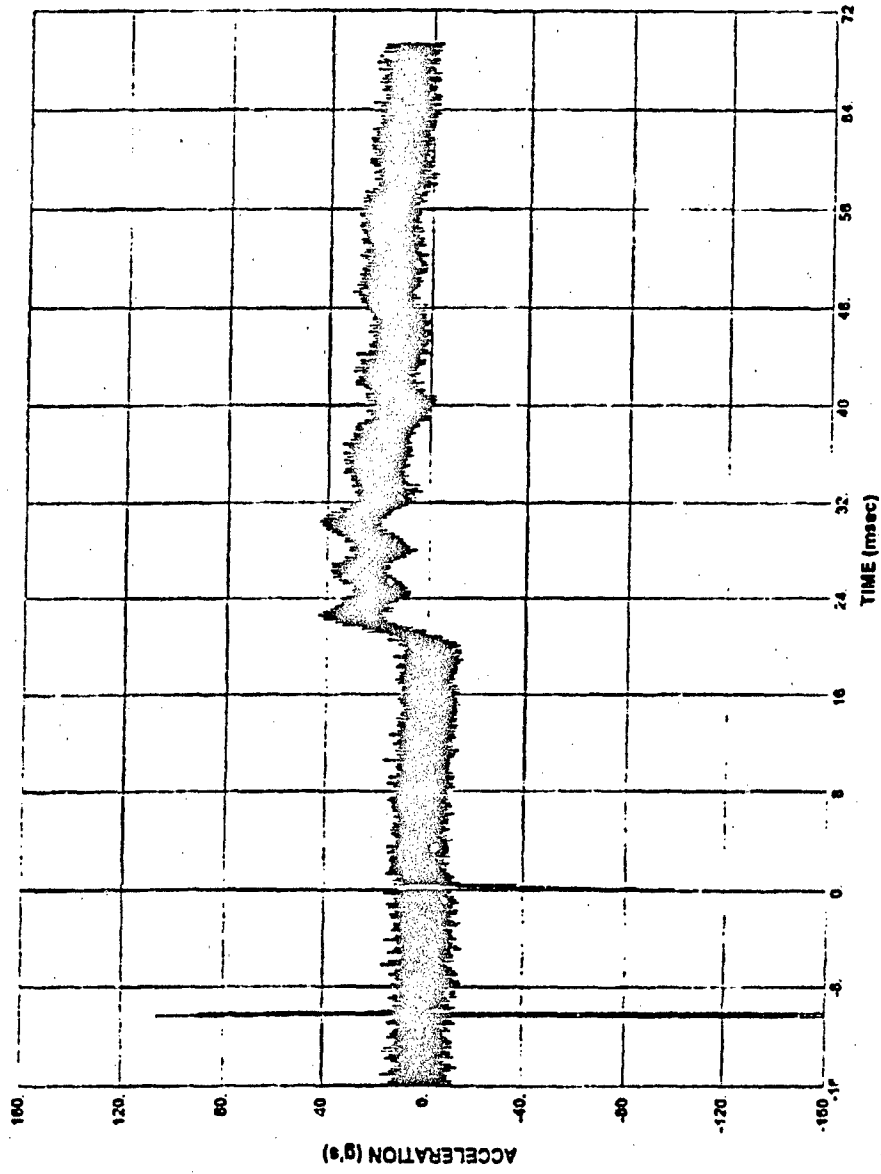
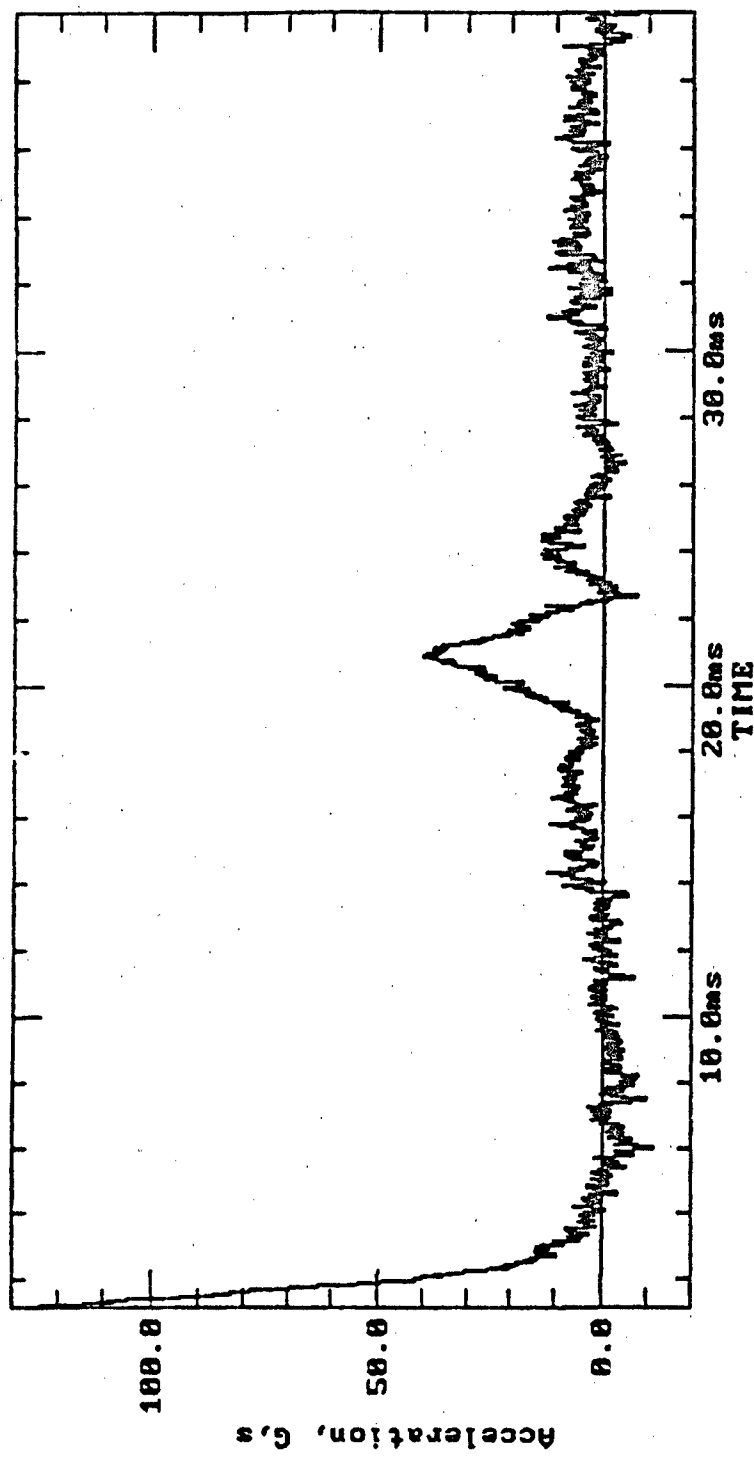


Figure C.9 Accelerometer A1, Test 1

262



ADA293552

Figure C.10 Accelerometer A2, Test 1

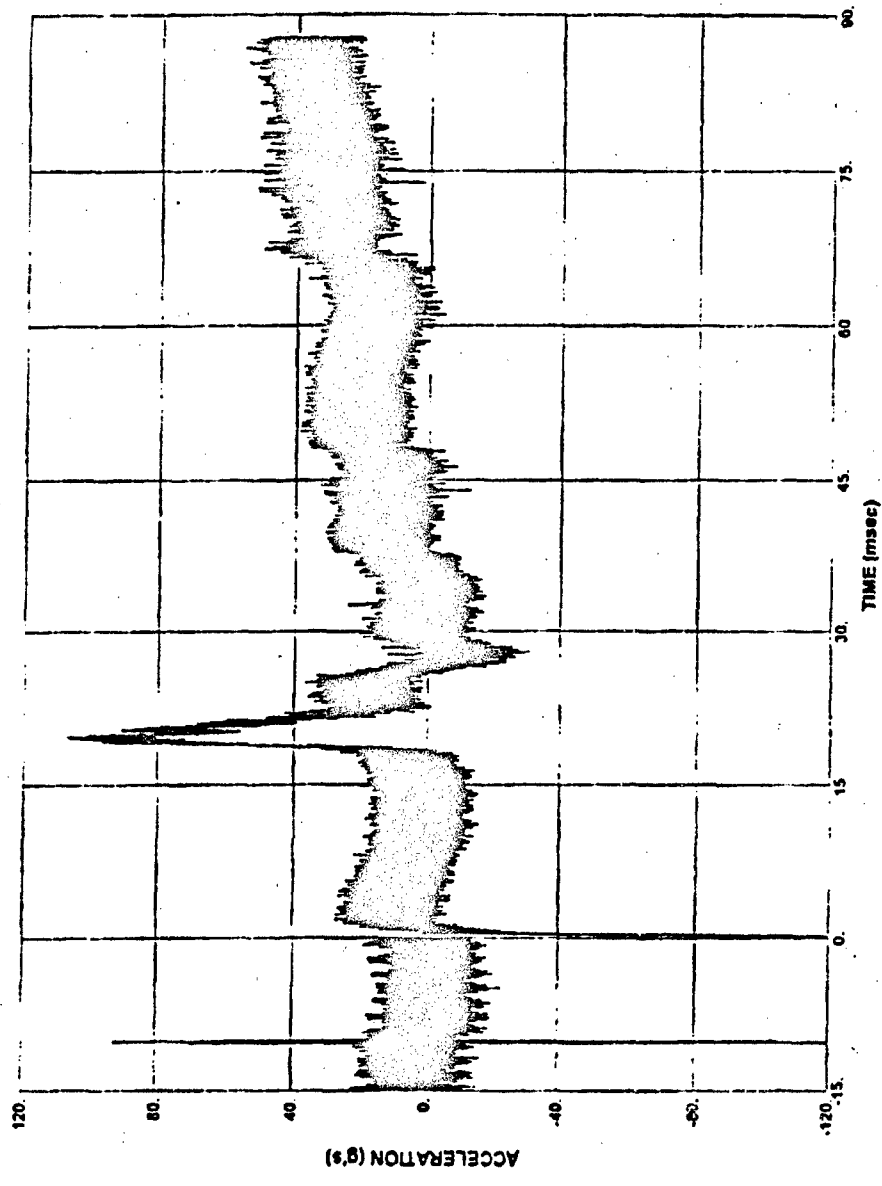


Figure C.11 Accelerometer A3, Test 1

264

ADA293552

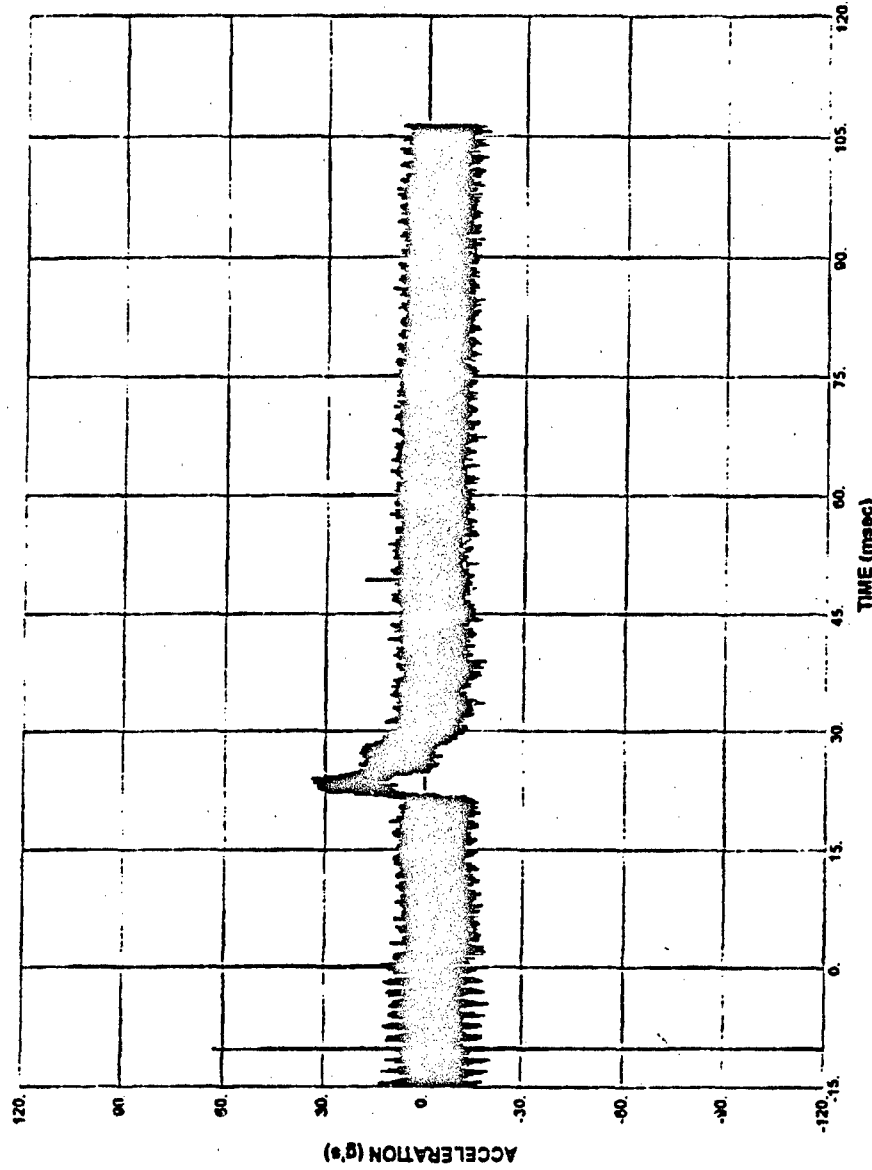


Figure C.12 Accelerometer A4, Test 1

265

ADA293552

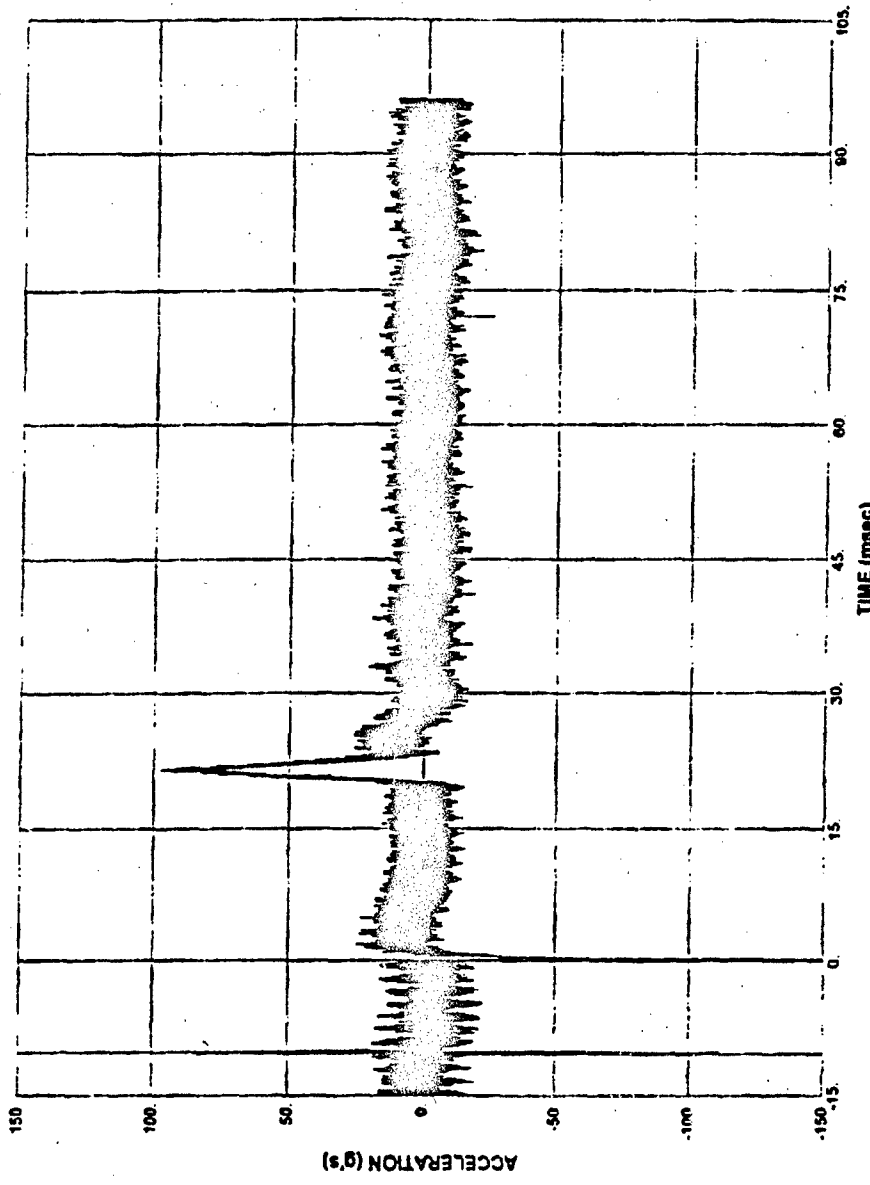


Figure C.13 Accelerometer A5, Test 1

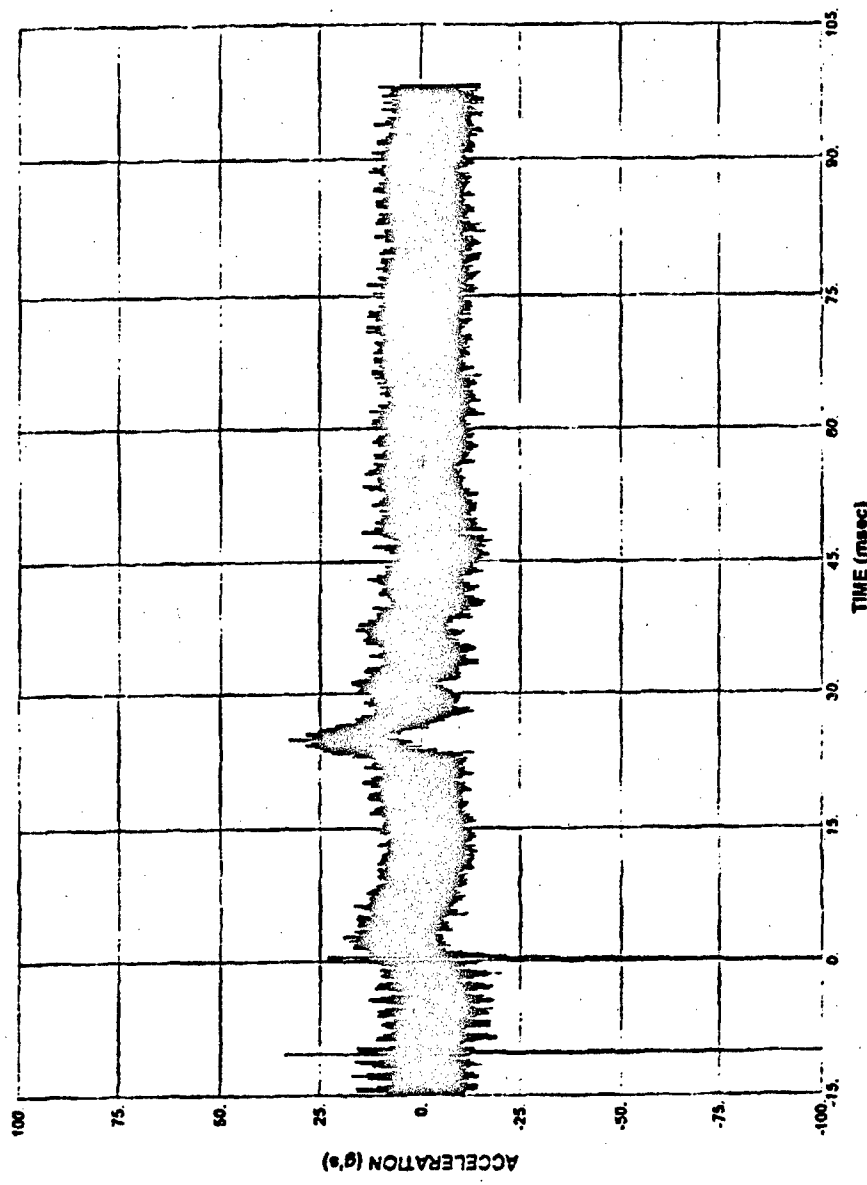


Figure C.14 Accelerometer A6, Test 1

267

ADA293552

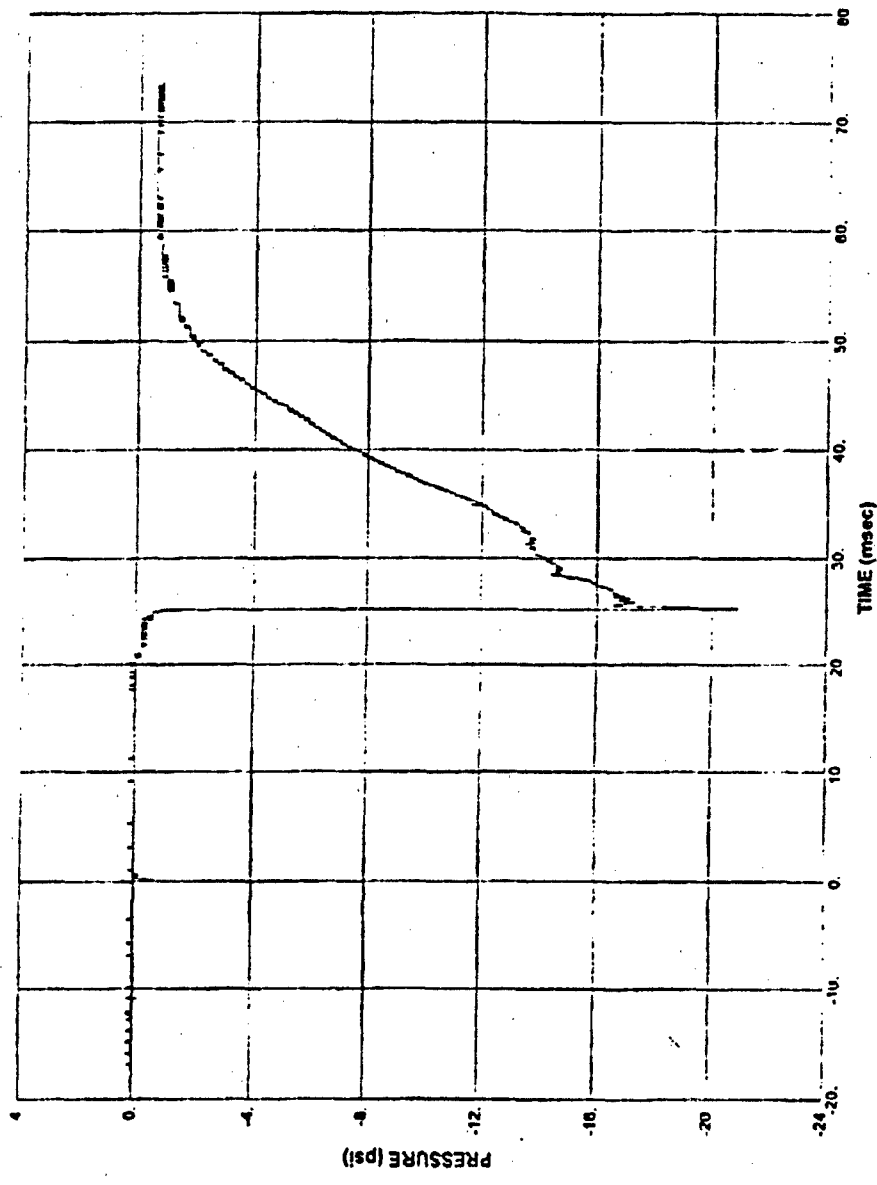


Figure C.15 Free-Field Pressure Gage F2, Test 2

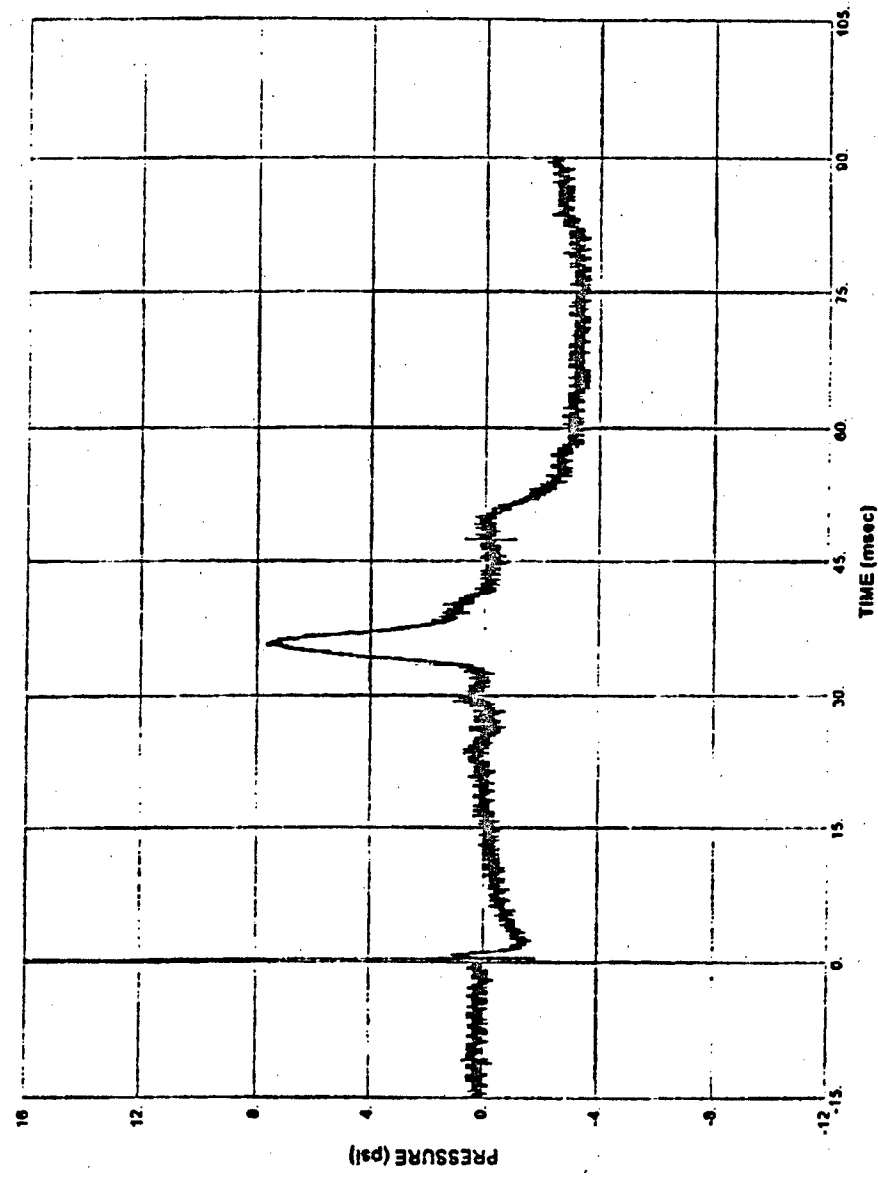
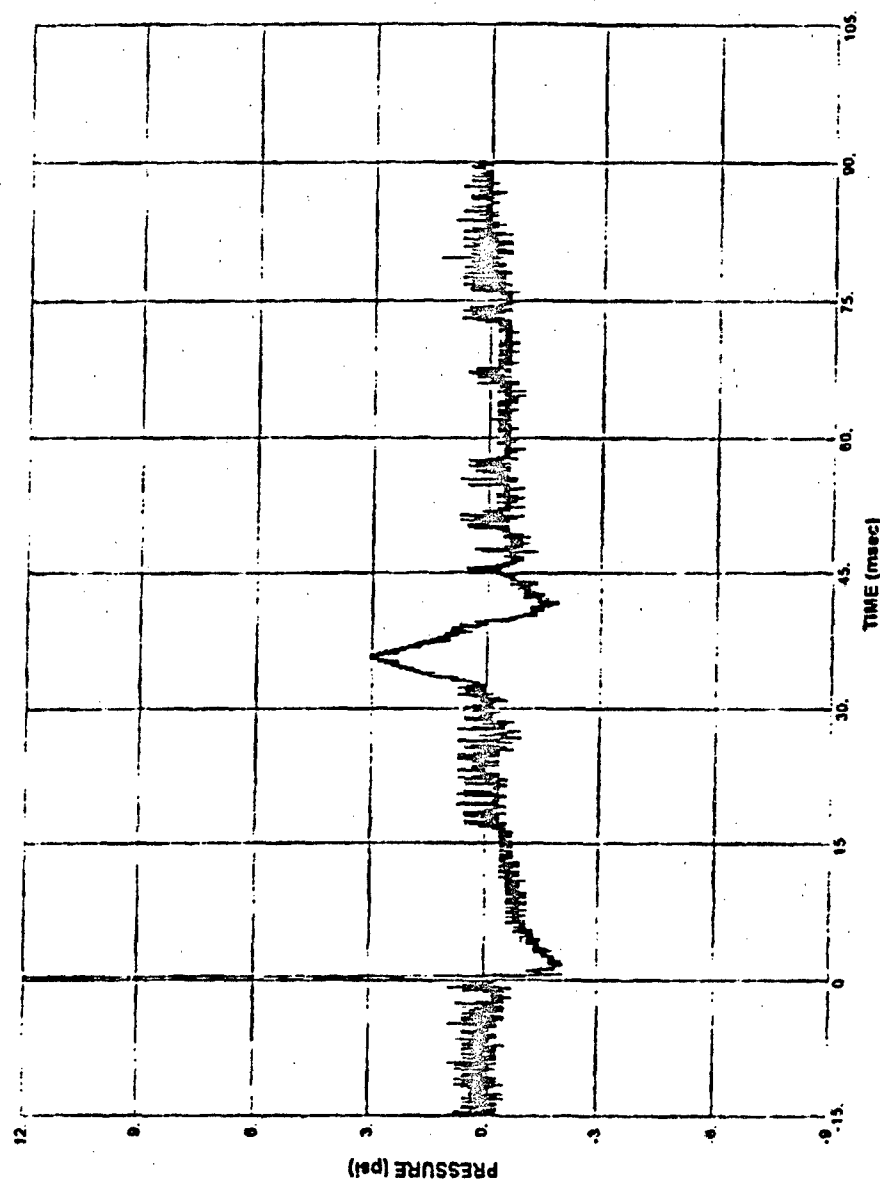


Figure C.16 Soil Pressure Interface Gage P1, Test 2



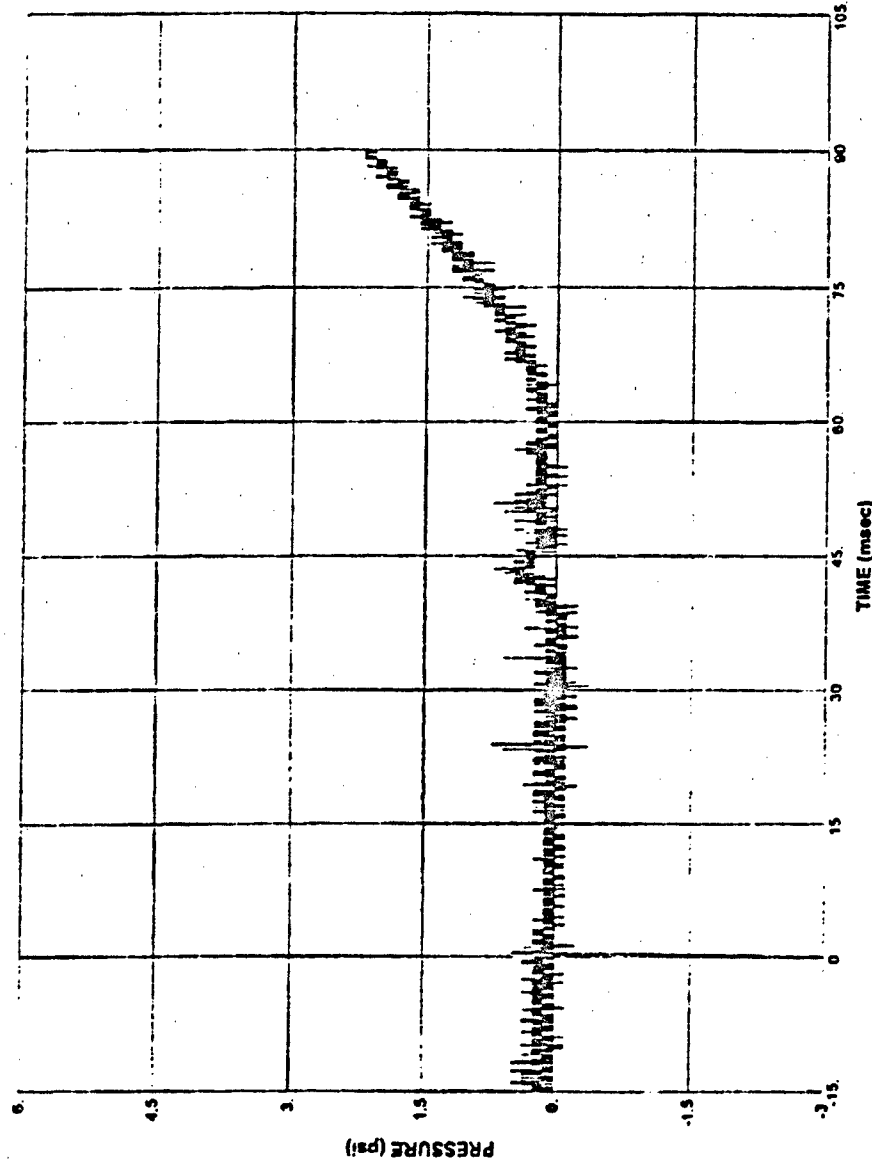


Figure C.18 Soil Pressure Int. face Gage P4, Test 2

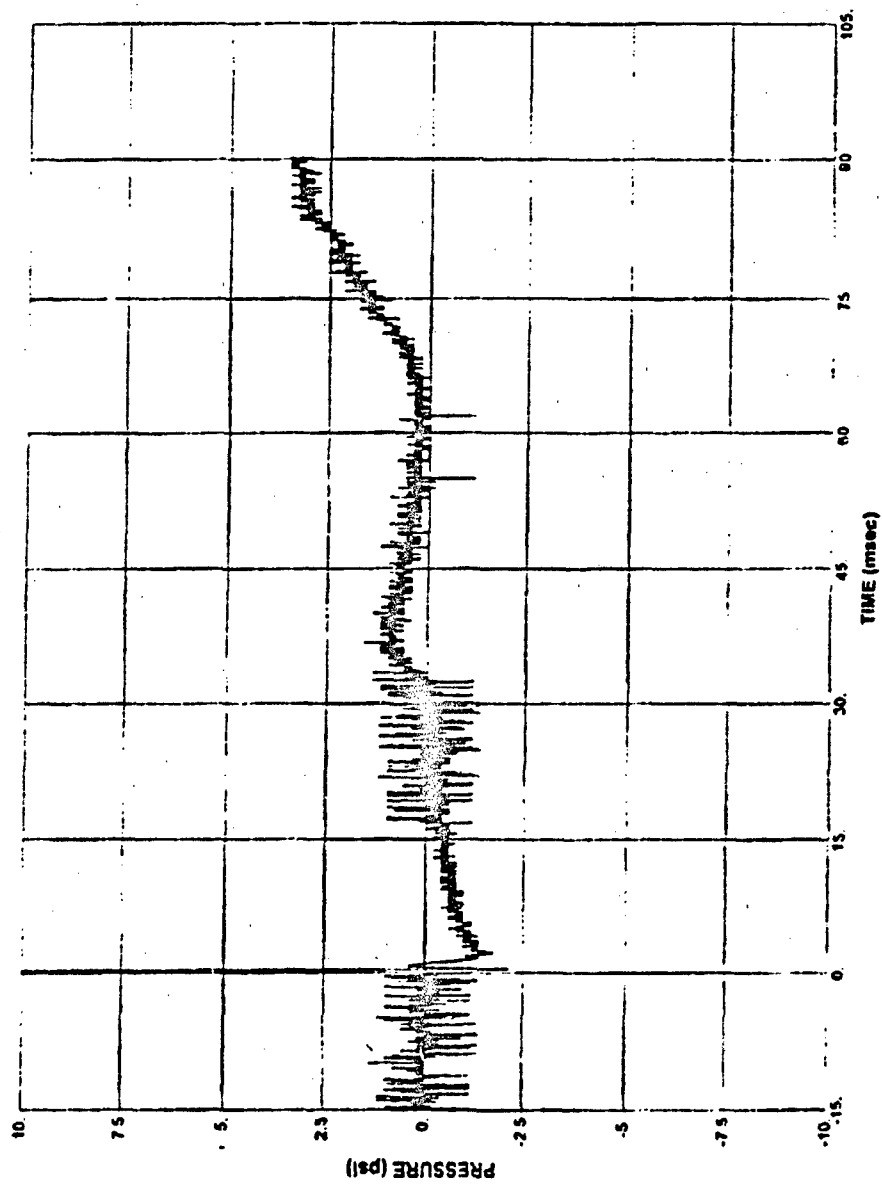


Figure C.19 Soil Pressure Interface Gage PS, Test 2

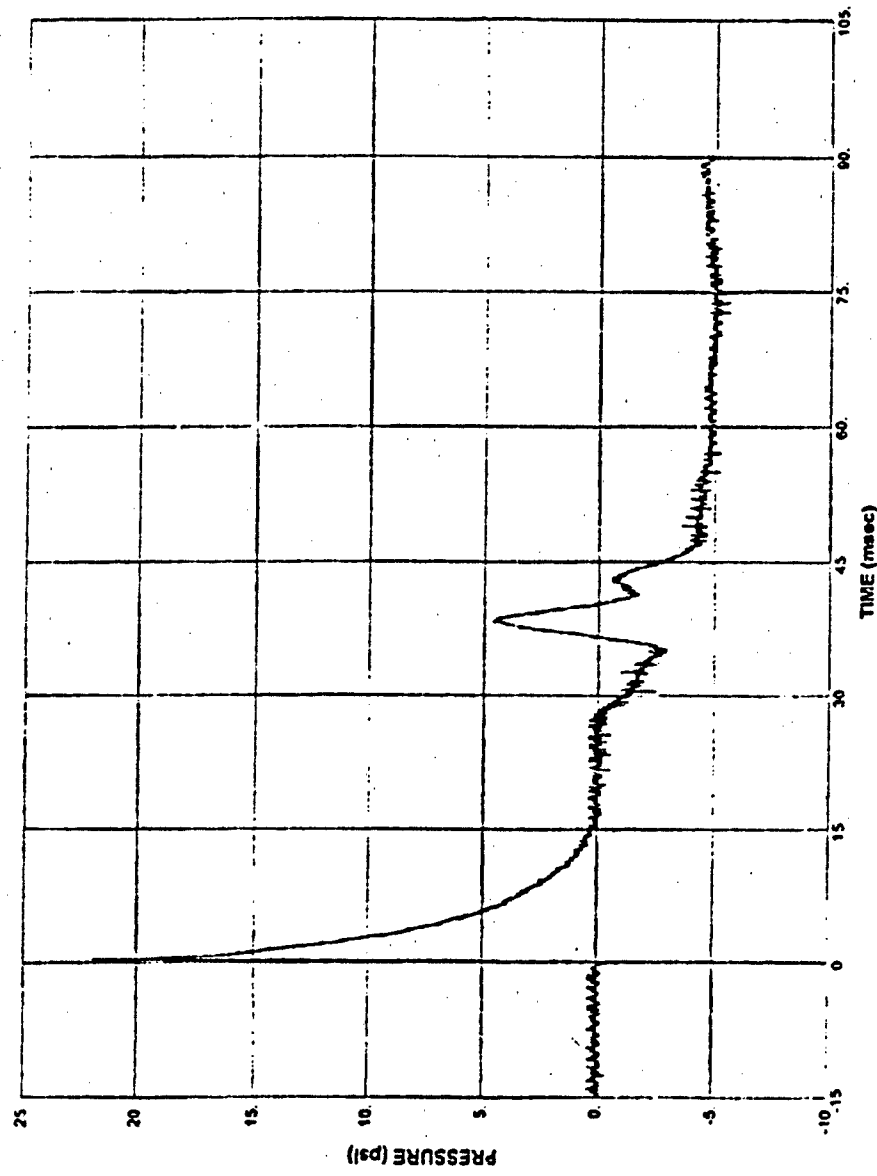


Figure C.20 Soil Pressure Interface Gage P6, Test 2

273

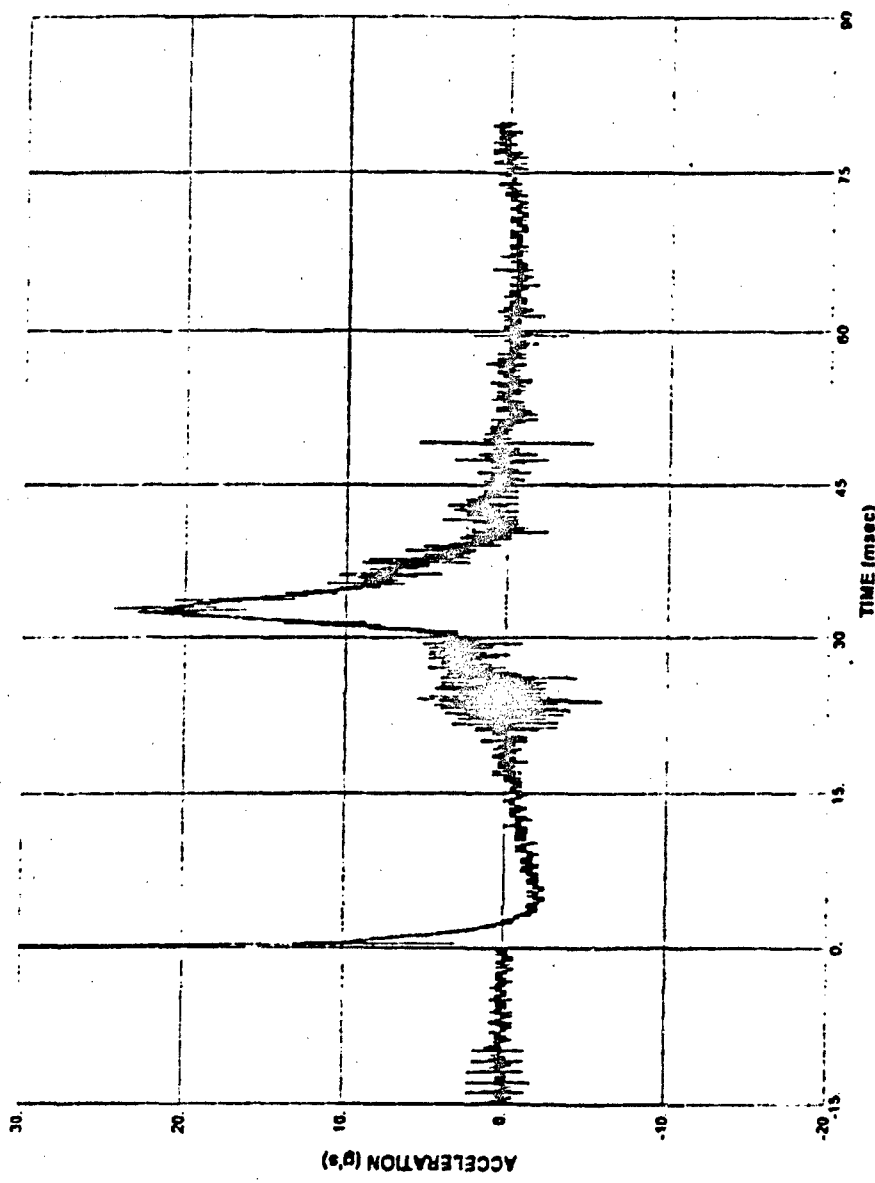


Figure C.21 Accelerometer A1, Test 2

274

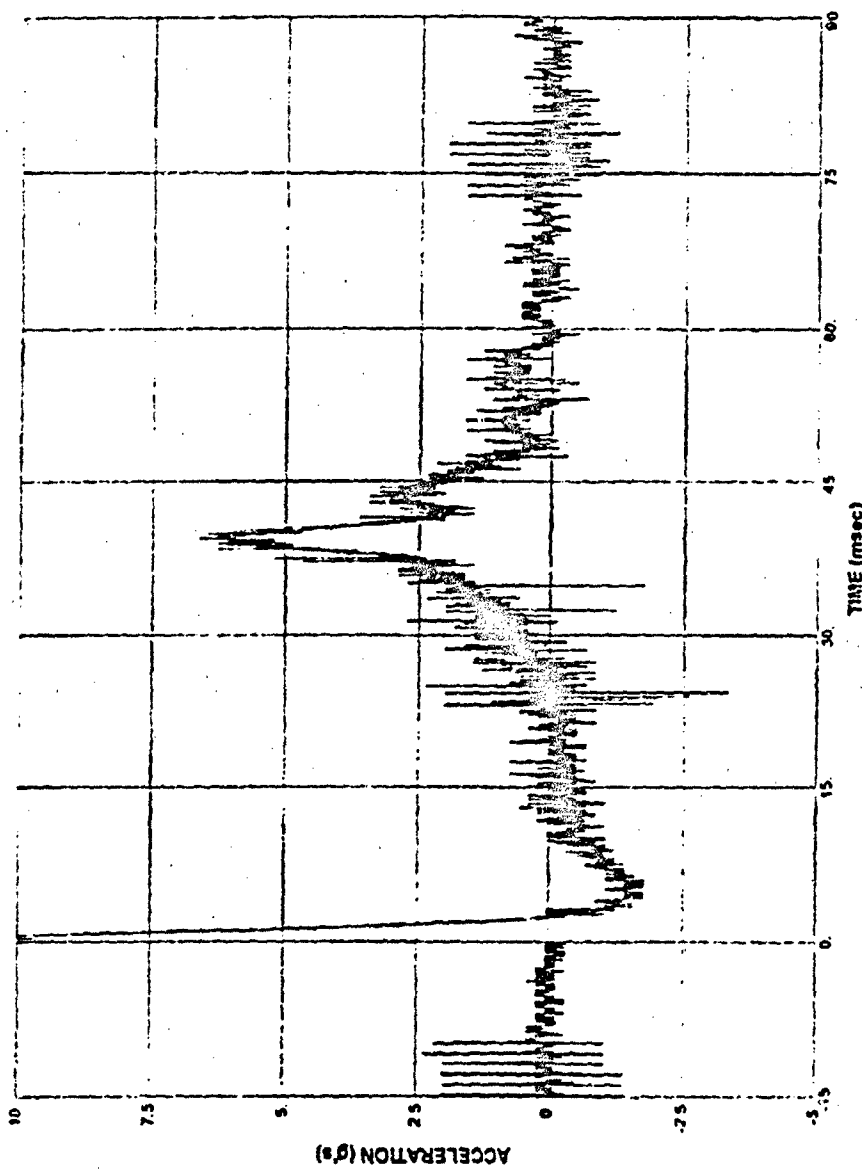


Figure C.22 Accelerometer A2, Test 2

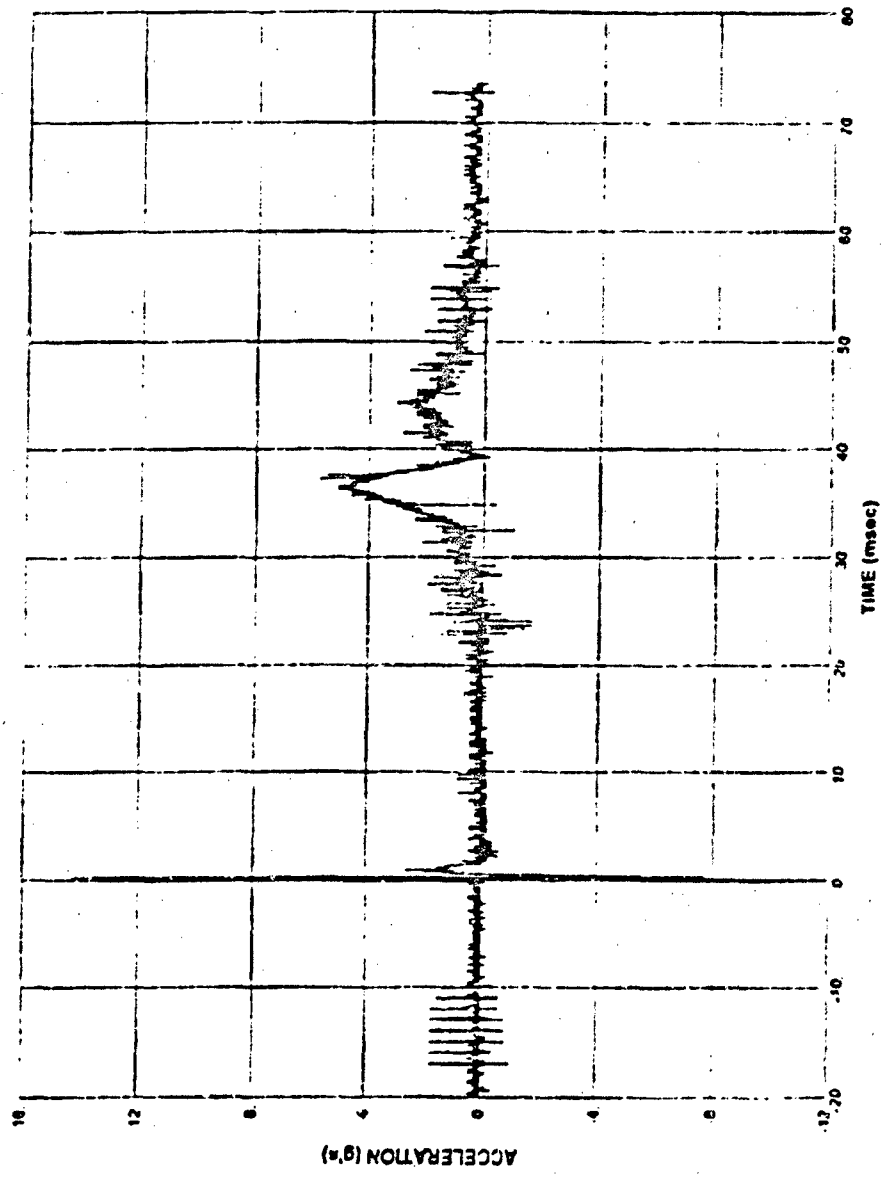


Figure C.23 Accelerometer A3, Test 2

276

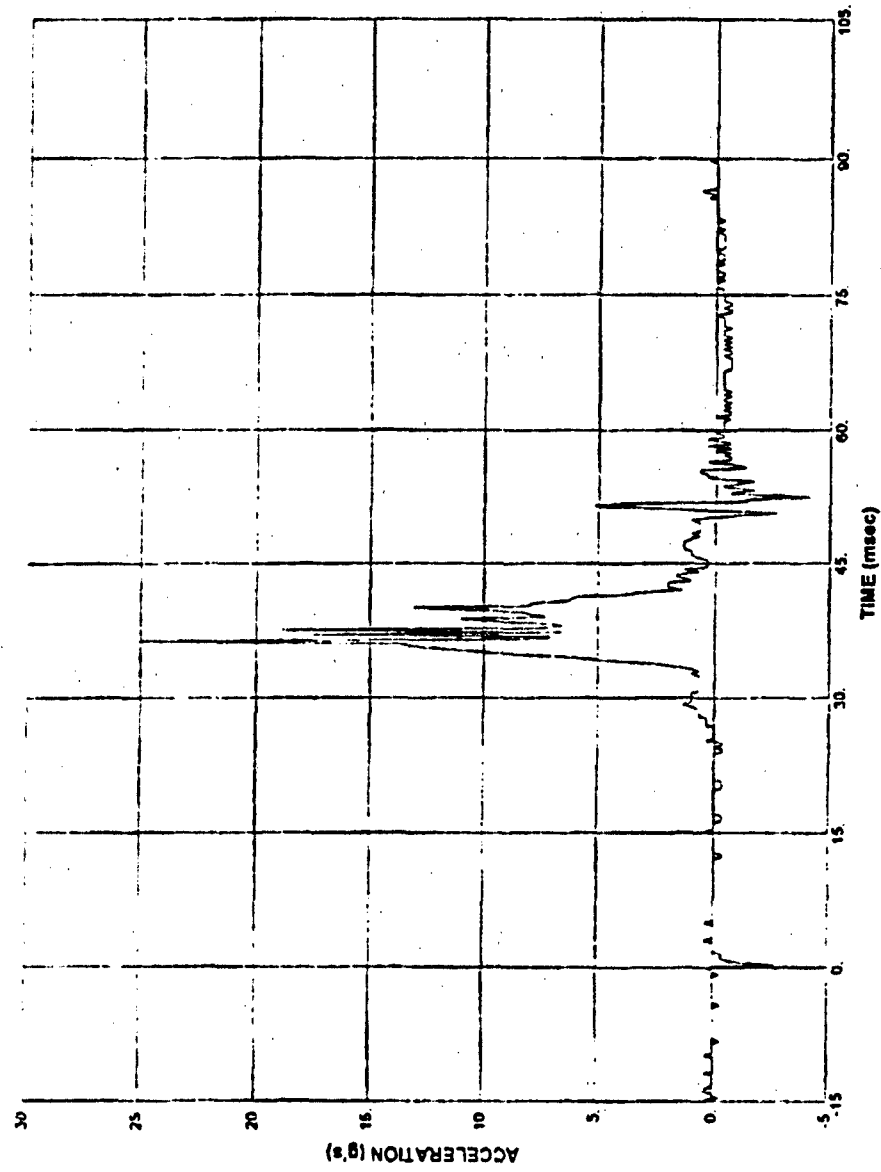


Figure C.24 Accelerometer A4, Test 2

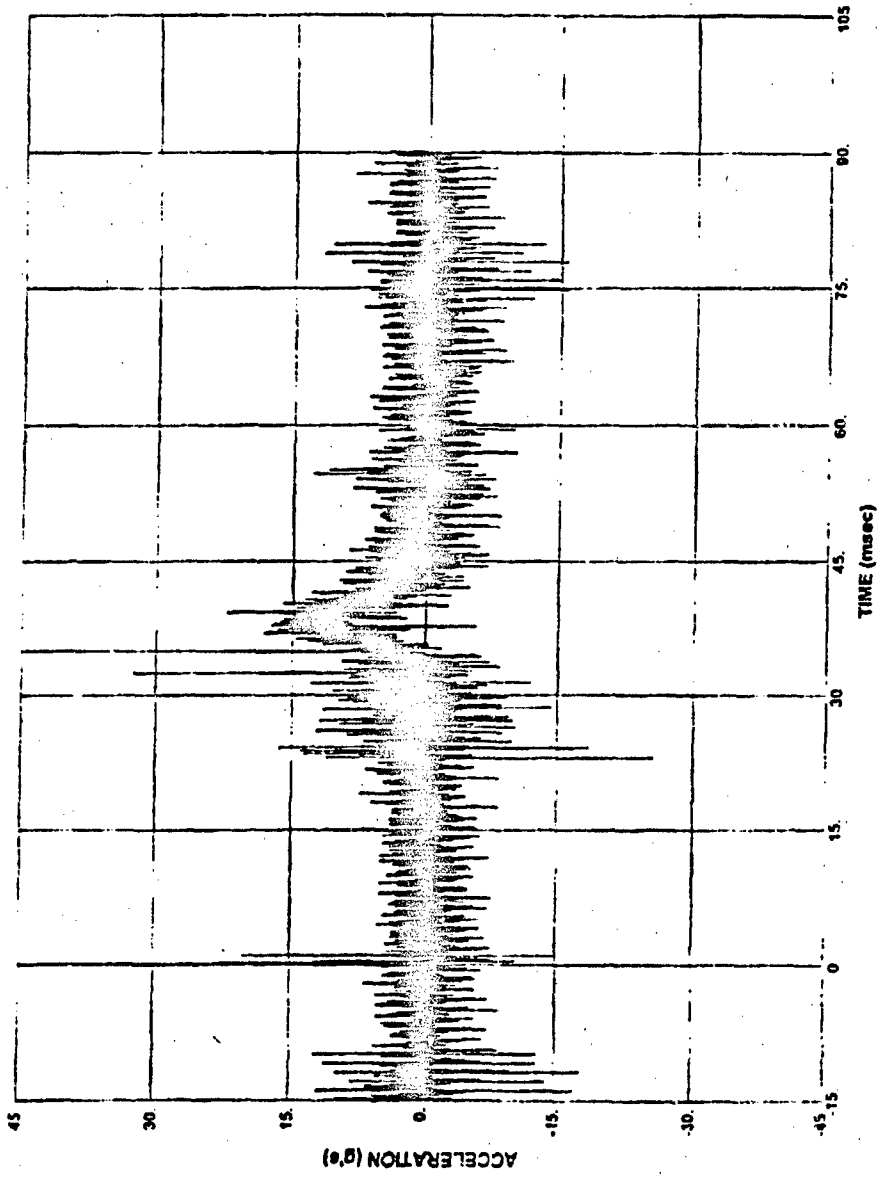


Figure C.25 Accelerometer A5, Test 2

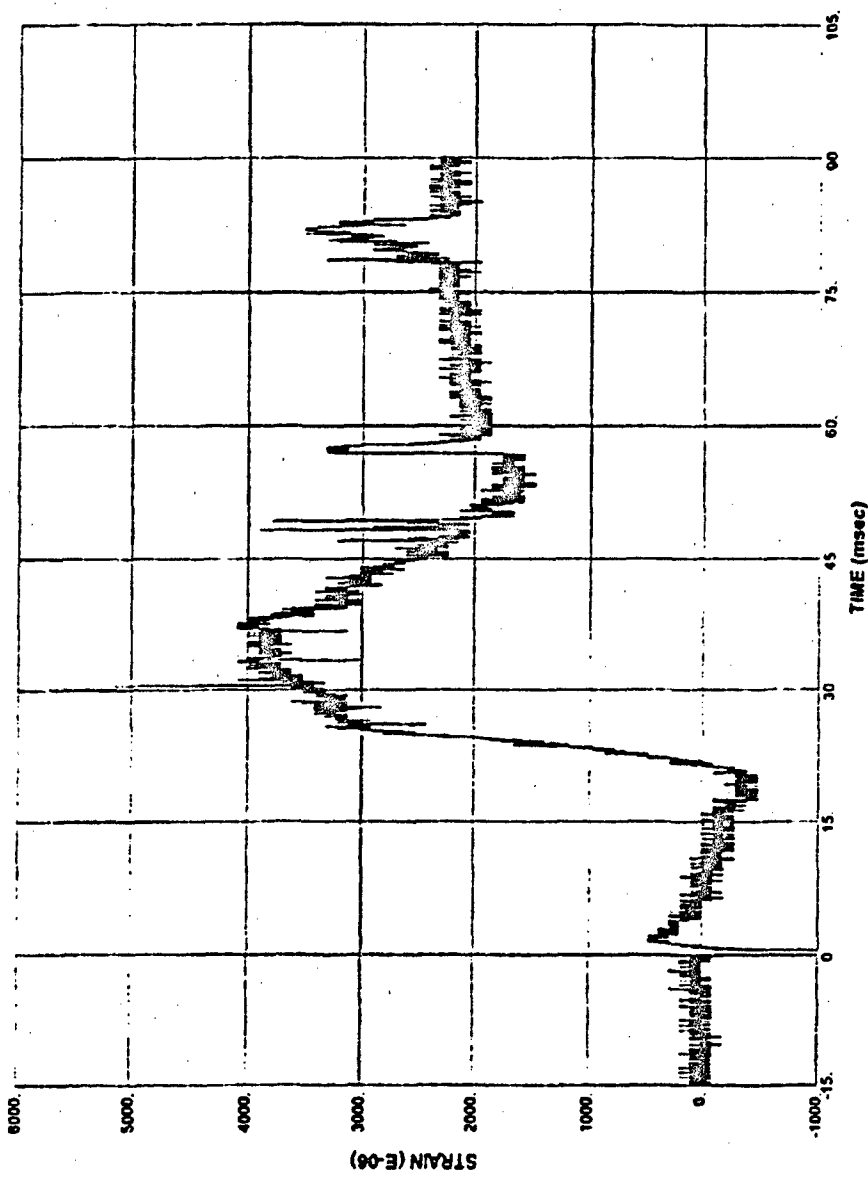


Figure C.26 Strain Gage S7, Test 2

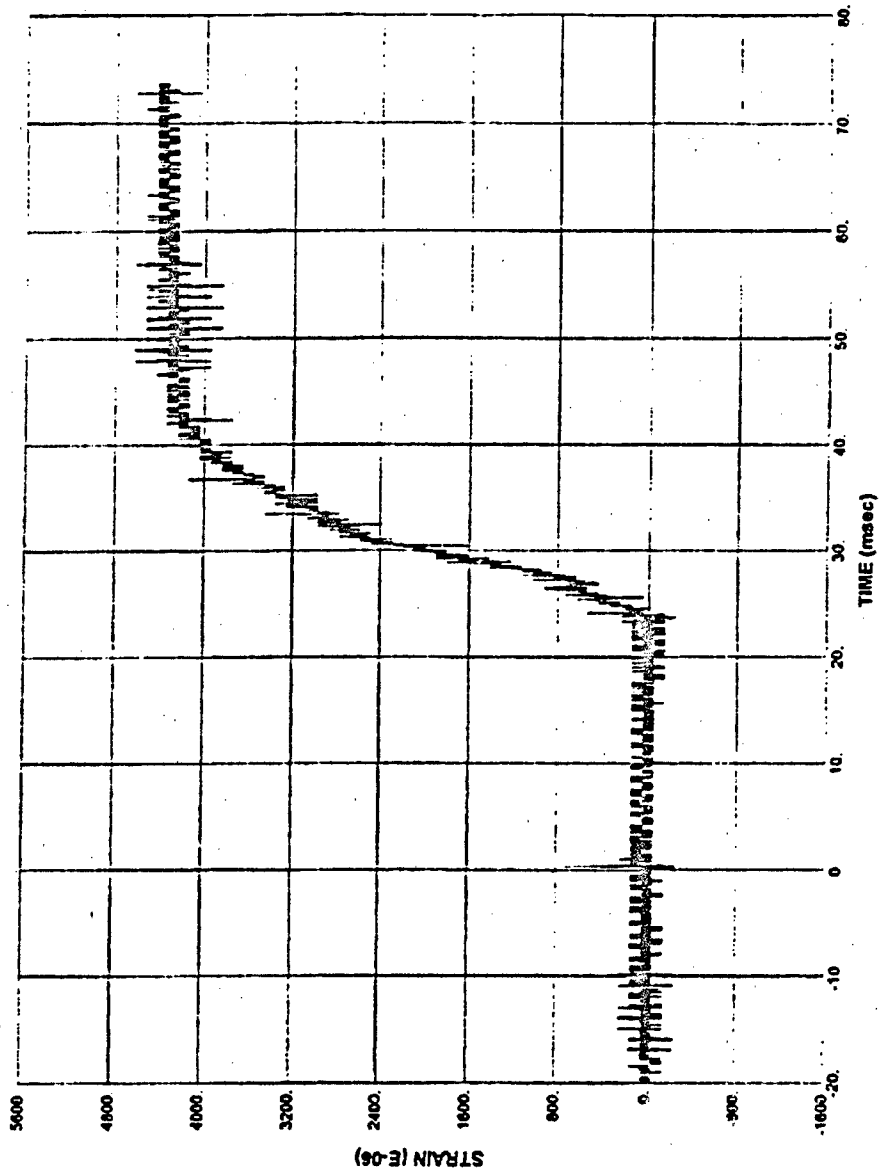


Figure C.27 Strain Gage S8, Test 2

280

ADA293552

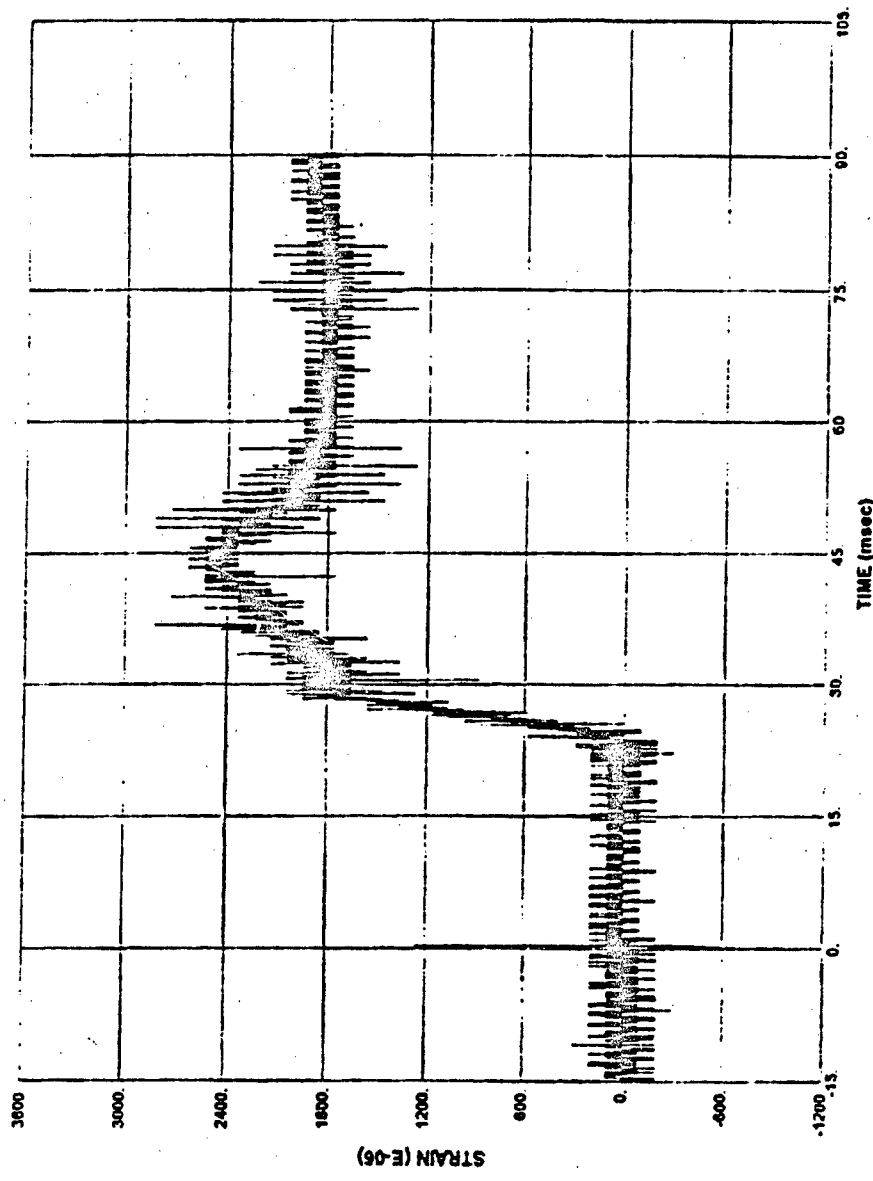


Figure C.28 Strain Gage S9, Test 2

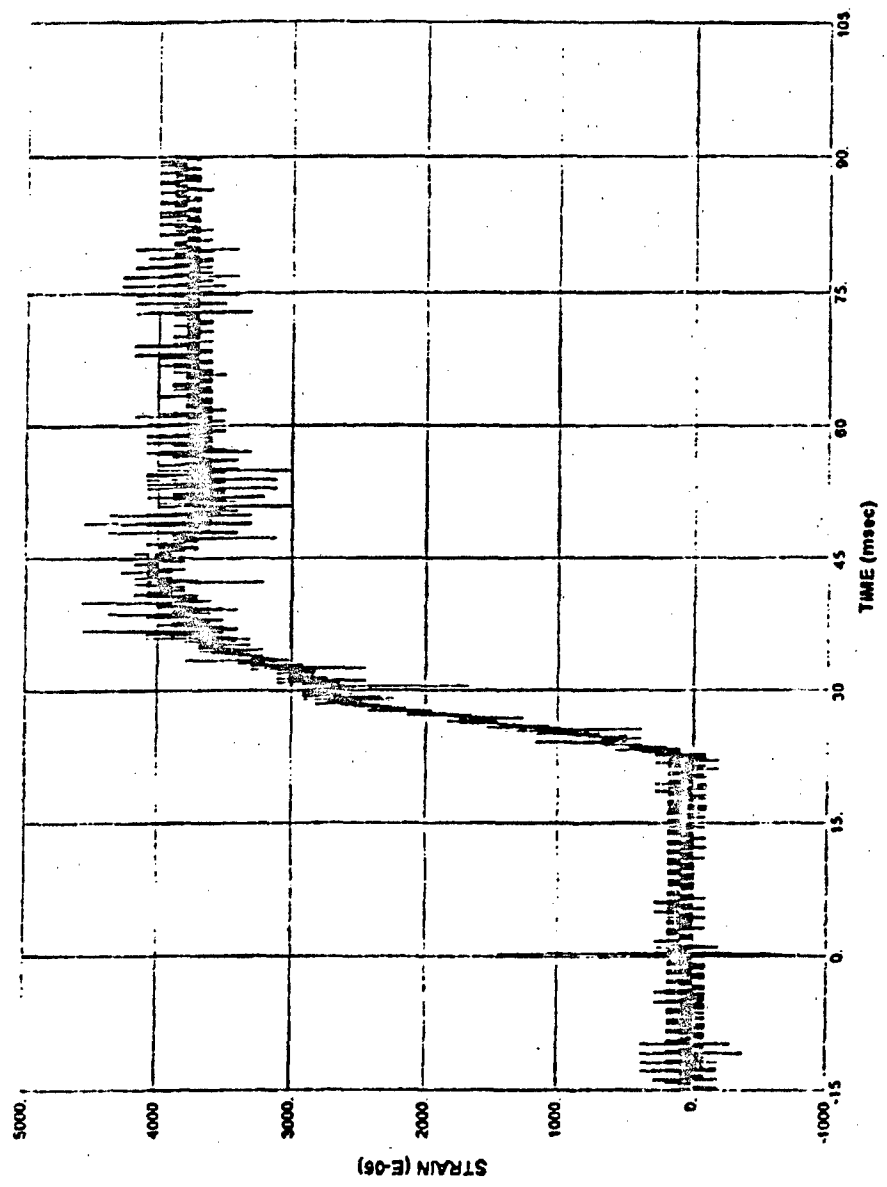


Figure C.29 Strain Gage S11, Test 2

282

ADA293552

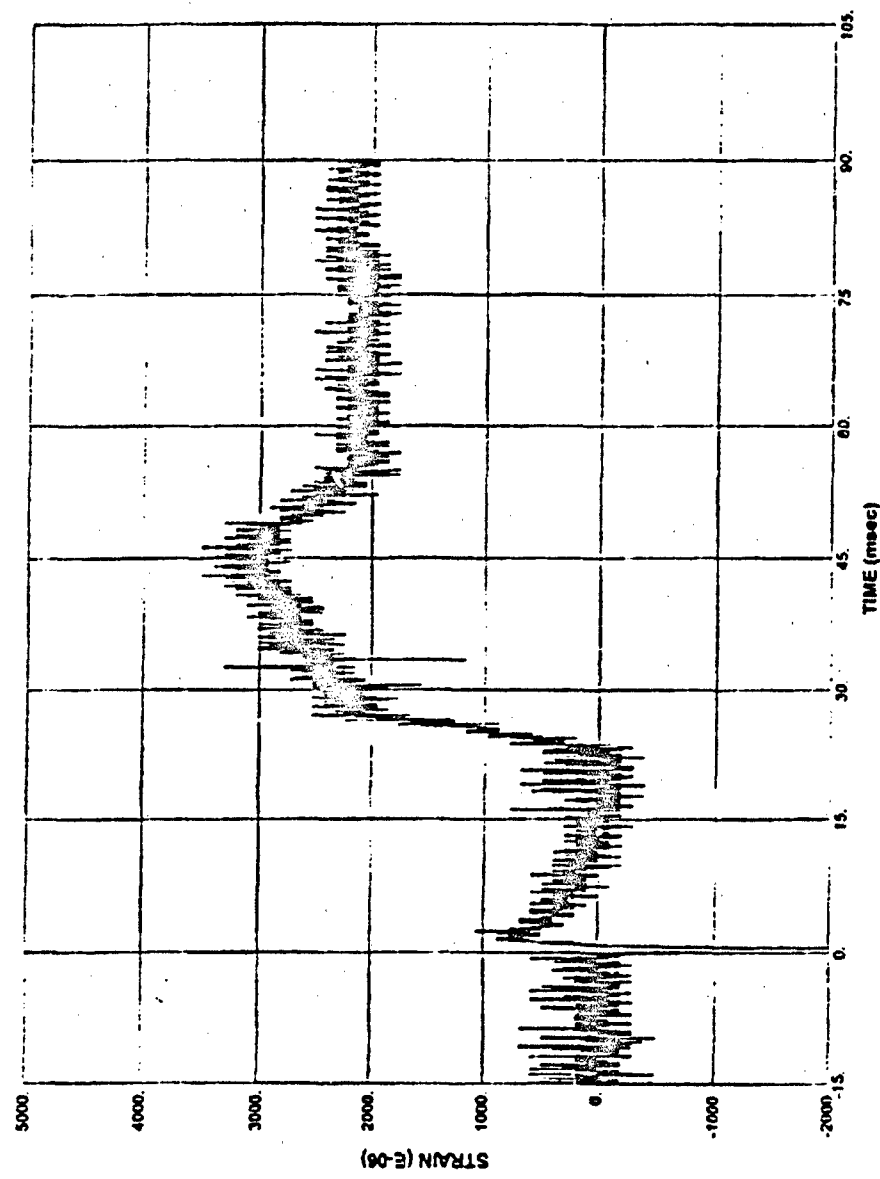


Figure C.30 Strain Gage S12, Test 2

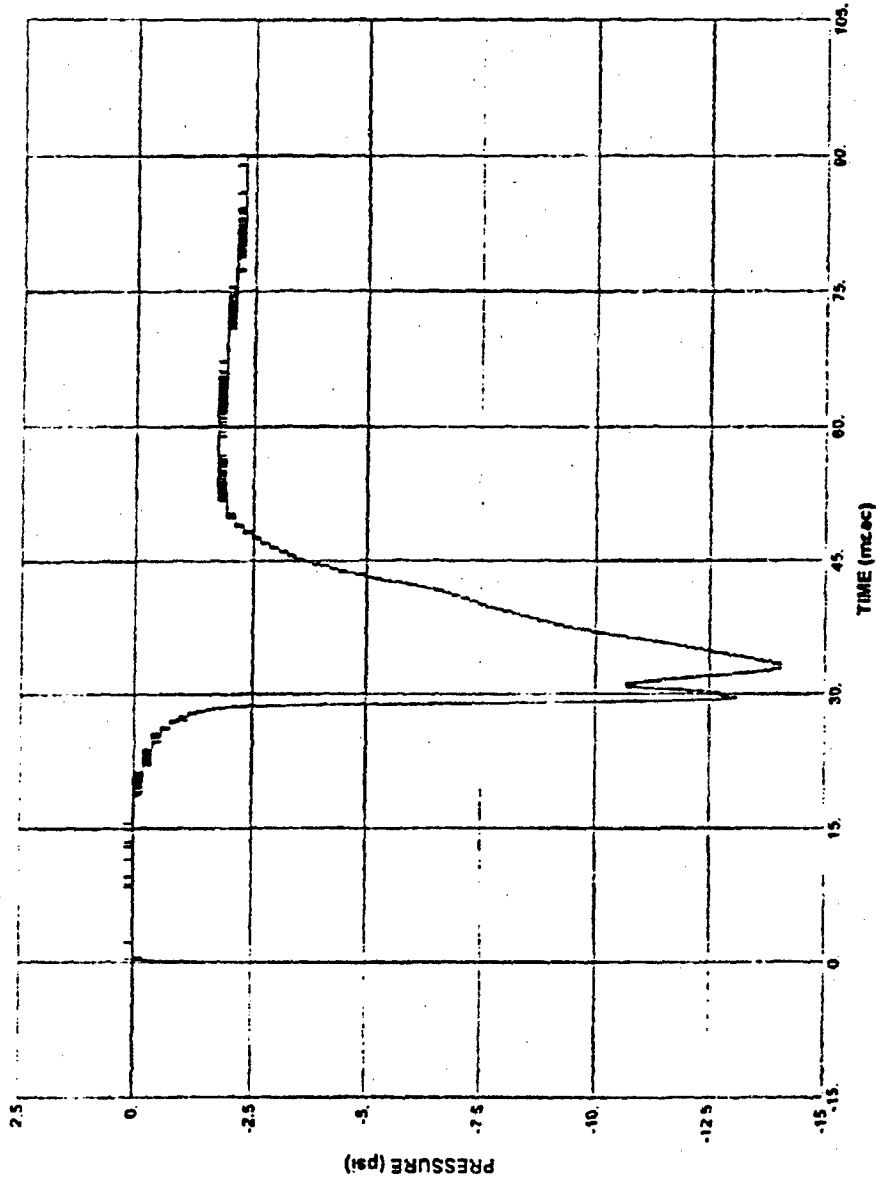


Figure C.31 Free-Field Pressure Gage F1, Test 3

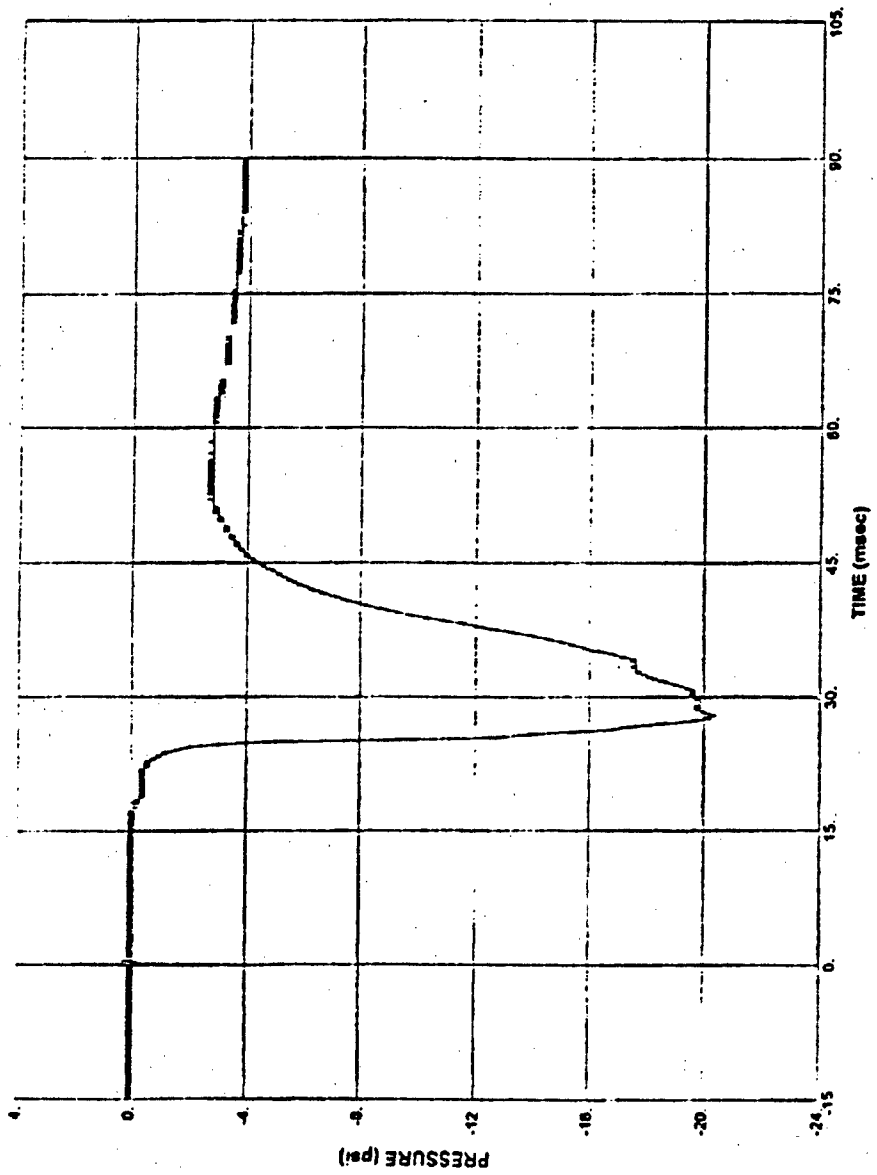


Figure C.32 Free-Field Pressure Gage F2, Test 3

285

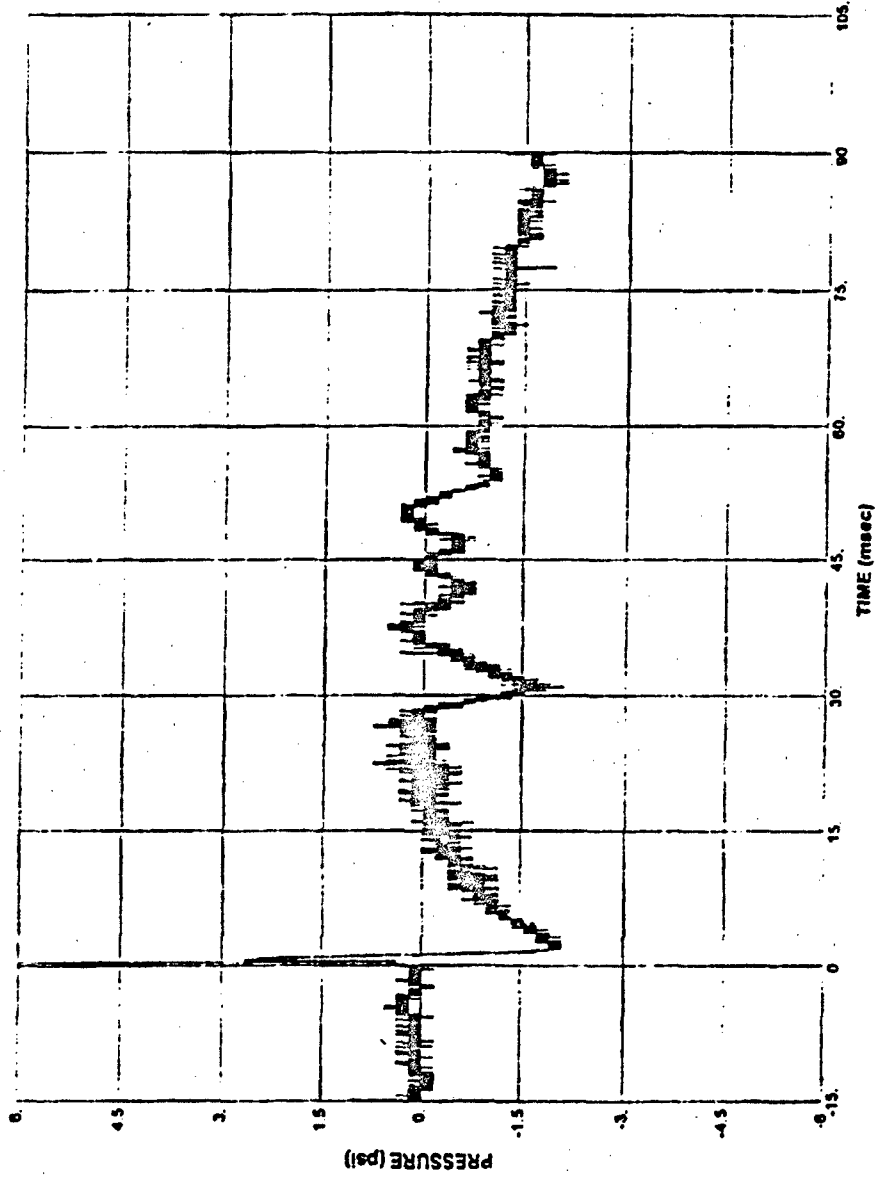


Figure C.33 Soil Pressure Interface Gage P1, Test 3

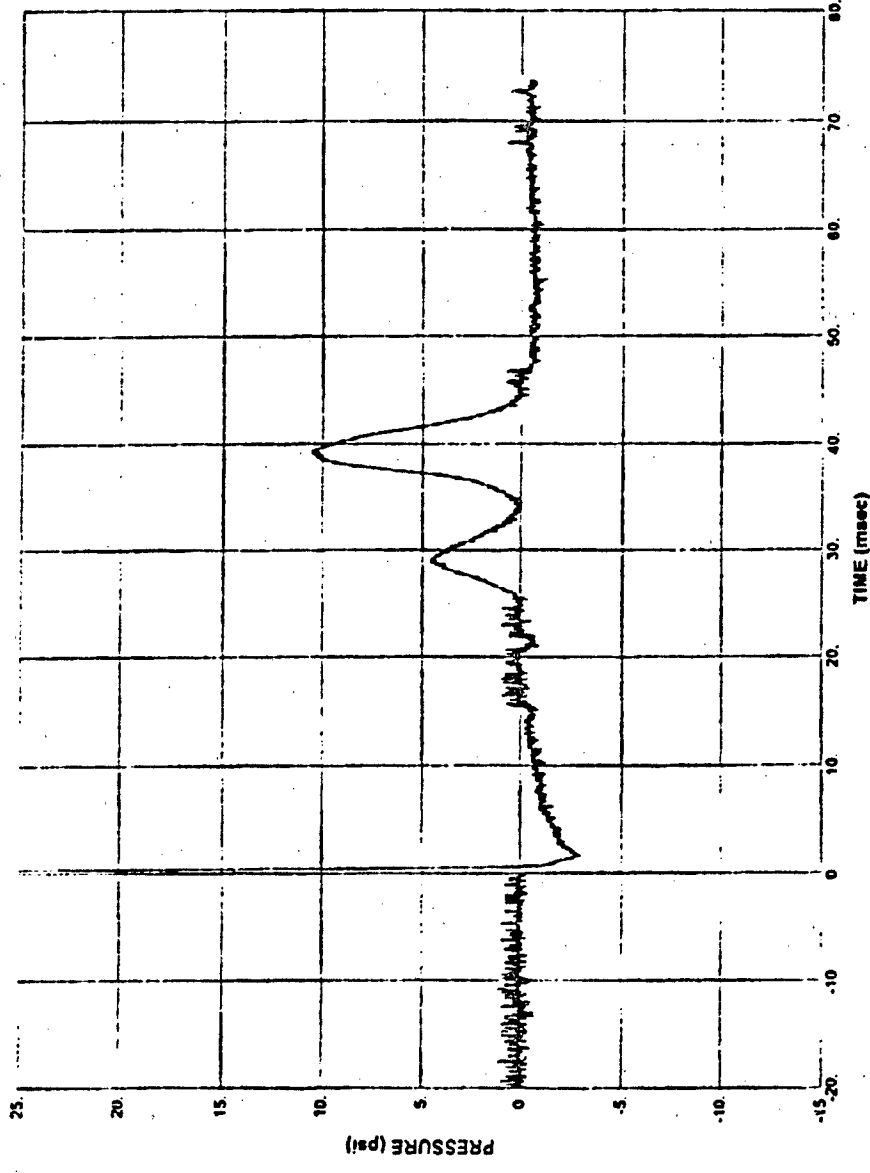


Figure C.34 Soil Pressure Interface Gage P2, Test 3

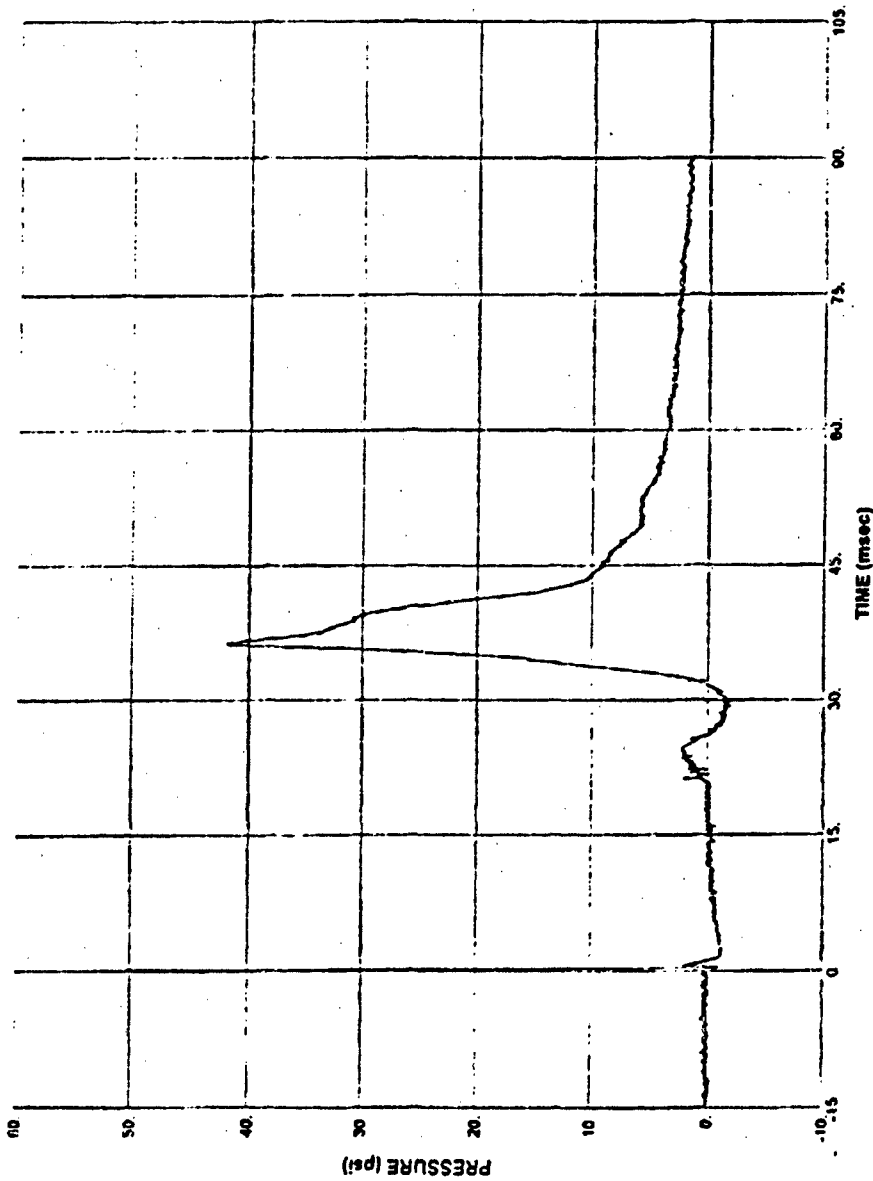


Figure C.35 Soil Pressure Interface Gage P3, Test 3

288

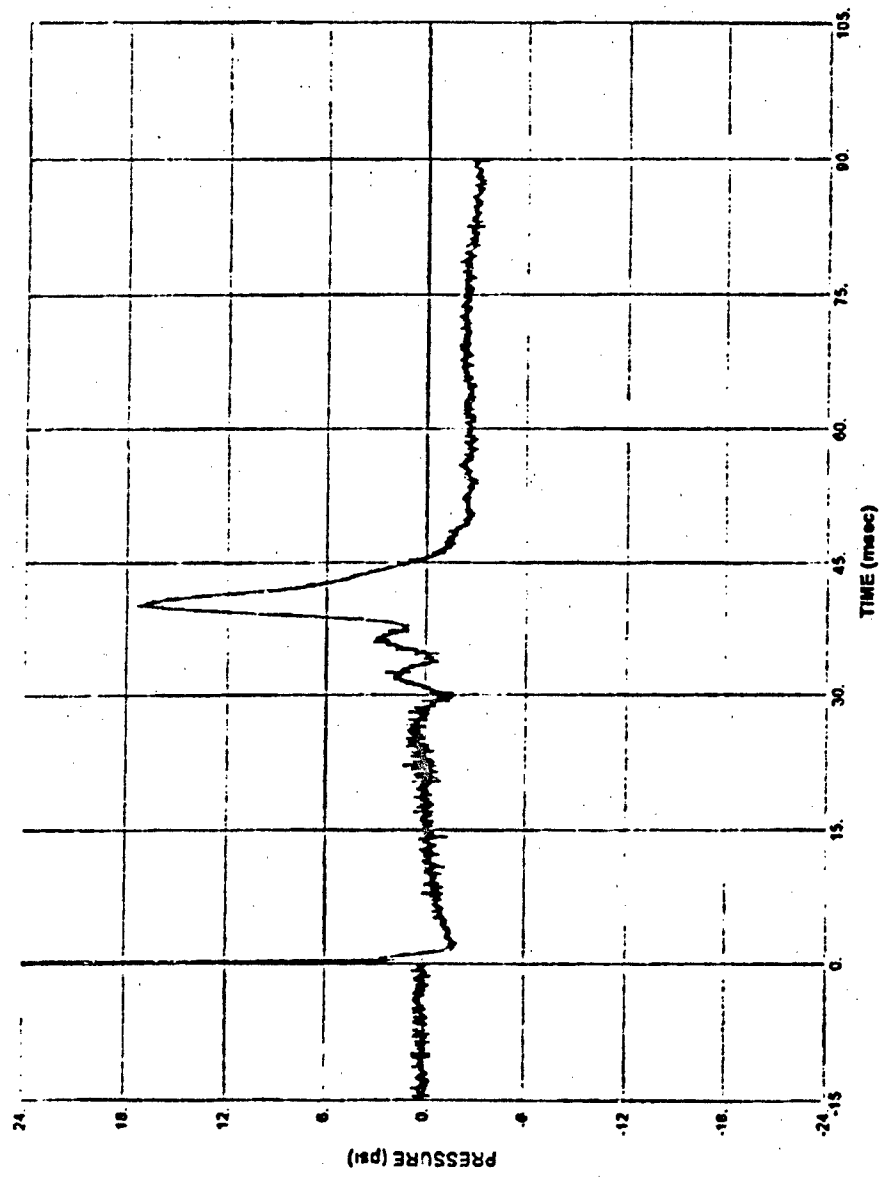


Figure C.36 Soil Pressure Interface Gage P4, Test 3

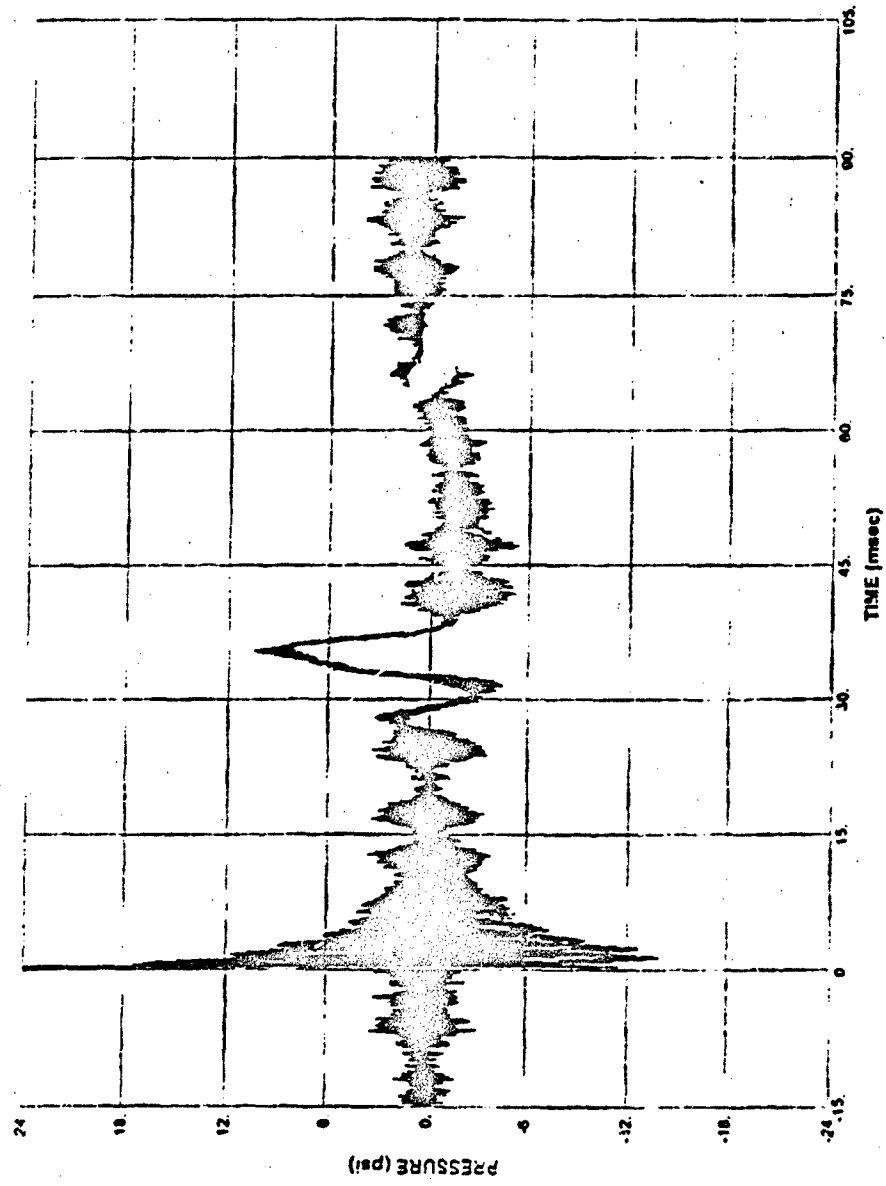


Figure C.37 Soil Pressure Interface Gage P5, Test 3

290

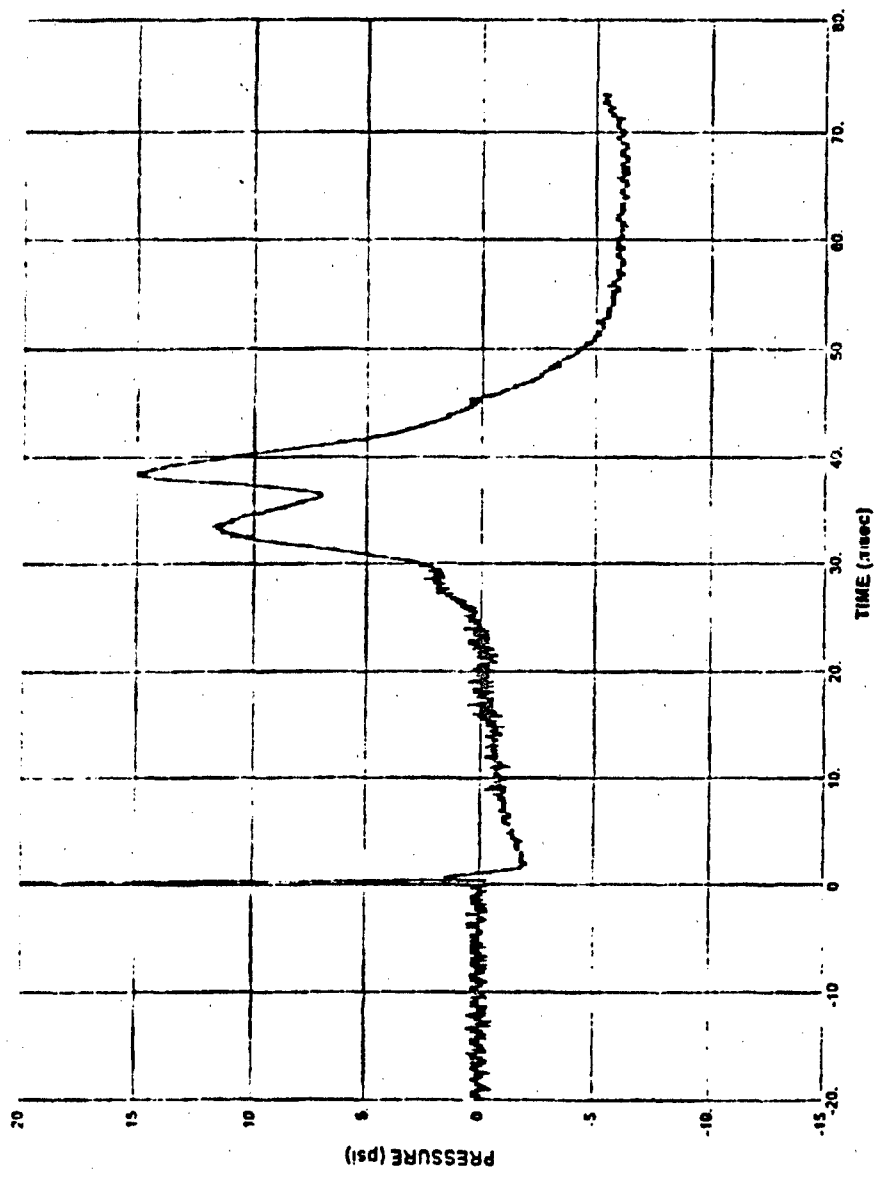
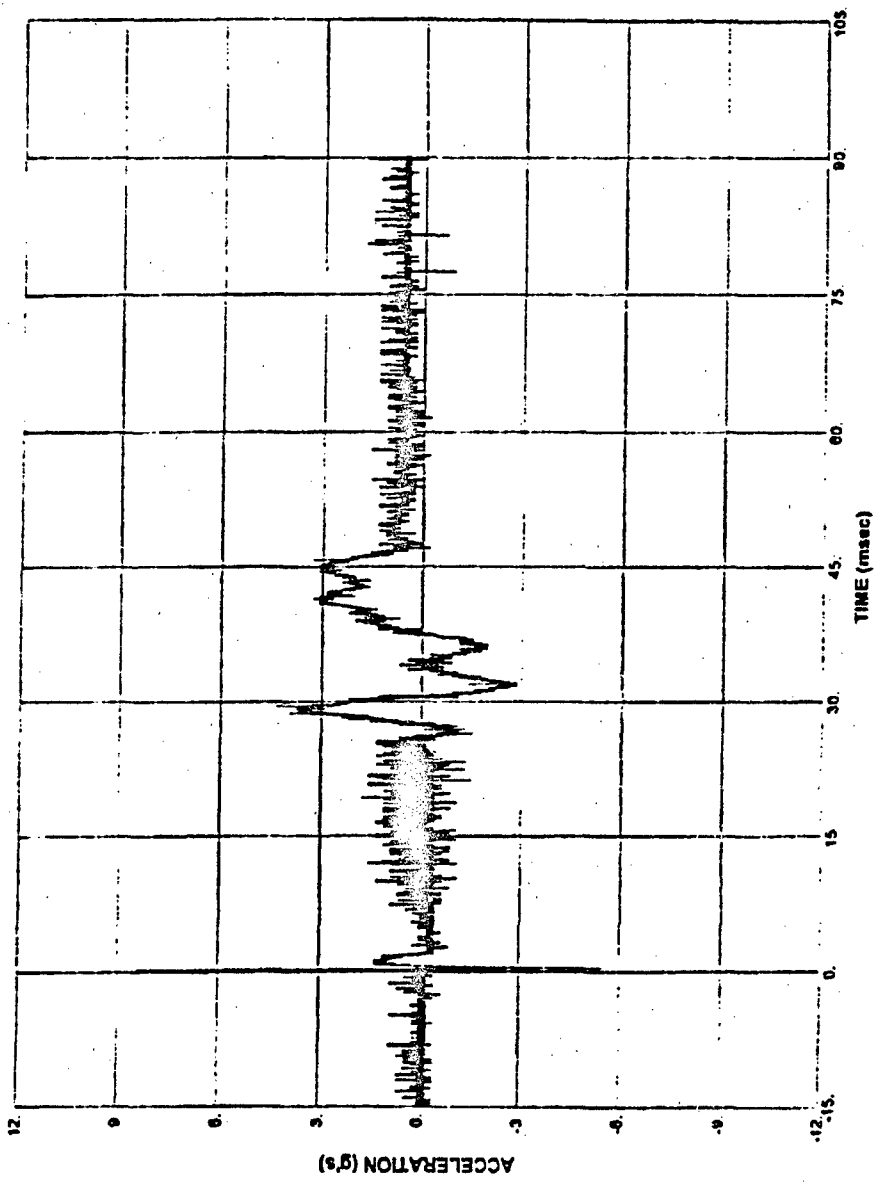


Figure C.38 Soil Pressure Interface Gage P6, Test 3

Figure C.39 Accelerometer A1, Test 3



ADA293552

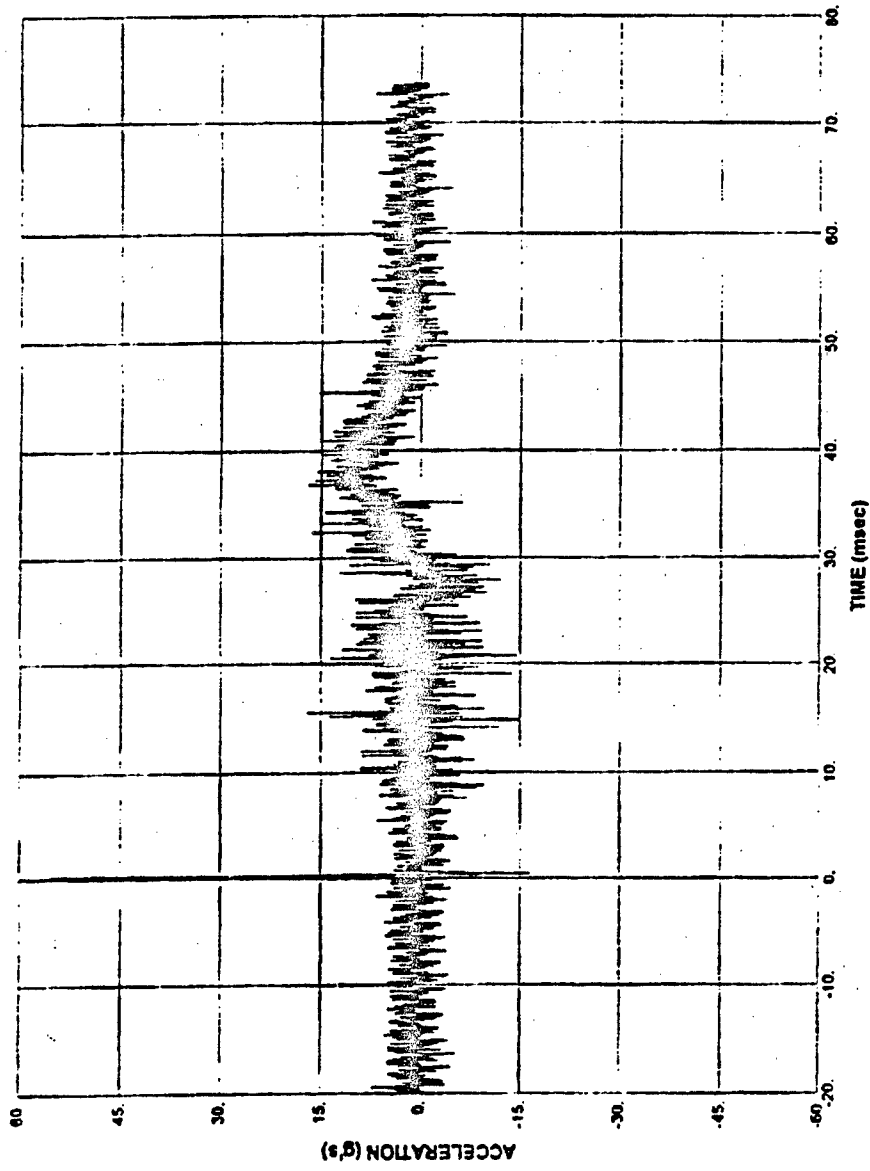


Figure C.40 Accelerometer A2, Test 3

293

ADA293552

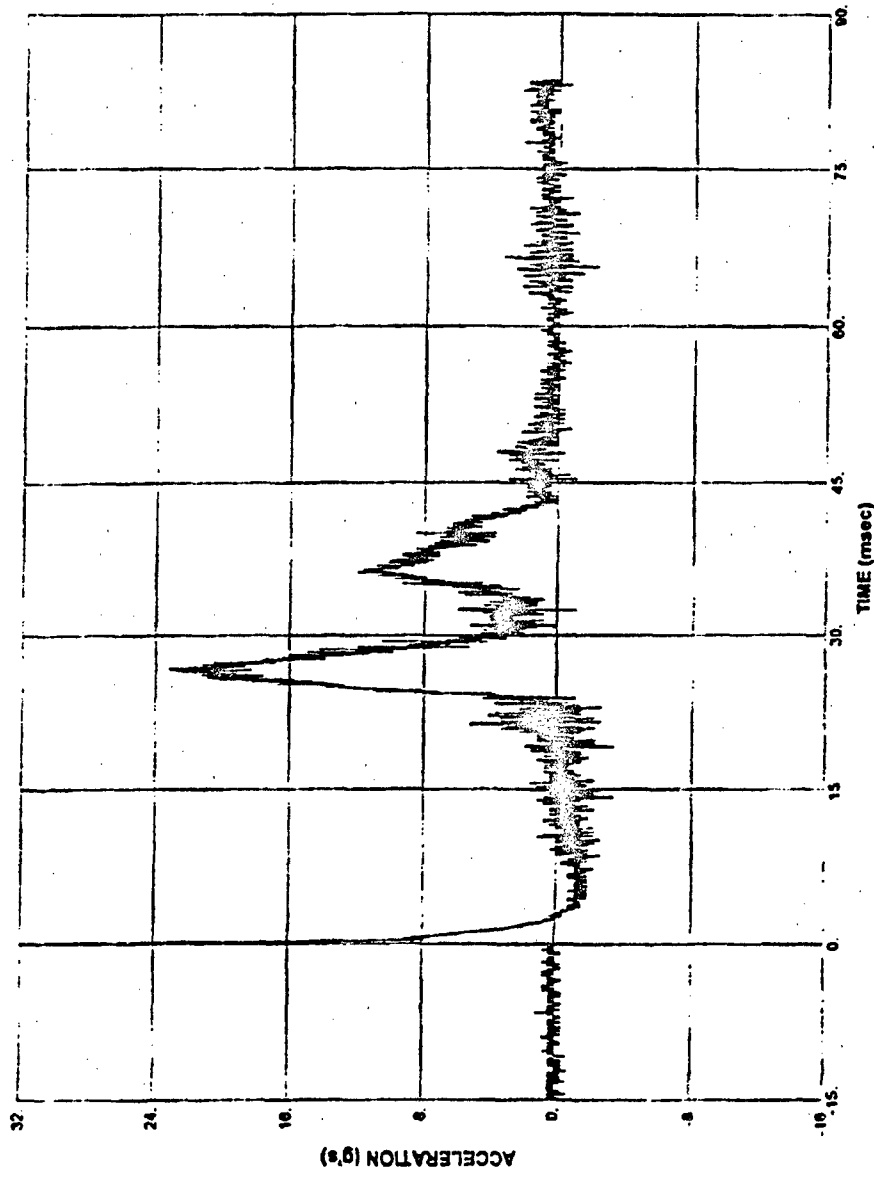


Figure C.41 Accelerometer A3, Test 3

294

ADA293552

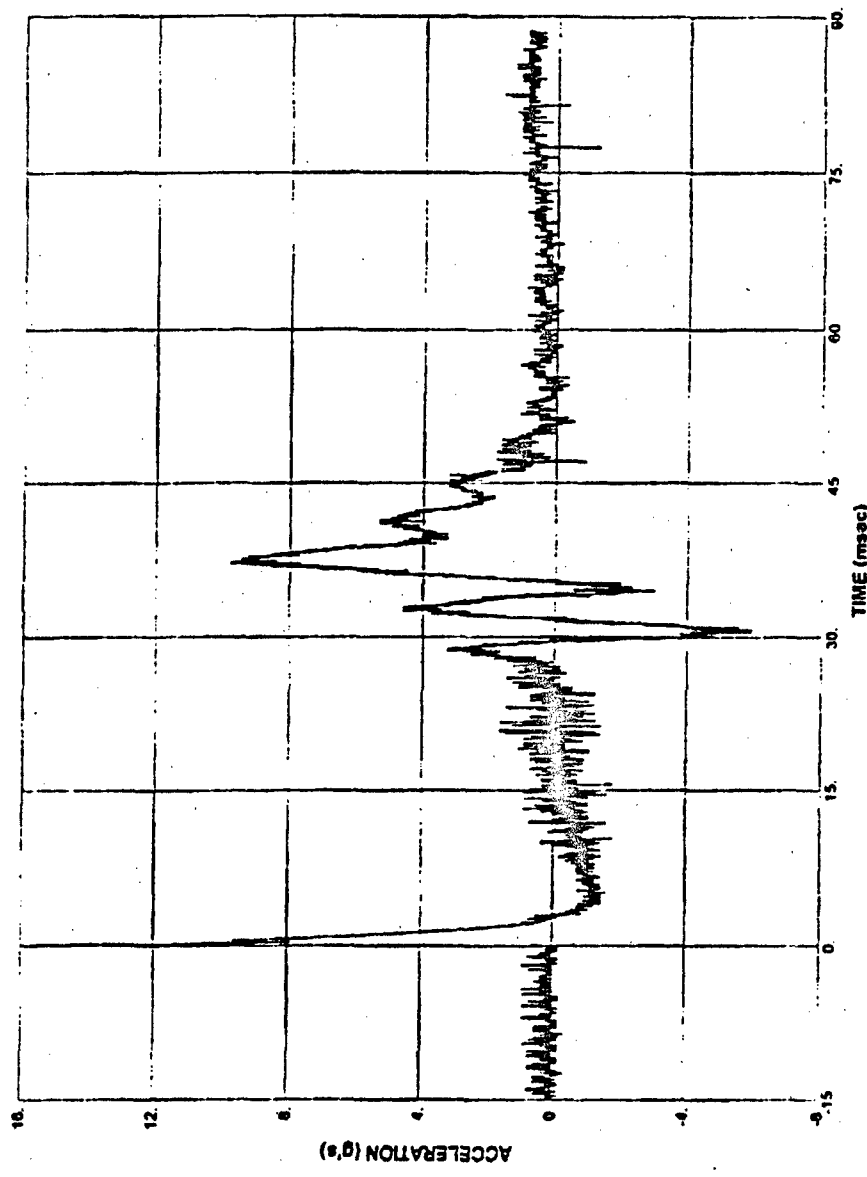


Figure C.42 Accelerometer A4, Test 3

295

ADA293552

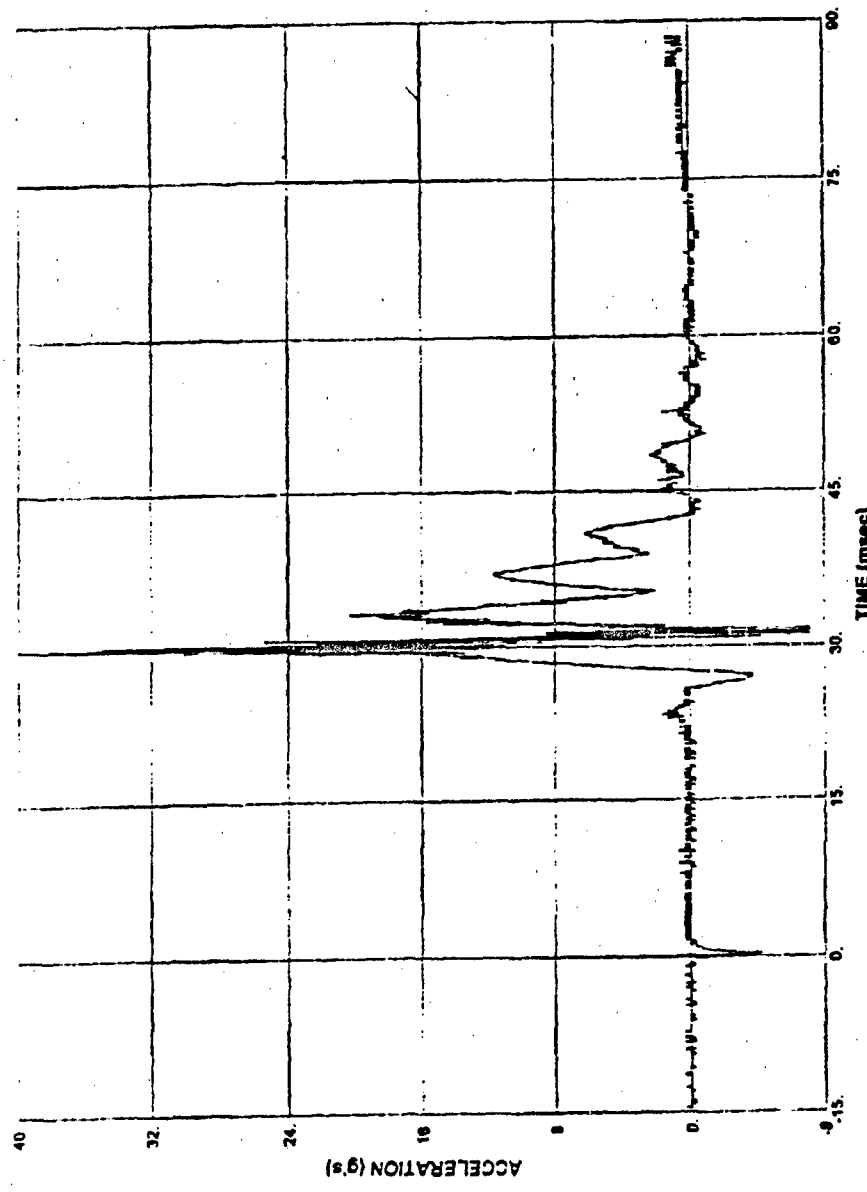


Figure C.43 Accelerometer A5, Test 3

296

ADA293552

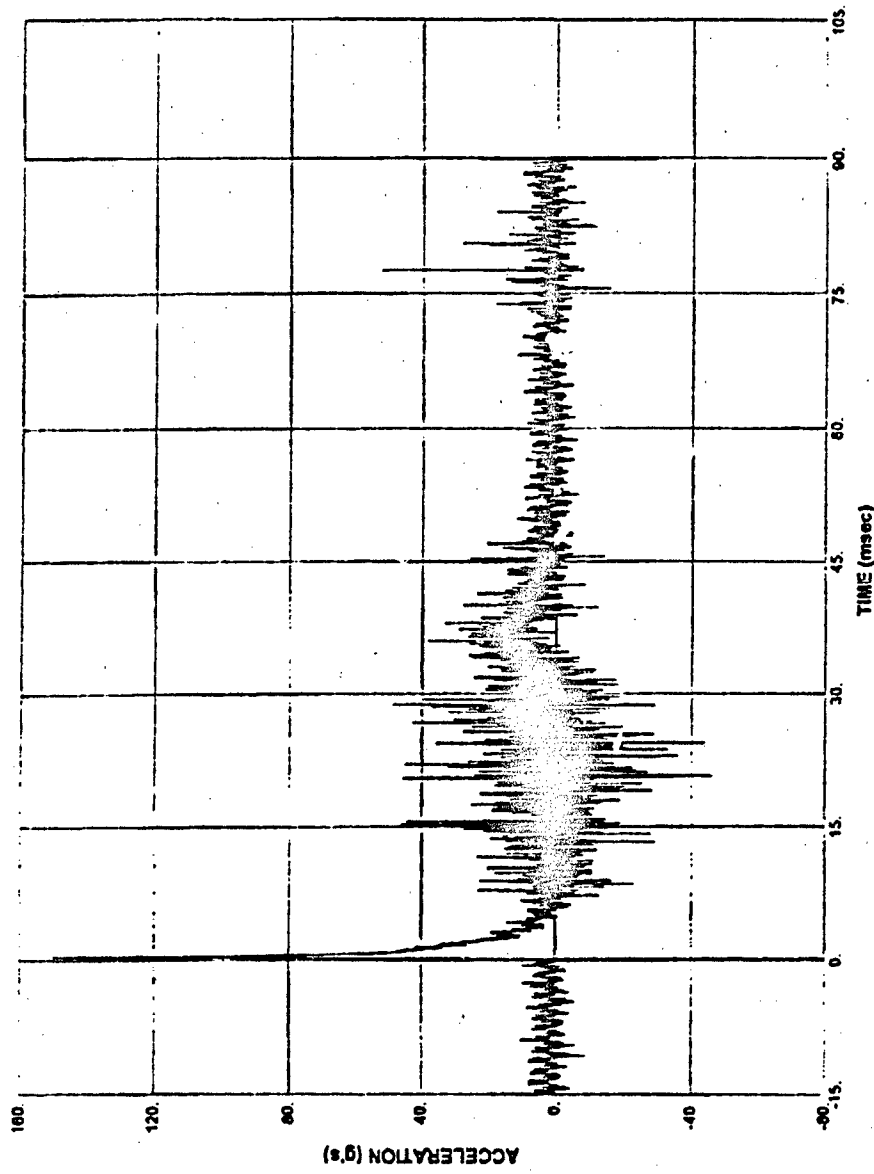


Figure C.44 Accelerometer A6, Test 3

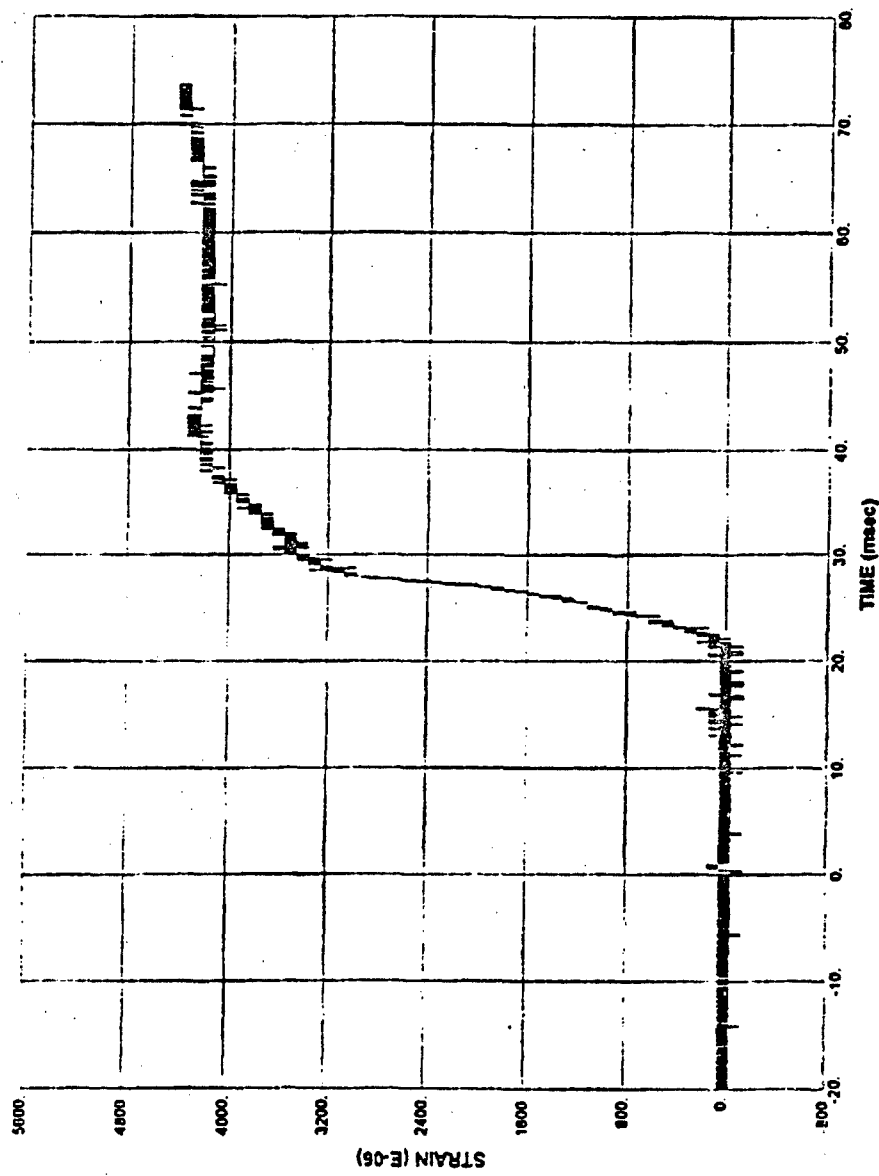


Figure C.45 Strain Gage S7, Test 3

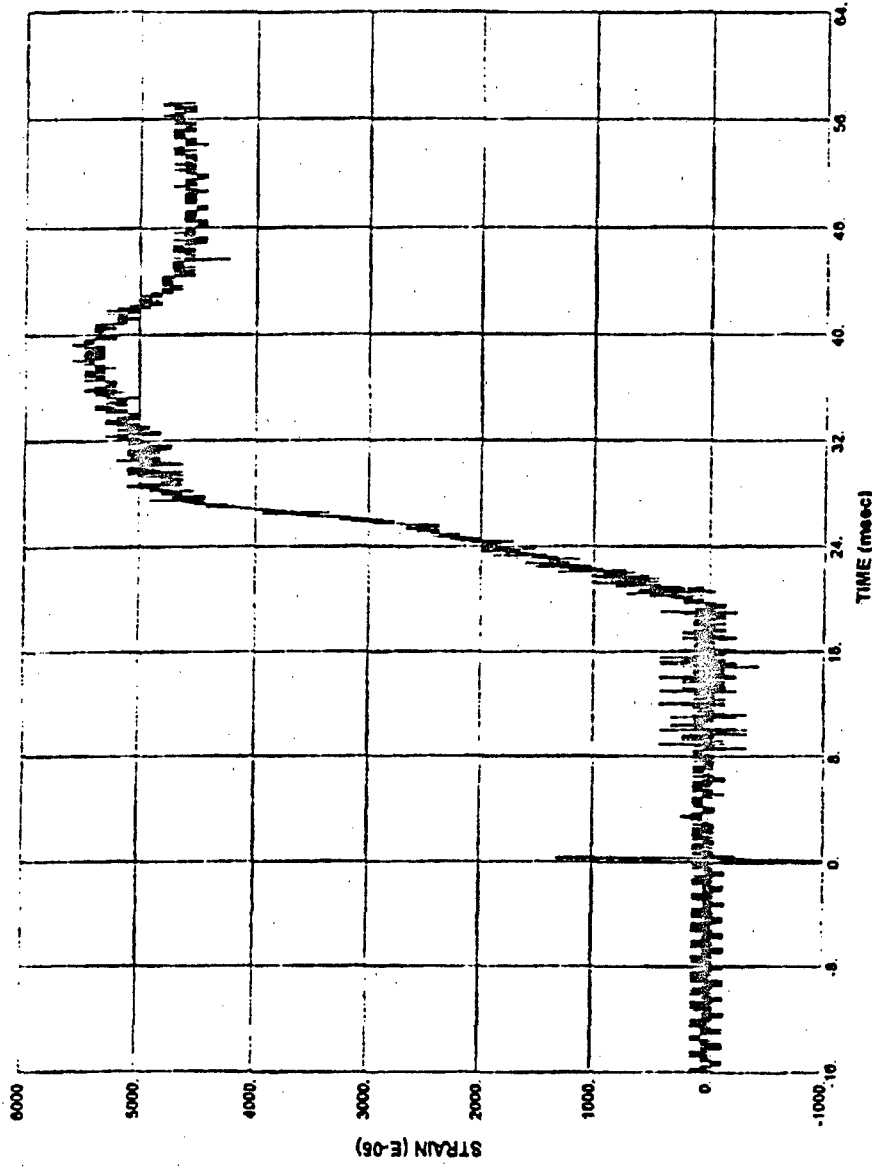


Figure C.46 Strain Gage S8, Test 3

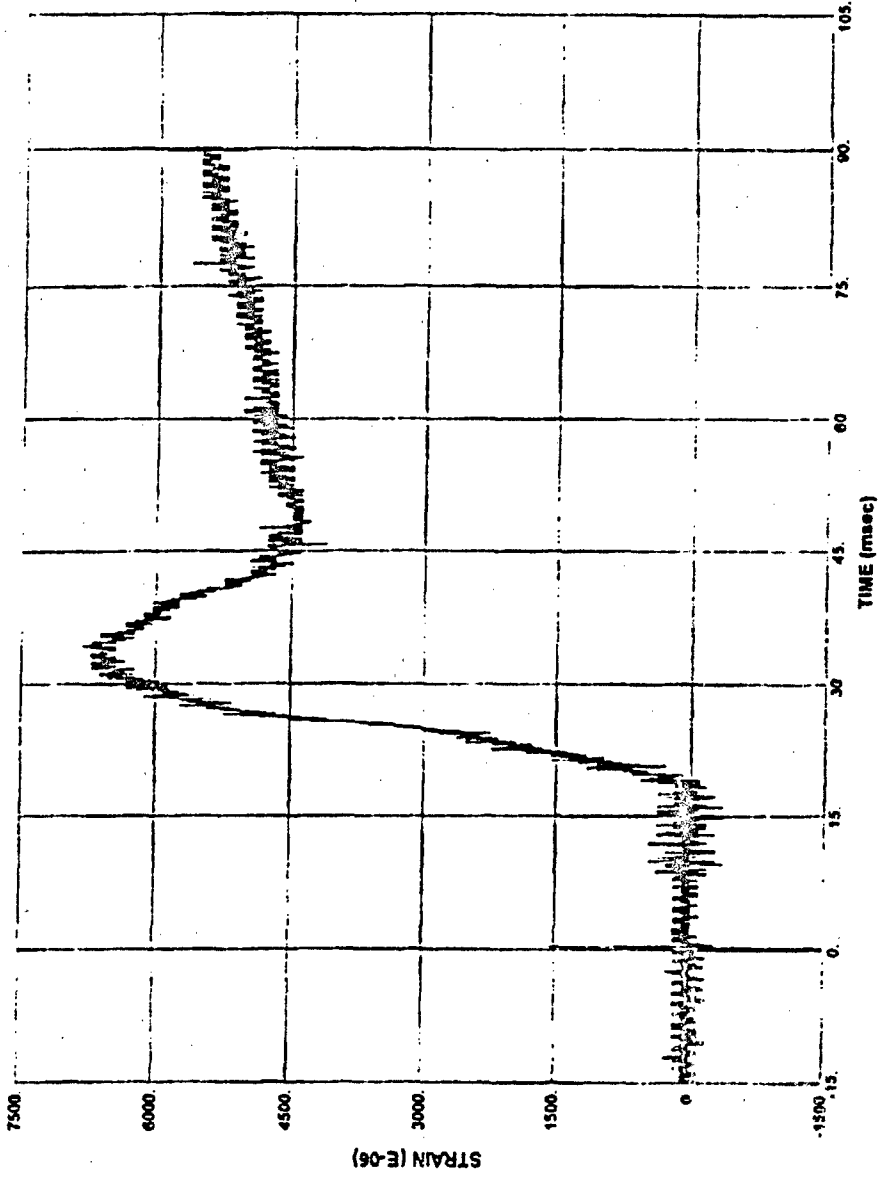


Figure C.47 Strain Gage S9, Test 3

300

ADA293552

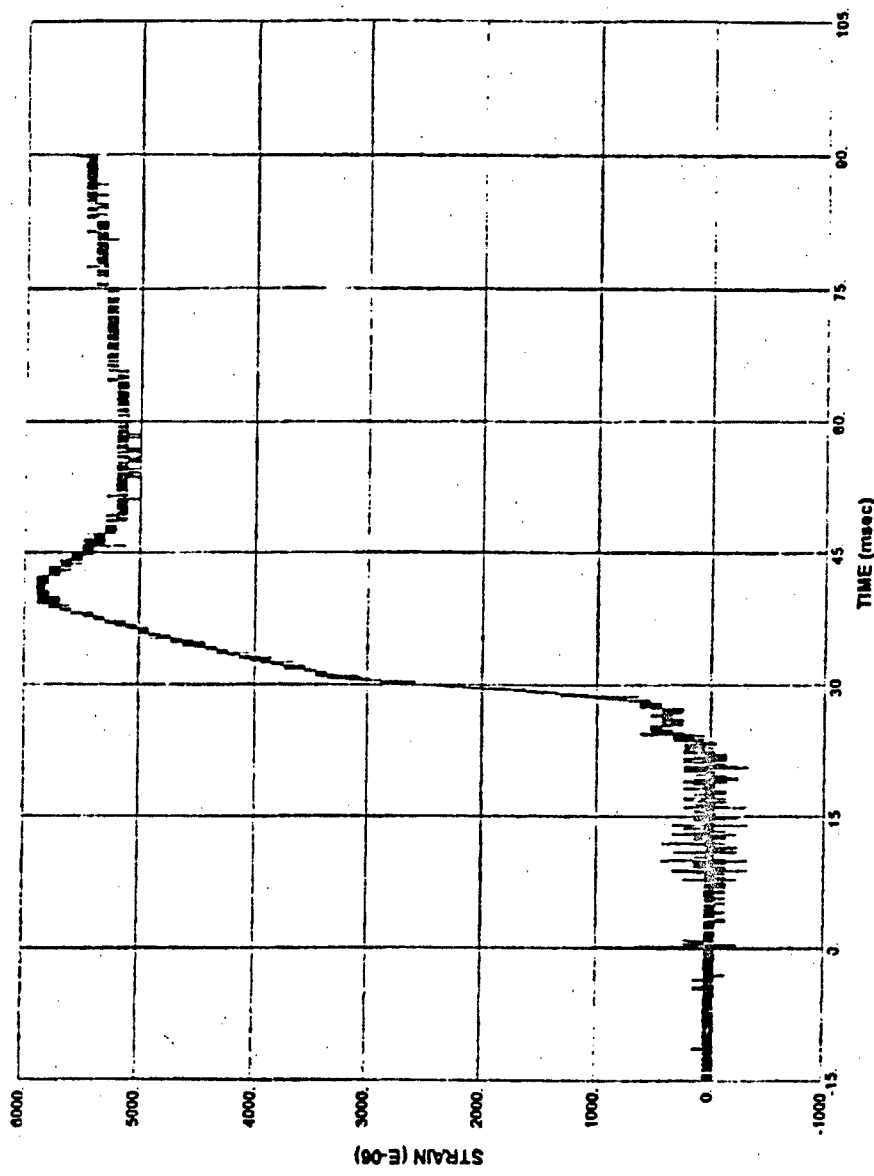


Figure C.48 Strain Gage S10, Test 3

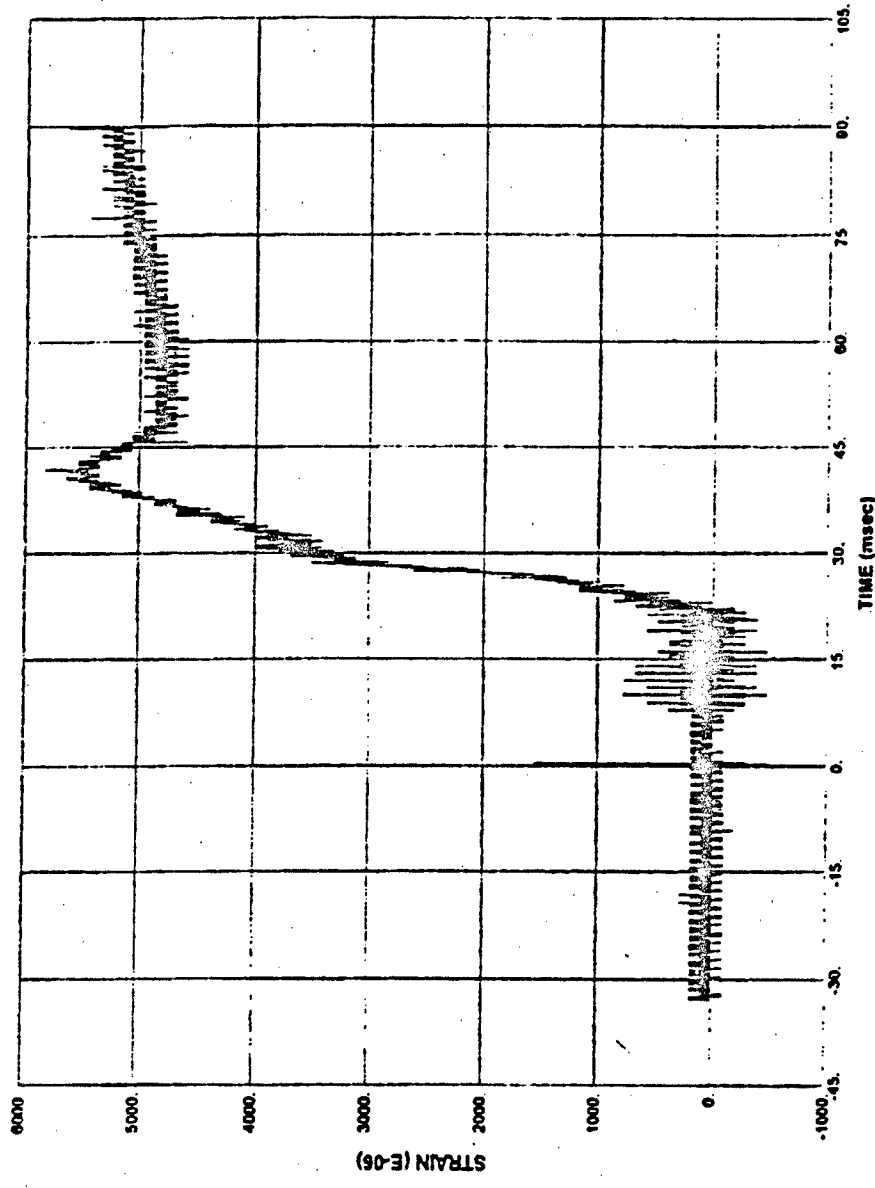


Figure C.49 Strain Gage SII, Test 3

302

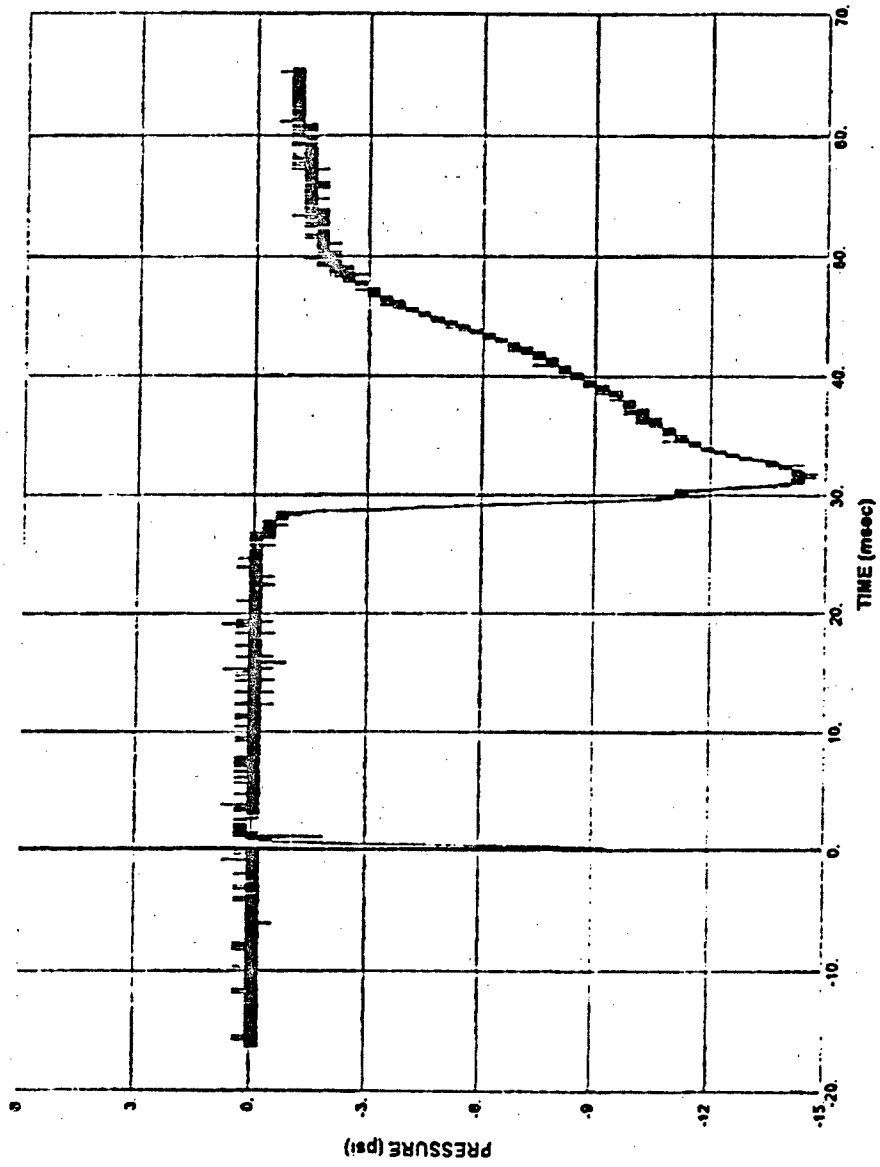


Figure C.50 Free-Field Pressure Gage F1, Test 4

303

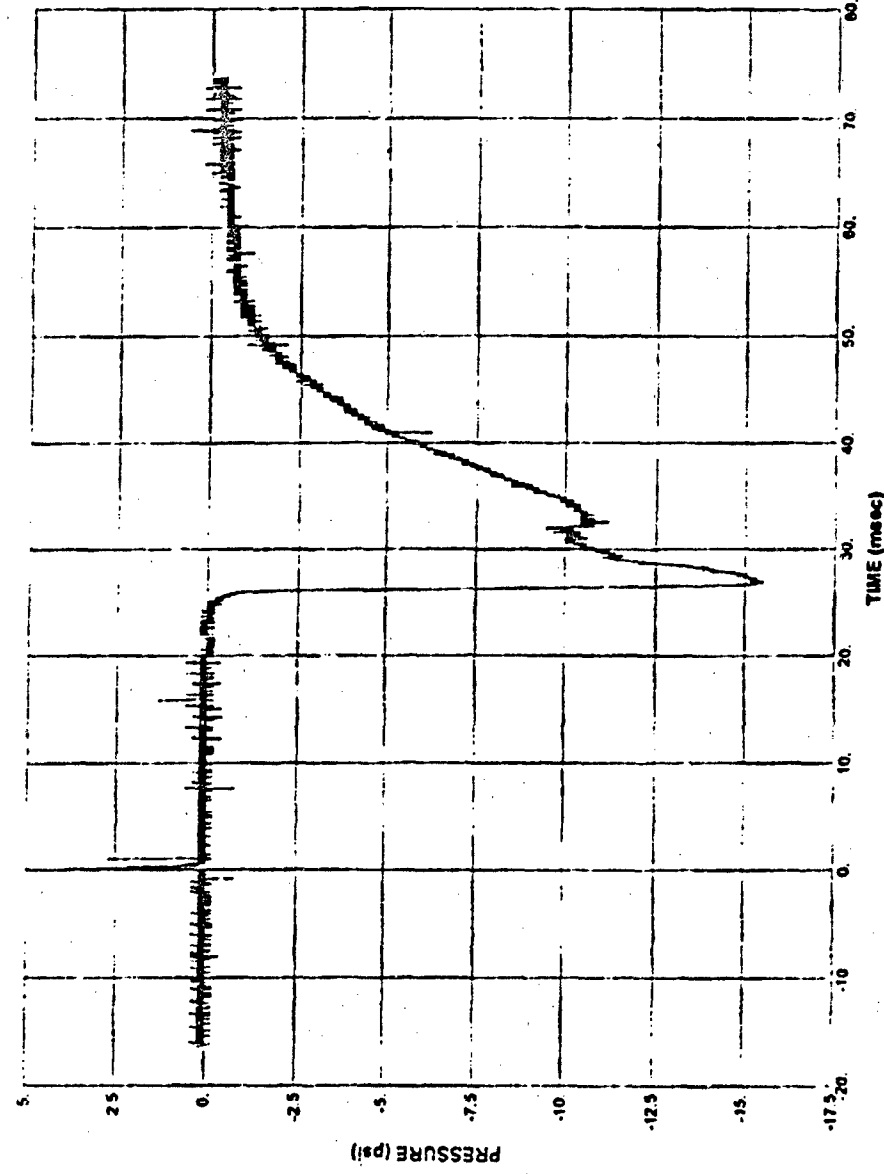


Figure C.51: Free-Field Pressure Gage F2, Test 4

304

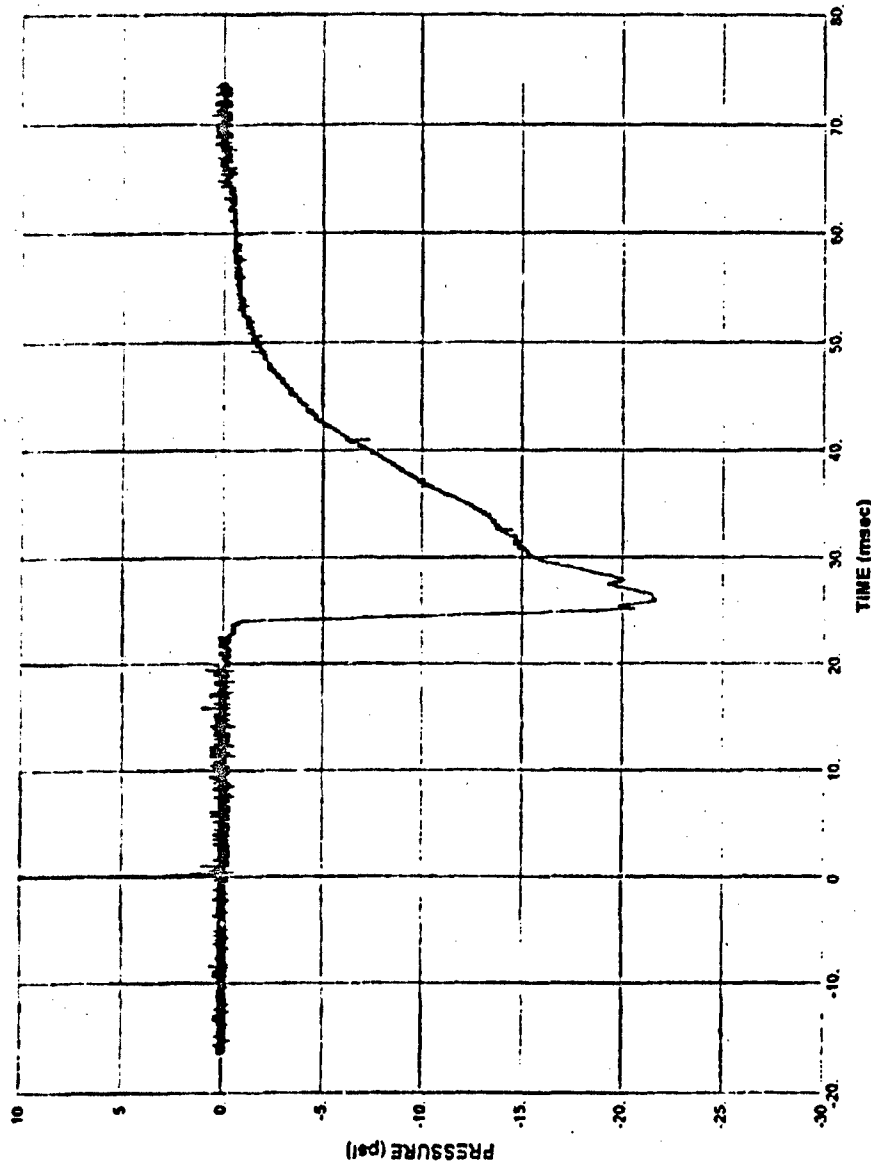


Figure C.52 Free-Field Pressure Gage F3, Test 4

305

ADA293552

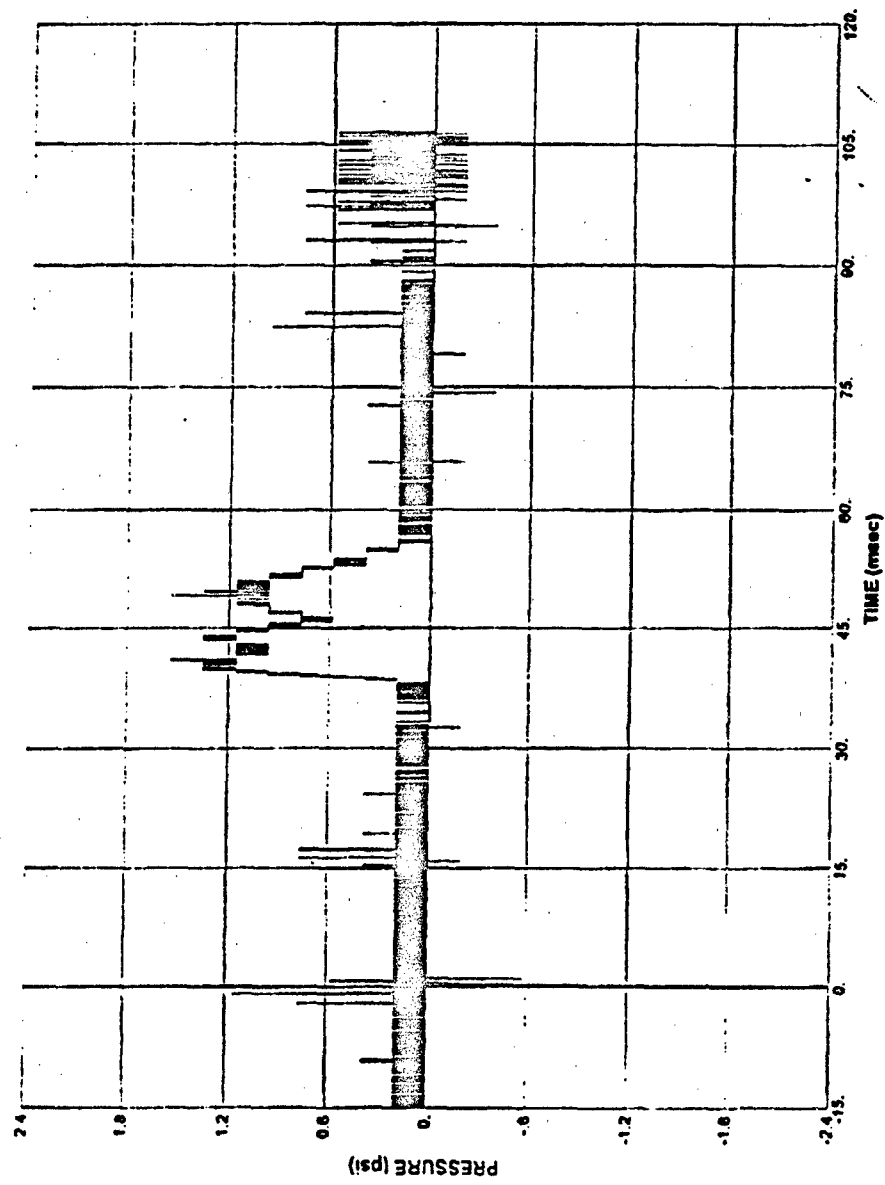


Figure C.53 Soil Pressure Interface Gage P1, Test 4

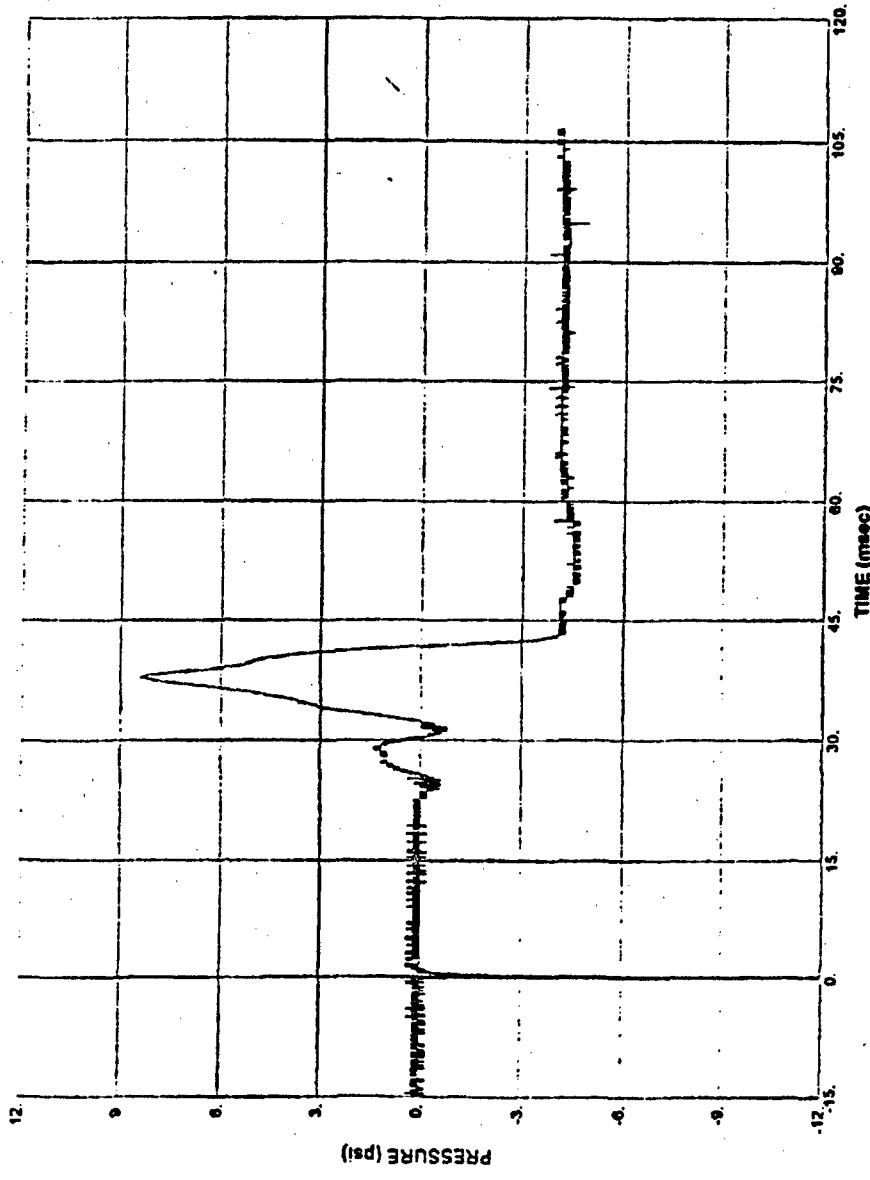


Figure C.54 Soil Pressure Interface Gage P2, Test 4

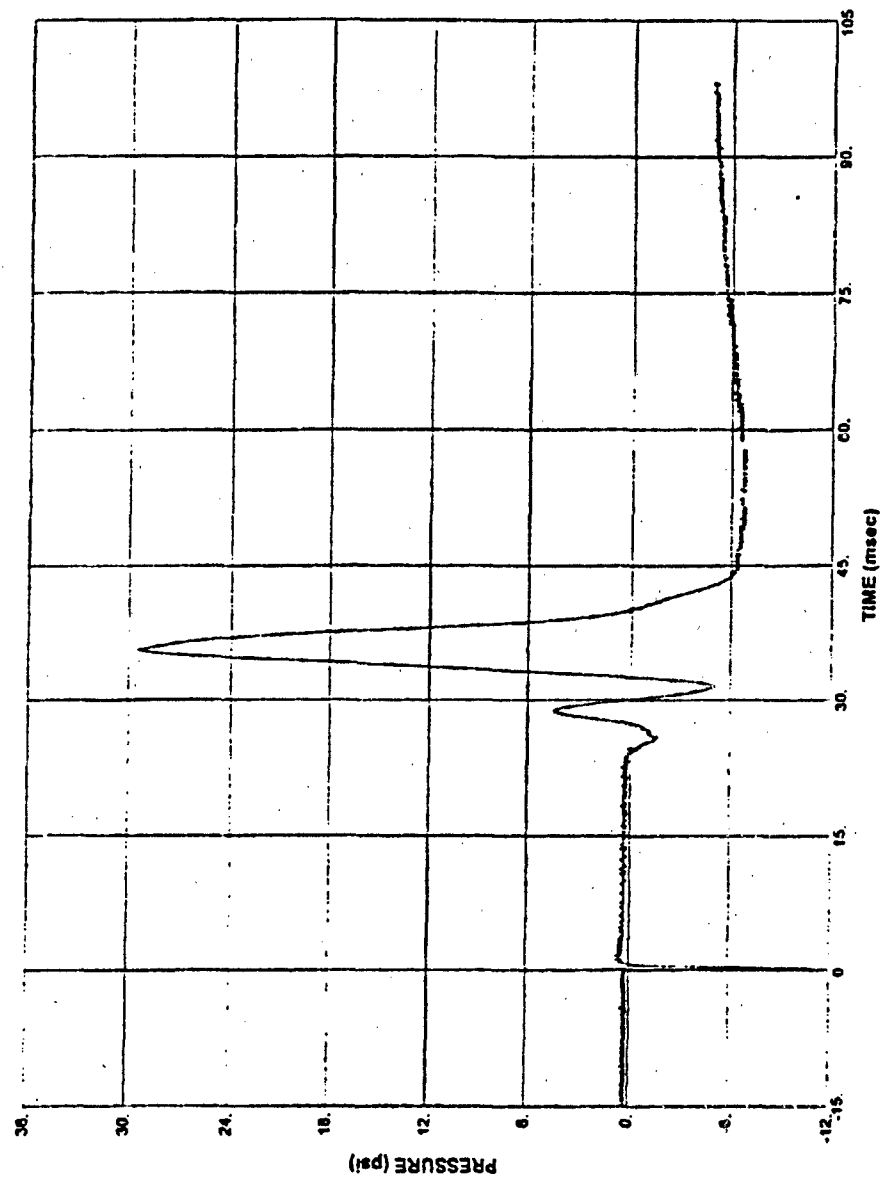


Figure C.55 Soil Pressure Interface Gage P3, Test 4

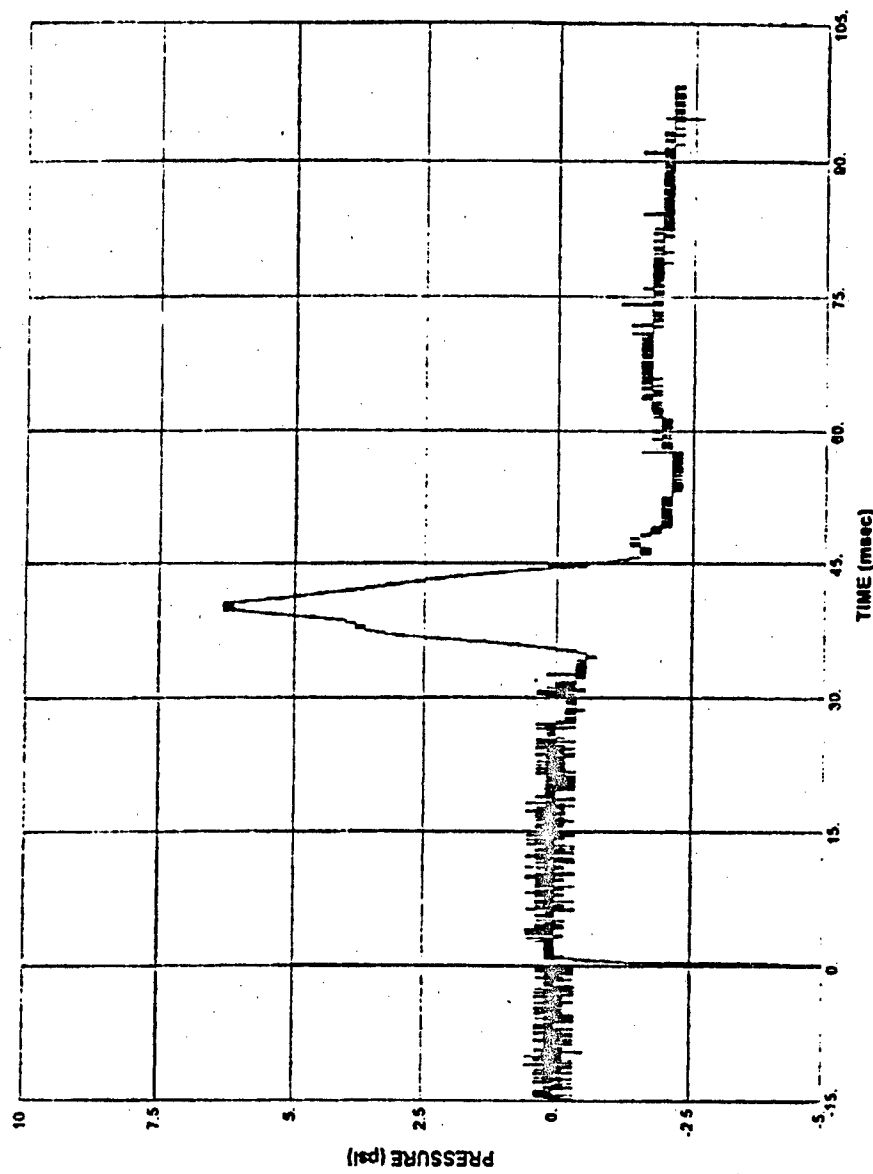


Figure C.56 Soil Pressure Interface Gage P4, Test 4

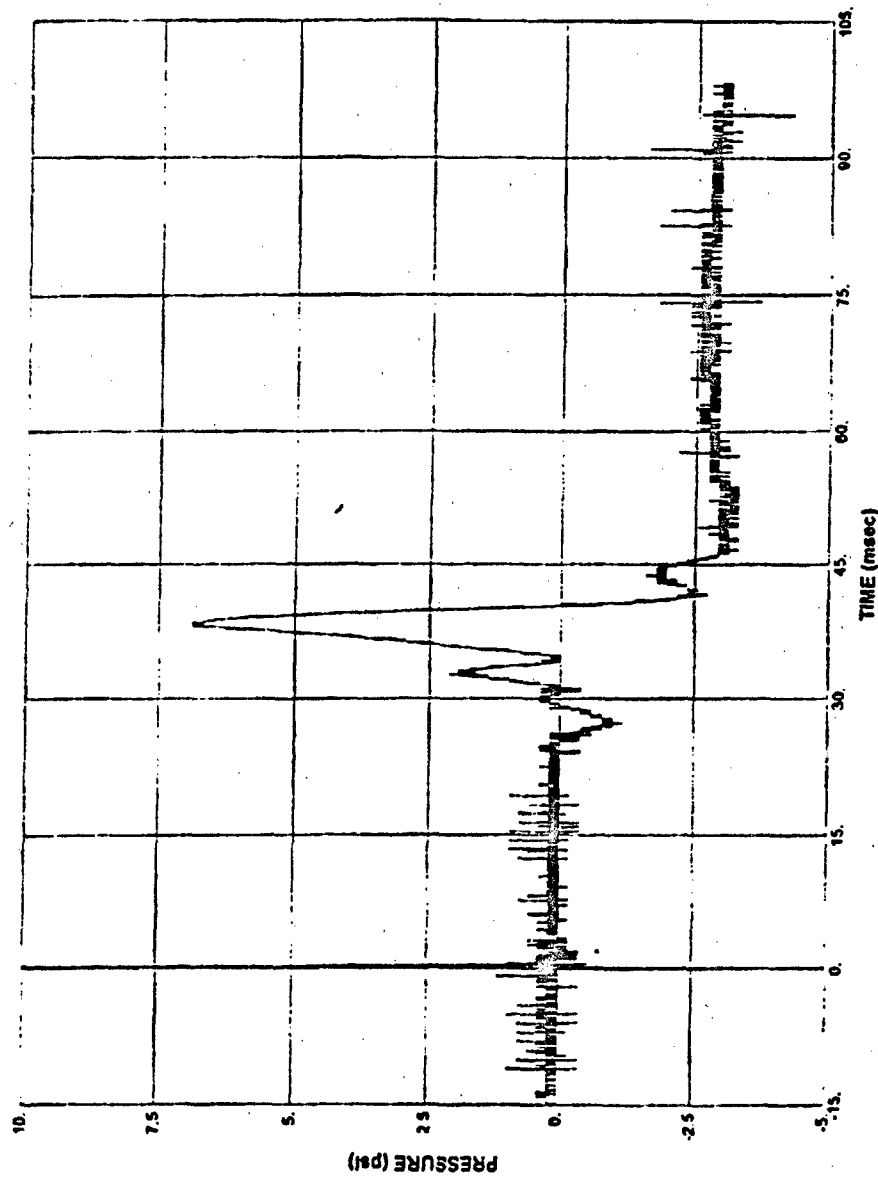


Figure C.57 Soil Pressure Interface Gage PS, Test 4

310

ADA293552

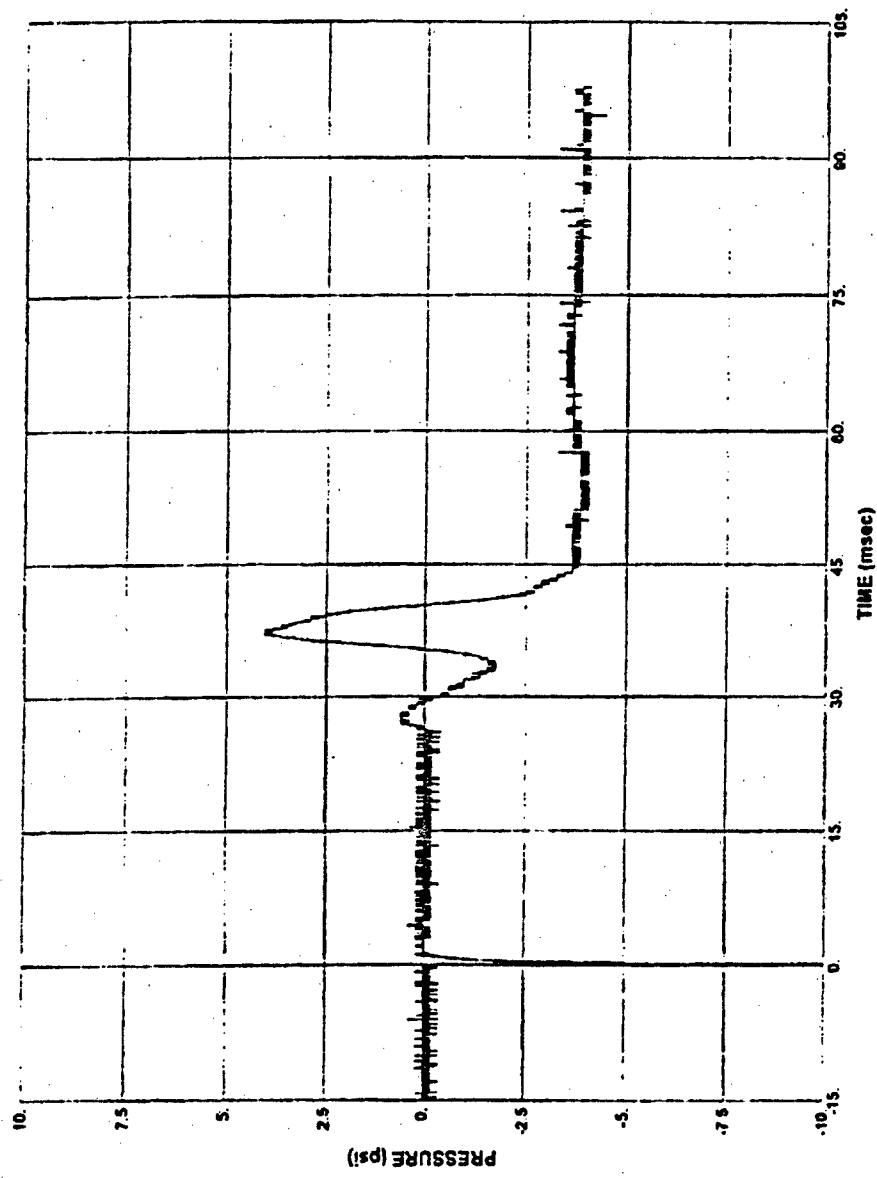


Figure C.58 Soil Pressure Interface Gage P6, Test 4

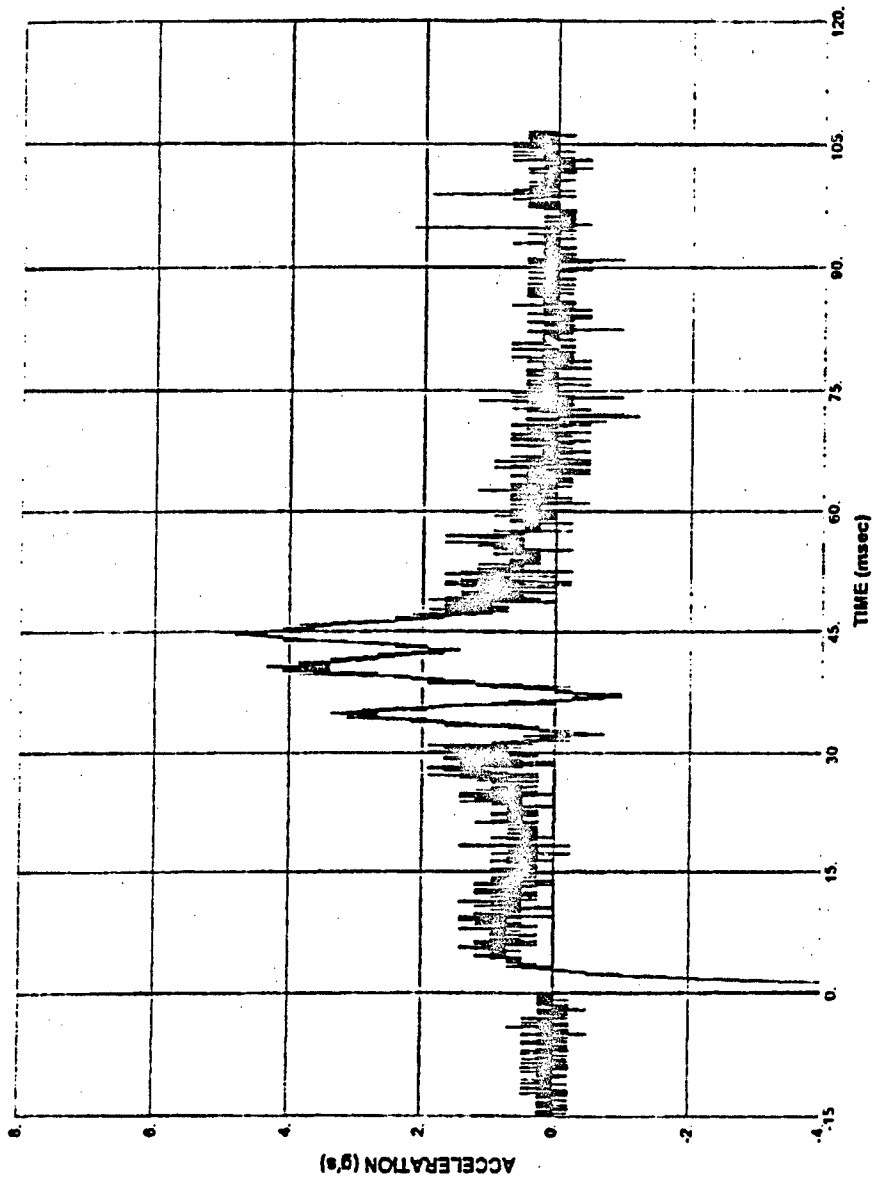


Figure C.59 Accelerometer A1, Test 4

312

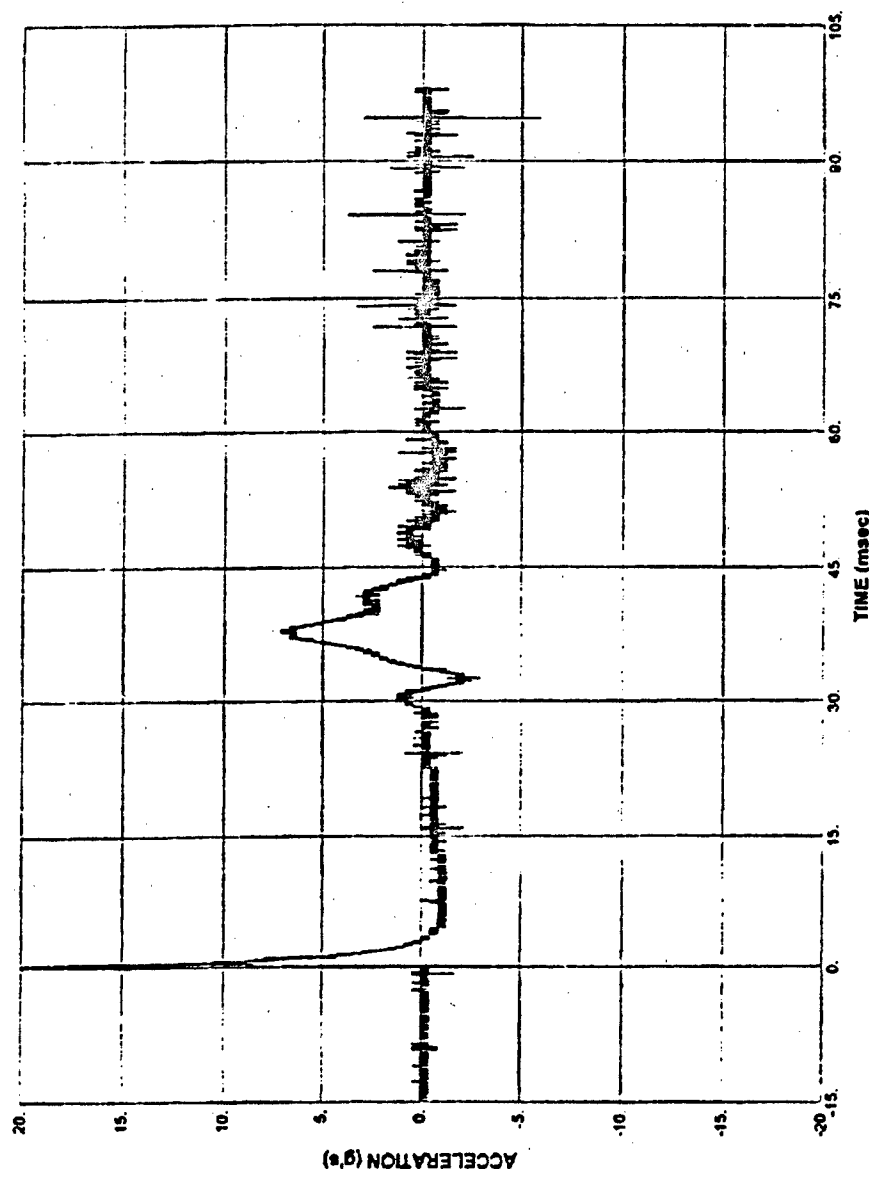


Figure C.60 Accelerometer A2, Test 4

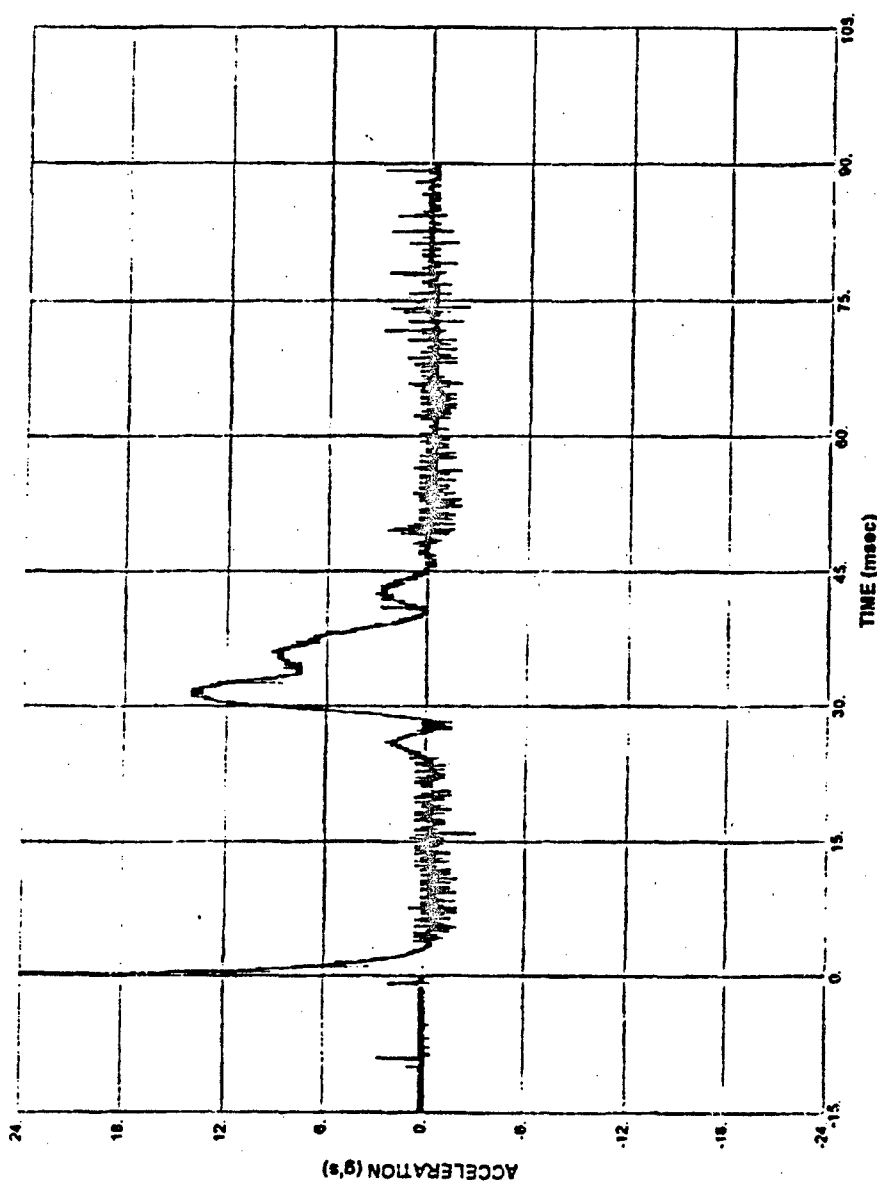


Figure C.61 Accelerometer A3, Test 4

314

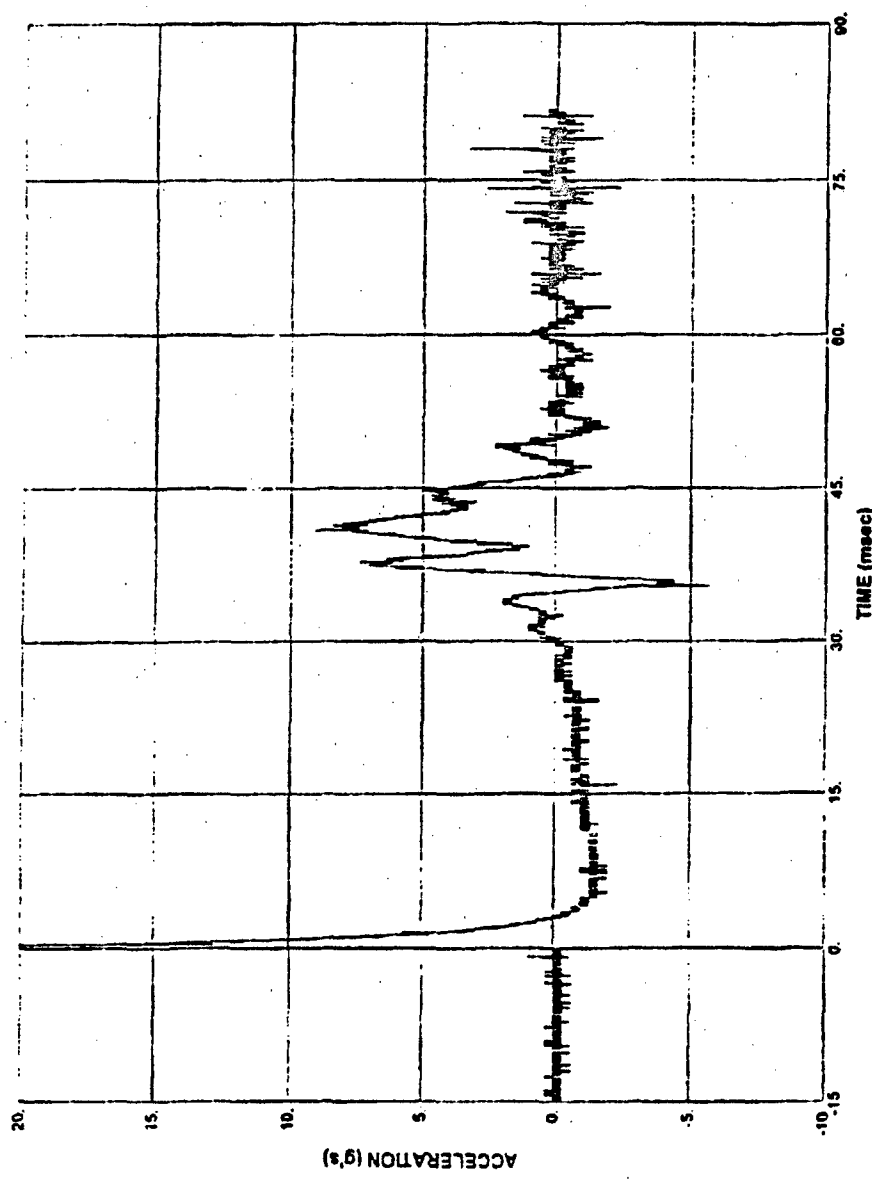


Figure C.62 Accelerometer A4, Test 4

315

ADA293552

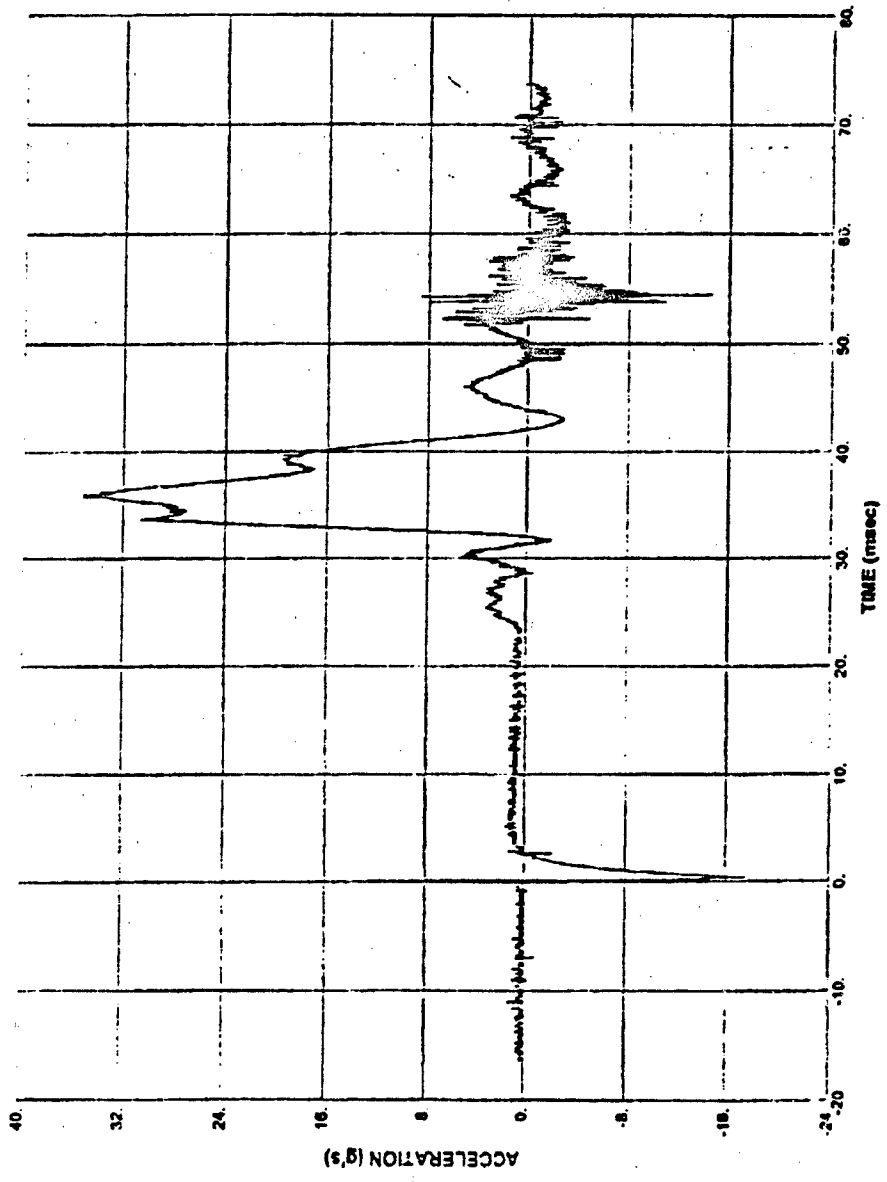


Figure C.63 Accelerometer A5, Test 4

316

ADA293552

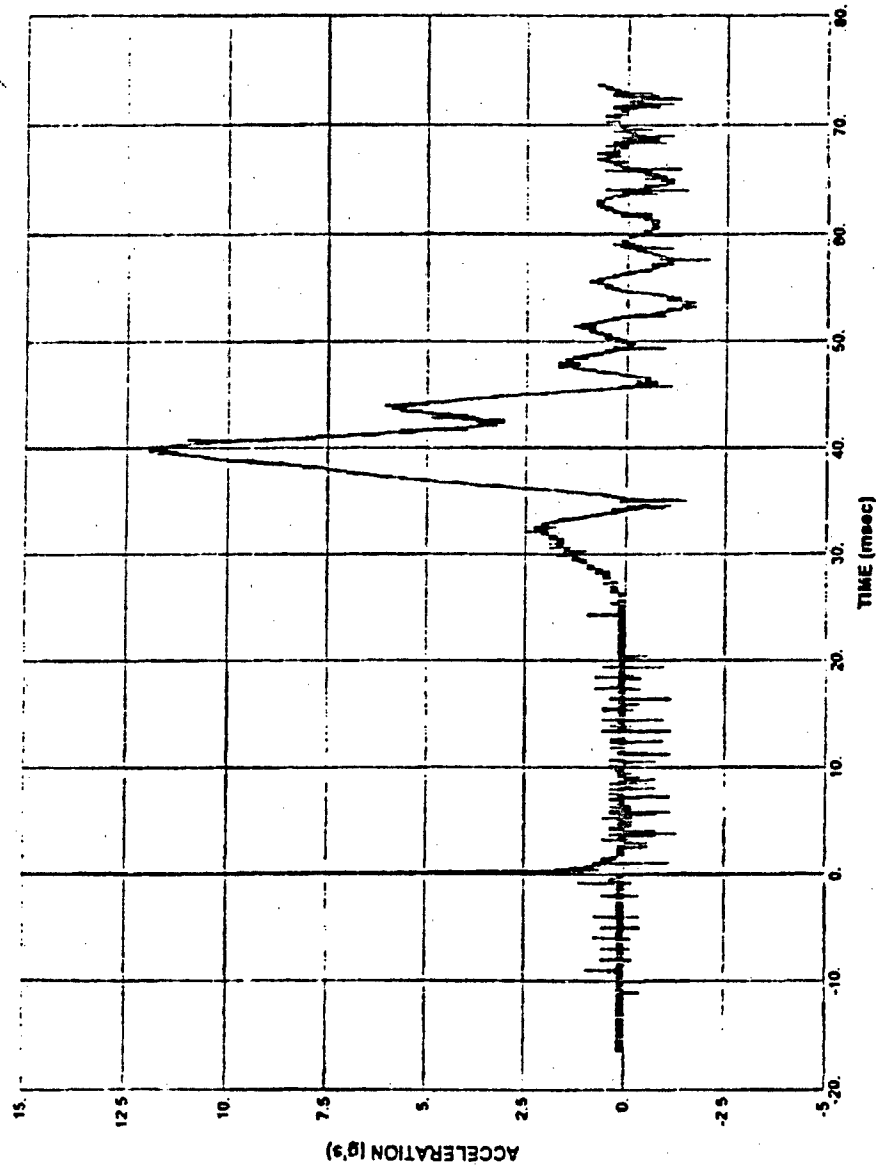


Figure C.64 Accelerometer A6, Test 4

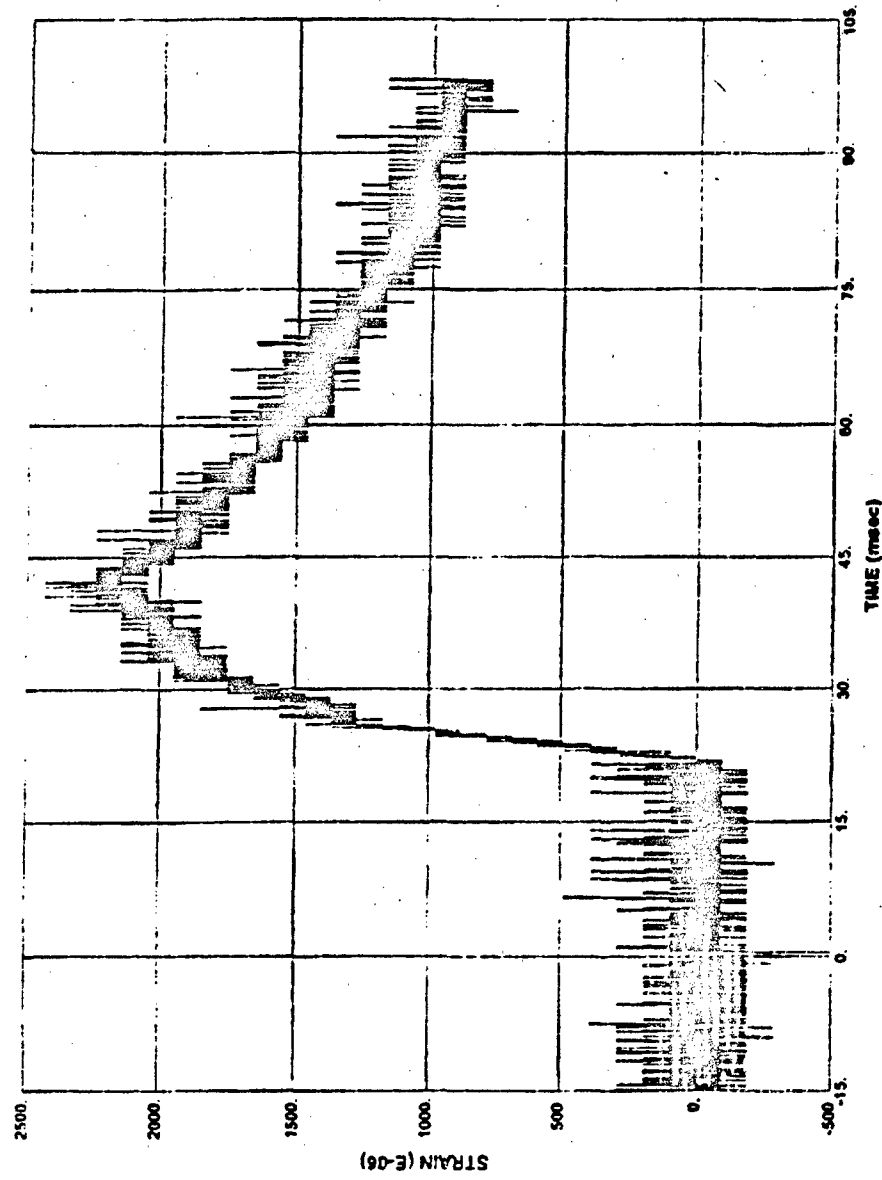


Figure C.65 Strain Gage S1, Test 4

318

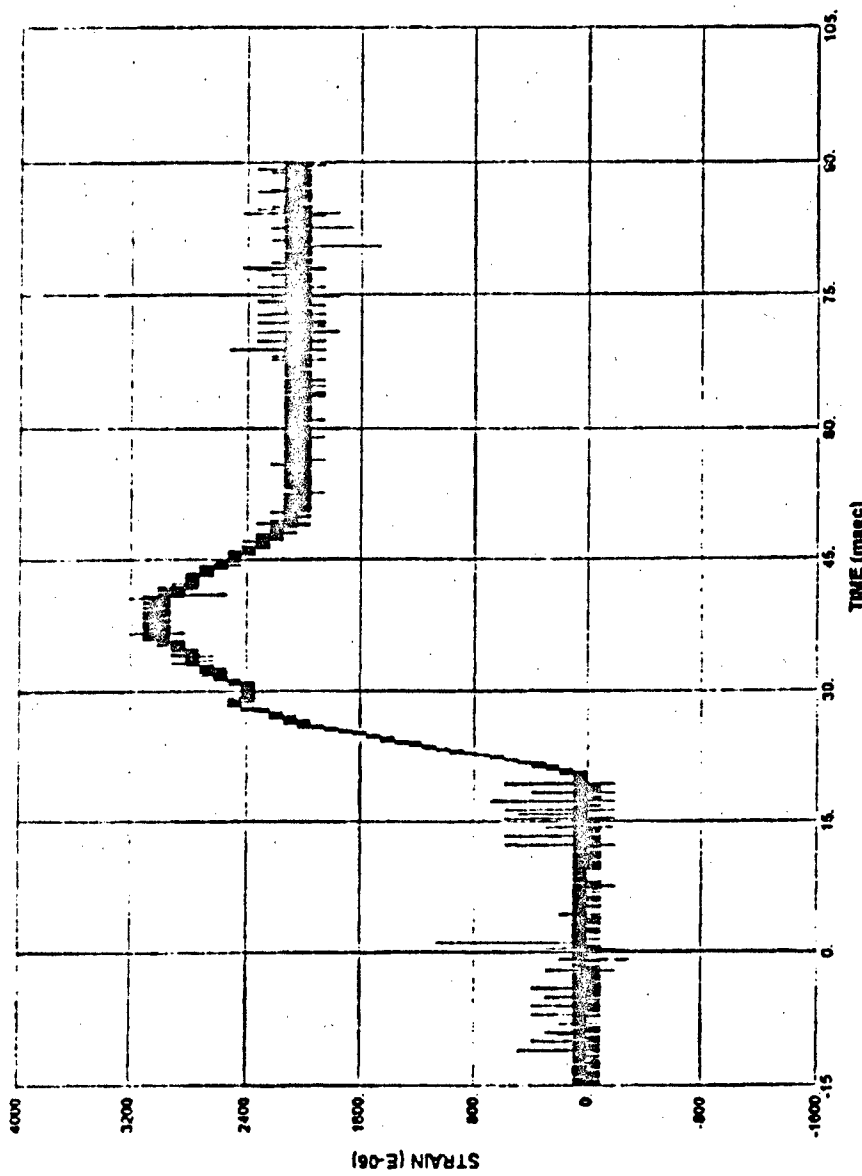


Figure C.66 Strain Gage S2, Test 4

319

ADA293552

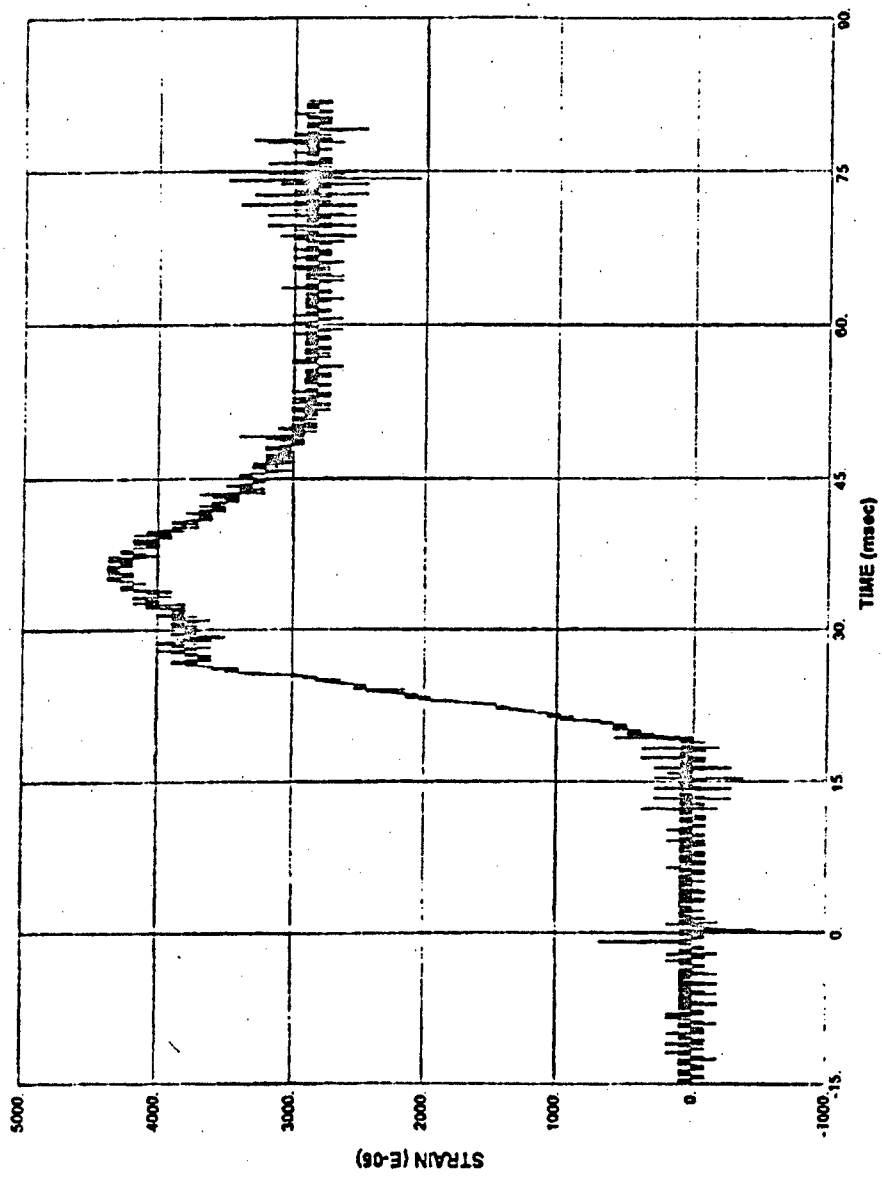


Figure C.67 Strain Gage S3, Test 4

320

ADA293552

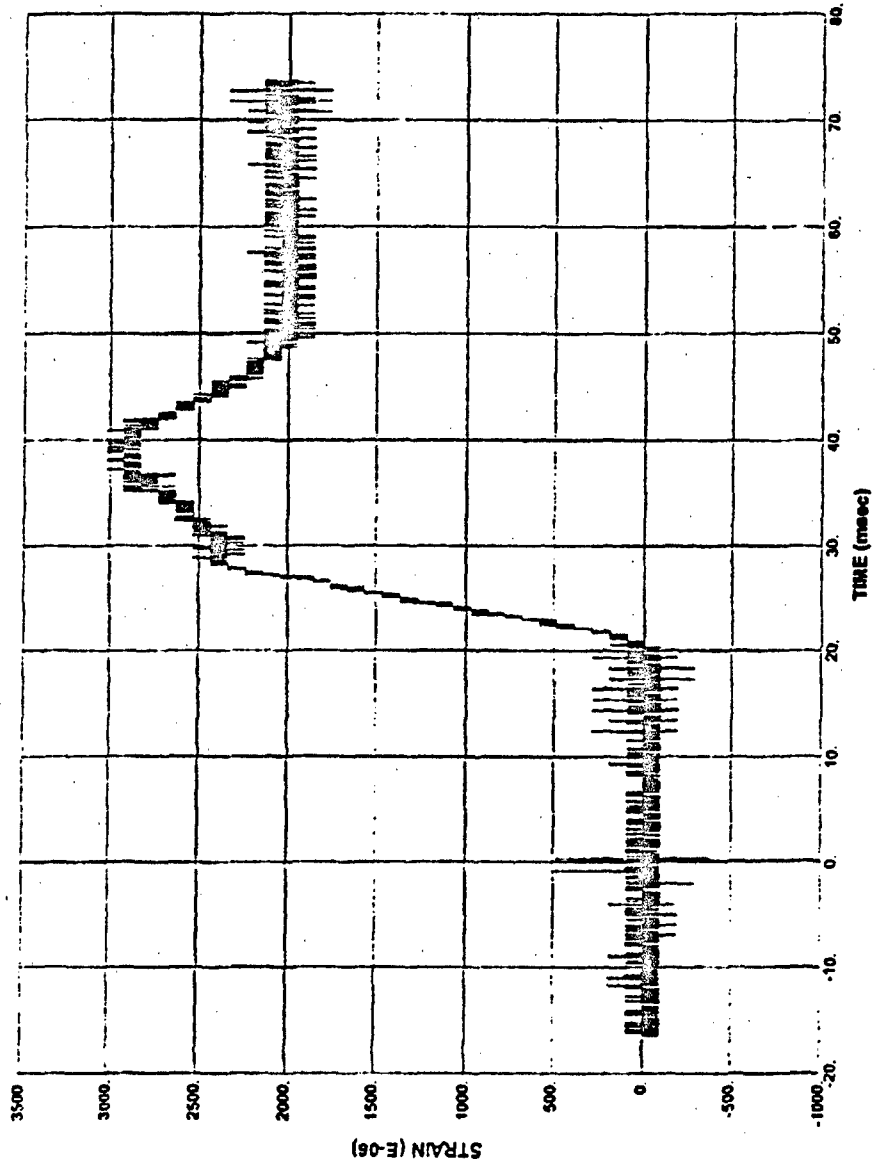


Figure C.68 Strain Gage S4, Test 4

321

ADA293552

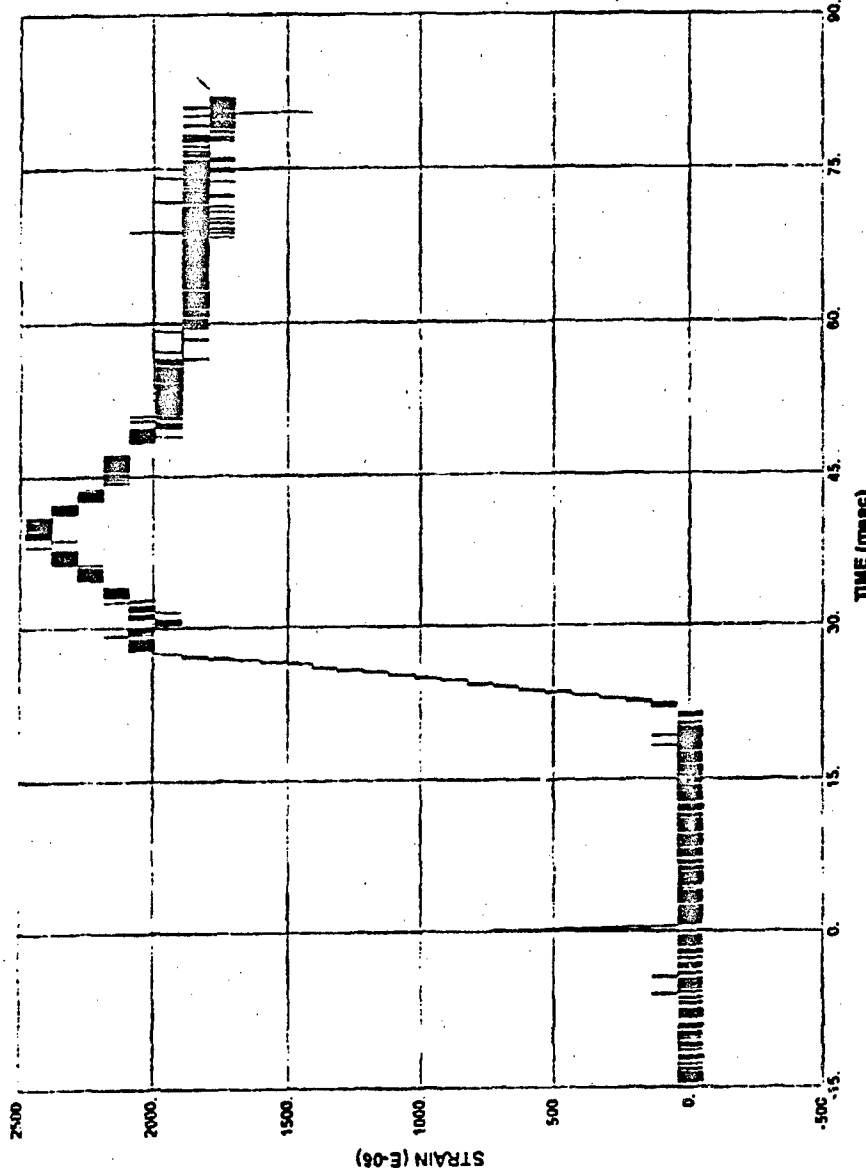


Figure C.69 Strain Gage S5, Test 4

322

ADA293552

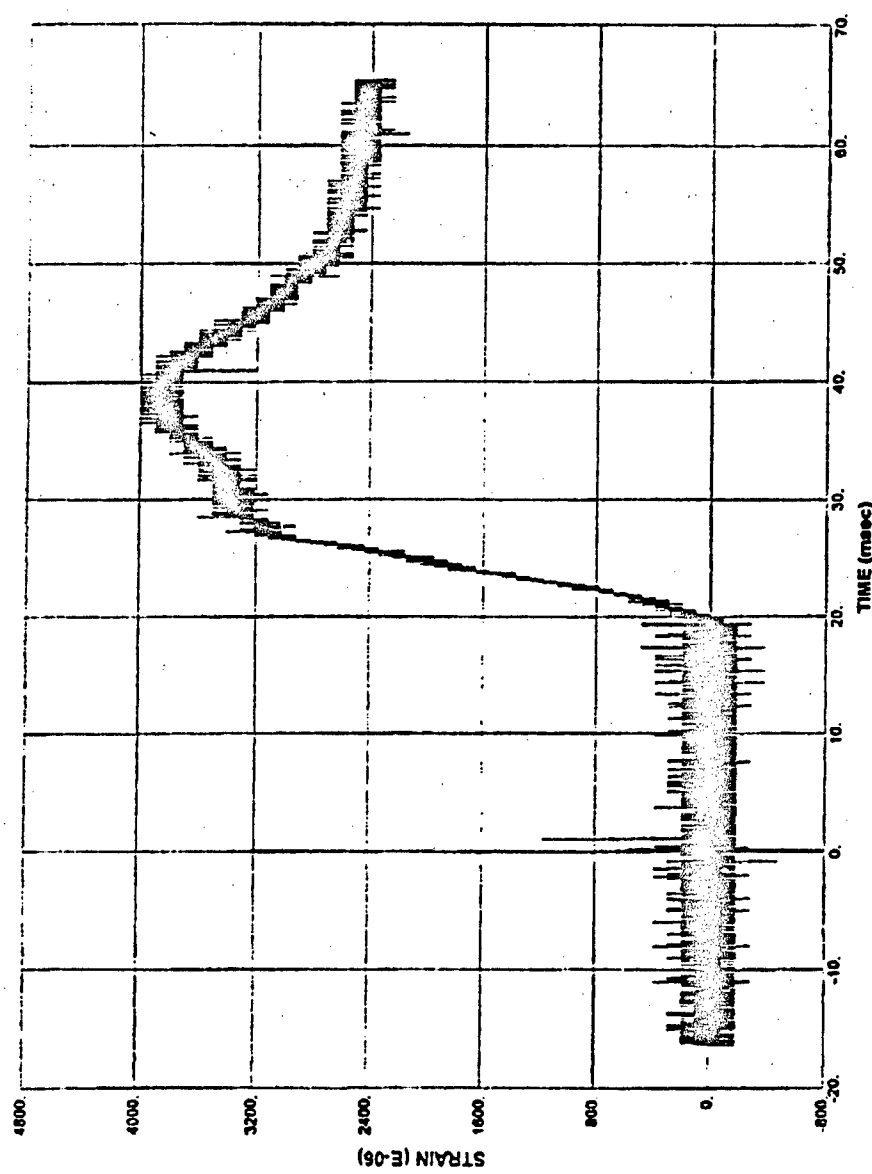


Figure C.70 Strain Gage S6, Test 4

323

ADA293552

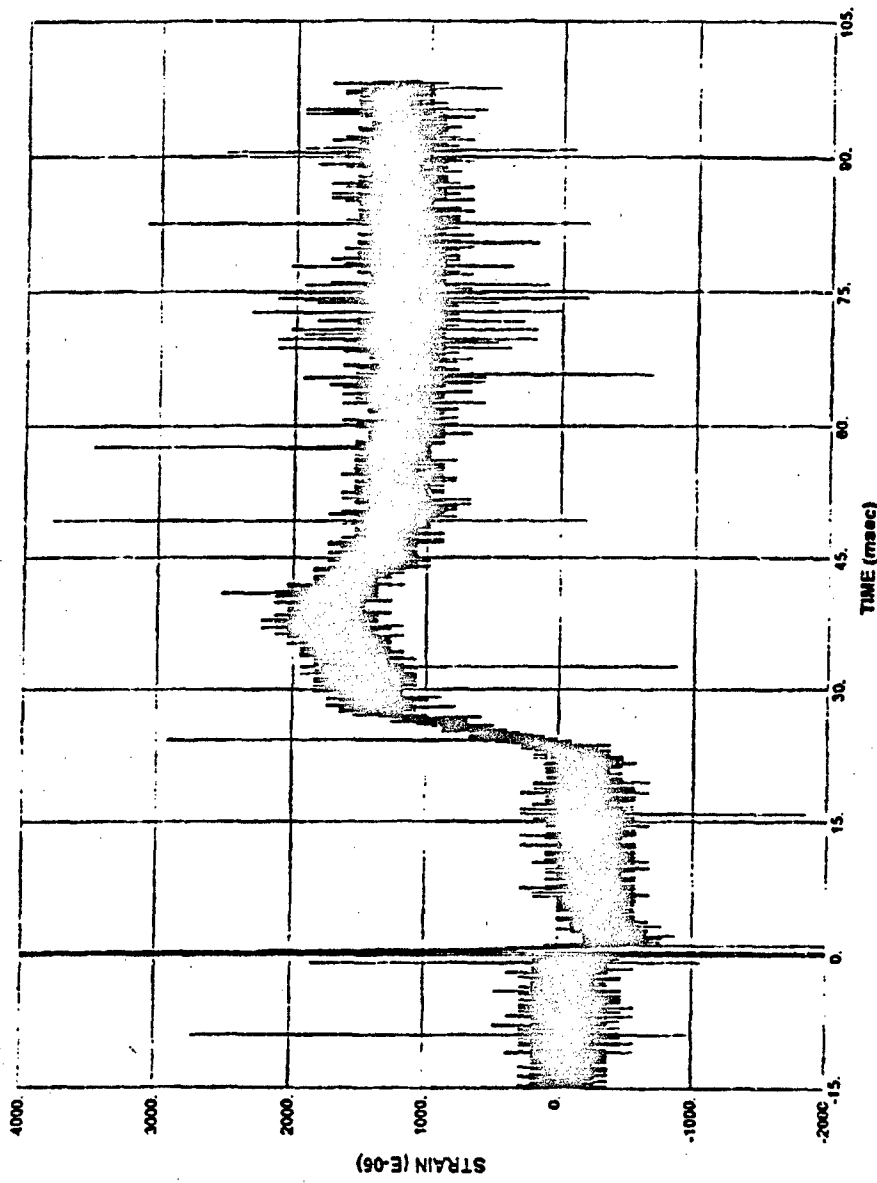


Figure C.71 Strain Gage S7, Test 4

324

ADA293552

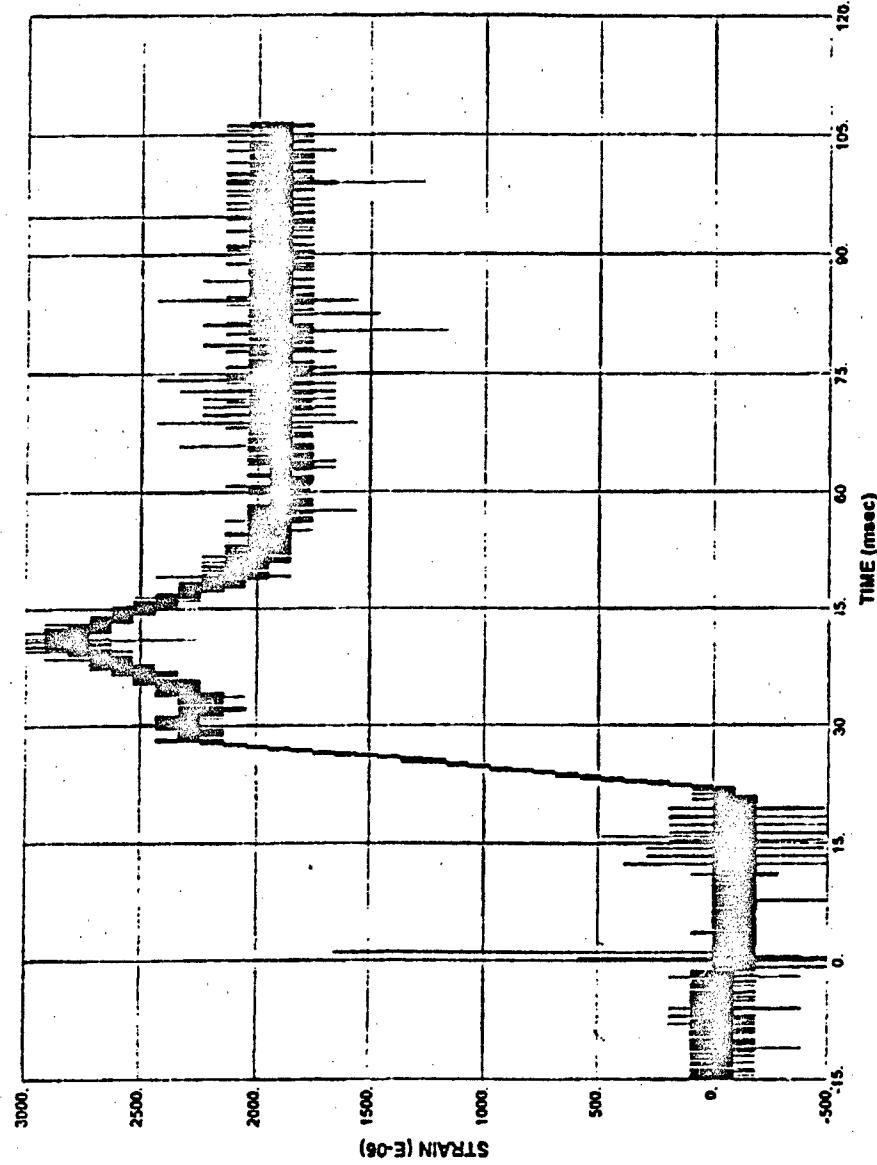


Figure C.72 Strain Gage S8, Test 4

325

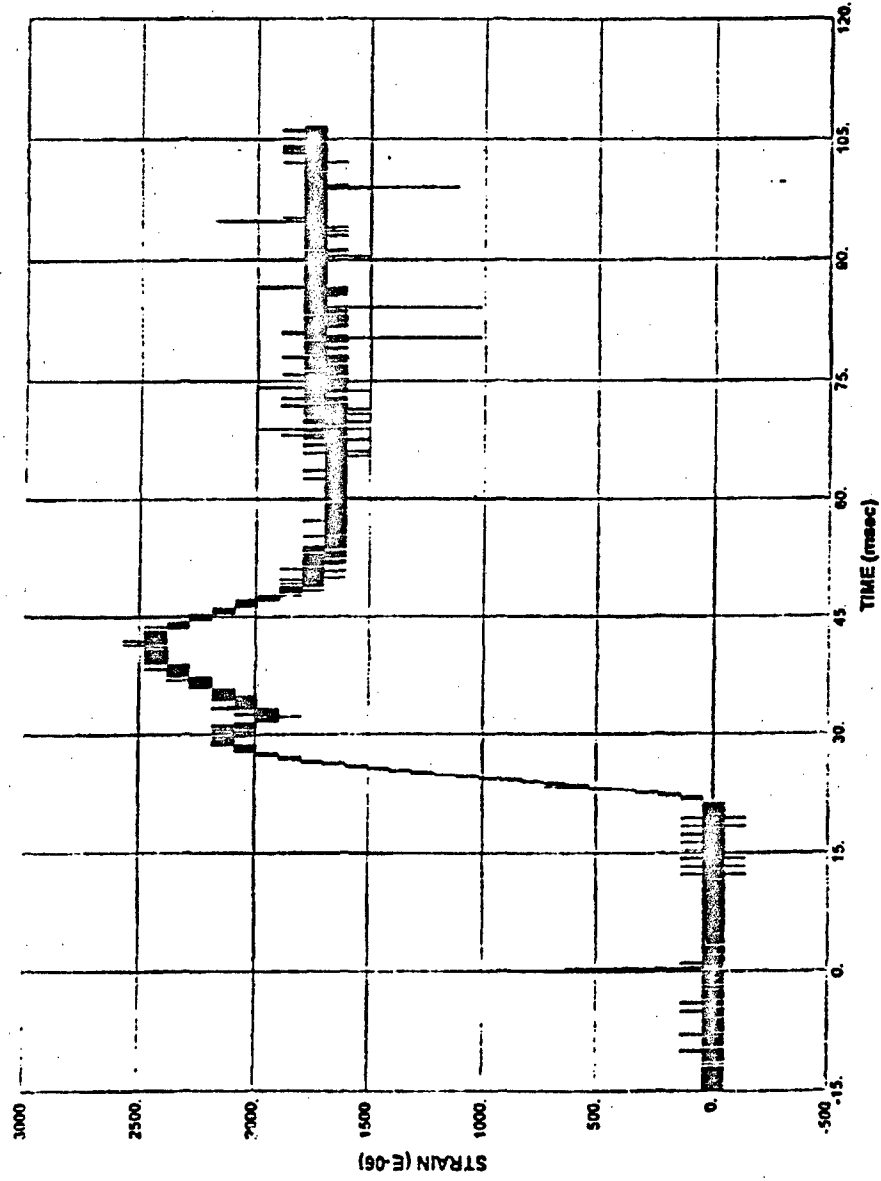


Figure C.73 Strain Gage SII, Test 4

326

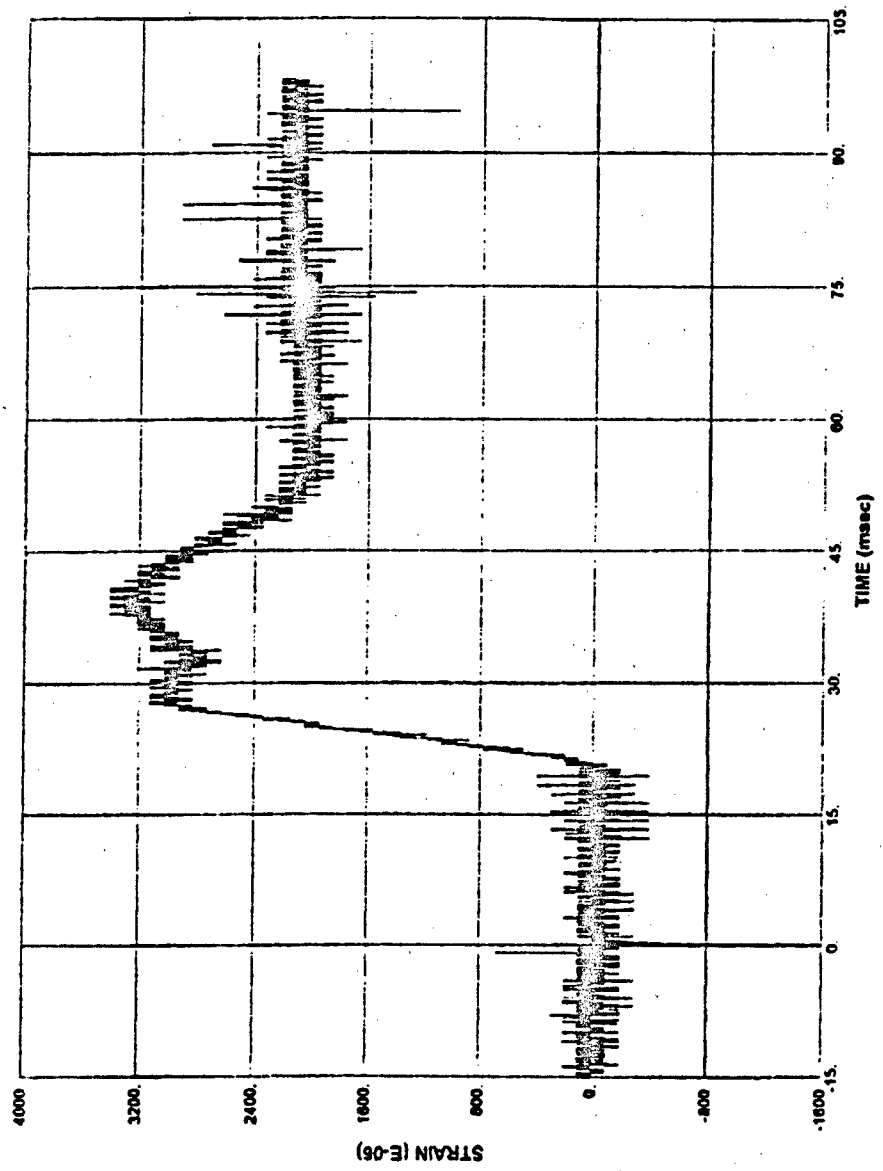


Figure C.74 Strain Gage SI2, Test 4

327

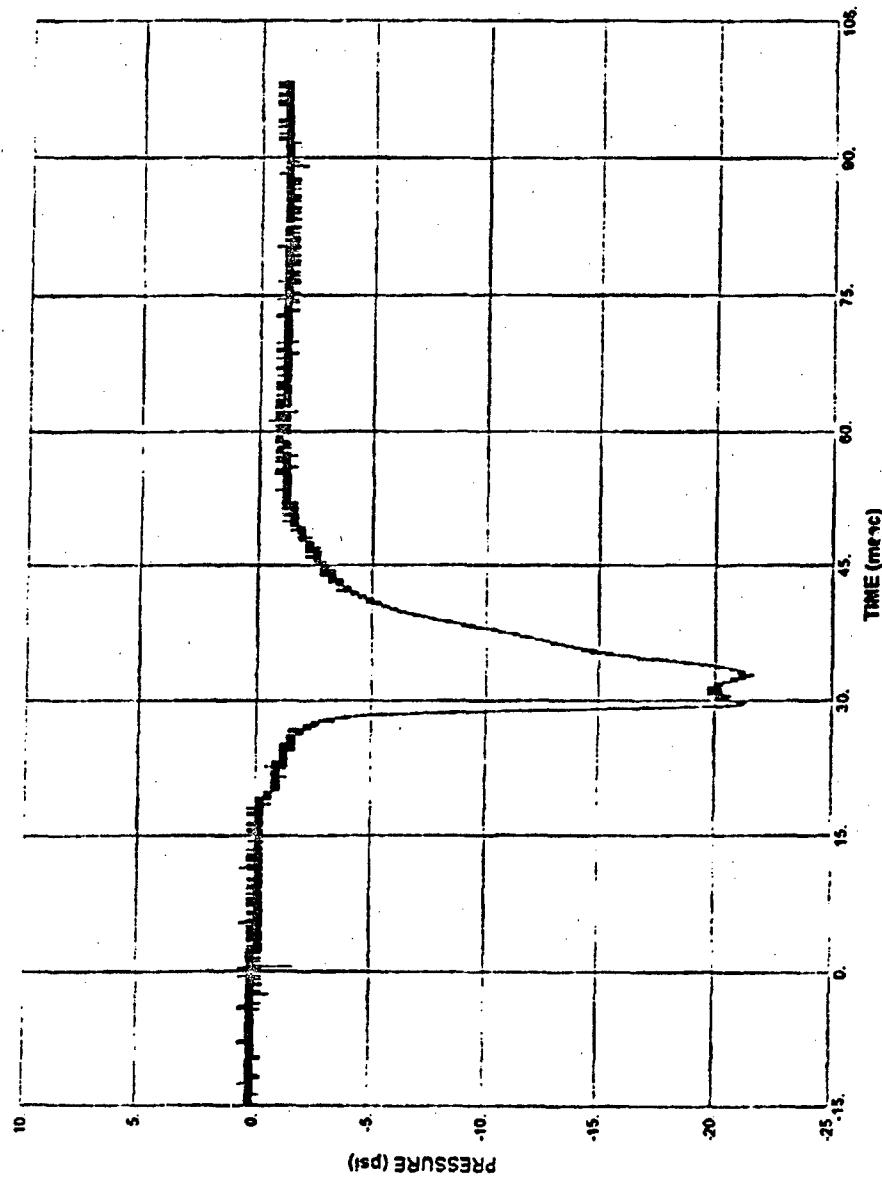


Figure C.75 Free-Field Pressure Gage F1, Test 5

328

ADA293552

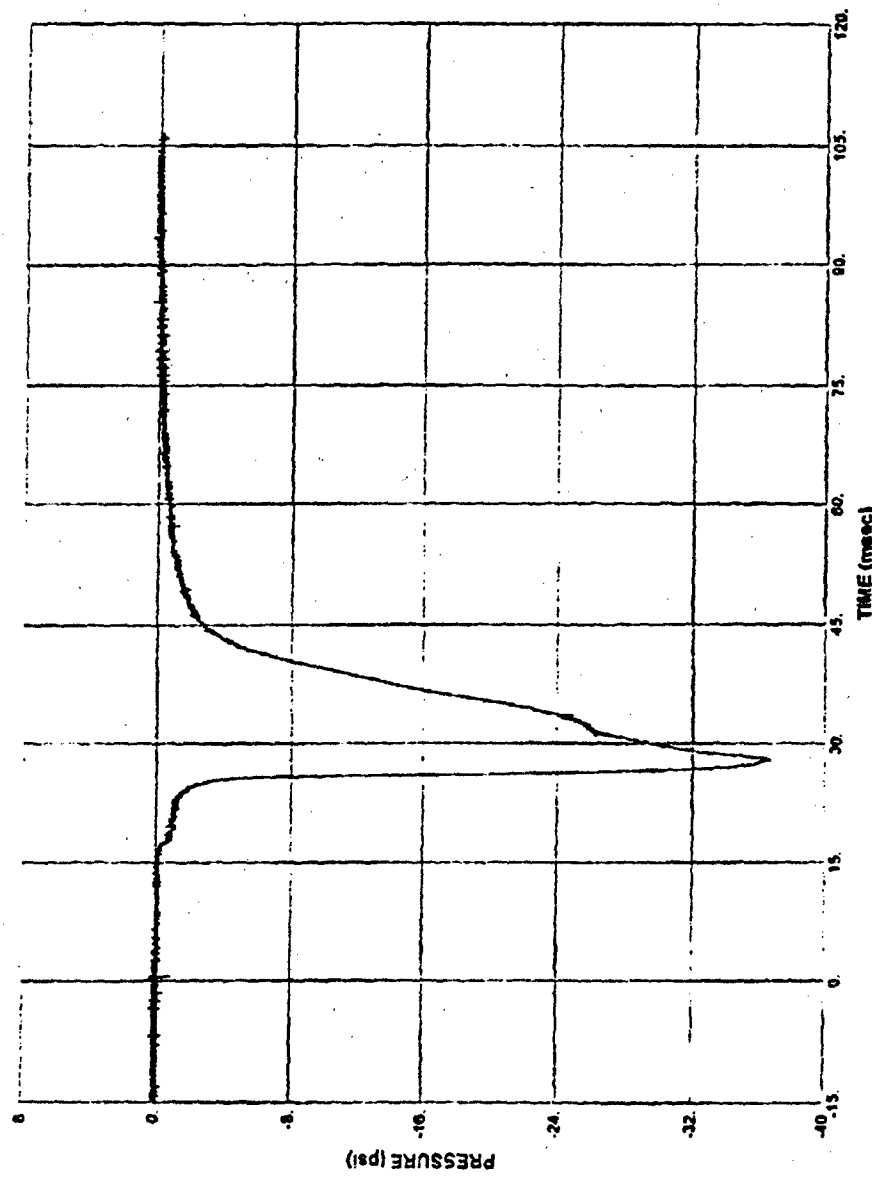


Figure C.76 Free-Field Pressure Gage F2, Test 5

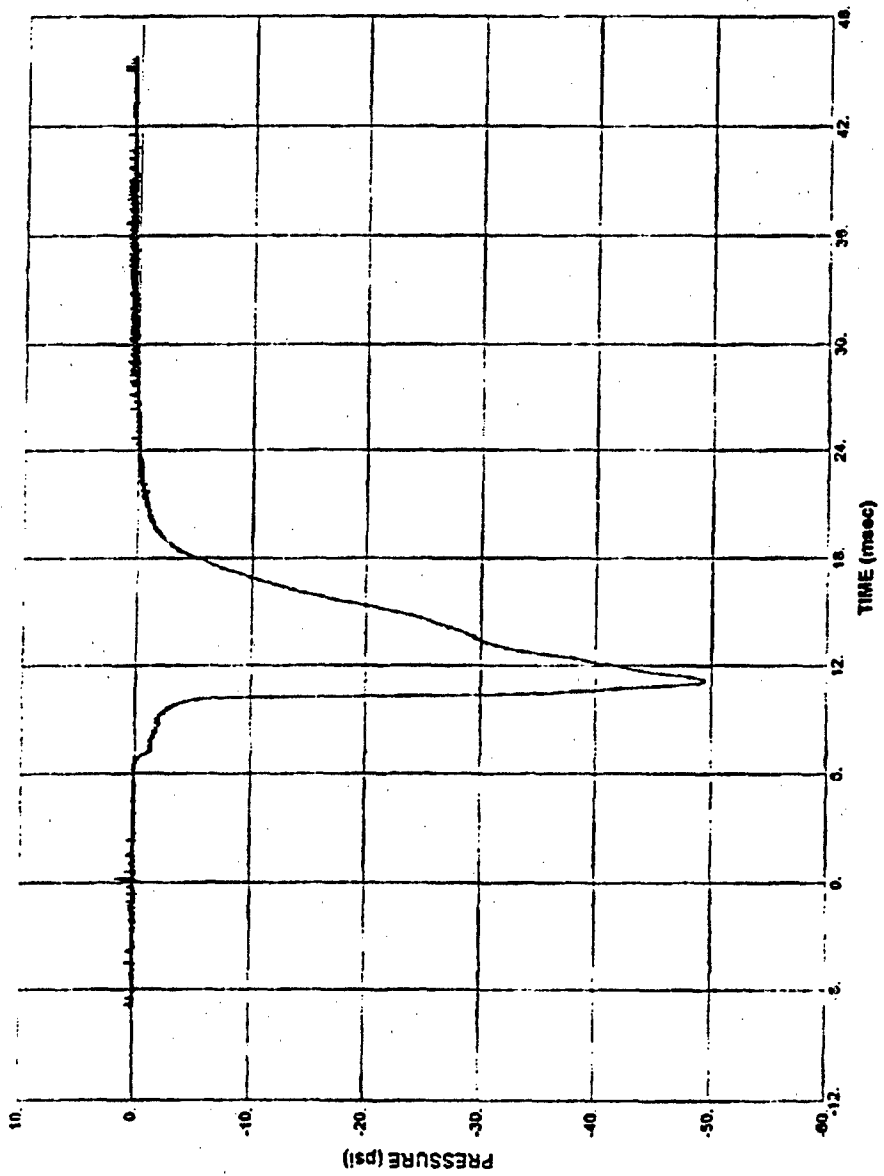


Figure C.77 Free-Field Pressure Gage F3, Test 5

330

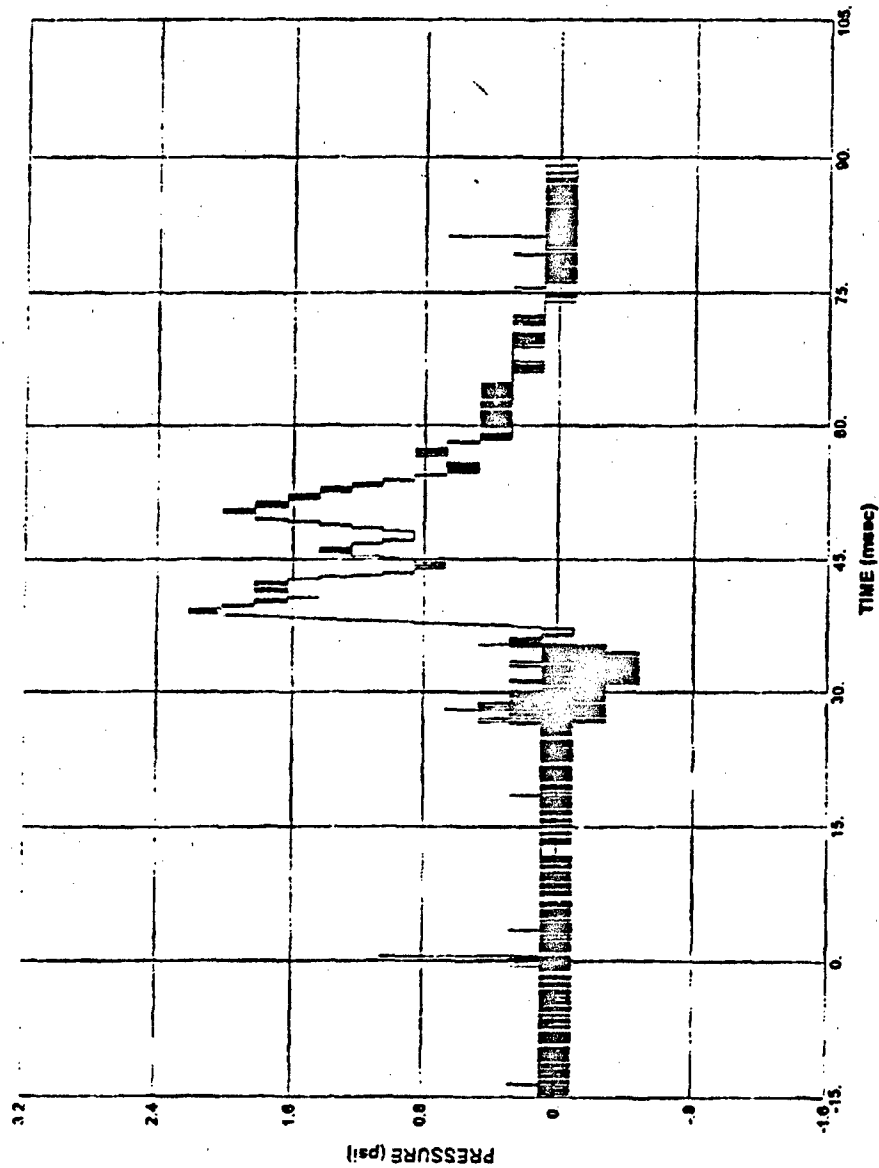


Figure C.78 Soil Pressure Interface Gage P1, Test 5

331

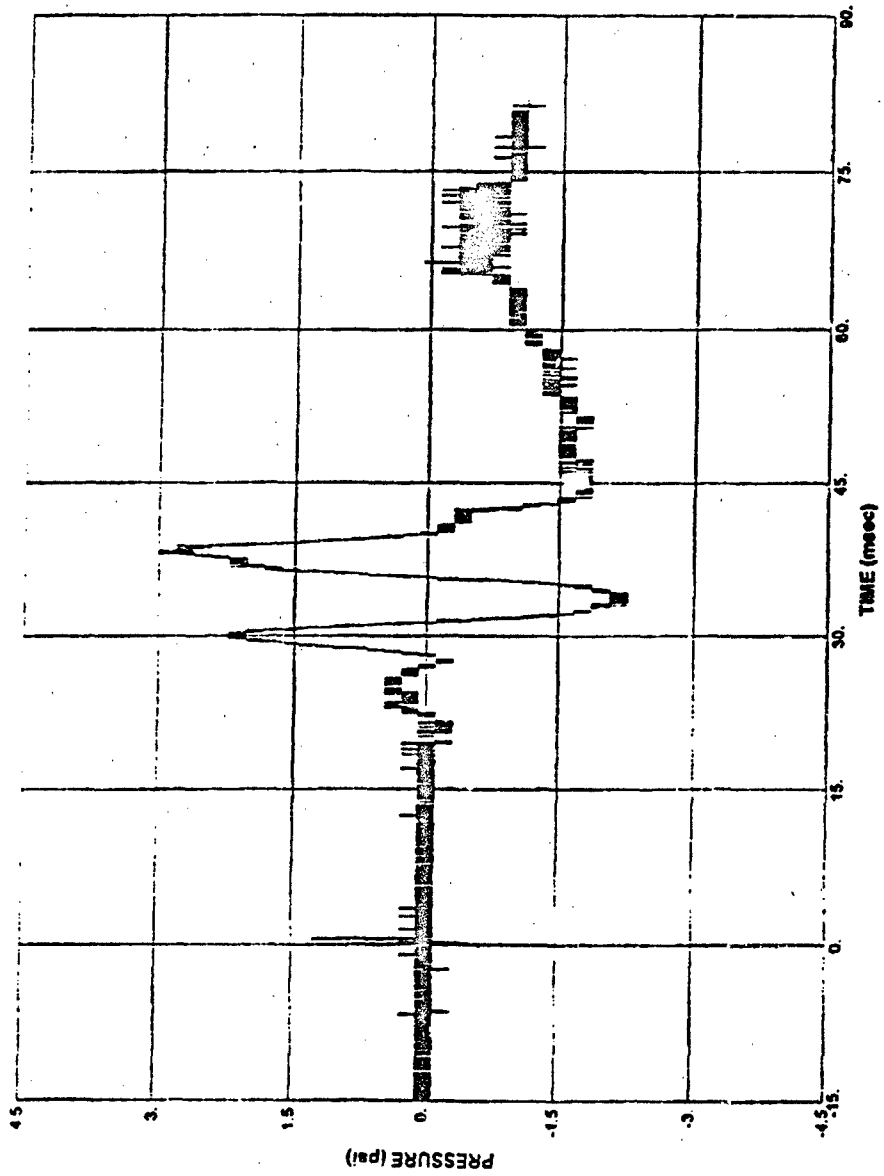


Figure C.79 Soil Pressure Interface Gage P2, Test 5

332

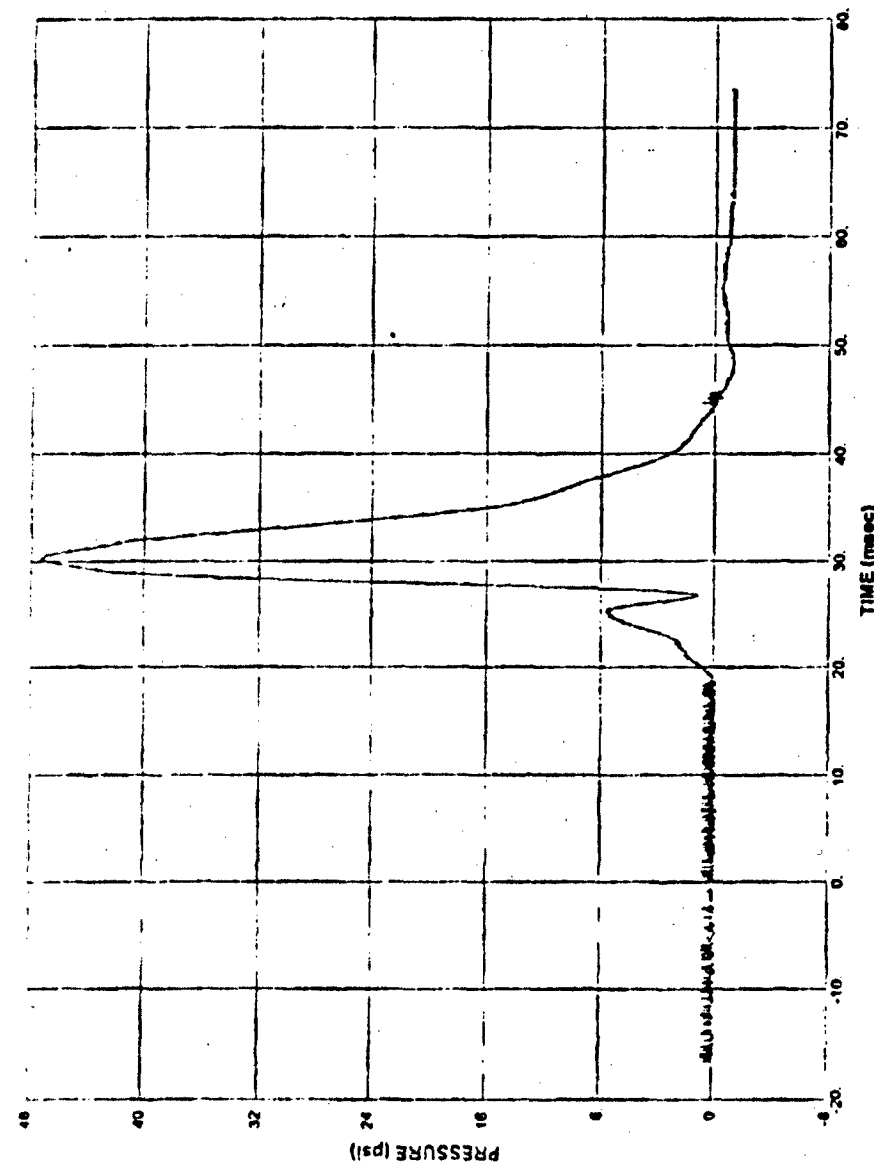


Figure C.80 Soil Pressure Interface Gage P3, Test 5

333

ADA293552

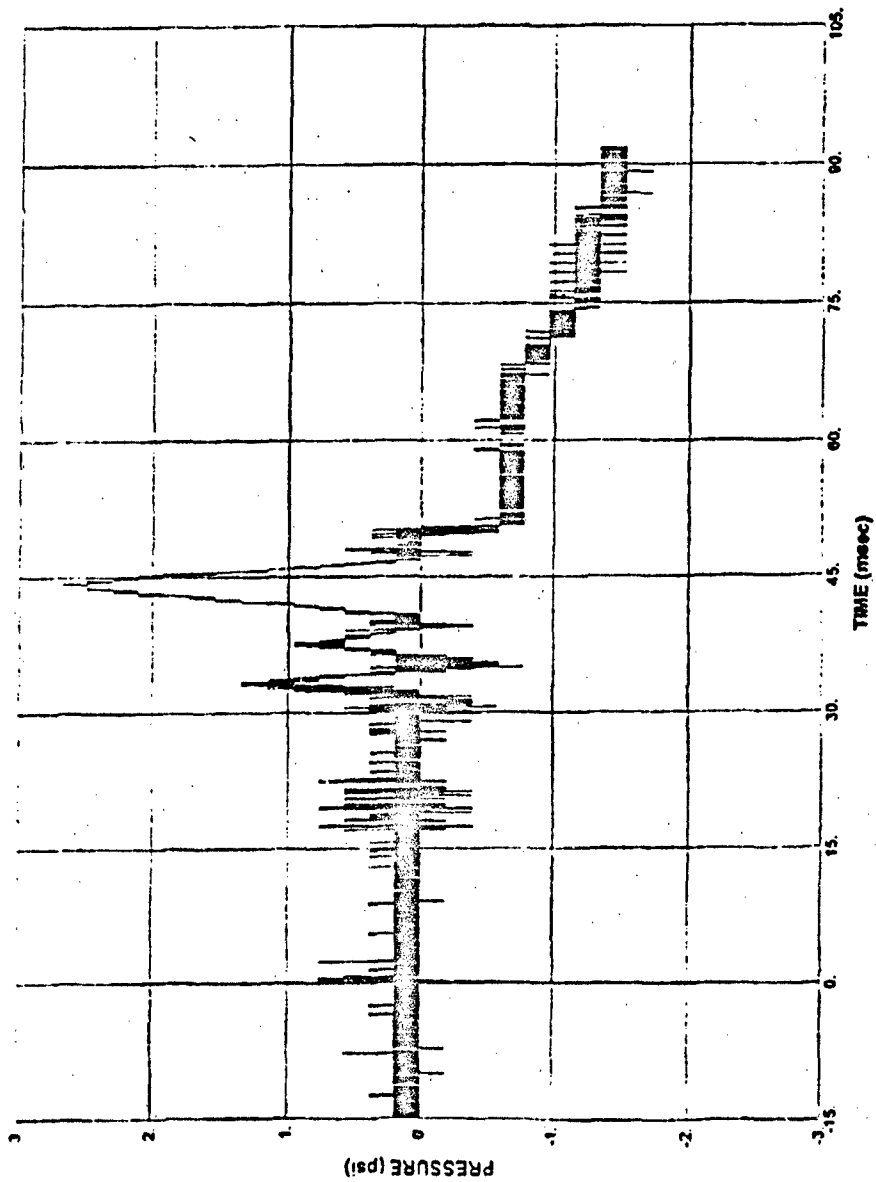


Figure C.81 Soil Pressure Interface Gage P4, Test 5

334

ADA293552

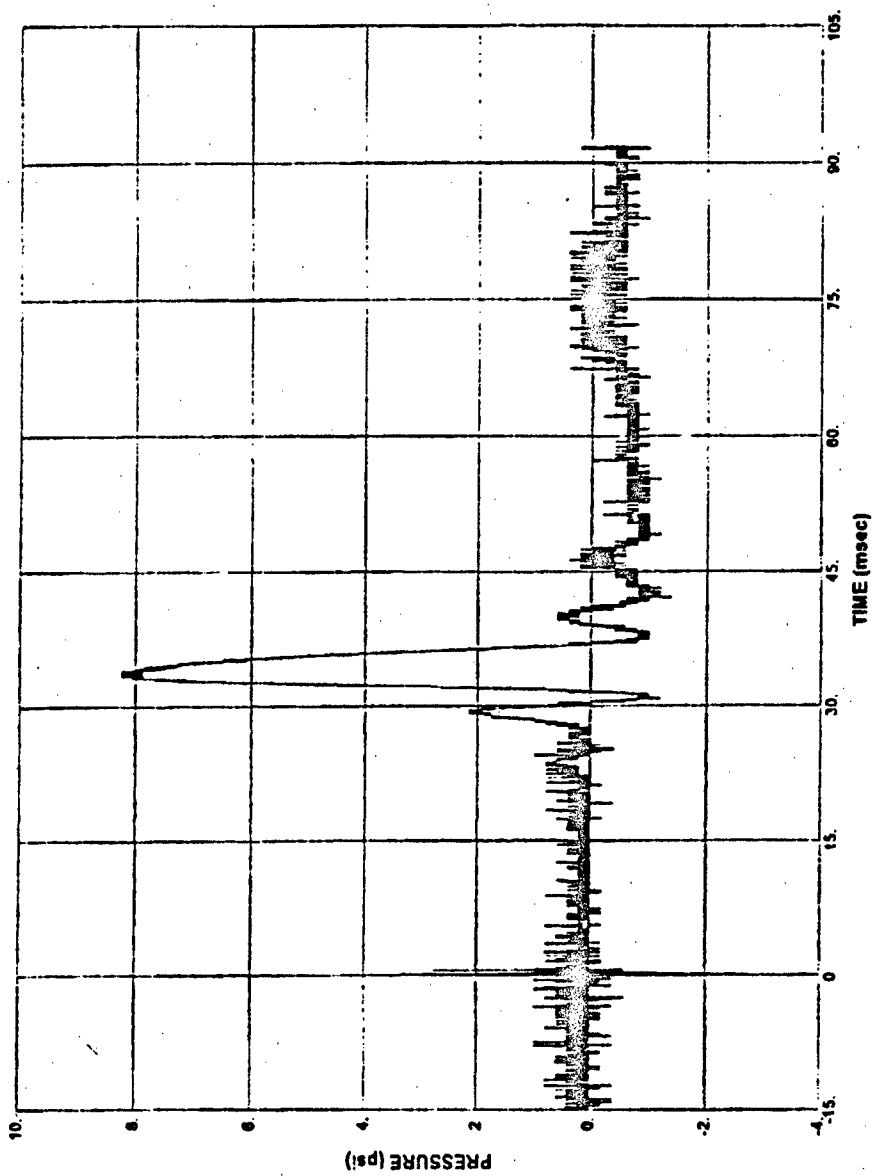


Figure C.82 Soil Pressure Interface Gage P5, Test 5

335

ADA293552

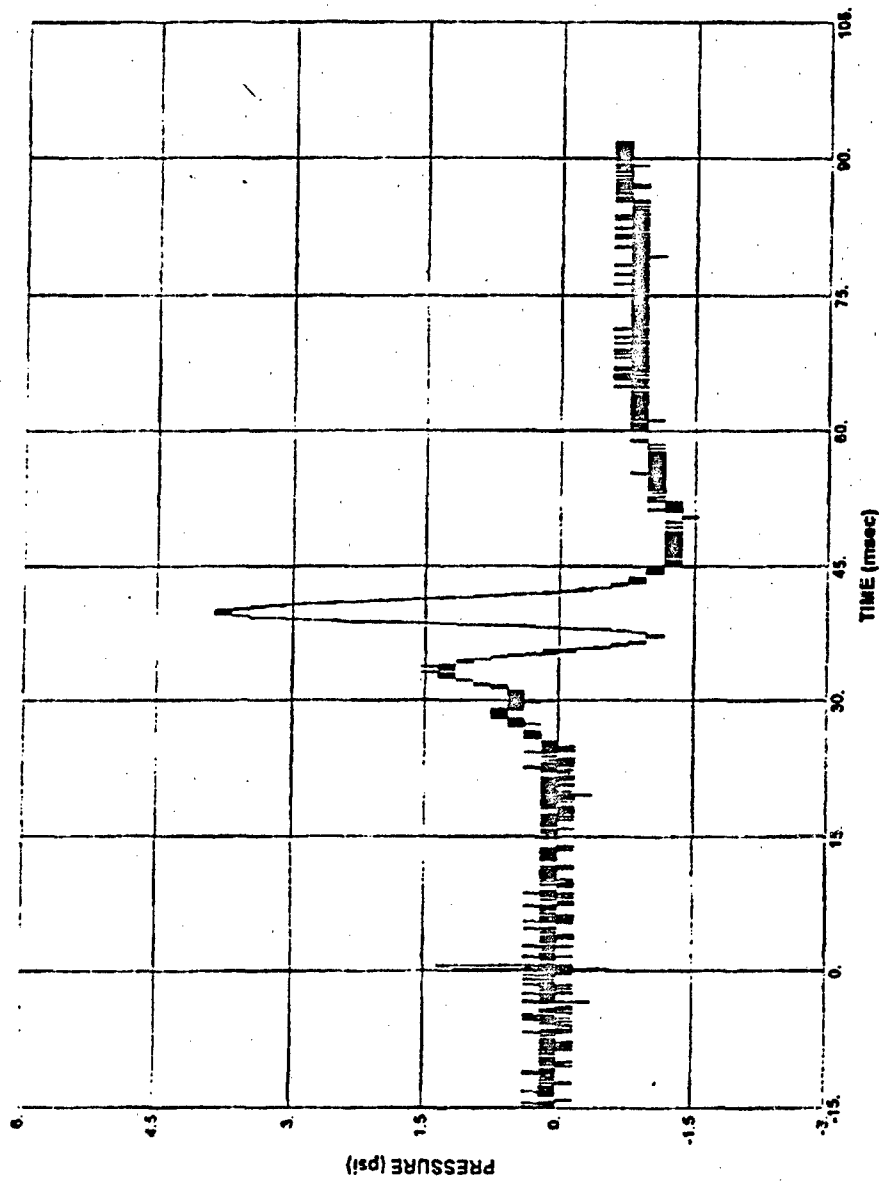


Figure C.83 Soil Pressure Interface Gage P6, Test 5

336

ADA293552

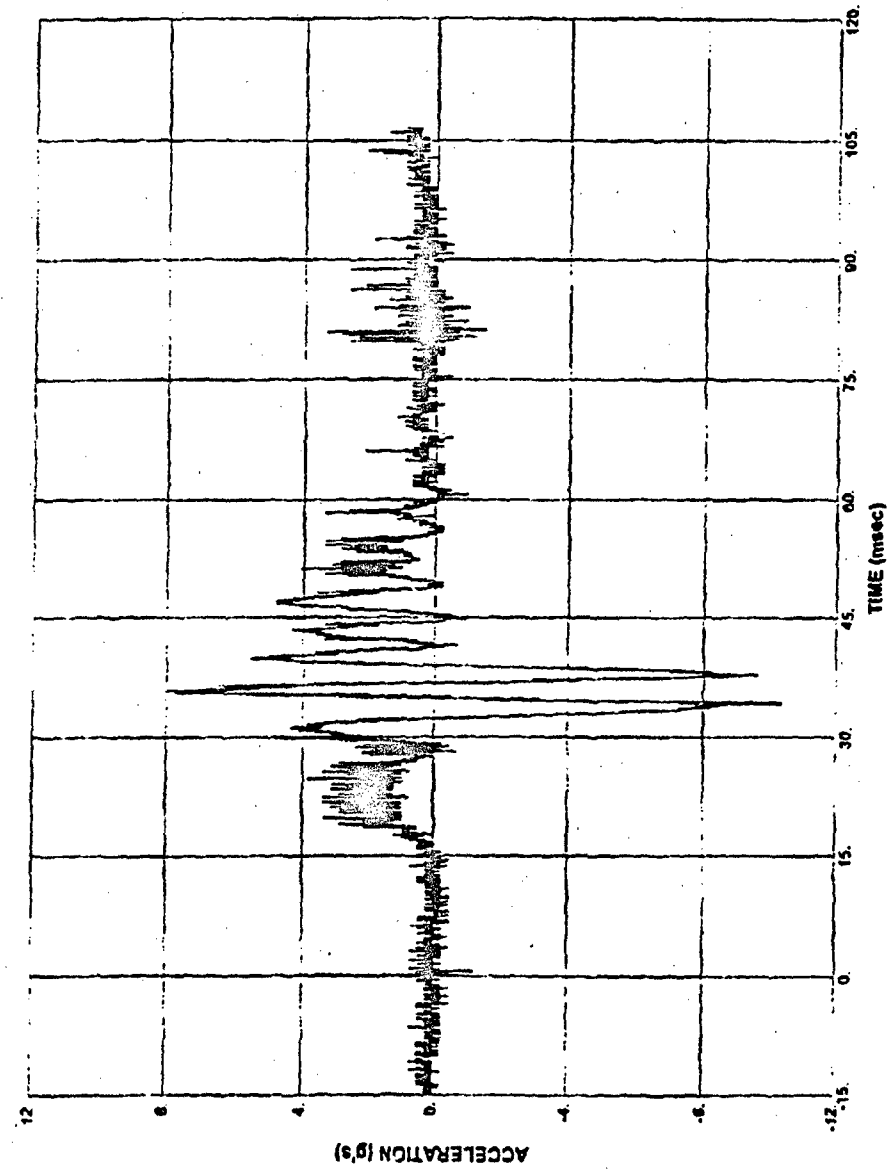


Figure C.84 Accelerometer A1, Test 5

337

ADA293552

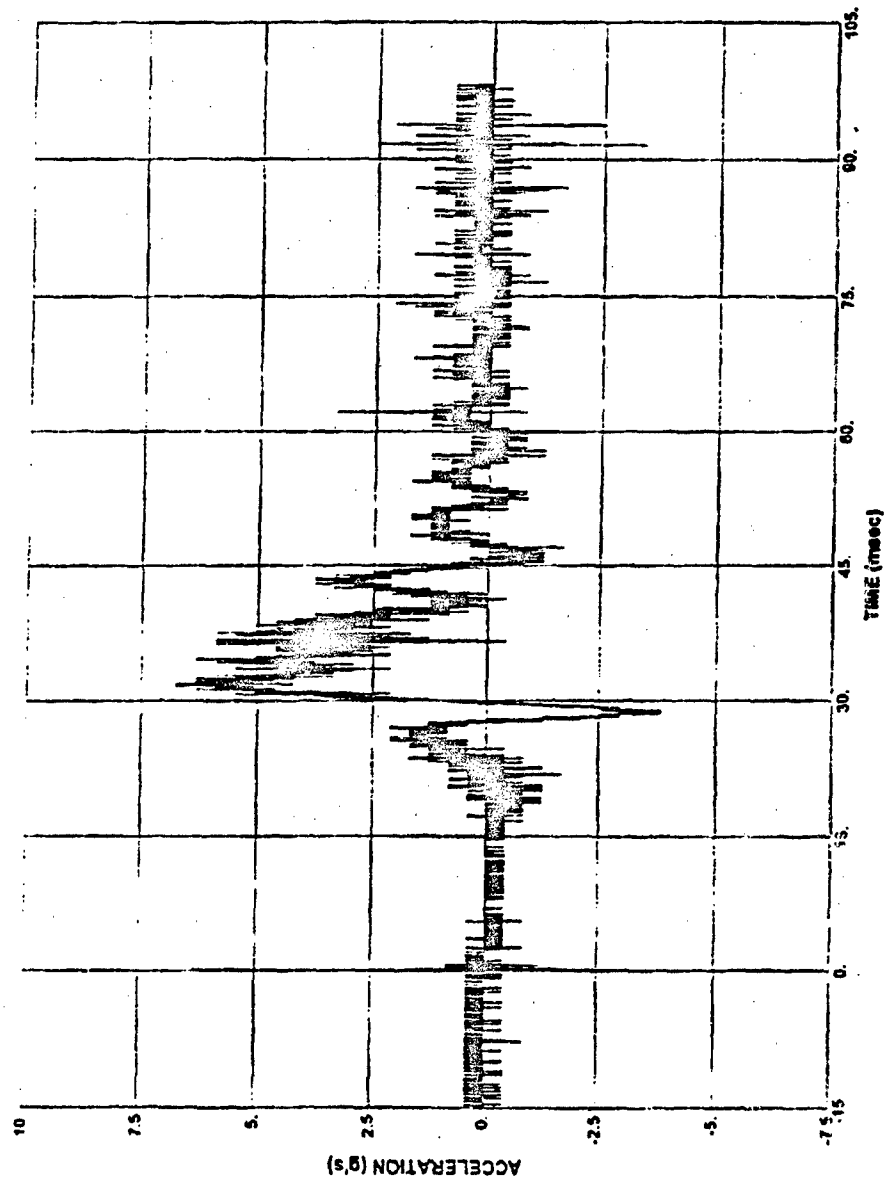


Figure C.85 Accelerometer A2, Test 5

338

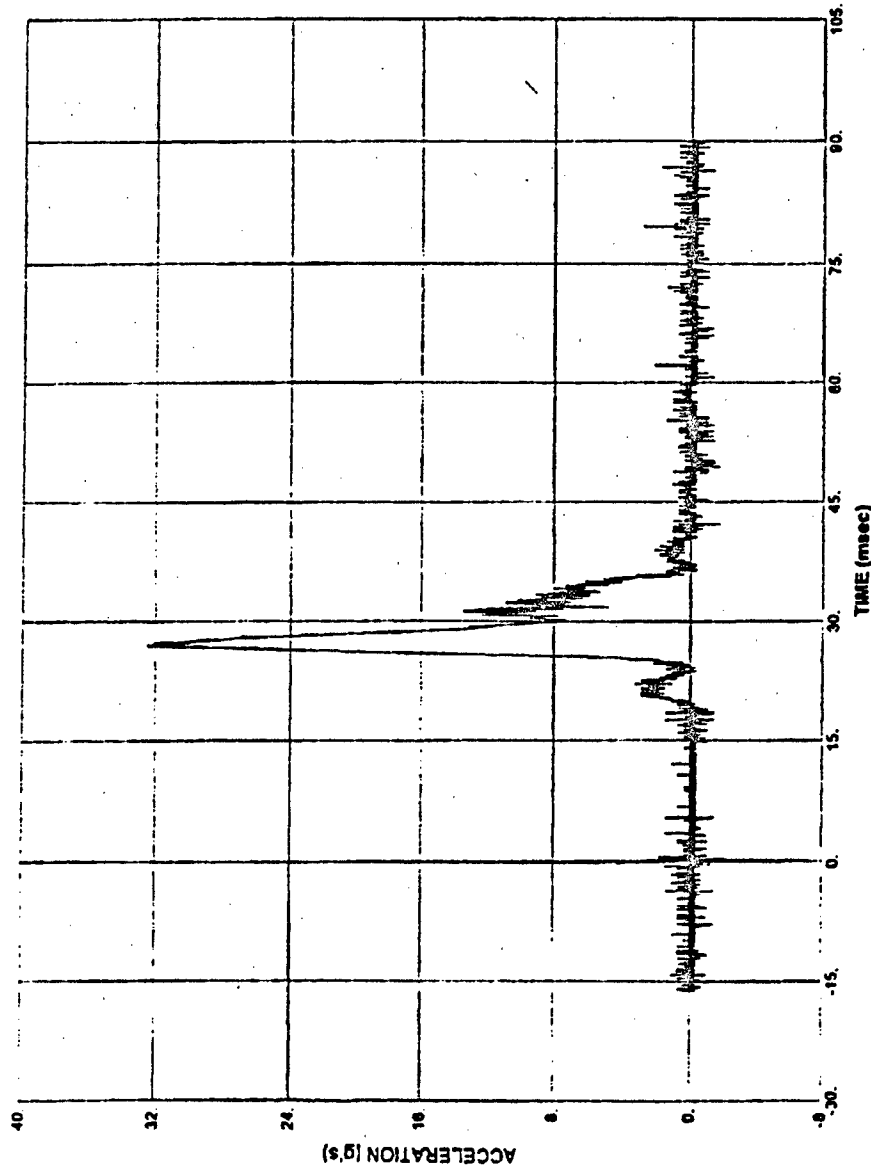


Figure C.86 Accelerometer A3, Test 5

339

ADA293552

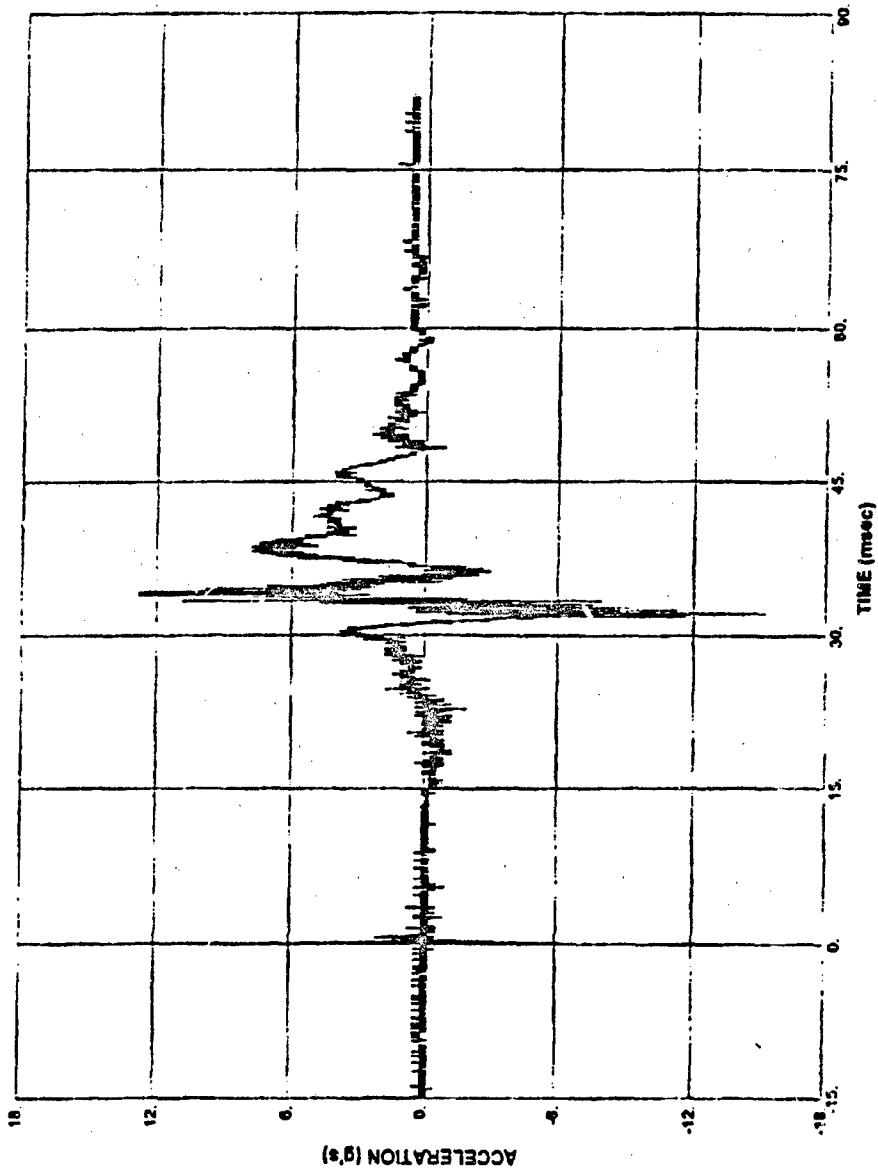


Figure C.87 Accelerometer A4, Test 5

340

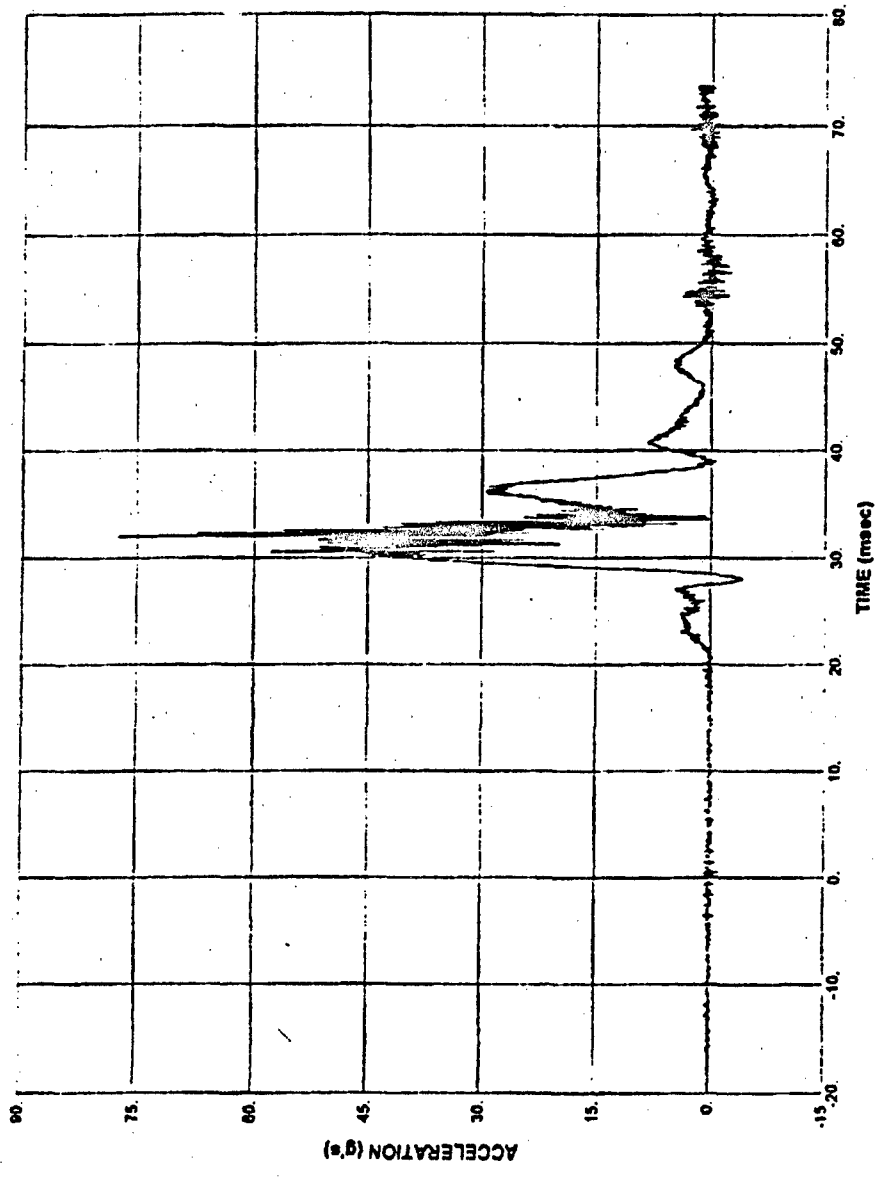


Figure C.88 Accelerometer A5, Test 5

341

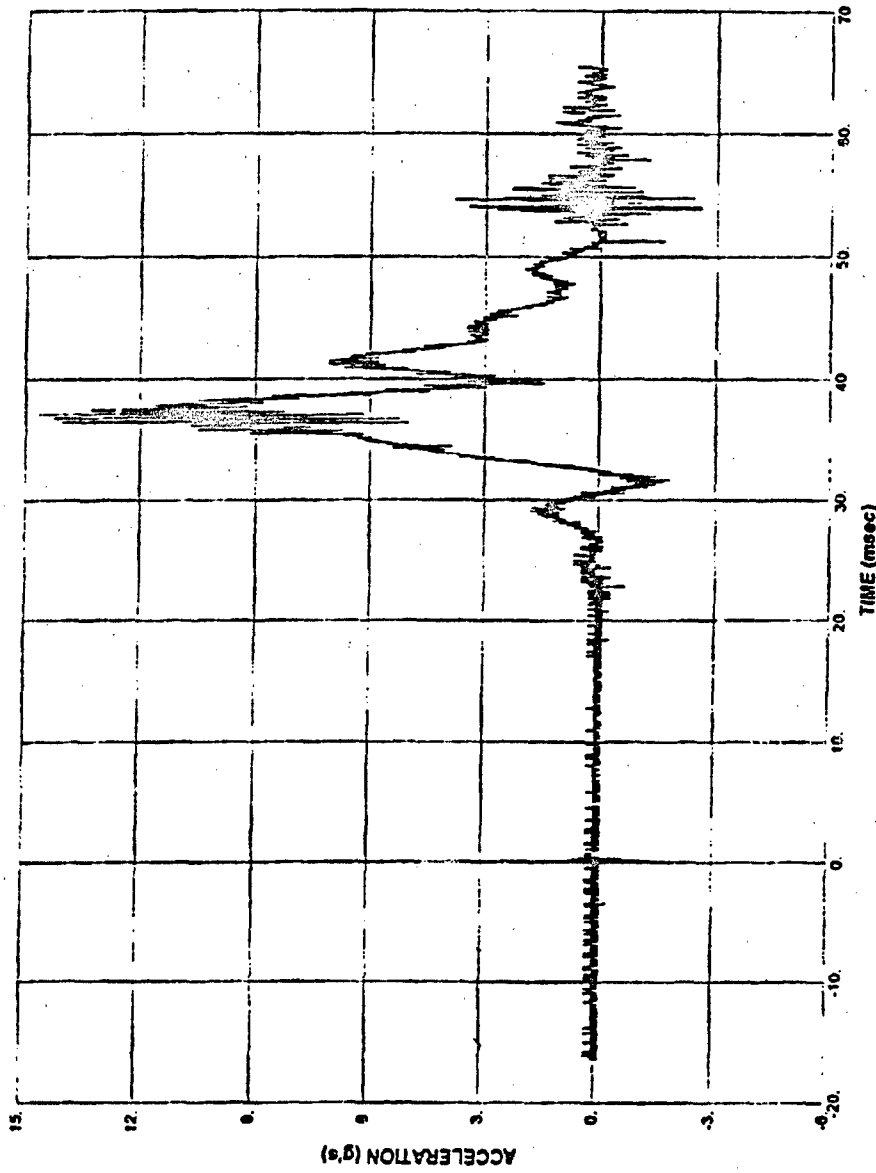


Figure C.89 Accelerometer A6, Test 5

342

ADA293552

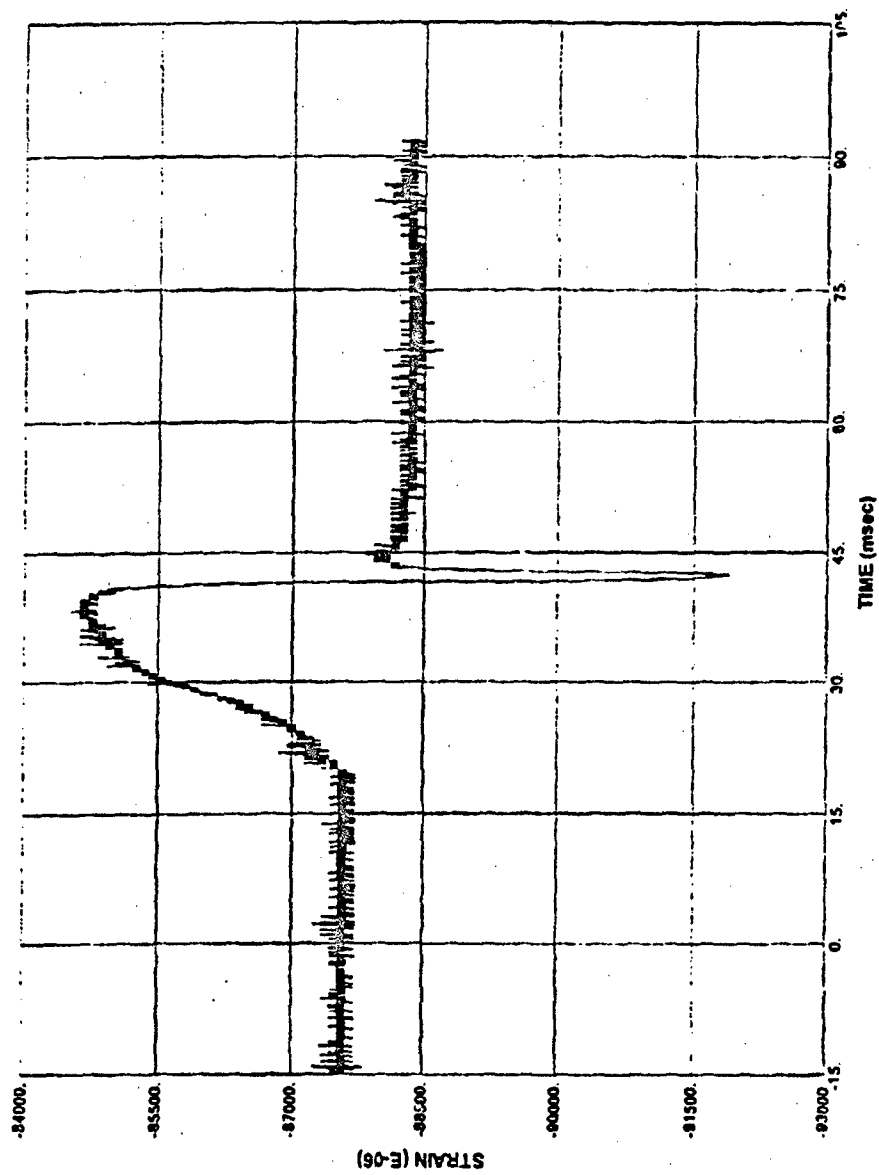


Figure C.90 Strain Gage S1, Test 5

343

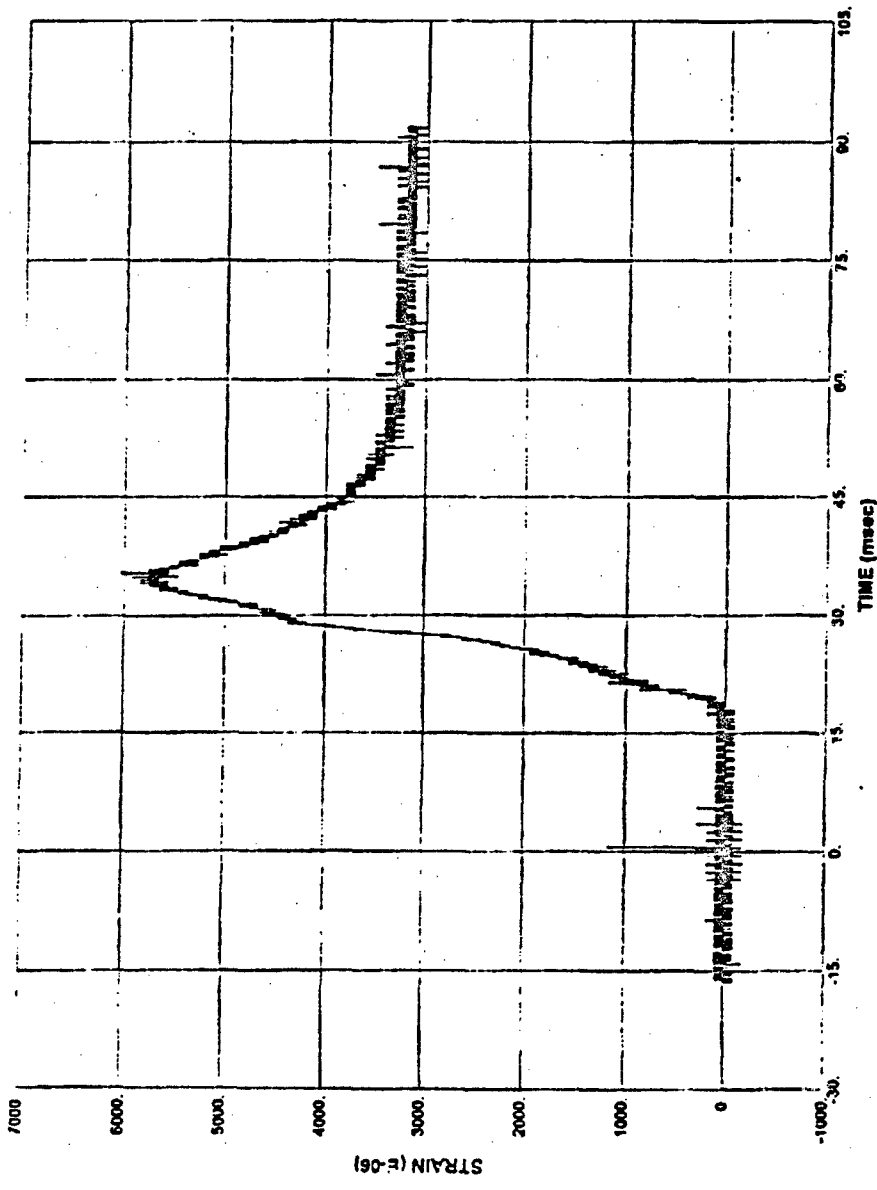


Figure C.91 Strain Gage S2, Test 5

344

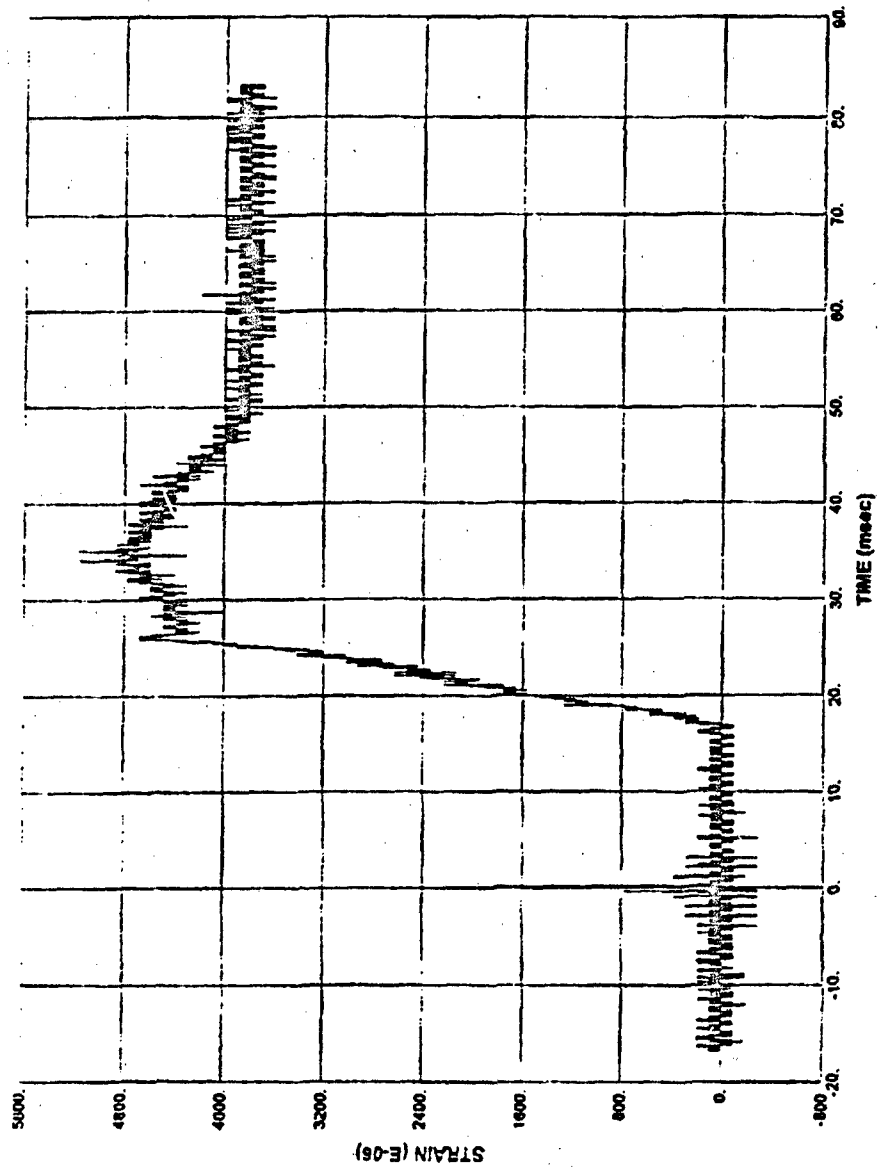


Figure C.92 Strain Gage S3, Test 5

345

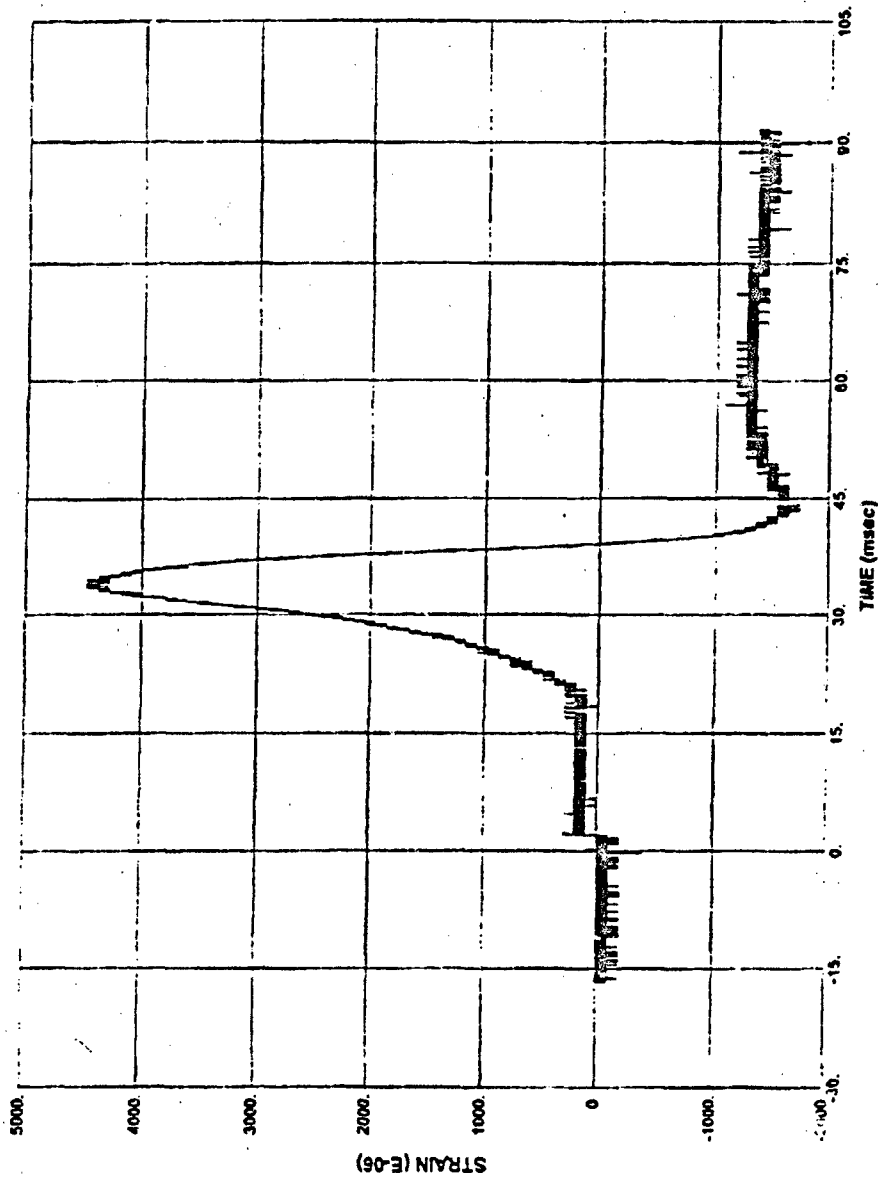


Figure C.93 Strain Gage S4, Test 5

346

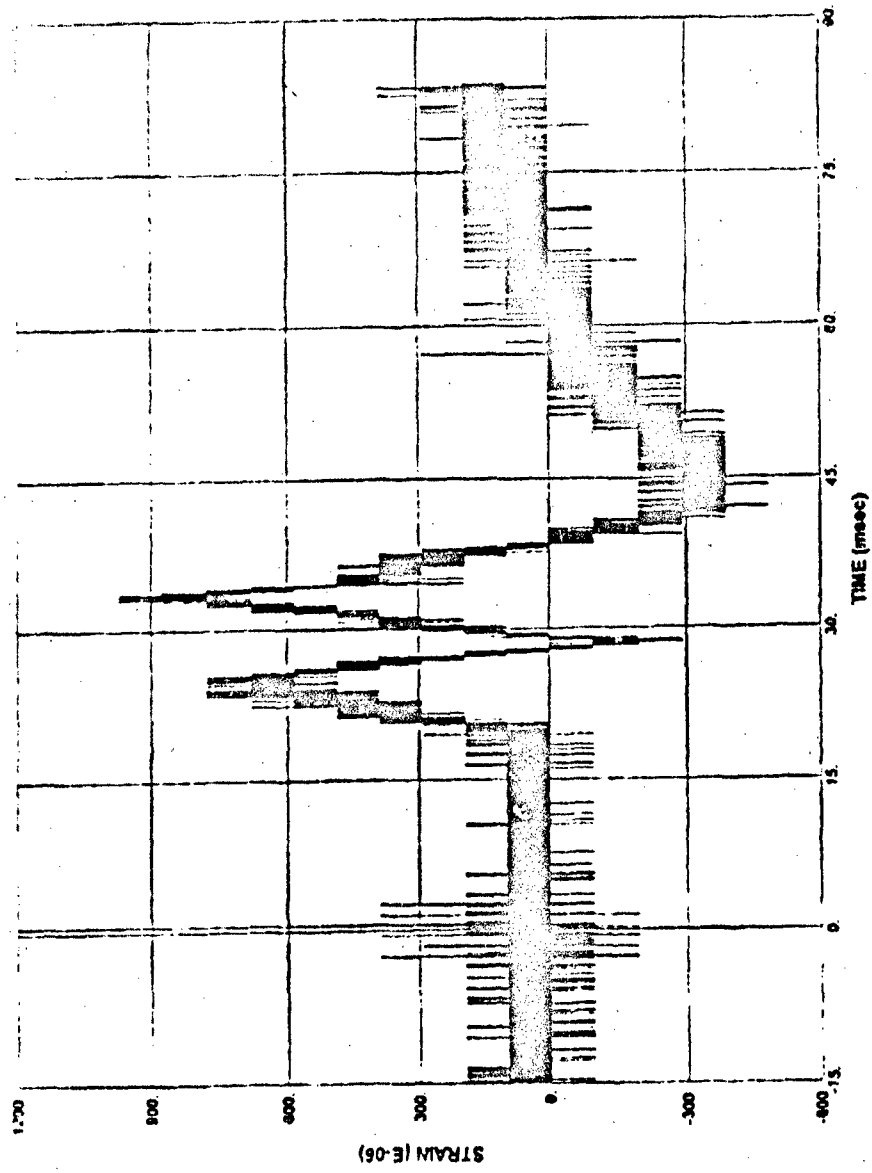


Figure C.94 Strain Gage S5, Test 5

347

ADA293552

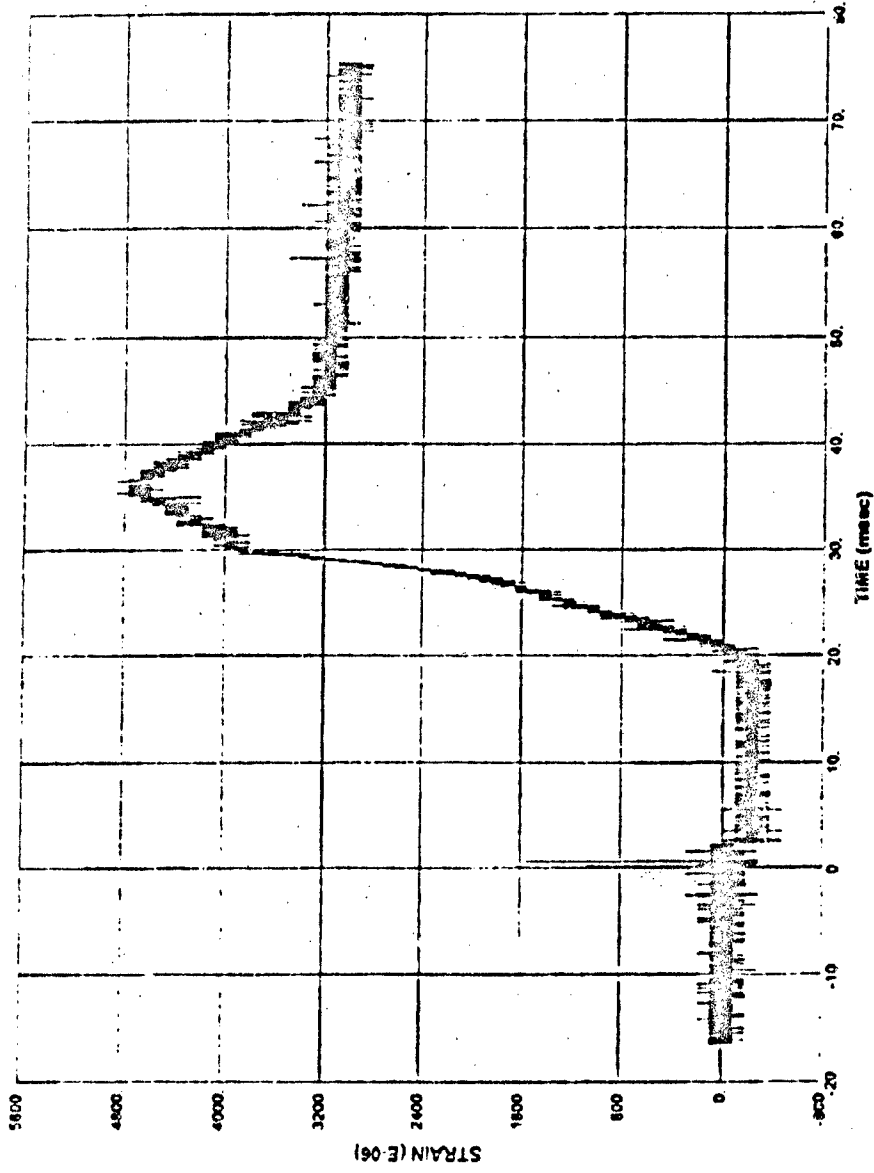


Figure C.95 Strain Gage S8, Test 5

348

ADA293552

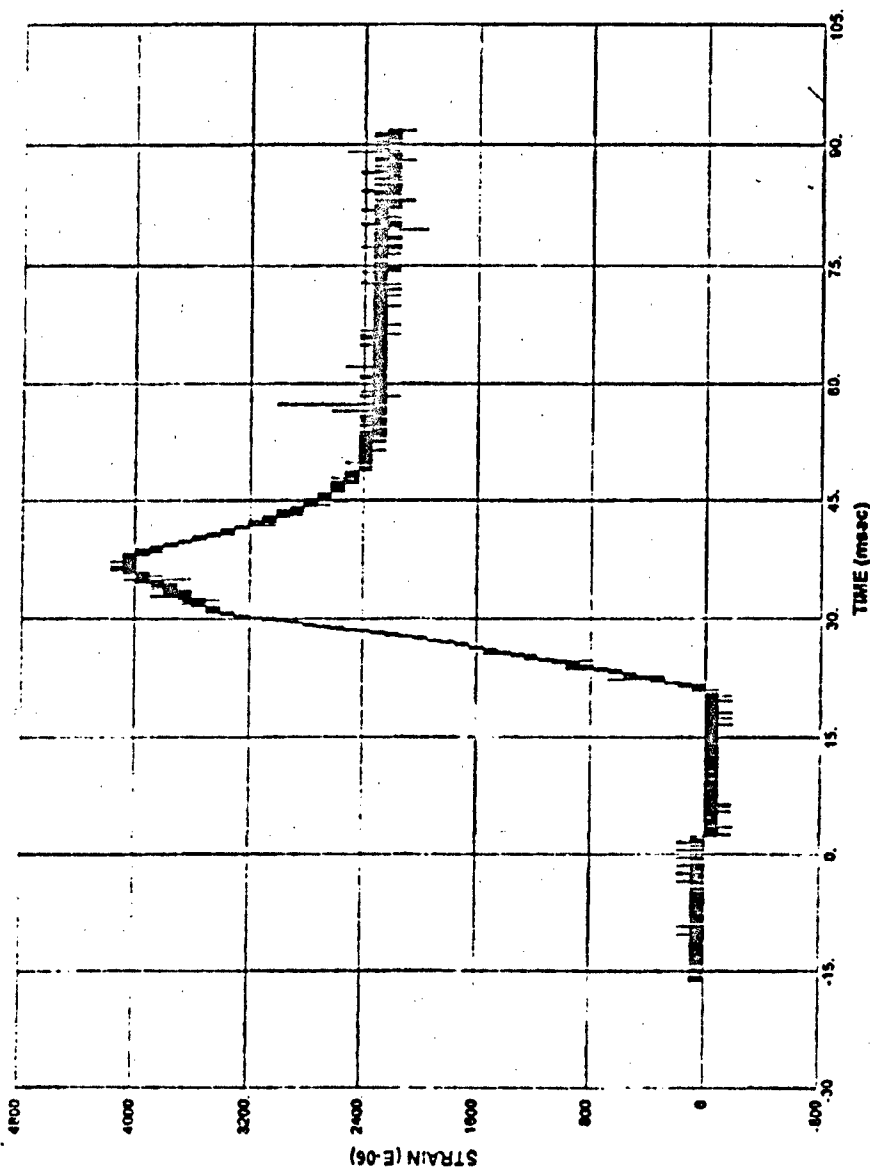


Figure C.96 Strain Gage SII, Test 5

349

ADA293552

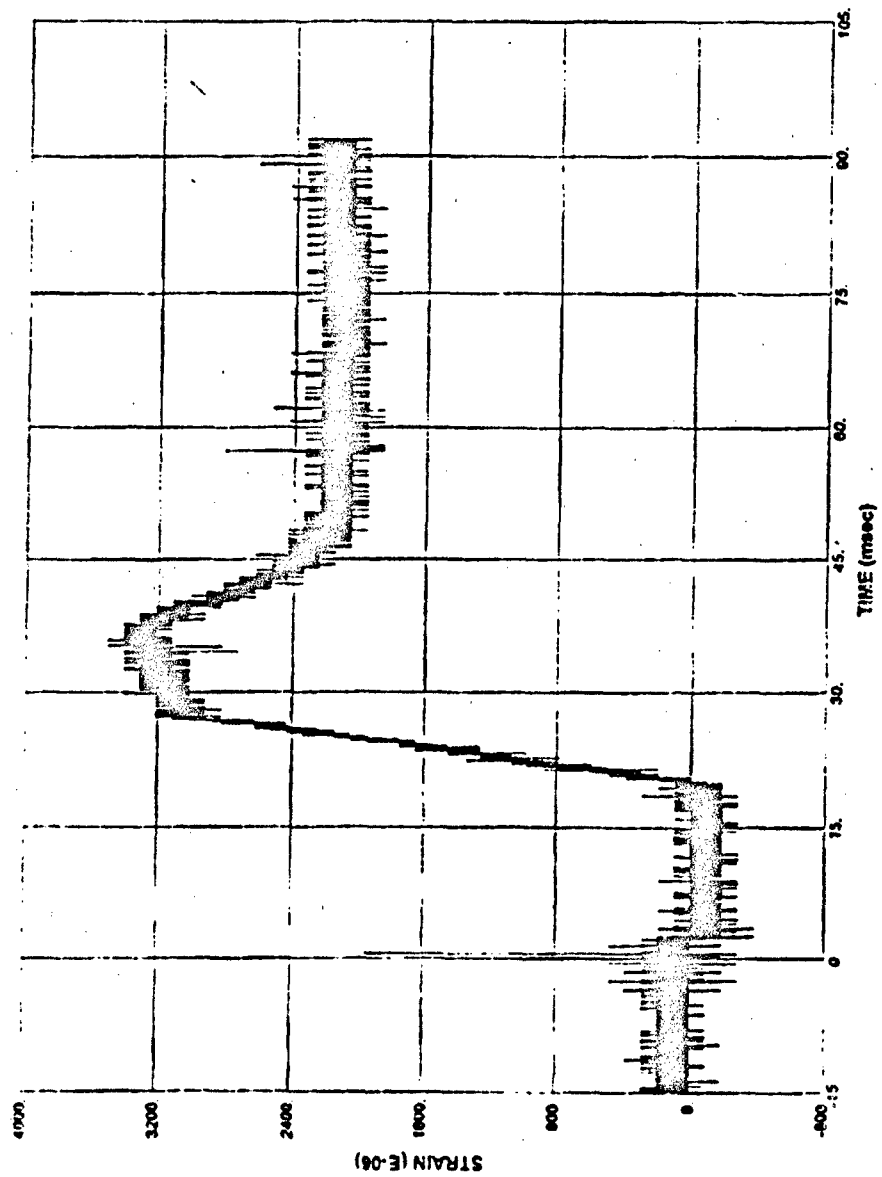


Figure C.97 Strain Gage S12, Test 5

350

BIBLIOGRAPHY

Al-Khafaji, A.W. and Tooley, J.R., Numerical Methods in Engineering Practice, Holt, Rinehart, and Winston, Inc., New York, 1986.

Anderson, J.C., The Seismic Design Handbook, edited by Farzad Naeim, Van Nostrand Reinhold, New York, New York, 1989.

Bachus, R.C., Fragaszy, R.J., Jaber, M, Olen, K.L., Yuan, Z., and Jewell.R. "Dynamic Response of Reinforced Soil Systems, Volume I and II," Report Number ESL-TR-92-47, Air Force Civil Engineering Support Agency, Tyndall Air Force Base, Florida, March 1993.

Baker, W.E., Explosions in Air, University of Texas Press, Austin, Texas, 1973.

Bangash, M.Y.H., Impact and Explosion: Analysis and Design, CRC Press, Inc. Boca Raton, FL, 1993.

Baylot, J.T., "Parameters Affecting Loads on Buried Structures Subjected to Localized Blast Effects," WES-TR-SL-92-9, US Army Engineer Waterways Experiment Station, Vicksburg, MS, April 1992.

Christopher, B.R.; Gill, S.A.; Giroud, J.P.; Juran, I; Mitchell, J.K.; Schlosser, F; and Dunncliff, J., "Reinforced Soil Structures: Volume I. Design and Construction Guidelines", Report Number FHWA-RD-89-043, U.S. Department of Transportation, Federal Highway Administration, McLean, Virginia, November, 1990.

Coltharp, D.R., Vitayaudom, K.P., and Kiger, S.A., "Semihardened Facility Design Criteria Improvement," Report Number ESL-TR-85-32, Air Force Engineering and Services Center, Tyndall Air Force Base, Florida, September 1985.

Crawford, R.E., et al, "Protection From Nonnuclear Weapons," Report Number AFWL-TR-70-127, Air Force Weapons Laboratory, Kirtland Air Force Base, New Mexico, February 1971.

Creighton, D.C., "Non-Normal Projectile Penetration in Soil and Rock: User's Guide for Computer Code PENCO2D," Technical Report SL-82-7, U.S. Army Engineer Waterways Experiment Station, Vicksburg, MS, September, 1982.

Das, B.M, Fundamentals of Soil Dynamics, Elsevier Science Publishers, New York, 1983.

Davies, M.C.R. and Williams, A.J., "Centrifuge Modelling the Protection of Buried Structures Subjected to Blast Loading," Structures Under Shock and Impact II, Proceedings of the Second International Conference, 1992, Portsmouth, U.K., P.S. Bulson, Editor, 16-18 June, 1992.

Dobratz, B.M. and Crawford, P.C., "Lawrence Livermore National Laboratory Explosives Handbook: Properties of Chemical Explosives and Explosive Simulants," Report Number UCRL-52997-Chg 2, January 1985.

Drake, J.L., and Little, C.D., "Ground Shock From Penetrating Conventional Weapons", Symposium Proceedings From The Interaction of Non-Nuclear Munitions With Structures, U.S. Air Force Academy, Colorado, May 1983, pp. 1-6.

Drake, J.L., Frank, R.A., and Rochefort, M.A., "A Simplified Method For The Prediction Of The Ground Shock Loads On Buried Structures," Symposium Proceedings From The Interaction of Conventional Munitions With Structures, Mannheim, FRG, March 1987, pp. 3-14.

Drake, J.L., Twisdale, L.A., Frank, R.A., Dass, W.C., Rochefort, M.A., Walker, R.E., Britt, J.R., Murphy, C.E., Slawson, T.R., and Sues, R.H., "Protective Construction Design Manual," Report Number ESL-TR-87-57, Air Force Engineering and Services Center, Tyndall Air Force Base, Florida, November, 1989.

Elias, V., "Tests on the Effects of Explosive Charges on Reinforced Earth Walls", Proceedings of the 18th Explosive Safety Seminar, San Antonio, Texas, September, 1978.

Eytan, R., "Short Distance Explosion Test in Armee Type Structure - Final report", (Published In Hebrew) (Confidential) Israel Air Force Civil Engineering Division, Engineering and Projects Branch, Tel Aviv, Israel, 1988.

Eytan, R., and Reid, R.A., "Reinforced Soil Ammunition Magazine: Full Scale Tests - 1990, Detailed Report" (Confidential), (Published in Hebrew), Israel Air Force Civil Engineering Division, Engineering and Projects Branch, Tel Aviv, Israel, and U.S. Air Force Civil Engineering Support Agency, Tyndall Air Force Base, Florida, July 1993.

Ferritto, J., Tancreto, J., and Hager, K., "Design Procedures and Effectiveness of Reinforced Earth Berms for Enhancing Facility Survivability", Report Number UG-0013, Naval Civil Engineering Laboratory, Port Hueneme, CA, March 1988.

Fluet, J.E., "Geosynthetics in North America: A Rigorous Attempt to Make a Short Story Long", Proceedings Geosynthetics '93 Conference, Vol. 1, Vancouver, British Columbia, Canada, 1993, page 6.

Headquarters, Department of the Army, "Fundamentals of Protective Design for Conventional Weapons," Technical Manual TM 5-855-1, November, 1986.

Heike, T.T., Patterson, M.A., and Kerr, J.R., "Geogrid Reinforced Containment Dykes for Mountainside Oil Tank Farm in Seismic Zone," Conference Proceedings, Geosynthetics '91, Atlanta, GA, 1991, pp. 861-878.

Henrych, J., The Dynamics of Explosion and Its Use, Elsevier Scientific Publishing Company, New York, 1979.

Hyde, D.W., ConWep (Conventional Weapons Effects), computer programs, United States Army Waterways Experiment Station, Vicksburg, MS, February 1988.

Hyde, D.W., "NATO Semi-Hardened Facility Test", Report Number ESL-TR-89-06, Air Force Engineering and Services Center, Tyndall Air Force Base, Florida, 1989.

Hyde, D.W., DPLOT/W, computer program, version 0.72.11.19, United States Army Waterways Experiment Station, Vicksburg, MS, undated.

Hyndman, D., Bultman, E., "Bitburg and Aircraft Revetment Tests - Conventional High-Explosives Blast and Shock (CHEBS) Tests 9 and 10", Report Number AFWL-TR-86-46, U.S. Air Force Weapons Laboratory, Kirtland Air Force Base, New Mexico, 1987.

Juran, I. and Chen, C.L., "Soil-Geotextile Pull-Out Interaction Properties: Testing and Interpretation," Transportation Research Board, No. 1188, Transportation Research Board, National Research Council, Washington, DC, 1988, pp. 37-47.

Juran, I., Knochenmus, G., Acar, Y.B., and Arman, A., "Pull-Out Response of Geotextiles and Geogrids (Synthesis of Available Experimental Data)," Proceedings of the Symposium on Geosynthetics for Soil Improvement, Geotechnical Special Publication No. 18, ASCE, Edited by R.D. Holtz, May 1988, pp. 92-111.

Koerner, R.M., Designing With Geosynthetics, Englewood Cliffs, New Jersey, Prentice-Hall, Inc., 1990.

Kolsky, H., Stress Waves in Solids, Dover Publications, Inc., New York, New York, 1963.

Lindholm, U.S., "Techniques in Metal Research," Edited by R.F. Bunshah, Vol. 5, Part 1, Interscience, N.Y., 1971.

Mitchell, J.K. and Villet, W.B., "Reinforcement of Earth Slopes and Embankments," National Cooperative Highway Research Program Report 290, Transportation Research Board, 1987, p. 323.

National Defense Research Committee, "Effects of Impact and Explosion,", Volume I, Office of Scientific Research and Development, Washington, D.C., 1946.

Newmark, N.M. and Haltiwanger, J.D., "Principles and Practices for Design of Hardened Structures", SWC-TDR-62-138, Air Force Special Weapons Center, Kirtland Air Force Base, NM, December 1962.

Oglesby, J.W., Mahmoodzadegan, B., and Griffin, P.M., "Evaluation of Methods and Materials Used to Attach Gages to Polymer Grids for High Strain Rate Conditions," Louisiana Transportation Research Center, Draft Report Number FHWA/LA-92/, Baton Rouge, LA, December 1992.

Ohrt, A., Personal communication, US Army Waterways Experiment Station, Vicksburg, MS, February, 1995.

Olen, K.L., Fragaszy, R.J., Purcell, M.R., and Cargill, K.W., "Dynamic Response of Reinforced Soil Systems: Phase II," Draft Report Submitted to the US Air Civil Engineering Laboratory, Tyndall Air Force Base, Florida, December, 1993.

Olen, K.L., Fragaszy, R.J., Purcell, M.R., and Cargill, K.W., "Response of Reinforced Soil Walls to Explosive Loading: Part I - Centrifuge Modeling," Proceedings of Geosynthetics '95 Conference, IFAI, Nashville, TN, 1995.

Purcell, M.R., Personal Communication, Applied Research Associates, Tyndall AFB, FL, February, 1995.

Reid, R.A., "Reinforced Soil Munitions Bunker Test", The Military Engineer, August 1990, Vol 82, Number 537, PP 51-52.

Reid, R.A., "Full-Scale Blast Test of a Reinforced Soil Bunker", Proceedings of the 5th Internationales Symposium Interaktion Kan Ventioneller Munition mit Schutzbauten, Monnheim, Federal Republic of Germany, April 1991.

Reid, R.A., Bachus, R.C., Olen, K.L., and Fragaszy, R., "Response of Geogrid-Reinforced Soil Subjected to Blast Loading", Proceedings of the Sixth International Symposium on Interaction of Nonnuclear Munitions With Structures", Panama City, Florida, May 1993, pp 253-258.

Reid, R.A. and Collier, J.G., "Response of Geogrid-Reinforced Retaining Wall to Explosive Loading: Part II - Full-Scale Tests", Proceedings of Geosynthetics '95 Conference, IFAI, Nashville, TN, 1995.

The Reinforced Earth Company Brochure "Family of Construction Technologies", McLean, Virginia, USA, 1990.

The Reinforced Earth Company Brochure, "Reinforced Earth Protective Structures for Industrial and Military Applications", undated, McLean, Virginia.

Richardson, G.N., Feger, D., Fong, A., and Lee, K.L., "Seismic Testing of Reinforced Earth Walls", Journal of the Geotechnical Engineering Division, ASCE, Vol 103, No. GT1, January 1977.

Robbins, P.E. and Riskowski, G.L., "Coefficient of Static Friction For Wood Bulkheads on Building Floors", Journal of the American Society of Agricultural Engineers, ASAE, Vol. 33, No. 6, November-December, 1990.

Rohani, B., "Shielding Methodology for Conventional Kinetic Energy Weapons," Technical Report SL-87-8, U.S. Army Engineer Waterways Experiment Station, Vicksburg, MS, 1987, Secret.

Ross, C.A., "Split-Hopkinson Pressure Bar Tests", Report Number ESL-TR-88-82, Air Force Engineering and Services Center, Tyndall Air Force Base, Florida, March 1989.

Scott, R.F. and Morgan, N.R., "Feasibility and Desirability of Constructing a Very Large Centrifuge for Geotechnical Studies," Report 760-170, National Science Foundation, Washington, D.C., 1977.

Sues, R.H., Murphy, C.E., and Frank, R.A., "Protective Construction Design Manual Change 5, Expedient hardening Methods for Structures Subjected to the Effects of Non-Nuclear Munitions", Report Number ESL-TR-87-57, Air Force Engineering and Services Center, Tyndall Air Force Base, Florida, June 1991.

Tensar Earth Technologies Inc., "Specification Sheets, UX 1400 HT and UX 1500 HT," Morrow, GA., 1992.

Tuan, C.Y. and Merkle, D.H., "Advanced Panel and Connection System For Reinforced Soil," Report Number ESL-TR-92-76, Air Force Civil Engineering Support Agency, Civil Engineering Laboratory, Tyndall Air Force Base, Florida, March 1993.

Underwood, J.M. and Westmoreland, M.K., "Penetration Countermeasures," Proceedings of the Sixth International Symposium on Interaction of Nonnuclear Munitions With Structures", Panama City, Florida, May 1993, pp. 50-55.

United States Office of Civil Defense, "Report of Bomb Tests on Materials and Structures", Washington, D.C., 1941.

Vesic, A.S., "Cratering By Explosives as an Earth Pressure Problem", Proceedings of the Sixth International Conference on Soil Mechanics and Foundation Engineering, Volume II, Montreal, Canada, September, 1965.

Veyera, G.E., Charlie, W.A., and Ross, C.A., "Strain-Rate Effects in Unsaturated Soils", Proceedings of the Sixth International Symposium on Interaction of Nonnuclear Munitions With Structures", Panama City, Florida, May 1993, pp 300-304.

Veyera, G.E., "Uniaxial Stress-Strain Behavior of Unsaturated Soil at High Strain Rates", Report Number WL-TR-93-3512, Air Force Wright Laboratories, Wright-Patterson AFB, OH, November 1993.

Whirley, R.G. and Hallquist, J.O., "DYNA3D A Nonlinear Explicit, Three-Dimensional Finite Element Code For Solid and Structural Mechanics - User Code," Report Number UCRL-MA-107254, Lawrence Livermore National Laboratory, Livermore, California, May 1991.

Waters, K.H., Reflection Seismology, John Wiley and Sons, New York, 1981.

Westine, P.S., and Friesenhahn, G.J., "Free-Field Ground Shock Pressures From Buried Detonations In Saturated and Unsaturated Soils", Symposium Proceedings From The Interaction of Non-Nuclear Munitions With Structures, U.S. Air Force Academy, Colorado, May 1983, pp. 12-16.

Yogendrakumar, M., Bathurst, R.J., and Finn, W.D.L, "Dynamic Response Analysis of Reinforced-Soil Retaining Wall", Journal of Geotechnical Engineering, ASCE, Vol. 118, No. 8, August, 1992.

Yuan, Z., Swan, R.H. and Cargill, K.W., "Final Report on Direct Shear and Pullout Testing, Phase II Study, Dynamic Response of Reinforced Soil Systems", laboratory report submitted by GeoSyntec Consultants to Applied Research Associates, Gulf Coast Division, Tyndall AFB, FL, December 22, 1993.

VITA

Richard Alan Reid was born on September 8, 1959 in Biddeford, Maine. He is the sixth child of Wallace and Virginia Reid. His elementary education was at Kennebunkport Consolidated School and Kennebunk High School. Supported by an Air Force Scholarship, he attended The Citadel in Charleston, SC from August 1977 to May 1981, where he earned his Bachelor's degree in Civil Engineering. After graduation, he was assigned to Ellsworth AFB, South Dakota, where he served as base environmental engineer and later, pavement engineer. In 1984 he was assigned to the Georgia Institute of Technology, earning a Master's in Civil Engineering, and completing his Ph.D. course requirements. In 1988 he was reassigned to the Air Force Civil Engineering Laboratory, Tyndall AFB, Florida, managing Civil Engineering research. He obtained his professional engineering license in Florida in 1990. In 1994, he left the Air Force, returning to Georgia Tech to complete his Ph.D. Upon completion of his Doctorate, he accepted a position as Assistant Professor of Civil Engineering at South Dakota State University, Brookings, SD.

He married Kathleen Ruth Kreger of Huron, SD on June 1, 1985, and they have three children, Lindsey Kathleen, Timothy Alan, and Rebecca Erin.